Deutsche Geodätische Kommission
der Bayerischen Akademie der Wissenschaften

Reihe C Dissertationen Heft Nr. 758

Tamara Bandikova

The role of attitude determination for inter-satellite ranging

München 2015

Verlag der Bayerischen Akademie der Wissenschaften
in Kommission beim Verlag C. H. Beck

ISSN 0065-5325 ISBN 978-3-7696-5170-6

Diese Arbeit ist gleichzeitig veröffentlicht in:
Wissenschaftliche Arbeiten der Fachrichtung Geodäsie und Geoinformatik der Leibniz Universität Hannover
ISSN 0174-1454, Nr. 318, Hannover 2015

Deutsche Geodätische Kommission

der Bayerischen Akademie der Wissenschaften

Reihe C Dissertationen Heft Nr. 758

The role of attitude determination for inter-satellite ranging

Von der Fakultät für Bauingenieurwesen und Geodäsie
der Gottfried Wilhelm Leibniz Universität Hannover
zur Erlangung des Grades
Doktor-Ingenieurin (Dr.-Ing.)
genehmigte Dissertation

von

Dipl.-Ing. Tamara Bandikova

München 2015

Verlag der Bayerischen Akademie der Wissenschaften
in Kommission bei der C. H. Beck'schen Verlagsbuchhandlung München

ISSN 0065-5325 ISBN 978-3-7696-5170-6

Diese Arbeit ist gleichzeitig veröffentlicht in:
Wissenschaftliche Arbeiten der Fachrichtung Geodäsie und Geoinformatik der Leibniz Universität Hannover
ISSN 0174-1454, Nr. 318, Hannover 2015

Adresse der Deutschen Geodätischen Kommission:

Deutsche Geodätische Kommission

Alfons-Goppel-Straße 11 ● D – 80 539 München

Telefon +49 – 89 – 23 031 1113 ● Telefax +49 – 89 – 23 031 - 1283 / - 1100
e-mail hornik@dgfi.badw.de ● http://www.dgk.badw.de

Prüfungskommission

Referent: Prof. Dr.-Ing. Jakob Flury
1. Korreferent: Prof. Dr.-Ing. Martin Horwath
2. Korreferent: apl. Prof. Dr. Gerhard Heinzel

Tag der mündlichen Prüfung: 28.09.2015

ISSN 0065-5325 ISBN 978-3-7696-5170-6

Non est ad astra mollis e terris via

-Seneca -

Abstract

The Gravity Recovery and Climate Experiment (GRACE) is the first and up to now the only satellite mission using the inter-satellite ranging observation technique for the determination of the static and time-variable Earth gravity field. The gravity field data are highly valuable for a large spectrum of geosciences as they contain information about mass distribution and mass transport within the Earth system, which cannot be gained from any other satellite data. Therefore, even after 13 years of successful mission operation, efforts are still ongoing to decrease noise of the GRACE gravity field models in order to reach the GRACE baseline accuracy. One of the most significant error sources are the untreated errors in the satellite observation data. Along with the primary GRACE scientific observations, i.e. the microwave inter-satellite ranging, precise orbit determination and ultra-sensitive accelerometry, which are needed for the gravity field recovery, the fourth fundamental observation is precise attitude determination. The precise attitude determination plays a crucial role not only for the in-orbit mission operation but also for the scientific data processing.

Our goal is to present a comprehensive study on the attitude determination, which for GRACE has not been carried out so far. Here we include thorough analysis of the characteristics and accuracy of the GRACE attitude determination sensors and attitude actuators with focus on star cameras, which are the primary attitude sensors. We also present detailed analysis of the characteristics of the inter-satellite pointing, which is one of the fundamental requirements for the inter-satellite ranging. Our review of processing algorithms for the in-flight and on-ground determination of the inter-satellite pointing angles revealed a large pointing bias (up to 3 mrad). This bias is caused by inconsistency between the calibration parameters related to the star cameras and to the ranging interferometer.

Furthermore, we show results of a full reexamination of the GRACE star camera Level-1A to Level-1B processing with emphasis on the data combination methods, which was carried out to find the source of the unexpectedly higher noise in the official SCA1B Release 02 solution. SCA1B RL02 contains systematically higher noise than nominally expected of about a factor 3-4. The data analysis revealed that the incorrect implementation of algorithms for the data combination in the official processing routines is the reason for the higher noise. In this study we also present the impact of the accuracy of the attitude data on the mission lifetime. While maintaining the inter-satellite pointing, the different performance of the star cameras critically affects the propellant consumption and the number of thruster activation cycles, which both are factors limiting the mission lifetime.

The results of our analysis not only contribute to the improvement of the current GRACE data products, but the experience from GRACE also provides information highly valuable for the development and design of the future gravity field satellite missions. As the technology of the primary measurement systems (inter-satellite ranging, orbit determination, accelerometry) is further improving, demands on the accuracy of the attitude determination are increasing. Therefore we also present a basic approach for the determination of the requirements on the measurement accuracy of the attitude determination sensors, on the accuracy of the calibration parameters related to the attitude sensors and on the in-flight and on-ground data processing.

Keywords: Gravity Recovery and Climate Experiment (GRACE); Attitude determination and control; Star cameras; Inter-satellite pointing; Gravity field satellite missions

Zusammenfassung

Gravity Recovery and Climate Experiment (GRACE) ist die erste und bislang einzige Satellitenmission, welche das sogenannte Inter-Satelliten-Ranging Verfahren, die Abstandsmessung zweier Satelliten zueinander, zur Bestimmung des statischen und zeit-variablen Erdschwerefeldes nutzt. Diese Schwerefelddaten sind für ein breites Spektrum der Geowissenschaften von größter Bedeutung, da die Informationen über die Masseverteilung und Massetransport im Erdsystem ermitteln, die mit keinem anderen Satellitenverfahren bestimmt werden können. Aus diesem Grund wird auch nach 13 erfolgreichen Jahren der Erdbeobachtung weiterhin an der Reduzierung des Rauschens der GRACE Schwerefeldmodelle gearbeitet, mit dem Ziel der maximalen Annäherung an die prädizierte Genauigkeit. Eine der signifikantesten Fehlerquellen sind nicht korrigierte Fehler in den Satellitenbeobachtungsdaten. Zusammen mit den primären GRACE Messverfahren, d.h. der Mikrowellen Abstandsmessungen, präzisen Bahnbestimmung und der ultra-sensitiven Beschleunigungsmessung, die für die Schwerefeldmodellierung erforderlich sind, stellt die präzise Lagebestimmung die vierte fundamentale Beobachtung dar. Die präzise Lagebestimmung spielt eine entscheidende Rolle nicht nur für den In-Orbit Missionsbetrieb, sondern auch für die wissenschaftliche Datenverarbeitung.

Unser Ziel ist eine umfassende Studie über die Lagebestimmung, die für GRACE in diesem Umfang noch nicht durchgeführt wurde, zu präsentieren. In dieser Arbeit stellen wir eine ausführliche Analyse über die Eigenschaften und Genauigkeit der GRACE Lagebestimmungssensoren und Lageaktuatoren vor. Der Fokus liegt auf den Sternkameras, welche die primären Lagesensoren darstellen. Zusätzlich wird eine detaillierte Analyse der Eigenschaften des Inter-Satelliten-Pointings bereitgestellt. Das Inter-Satelliten-Pointing, d.h. die präzise Orientierung der GRACE Satelliten zueinander, ist eine der fundamentalen Grundvoraussetzungen für die Abstandsmessung zwischen den Satelliten. Unsere Überprüfung der Algorithmen für die Bestimmung der Pointingwinkel, welche bei dem Onboard- und Onground-Processing verwendet werden, zeigt einen großen Bias (bis zu 3 mrad) der Pointingwinkel auf. Dieses Bias wird durch Inkonsistenzen zwischen den Kalibrierungsparametern der Sternkameras und Abstandsmesser verursacht.

Des Weiteren stellen wir die Ergebnisse einer vollständigen Überprüfung der Sternkameradatenprozessierung von Level-1A zu Level-1B vor. Der Fokus liegt dabei auf den Datenkombinationsmethoden. Diese Überprüfung wurde durchgeführt, um die Ursache des erhöhten Rauschens in den offiziellen Sternkameradaten, d.h. SCA1B Release 02, zu ermitteln. SCA1B RL02 weist ein systematisch erhöhtes Rauschen um den Faktor 3-4 auf. Die Datenanalyse zeigt, dass die Fehlerursache in der inkorrekten Implementierung der Algorithmen für die Sternkameradatenkombination in den offiziellen Verarbeitungsroutinen liegt. Zusätzlich stellen wir den Einfluss der Lagedatengenauigkeit auf die Missionslebensdauer dar. Während der präzisen Orientierung der Satelliten zueinander wird der Treibgasverbrauch und die Anzahl der Düsenaktivierungen, welche beide zu den limitierenden Faktoren der Missionslebensdauer gehören, entscheidend durch die unterschiedliche Messgenauigkeit der Sternkameras beeinflusst.

Die Ergebnisse unserer GRACE-Datenanalyse stellen nicht nur die Grundlage für die Verbesserung der bestehenden GRACE Datenprodukten dar. Die gewonnenen Erfahrungen bieten auch wertvolle Informationen für die Entwicklung und das Design künftiger Schwerefeldsatellitenmissionen. Da die Technologie der primären Messsysteme, d.h. der Abstandsmessung, der Bahnbestimmung und der Beschleunigungsmessung stetig verbessert wird, steigen auch die Ansprüche an die Genauigkeit der Lagebestimmung stetig. Daher stellen wir zusätzlich einen grundlegenden Ansatz vor, zur Bestimmung der Anforderungen an die Messgenauigkeit der Lagebestimmungssensoren an die Genauigkeit der relevanten Kalibrierungsparameter sowie die Onboard- und Onground-Verarbeitung der Beobachtungsdaten.

Keywords: Gravity Recovery and Climate Experiment (GRACE); Lagebestimmung und Lageregelung; Sternkameras; Inter-Satelliten Pointing; Schwerefeldsatellitenmissionen

Contents

*The journey is what brings us happiness,
not the destination.*

- Dan Millman -

1 Introduction

1.1 Motivation

The Earth's gravity field determination along with the determination of the shape of the Earth and its orientation in space have ever been the fundamental objectives of geodesy. As the gravity field and its changes reflect the mass distribution and mass transport in the Earth system, its knowledge is fundamental for many sciences such as solid Earth physics, geodynamics, hydrology, oceanography, navigation, spaceflight, geodesy and others. From the gravimetric measurements on and above the Earth's surface, information about the geoid, continental water storage variations, ice mass balance, glacial isostatic adjustment, post-seismic deformation, tidal deformations of the Earth crust due to the gravitational attraction of the Sun and the Moon, sea level changes and many other phenomena can be derived. Some of these processes have a crucial impact on the human society and thus the need arises to globally monitor the gravity variations more precisely.

The first absolute gravity measurements were carried out around the turn of the 17th and 18th century by means of diverse types of pendulum. The first spring-based relative gravimeters were developed in the first half of the 20th century and later on the absolute gravimeters based on rise-and-fall and free-fall methods were built, which were significantly more accurate than the pendulum gravimeters (Torge, 1989). The technology development in the last few decades allowed to build highly precise relative superconducting gravimeters (Goodkind, 1999), and currently absolute quantum gravimeters are under development (de Angelis *et al.*, 2009). With these instruments it is possible to perform the gravity measurements only pointwise. Later, regional measurements have been possible by means of airborne and ship-borne instruments. However, the determination of the global gravity field was not possible before using measurements from space. The very first satellite, Sputnik 1, was launched in 1957 and since then the number of launched satellites has raised exponentially. The satellite orbits are perturbed by the inhomogeneous mass distribution within the central body and so it is possible to recover the gravity field from the orbit tracking data. One of the first global Earth's gravity field models was presented in 1966 by Lundquist and Veis (1966). The accuracy of the first models was rather low, though.

At the beginning of the new millennium, three geodetic satellites dedicated exclusively to the observation of the Earth's gravity were launched: the Minisatellite Challenging Payload (CHAMP) in 2000 (Reigber *et al.*, 1999), the Gravity Recovery and Climate Experiment (GRACE) in 2002 (Tapley *et al.*, 2004) and the Gravity Field and Steady-State Ocean Circulation Explorer (GOCE) in 2009 (ESA, 1999). Each mission is based on different measurement techniques which are: orbit tracking and accelerometry for CHAMP, orbit tracking, inter-satellite ranging and accelerometry for GRACE and finally orbit tracking and gravitational gradiometry for GOCE. From the observation data, global models of the static gravity field have been computed with previously unprecedented accuracy. GRACE and GOCE data complement each other well, resulting in combined models computed up to spherical harmonic degree and order 250 such as GOCO03S (Mayer-Gürr *et al.*, 2012). Besides, the static gravity field is further determined from combination of the terrestrial and satellite gravity data, including altimetry-derived and airborne data. The latest global model is EIGEN-6C4 derived up to the spherical harmonic degree and order 2190 which corresponds to approx. 9 km spatial resolution (Förste *et al.*, 2014).

Along with the determination of the static gravity field, the GRACE observations allow the determination of time variations of the gravity field. Due to the orbital configuration and the inter-satellite ranging measurement technique, enough data for gravity field recovery are collected already within 30 days and thus up-to-date models with sufficient accuracy are released usually on monthly basis. The importance of the availability of the monthly field models for geosciences has been further enhanced thanks to the GRACE unexpected long lifetime. Until today, the originally planned 5 years of operation have been exceeded more than 2.5 times.

GRACE is the very first gravity field satellite mission based on inter-satellite ranging technique. The concept of relative velocity observation between a pair of satellites flying in the same orbit separated by a distance of 200 km was originally described by Wolff (1969). The inter-satellite ranging technique demonstrated well its strengths and so far it is considered to be the most favorable observation technique for resolving the long and medium wavelengths of the static gravity field at annual and seasonal time-scales. It is notable that the GRACE mission concept was also chosen for the observation of the lunar gravity field. The Gravity Recovery and Interior Laboratory (GRAIL) successfully operated from March 2012 to December 2012 and provided so far the most accurate Moon's gravity field (Zuber *et al.*, 2013).

Precise knowledge of the gravity field and especially its temporal variations has become more and more important over the last decades and therefore the gravity field observation from space will continue. The next satellite mission dedicated to Earth's gravity field observation, the GRACE Follow-On, is planned to be launched in 2017 (Watkins *et al.*, 2013). The spacecraft design and operation principle is very similar to GRACE. Along with the primary observations based on the microwave inter-satellite ranging, the changes in inter-satellite range will be measured by the laser ranging interferometer. The successful technology demonstration of the laser interferometry in space might open the door to the next generation of the gravity field satellite missions. Concepts of the next generation of the gravity field missions are already under development, such as the e^2.motion mission concept, considering two pairs of satellites and laser ranging interferometry as the primary observation technique (NGGM-D Team *et al.*, 2014). Such constellations promise substantially improved gravity field models.

One of the fundamental requirements of the inter-satellite ranging technique is the precise inter-satellite pointing whose realization differs for the microwave and the laser ranging. In case of the microwave ranging, precise orientation of the two spacecraft with their ranging antennas towards each other is required. In case of the laser ranging, precise alignment of the received laser beam and the local oscillator beam needs to be maintained. The precise inter-satellite pointing has high demands on precise attitude determination and control of the satellites. Precise attitude determination is important not only for the in-orbit maintenance of the inter-satellite pointing, but also for the post-processing of the inter-satellite ranging observations, accelerometer measurements and the GPS observations, which are needed for the gravity field recovery. Several extensive studies were published on the GRACE precise orbit determination e.g. Kang *et al.* (2006); Jäggi *et al.* (2007); Montenbruck *et al.* (2005); van Helleputte and Visser (2008), on the inter-satellite ranging technique e.g. Thomas (1999); Kim (2000); Kim and Tapley (2002); Wang (2003); Ko (2008) and on the GRACE accelerometry e.g. Flury *et al.* (2008); Frommknecht (2008); Peterseim (2014). Concerning the attitude determination, only a few research studies have been released which included the star camera sensor analysis e.g. Frommknecht (2008); Bandikova *et al.* (2012); Inacio *et al.* (2015), the attitude data processing e.g. Bandikova and Flury (2014); Klinger and Mayer-Gürr (2014) or the attitude error propagation into gravity field e.g. Horwath *et al.* (2010); Inacio *et al.* (2015). However, no comprehensive study on GRACE attitude determination has been published so far.

Profound knowledge of the GRACE onboard laboratory and the observation techniques is necessary not only for improvement of the current GRACE gravity field models, but also for the development of the future gravity field satellite missions. Thanks to the unexpectedly long mission operation, analysis of long data time series is possible which provides precious insight into the characteristics and accuracy of the onboard sensors and instruments. The analysis of GRACE star camera attitude data will help to understand the characteristics of the onboard star camera sensors and to reveal systematics which, if not corrected, negatively influence the mission performance as well as the accuracy of the other three fundamental observations. The laser ranging, which will be implemented on GRACE Follow-On and possibly on the future missions as well, has even higher requirements on the precise attitude determination and control. Therefore it is necessary to gain maximal experience from GRACE which will be considered during the design development and operation of the future missions.

1.2 Goal

The goal of this thesis is to present the role of attitude determination for the gravity field satellite missions based on inter-satellite ranging measurement technique and to demonstrate how the quality of the attitude data influences the gravity field models as well as the mission lifetime, cf. Figure 1.1. We analyze the data from GRACE, so far the only operating mission using the inter-satellite ranging technique, and take the benefit from the availability of long time series of sensor data.

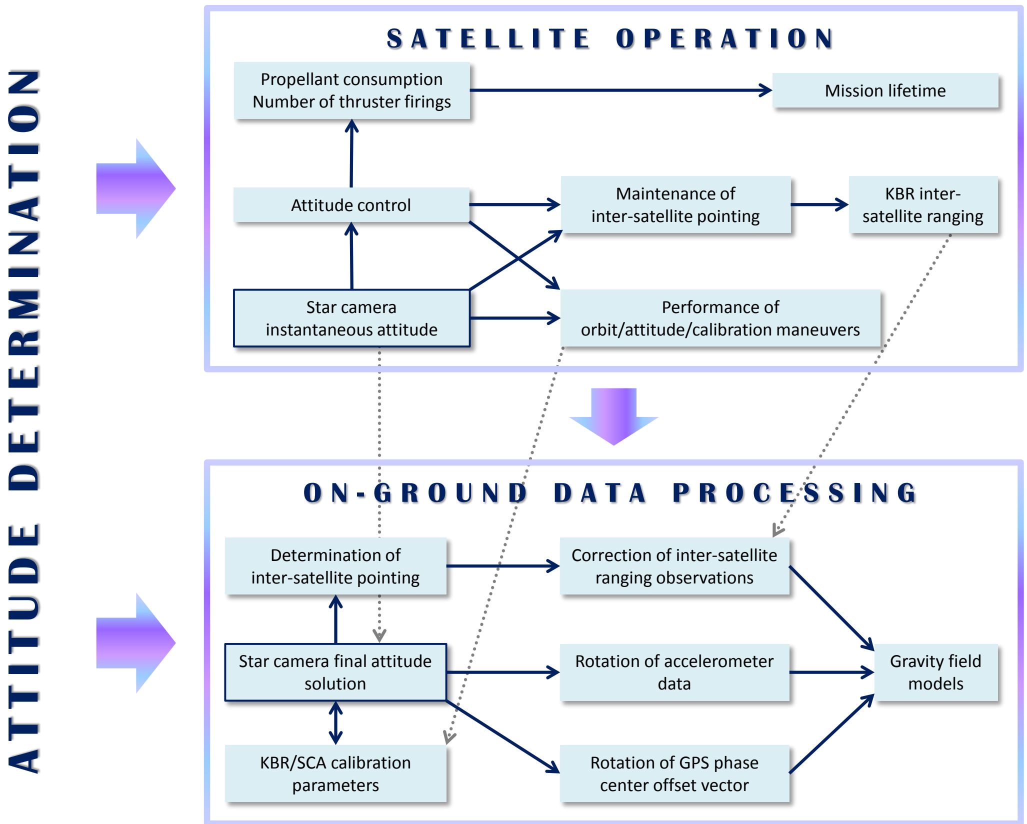

Figure 1.1: The role of attitude determination for inter-satellite ranging mission

We present the impact of the attitude determination on satellite operation as well as on the on-ground data processing. The thesis is based on five cornerstones:

The first cornerstone is the analysis of the characteristics and accuracy of the GRACE attitude determination sensors and attitude actuators (see Chapter 3). The main focus is put on star cameras, which provide the most accurate attitude information compared to all other available sensors and therefore the star camera data are fundamental for mission operation as well as for the processing of the observations needed for gravity field modeling.

The inter-satellite ranging measurement technique is unique due to its fundamental requirement on precise inter-satellite pointing, for which precise attitude determination is essential. Thus the second cornerstone is the analysis of the characteristics and accuracy of GRACE inter-satellite pointing (see Chapter 4). The focus of our analysis is put on the in-flight maintenance and on-ground determination of the inter-satellite pointing, as well as on its characteristics and accuracy in relation to the attitude determination and control.

The third cornerstone is the improvement of the GRACE star camera attitude data and the analysis of the effect on the fundamental observations needed for gravity field recovery, i.e. on inter-satellite ranging observations, accelerometer data and orbit tracking data (see Chapter 5). As the star cameras are the key sensors for attitude determination, the highest possible accuracy of the attitude data is of high importance and priority.

The accuracy of the attitude determination has impact not only on the accuracy of the gravity field models, but also it significantly affects the mission operation. While maintaining the inter-satellite pointing, the quality of the attitude data critically influences the propellant consumption, which is one of the factors limiting the mission lifetime. For this reason, the demonstration of the impact of the accuracy of measured attitude data on the mission lifetime is the fourth cornerstone of this thesis (see Chapter 6).

And finally the fifth cornerstone is the presentation of suggestions related to attitude determination issues for the future gravity field satellite missions based on inter-satellite ranging technique. The results of this thesis go beyond the GRACE mission itself. As the GRACE mission is the first inter-satellite ranging mission, the experience from GRACE provides highly valuable information for the development, design and operation of the future missions (see Chapter 7).

1.3 Prior publications

Some of the results presented in this thesis were already published as original articles in an internationally acknowledged research journal:

- Bandikova T., Flury J., Ko U.-D. (2012): Characteristics and accuracies of the GRACE inter-satellite pointing, Advances in Space Research 50(1):123-135. doi: 10.1016/j.asr.2012.03.011
- Bandikova T., Flury, J. (2014): Improvement of the GRACE star camera data based on the revision of the combination method, Advances in Space Research 54(9):1818-1827. doi:10.1016/j.asr.2014.07.004

The results presented in the first research article have been further complemented and are incorporated in Chapters 3 and 4. The results presented in the second research article are included in the first part of Chapter 5 and are complemented by the analysis of the impact of the improved star camera data on the scientific observations and on the gravity field. The results of this analysis are introduced in the second part of Chapter 5. The first publication received the Outstanding Paper Award for Young Scientists presented by the Committee on Space Research (COSPAR) in 2014.

To fly as fast as thought,
you must begin by knowing
that you have already arrived.

- Richard Bach -

2 GRACE mission fundamentals

2.1 Mission success

GRACE is a joint mission of the National Aeronautics and Space Administration (NASA) and the German Aerospace Center (DLR) (Tapley *et al.*, 2004). It was launched on March 17^{th} 2002 on Rockot launch vehicle from the Plesetsk cosmodrome in Russia. The mission is operated by the German Space Operations Center (GSOC) and it consists of two identical satellites named GRACE-A and GRACE-B or Tom and Jerry (Figure 2.1). With now more than 13 years of operation, the predicted mission lifetime of 5 years has been exceeded by more than 2.5 times.

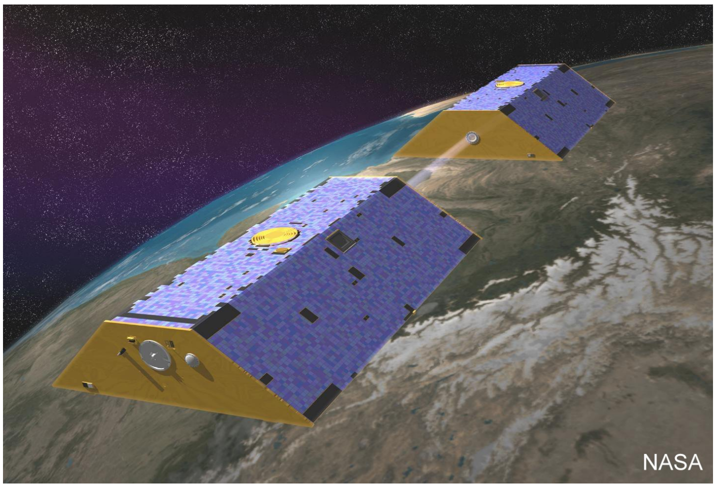

Figure 2.1: The Gravity Recovery and Climate Experiment (GRACE)

The primary mission's goal is the determination of the static and time-variable Earth's gravity field. GRACE can be considered as so far the most successful satellite mission for Earth's gravity field observation due to its great impact on the wide spectrum of geosciences. The precise knowledge of the global Earth' gravity field is essential for many geophysical, geodynamical and geodetical applications as for example:

- for the determination of the *continental water storage variations*, i.e. ground water variations (Rodell *et al.*, 2009), snow cover and permafrost variations (Vey *et al.*, 2013), evapotranspiration in specified regions (Rodell *et al.*, 2004), seasonal and inter-annual river basin water storage changes (Frappart *et al.*, 2012), human influences on regional water storage changes (Famiglietti and Rodell, 2013), etc. Information about the continental water storage is needed for understanding the Earth ecosystem, for water resource management or for exploring environmental solutions.

- for observation of the *ice mass balance in Antarctica, Greenland and Alaska* (Velicogna and Wahr, 2006; Sasgen *et al.*, 2013; Svendsen *et al.*, 2013; Luthcke *et al.*, 2006, 2008; Cazenave and Llovel, 2010; Baur *et al.*, 2013). Using the GRACE data, it was possible to quantify the ice sheet mass loss and to estimate the effect on the global sea level rise for the first time.
- for observation of the *phenomena related to solid Earth geophysics*, such as glacial isostatic adjustment in northern Europe and Canada (Steffen *et al.*, 2008; Müller *et al.*, 2012; A *et al.*, 2013) or co- and post-seismic deformations of the Earth crust (Han *et al.*, 2006; Wang *et al.*, 2011, 2012).
- the precise knowledge of the gravity field is fundamental for many *geodetic techniques* like leveling based on the Global Positioning System (GPS) (Hofmann-Wellenhof and Moritz, 2005), precise satellite orbit determination and prediction (Montenbruck and Gill, 2000) or definition of the height system and geodetic reference frames (Torge and Müller, 2012).

Along with the gravity field data, GRACE provides globally distributed data from atmospheric sounding using the GPS signals. These radio occultation data are valuable for atmospheric and climate research and weather modeling and forecasting (Wickert *et al.*, 2005, 2009).

2.2 Orbit

The GRACE satellites are placed in a low Earth orbit at slowly decaying altitude of 500 km (in 2002) to 420 km (in 2014). The twins fly in co-planar, nearly polar orbit with inclination of 88.93° - 89.10° and nearly circular orbit with characteristic eccentricity of 0.0010 - 0.0025. The right ascension of the ascending node is progressing very slowly with a period of ca. 8 years. The orientation of the orbital plane relative to the Sun (β' angle) is changing with a period of ca. 322 days (cf. Appendix D.2). The complete orbital configuration can be found at http://www.csr.utexas.edu/grace/.

It takes approximately 93 min to finish one revolution which results in 15.5 revolutions per day. The orbit is selected in such a way that within a month sufficient spatial data coverage is available (cf. Figure 2.2) and so that an up-to-dated gravity field model can be computed. The two satellites are separated by distance of 220±50 km which is maintained by regular orbital maneuvers. Due to the separation distance, the trailing satellite passes over a certain region approx. 28 s after the leading satellite. So far, the positions of the leading and the trailing satellite have been switched four times. The first swap maneuver was carried out in December 2005 when the GRACE-B satellite replaced the GRACE-A satellite in its leading position. The second swap maneuver was performed in July 2014, followed by maneuvers in December 2014 and June 2015 (Witkowski and Massmann, 2014).

2.3 Measurement principle

The GRACE measurement principle is based on three fundamental techniques: the precise orbit determination, inter-satellite ranging and accelerometry as illustrated in Figure 2.3. The gravity observation from space is based on the fact that the satellite's orbit is perturbed by the attraction of the inhomogeneously distributed Earth's mass. Therefore the precise orbit determination is the primary observation technique, see Section 2.3.1.

As the two satellites are flying in a co-planar orbit separated by a distance of 220±50 km, the sensed orbit perturbation is slightly different for each satellite, which results in continuous inter-satellite range variations. The relative range rates reflect directly the gravitational

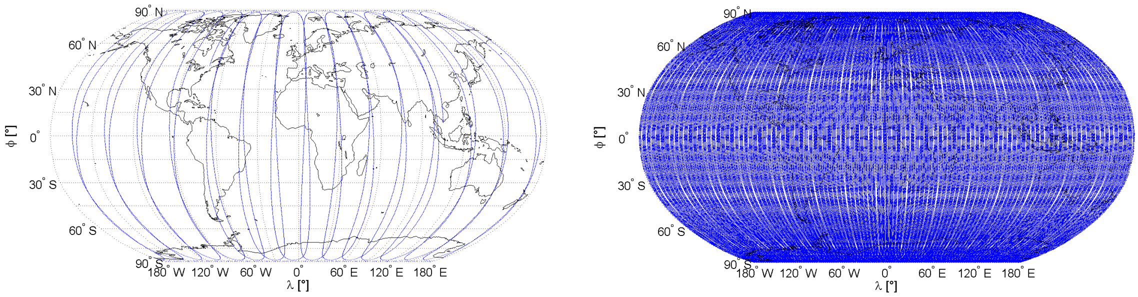

(a) (b)

Figure 2.2: GRACE groundtrack after 1 day (a) and after 30 days (b)

potential at the position of the satellites at the time of measurement. They are obtained from the inter-satellite ranging which is described more in Section 2.3.2.

It is not only the gravitational attraction of the Earth but also the gravitational attraction of the Sun, the Moon and other celestial bodies, which perturb the satellite's orbit. All these forces have to be precisely modeled and removed from the observations. Along with the gravitational forces, non-gravitational forces such as air-drag, solar radiation pressure and Earth albedo act on the satellite vehicle. In order to obtain the orbit perturbations caused solely by the gravitational attraction of the Earth mass, these non-gravitational forces are sensed by ultra-sensitive accelerometers (cf. Section 2.3.3) and subsequently reduced from the original observations as well.

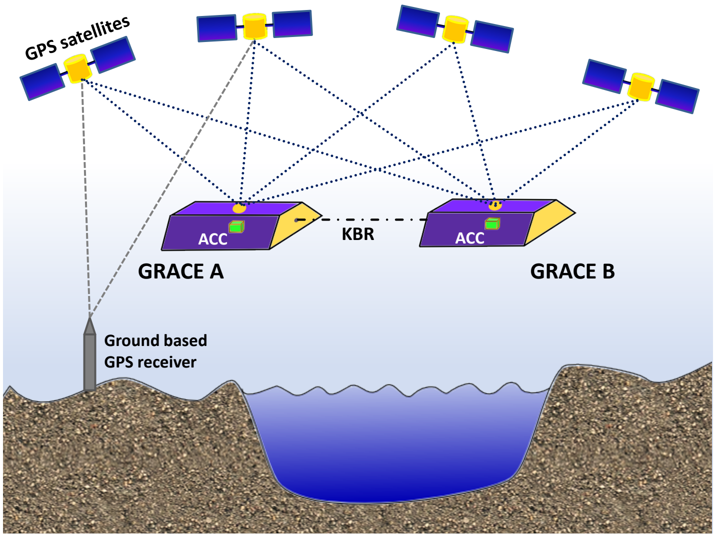

Figure 2.3: GRACE measurement principle is based on three key observation techniques: orbit tracking using the GPS satellites, inter-satellite ranging using the K-band ranging (KBR) interferometer, and precise accelerometry performed by the accelerometer (ACC) located in the center of mass of each satellite

2.3.1 Precise orbit determination

The GRACE orbit tracking is performed primarily using the GPS system. The GPS signals for navigation are received by the JPL Black Jack GPS receiver via one main antenna located on the top. For redundancy, a back-up navigation antenna is mounted on the rear panel of the satellite. The GPS receiver tracks up to 14 dual frequency signals. The description of the GPS signals, measurement principle and data processing can be found e.g. in Hofmann-Wellenhof *et al.* (2008). Additionally, the orbit is tracked from the ground stations using the Satellite

Laser Ranging (SLR) observation technique. For these purposes, a laser retro-reflector is mounted on the nadir panel of each satellite. The SLR observations are then used for validation of the GPS-based orbits. The precise orbit determination is performed on-ground, by applying so called kinematic, dynamic or reduced dynamic approach, cf. e.g. Kang *et al.* (2006); Jäggi *et al.* (2007); Liu (2008). The current accuracy of the GRACE orbits is 2-3 cm.

2.3.2 K-band inter-satellite ranging

The inter-satellite ranging is performed by the K-Band microwave Ranging (KBR) interferometer as a dual one way ranging (Thomas, 1999). This means that each satellite is both transmitting and receiving the carrier signal which is modulated on two frequencies, K-band (24 GHz) and Ka-Band (32 GHz). Because the inter-satellite ranging is carried out between the KBR antenna horns which are mounted at the front panel of each satellite, consequently, the leading satellite must be turned about 180 ° about its z-axis. Additionally, both satellites fly with 1 ° pitch offset relative to the satellite's velocity vector (Figure 2.4).

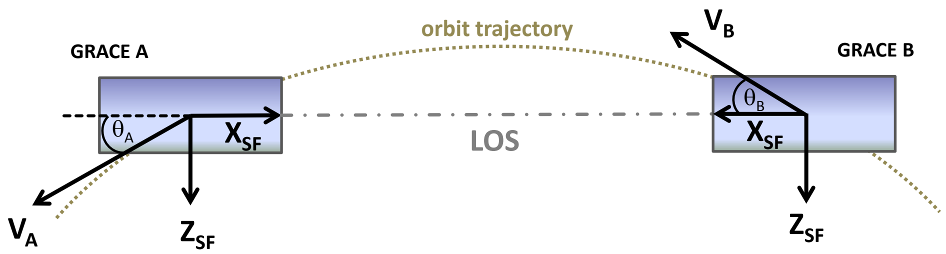

Figure 2.4: Orientation of the GRACE satellites relative to the orbit trajectory while maintaining the inter-satellite pointing, which allows the inter-satellite ranging. The leading satellite is turned about 180° about the z-axis, both satellites fly with an 1 ° pitch offset (θ_A, θ_B) relative to the satellite's velocity vectors ($\mathbf{v_A}, \mathbf{v_B}$). The definition of the $\mathbf{x}_{SF}, \mathbf{y}_{SF}, \mathbf{z}_{SF}$ axes can be found in A.2

The primary observation is the biased range which is obtained by combination of the dual one way phase measurements. The inter-satellite range rates and range accelerations needed for the gravity field determination, are obtained numerically as the first and second time derivatives of the biased range. The inter-satellite ranging is performed with μm precision. The measurement requires the KBR antenna phase centers to be aligned with the line-of-sight (LOS) within a few miliradians. More details about the inter-satellite pointing are provided in Chapter 4.

The KBR assembly consists of a single horn antenna for both transmission and reception of the dual-band microwave signals, of an Ultra-Stable Oscillator (USO) and frequency convertors, which up-convert the reference frequency generated by the USO to the carrier frequency and also down-convert the received signal from the other satellite (cf. Figure 2.5). The outcoming and incoming signals are processed in the Instrument Processing Unit (IPU) where one way phase measurements are generated and delivered to the On-Board Data Handler (OBDH) of each satellite and then sent to the ground stations. Subsequent data processing is done on-ground. The one way phase measurements are combined and corrected for systematic effects. After multiplication of the dual one way phase measurement with the wavelength, instantaneous biased range is obtained. Then final digital filtering is performed to obtain the biased range, range rate and range acceleration. For more details see e.g. Thomas (1999); Kim (2000).

The resulting dual one way range $R(t)$ between the center of mass of each satellite at a certain time epoch t is obtained as (Kim and Tapley, 2002):

$$R(t) = \rho(t) + \Delta\rho_{TOF} + I + AOC + B + \Delta\rho_{err} \tag{2.1}$$

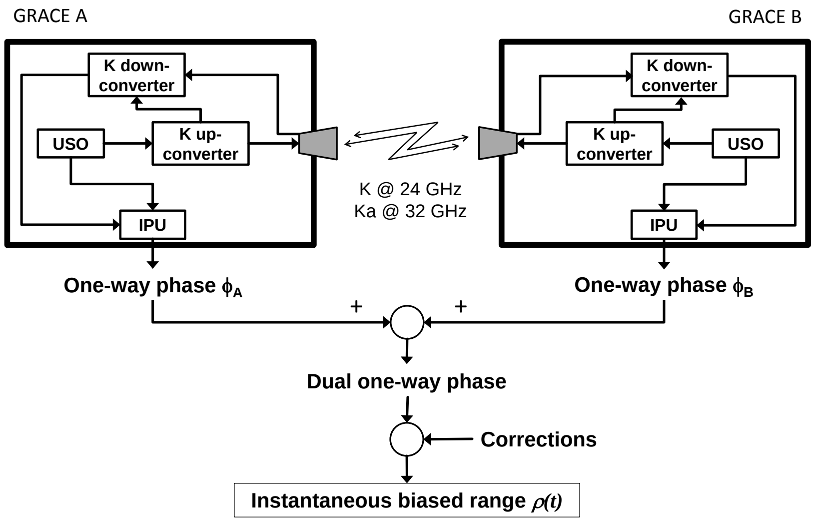

Figure 2.5: The principle of dual one way ranging system as implemented on GRACE after Thomas (1999); Kim and Tapley (2002)

where

$\rho(t)$	...	instantaneous range at epoch t
$\Delta\rho_{TOF}$	...	light time correction which accounts for the satellite motion during the signal time of flight
I	...	ionospheric delay due to signal propagation through the residual atmosphere
AOC	...	antenna offset correction which relates the measured range (which is originally related to the phase center of the KBR antenna horns) to the satellites' center of mass (cf. Section 4.5)
B	...	range bias due to unknown phase ambiguity values in the one way phases
$\Delta\rho_{err}$	...	measurement error

The measurement error $\Delta\rho_{err}$ is composed of

$$\Delta\rho_{err} = \Delta\rho_{osc} + \Delta\rho_{time} + \Delta\rho_{sys} + \Delta\rho_{mp} + \Delta\rho_{other} \tag{2.2}$$

where

$\Delta\rho_{osc}$	...	oscillator noise which depends on the oscillator characteristics and the noise cancellation efficiency of the dual one-way ranging system
$\Delta\rho_{time}$	...	time tag related error arising due to applying of time tag correction with the aid of the GPS measurements
$\Delta\rho_{sys}$	...	system noise due to the receiver instrument noise
$\Delta\rho_{mp}$	...	multipath noise due to indirect signals that arise due to imperfect inter-satellite pointing; can be modeled as 3 μm per milliradian attitude variation
$\Delta\rho_{other}$	...	other errors represent negligible error sources

The expected error level of the KBR range measurement is determined by the oscillator and system noise which are the two biggest error sources (Figure 2.6). The system noise $\Delta\rho_{sys}$ for range can be approximated by white noise of $1\mu\text{m}/\sqrt{\text{Hz}}$. The oscillator noise for range, for the case when timing is derived from GPS receiver clock, can be modeled as (Thomas, 1999)

$$\Delta\rho_{osc} = \left(\frac{1}{2}\left|(1-e^{-2\pi i f\tau})\right|^2\left[0.029+\frac{77}{f^2}+\frac{5.3}{f^3}+\frac{0.0059}{f^4}\right]\right)^{-1/2} \mu\text{m}/\sqrt{\text{Hz}} \tag{2.3}$$

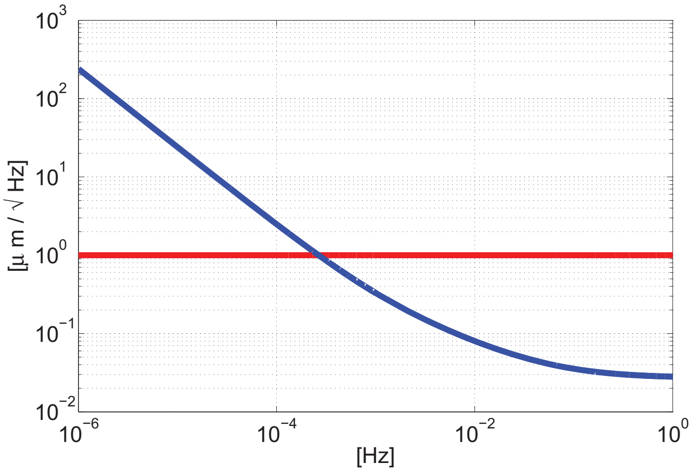

Figure 2.6: The total error of the KBR range measurement is dominated by two error sources: the oscillator noise (blue) and the system noise (red)

2.3.3 Precise accelerometry

The SuperSTAR three-axis capacitive acclerometer (ACC) manufactured by the Office National d'Études et de Recherches Aérospatiales (ONERA) (Touboul *et al.*, 1999) is mounted in the center of mass of each satellite. The sensor unit consists of a proof mass surrounded by an electrode cage. The titanium proof mass with dimensions of 40 x 40 x 10 mm^3, is kept motionless in the center of mass (CoM) of the satellite by servo-controlled electrostatic forces generated by the cage electrodes. The electrostatic force is proportional to the acceleration of the spacecraft caused by the non-gravitational forces acting on the satellite, i.e. the drag of residual atmosphere, solar radiation pressure and Earth albedo. Along with these naturally caused accelerations, the accelerometer also senses artificial accelerations such as accelerations due to thruster firings, heater switches and others, which need to be eliminated from the observations in the post-processing (Flury *et al.*, 2008; Peterseim, 2014). Furthermore, from the linear accelerations not only the non-gravitational forces acting on the satellite, but also atmospheric density can be derived (Doornbos *et al.*, 2009). In case the accelerometer is not precisely located in the satellite's CoM, the measured linear accelerations contain additional signal due to satellite's angular motion and gravity gradients. To minimize this effect, CoM calibration is performed regularly using the Mass trim system (Wang, 2003). More details on the accelerometer sensor and measurement principle can be found e.g. in Touboul *et al.* (1999); Frommknecht (2008).

The accelerometer has two high sensitive axes, the radial and along-track axes, and one less sensitive axis, the cross-track axis. The linear acceleration can be determined with the accuracy of $10^{-10}\mathrm{ms}^{-2}/\sqrt{\mathrm{Hz}}$ for the high sensitive axes, and with $10^{-9}\mathrm{ms}^{-2}/\sqrt{\mathrm{Hz}}$ for the less sensitive axis within the high frequency band (Hudson, 2003), cf. Figure 2.7. The error models are defined as follows (Stanton, 2000):

for the high sensitive axes:

$$E(f) = (1 + 0.005/f) \times 10^{-20}\mathrm{m}^2\mathrm{s}^{-4}/\mathrm{Hz} \tag{2.4}$$

for the less sensitive axis:

$$E(f) = (1 + 0.1/f) \times 10^{-18}\mathrm{m}^2\mathrm{s}^{-4}/\mathrm{Hz} \tag{2.5}$$

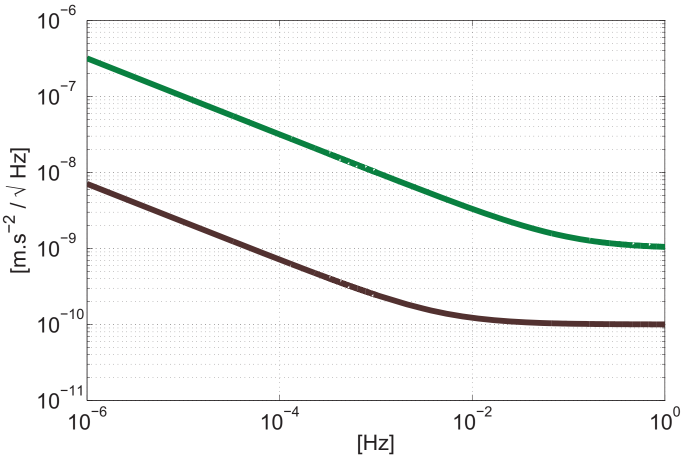

Figure 2.7: Error model of the linear accelerations sensed by the SuperSTAR accelerometer along the high sensitive axes (brown) and less sensitive axis (green)

Along with the linear accelerations, the accelerometer also senses the angular accelerations of the spacecraft. The angular accelerations are determined with an accuracy up to $5 \cdot 10^{-6}\,\mathrm{rad} \cdot \mathrm{s}^{-2}/\sqrt{\mathrm{Hz}}$ about the high sensitive axes, and $2 \cdot 10^{-7}\,\mathrm{rad} \cdot \mathrm{s}^{-2}/\sqrt{\mathrm{Hz}}$ about the less sensitive axis (Hudson, 2003). Although the accelerometer is not seen as one of the attitude determination sensors, it provides additional attitude information which can be used in the post-processing for attitude data fusion (Frommknecht, 2008; Klinger and Mayer-Gürr, 2014).

2.4 Sensors and instruments

With 487 kg of initial total mass and size of 1942 x 3123 x 720 mm, the GRACE spacecraft belong to the category of small satellites. The GRACE satellites carry onboard several scientific sensors and instruments together with other instruments and devices needed for the satellite operation (Figure 2.8). The illustrated components are (http://www.csr.utexas.edu/grace/):

K-Band Ranging Assembly

USO	Ultra-Stable Oscillator provide a frequency standard for KBR ranging and for GPS navigation
KBR horn	K-Band Ranging horn transmits and receives the K-band (24 GHz) and Ka-band (32 GHz) carrier signals between the satellites
Sampler	Sampler upconverts the reference frequency to 24 and 32 GHz and downcoverts and samples the incoming carrier phase
IPU	Instrument Processing Unit is used for sampling and digital signal processing of the K-band carrier phase signals, of the GPS signals as well as of the star camera attitude data

Science Instruments Systems

GPS Nav Antenna	GPS Navigation Antenna is the main antenna receiving the GPS navigation signals
GPS Bkup Antenna	GPS Back-up Antenna is back-up antenna for the main navigation antenna
GPS Occ Antenna	GPS Occultation Antenna is used for radio occultation
ACC SU	Accelerometer Sensor Unit consists of the proof-mass placed inside an electrode cage

ACC ICU	Accelerometer Interface Control Unit supplies power to ACC SU and performs digital signal processing for accelerometer
LRR	Laser Retro-Reflector is needed for satellite laser ranging from the ground stations

Spacecraft Housekeeping & Data Handling System

OBDH	On-Board Data Handler is the central computer of the spacecraft and is needed for the management of the science and housekeeping data and spacecraft health functions
RFEA	Radio-Frequency Electronics Assembly prepares the data obtained from OBDH for the S-Band transmission to the ground data system
S-Band Boom	S-Band Boom is the primary system for ground communication
SZA (TX/RX)	S-band Zenith Transmitter (TX) and Receiver (RX) Antenna are back-up systems for ground communication
PCDU	Power Conditioning and Distribution Unit covers all tasks for power distribution and control on-board the spacecraft
Batteries	The Nickle-Hydrogen common pressure vessel cells, with initial 16 Amp-hr capacity, provide the power storage for the spacecraft

Mass Trim System

MTM	Mass Trim Mechanism
MTE	Mass Trim Electronics
	MTM and MTE are needed for placing the accelerometer proof mass at the spacecraft's center of gravity

Attitude & Orbit Control System (AOCS)

SCA	Star Camera is the primary sensor for attitude determination
CESS	Coarse Earth/Sun Sensor is an additional attitude determination sensor with lower accuracy than SCA
Gyro	Gyroscope provides 3-axis attitude rate information
Magnetometer	Förster magnetometer senses the Earth's magnetic field and provides additional attitude rate information
ATH	10 mN Thrusters are used for attitude control
OTH	40 mN Thrusters are used for orbit control
Tank	tank is a pressure vessel which initially contained 16 kg of gaseous nitrogen
MTQ	Magnetic Torquers are the primary attitude actuators

2.5 Data levels

The science instrument and housekeeping data are regularly downlinked on the S-band frequency to the ground stations localized in Weilheim, Neustrelitz (both in Germany) and Ny-Ålesund (Spitzbergen, Norway). The data are further collected in the Raw data center and stored as **Level-0** data. The Level-0 data are further processed to Level-1A, Level-1B and Level-2 data (Watkins *et al.*, 2000; Bettadpur, 2012) by the Science data system, which includes the Jet Propulsion Laboratory (JPL), the University of Texas Center for Space Research (CSR) and the German Research Center for Geosciences (GFZ).

The **Level-1A** data are essentially the Level-0 data converted from the binary encoded measurements into engineering units. They contain editing and quality control flags and ancillary data products needed for Level-1A to Level-1B processing.

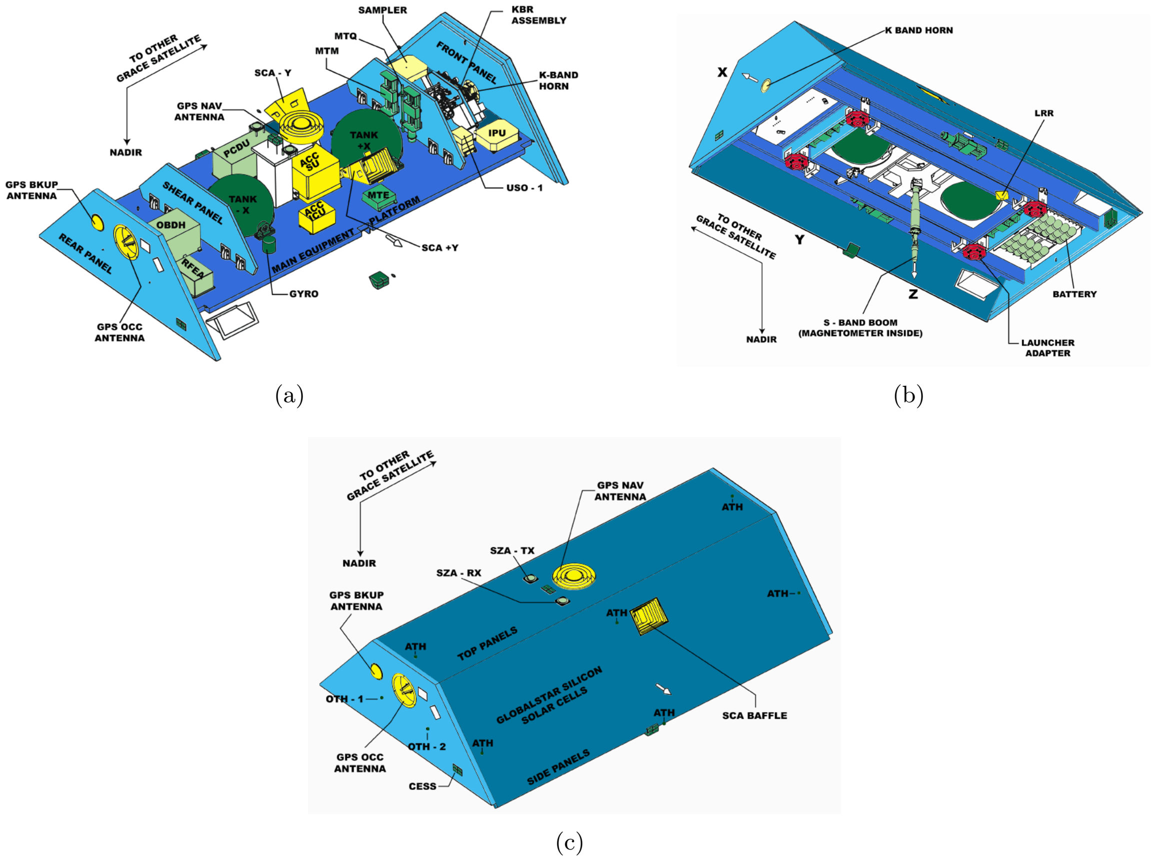

Figure 2.8: The overview of GRACE payload, for abbreviation explanation see text (©NASA)

The final product of the science and housekeeping data is the **Level-1B** data, which is derived from Level-1A data, correctly time-tagged, down-sampled and given in conventional reference frames. The Level-0 to Level-1B processing is performed by JPL. Detailed product description can be found in Case *et al.* (2010).

The **Level 2** data contain the monthly and static gravity field models which are derived from the Level-1B data. The gravitational potential is modeled using spherical harmonic functions (SH), therefore the Level-2 data product contain solely the SH coefficients and their errors. The Level-1B to Level-2 data processing is performed independently by several analysis centers e.g. JPL (Yuan *et al.*, 2012), CSR (Bettadpur and the CSR Level-2 Team, 2012), GFZ (Dahle *et al.*, 2014), Le Centre national d'études spatiales/Le Groupe de Recherche de Géodésie Spatiale (CNES/GRGS) (Bruinsma *et al.*, 2010), AIUB (Astronomical Institute of the University of Bern) (Beutler *et al.*, 2010), and others. Slight differences exist between these models caused by the applied mathematical approaches which are different for every center and by different background models used in the data processing.

The analysis results presented in this thesis are based on the GRACE data products listed in Table 2.1. The analysis is based on data primarily from year 2008. The reason for this choice is the fact that in 2008 the mission was operating during solar cycle minimum, thus the disturbing influence of solar activity on the satellite's performance was minimal.

2.6 Reference frames

The GRACE sensor data are provided in different reference frames, which will be introduced in the context of the following chapters. The overview of the reference frames and their definition can be found in Appendix A.

Table 2.1: List of GRACE data products used for the analysis presented in this thesis

data level	product	description
Level-0	THAD	AOCS data
	THBB	Pt1000 thermistor data
	THBC	YSI thermistor data
	THCE	CESS temperature data
Level-1A	SCA1A	star camera data
Level-1B	ACC1B	accelerometer science data
	CLK1B	satellite clock solution
	GNV1B	GPS orbit solution
	KBR1B	KBR ranging data
	MAG1B	magnetometer data and magnettorquer activation data
	MAS1B	spacecraft mass data
	QSA1B	SCA/ACC calibration parameters
	QKS1B	SCA/KBR calibration parameters
	SCA1B	star camera data
	THR1B	thruster activation data
	TNK1B	gas tank sensor data
	VGN1B	vector offset for the GPS main navigation antenna
	VKB1B	KBR antenna phase center offset
Level-2	GSM-2	geopotential SH coefficients

2.7 Gravity field models

From the GRACE observations, both the static and the monthly gravity field models are determined. The static field represents the mean value of the gravitational potential over a long time span and is usually computed from several years of observation data. In contrast, the monthly models are computed from the observations collected within 30 days. Based on the monthly models, temporal variations of the gravitational potential are computed, from which the changes in the mass distribution and mass transport in the Earth system are derived. Due to the limited amount of observation data, the monthly models are computed up to SH degree and order 60 or 90, whereas the models of the static field are estimated up to SH degree and order 160-200. For illustration, Figure 2.10 shows the static gravity field model GGM05s (Tapley *et al.*, 2013) in terms of geoid, whereas Figure 2.11 shows the geoid variations with respect to the mean field for the whole year 2008. The geoid variations were derived from CSR Release 05 monthly models, which represent the current latest solution.

Since the beginning of the mission, the accuracy of the gravity field models has been significantly improved as demonstrated in Figure 2.9. The figure shows the error degree amplitudes of the gravity field models generated by CSR for October 2006 according to the processing standards set for Release 01 (RL01), RL04 and RL05. In addition, the accuracy level of these solutions is compared to GRACE baseline. The GRACE baseline represents the target accuracy of the monthly gravity field models which was predicted from a pre-launch simulation model, where the measurement accuracy of the science instruments and of orbit determination were taken into account (Kim and Tapley, 2002). Although the overall accuracy increased substantially in the last years, the GRACE baseline accuracy has not been reached yet. Today, almost an order of magnitude remains between the current and the predicted level of accuracy of the monthly models. The most significant factors contributing to the error budget are the unmodeled sensor and instrument errors and the uncertainties in the calibration parameters, cf. e.g. Flury *et al.* (2008); Horwath *et al.* (2010); Bandikova and Flury (2014); Inacio *et al.* (2015), the aliasing effects coming from improper time and spatial sampling and the uncertainties in the atmospheric, oceanic and tidal models, cf. e.g. Han *et al.* (2004); Ray and Luthcke (2006); Zenner (2013). Yet, efforts are still ongoing to improve the accuracy of the input observation data and the background models as well as the mathematical approaches for the gravity field determination.

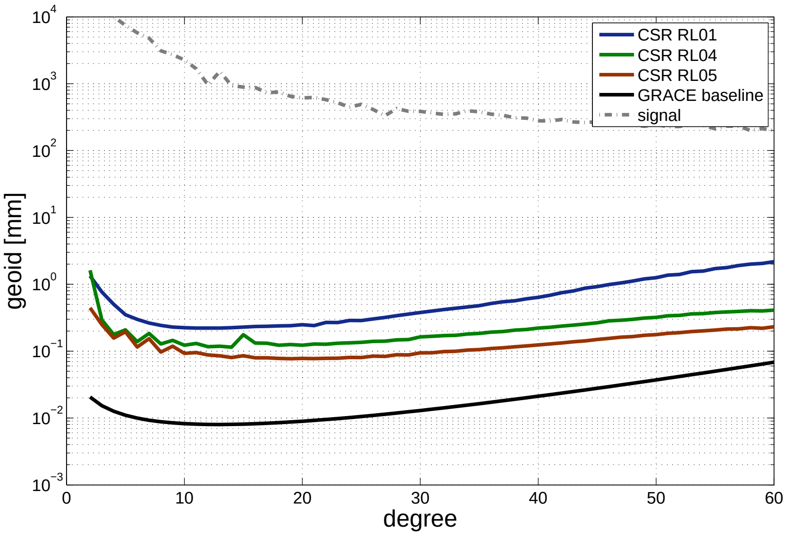

Figure 2.9: Comparison of the GRACE baseline accuracy with the accuracy of the monthly gravity field models for October 2006 generated by CSR according to the processing standards for RL01, RL04 and RL05, expressed in terms of error degree amplitudes as a function of SH degree. Although the GRACE baseline has not been reached yet, a significant improvement of the accuracy of the GRACE monthly gravity field models has been achieved over the years

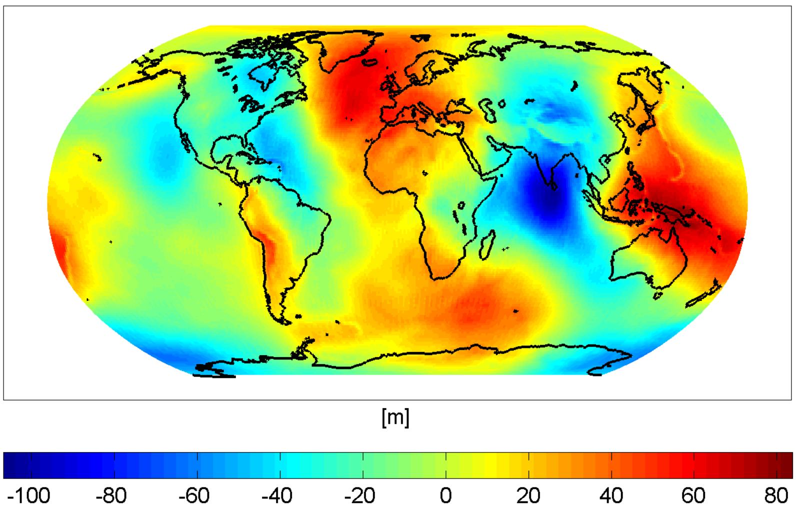

Figure 2.10: The Earth's static gravity field in terms of geoid up to SH degree and order 180, derived from the GGM05s model

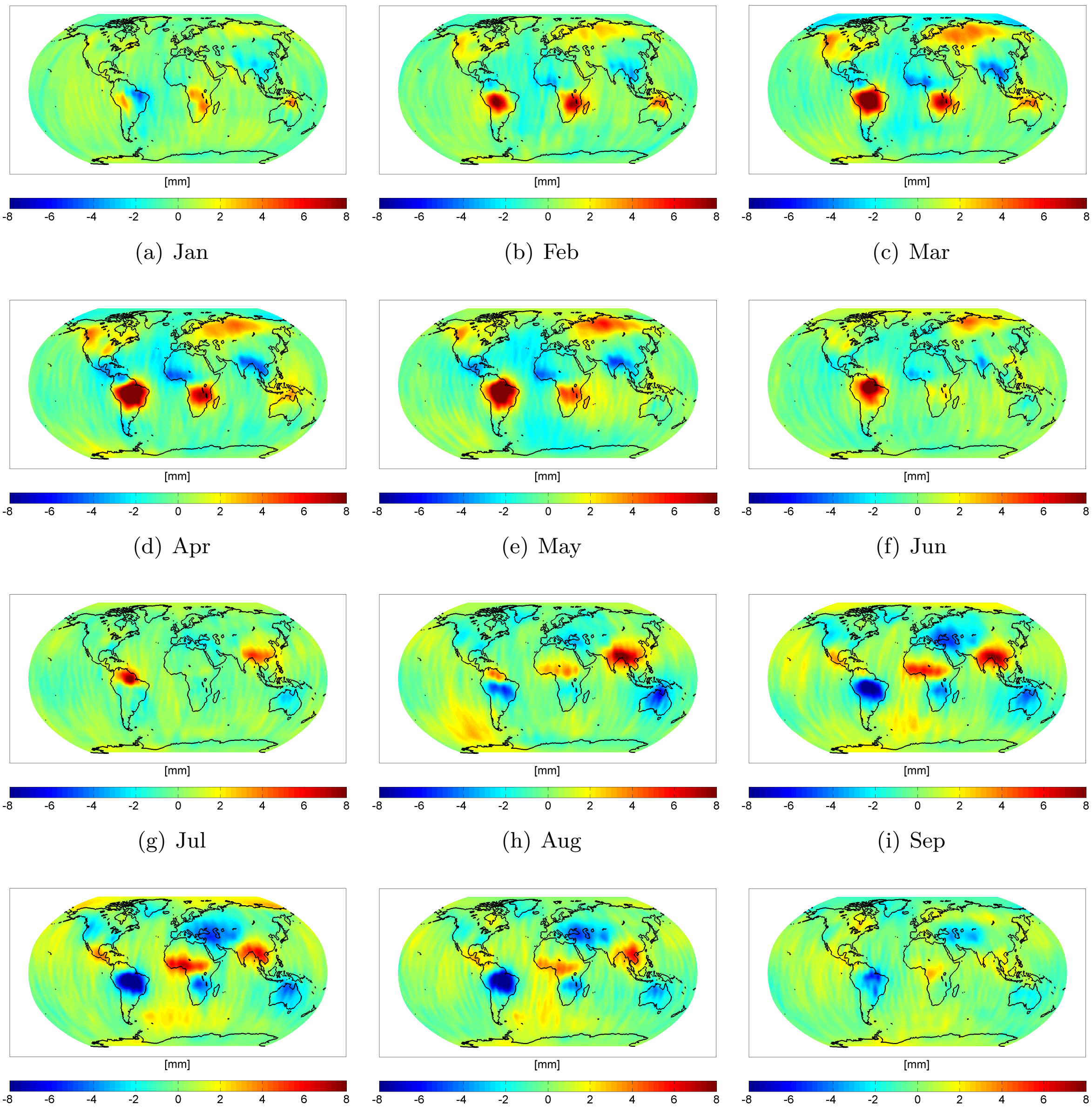

(a) Jan (b) Feb (c) Mar

(d) Apr (e) May (f) Jun

(g) Jul (h) Aug (i) Sep

(j) Oct (k) Nov (l) Dec

Figure 2.11: The variations of the gravitational potential with respect to the static field (GGM05s) in terms of geoid, derived for the whole year 2008 from the GRACE monthly gravity field solutions released as CSR RL05, modeled up to SH degree and order 60, filtered with Gaussian filter of 300 km radius

Shoot for the moon, even if you miss
you will land among the stars.

- Les Brown -

3 Characteristics of the GRACE attitude determination and control

3.1 Introduction to attitude determination and control

The attitude determination and control is one of the key tasks for almost every satellite mission because it secures the fundamental requirements for mission operation. Such requirements may be for example orientation of the solar arrays towards the Sun, orientation of the RX/TX antennas towards the Earth or, as in case of GRACE, maintenance of the inter-satellite pointing. In case the attitude determination and control system fails, in the worst case the mission may be lost. The attitude is defined as the orientation of the spacecraft. Attitude determination is a process of estimating the attitude based on sensor measurement. Attitude control is then a process of maintaining or changing the attitude using either natural forces or actuators. The theory to the satellite's attitude determination and control system is well described e.g. by Wertz (2001).

The attitude determination and control is to be distinguished from the orbit determination and control. The position of a spacecraft informs us about where the satellite's center of mass is located in space, whereas the attitude describes the motion about this center of mass. The orbit changes are due to forces acting on the spacecraft, while the attitude changes are caused by torques. The orbit maneuvers are mostly performed at intervals of days or months, however, the attitude maneuvers are performed usually with 1 Hz to 10 Hz sampling. The orbit determination is carried out using GPS technology or tracking from ground stations, e.g. SLR, whereas for the attitude determination Sun/Earth/Star sensors and others are used. The orbit control is usually commanded from ground compared to the attitude control which is performed autonomously onboard the spacecraft and in real time.

For GRACE, the need of precise attitude determination and control is absolutely crucial for fulfilling to mission goal. On the one hand, it enables the inter-satellite pointing, which is the fundamental requirement for inter-satellite ranging. It also allows performance of in-orbit calibration maneuvers, battery saving maneuvers, satellite swap maneuvers, etc., which are needed for successful mission operation. On the other hand, precise information about spacecraft's attitude is essential for the processing of the KBR ranging, GPS and accelerometer measurements that are needed for gravity field recovery. Hence any inaccuracies or untreated systematic errors in the attitude data will directly propagate to the gravity field models. For GRACE, the attitude as well as the orbit determination and control system are implemented in the AOCS satellite subsystem.

Elements of the attitude determination and control system

The attitude determination and control systems consist of sensors, actuators, electronics and software. Based on the mission requirements, these systems differ in their accuracy, complexity and costs. Usually there is more than one attitude sensor as well as more than one attitude actuator implemented onboard. This is not only for back-up purposes, but also because no one sensor can fulfill all requirements on the satellite operation. Each sensor has its characteristic advantages and disadvantages, which are exploited in different mission operational modes.

The spacecraft's attitude is continuously perturbed by both external and internal disturbing torques, such as aerodynamic torques, magnetic torques, Earth's gravitational torques, solar radiation torques or due to propellant motion inside the tanks or any other intentional or unintentional mass motion within the spacecraft. It is the task of the attitude control system to maintain or to change the current attitude by applying control torques on the spacecraft. The attitude determination and control operates in a close loop as sketched in Figure 3.1. Based on the attitude sensor measurement, the instantaneous satellite's attitude can be estimated. The absolute orientation of the spacecraft is determined relative to other celestial objects like the Earth, the Sun, stars or the Earth's magnetic field. Additionally, relative orientation of the spacecraft can be estimated by measuring the attitude rate of change by e.g. a gyroscope or magnetometer. In the next step, the estimated instantaneous attitude is compared to the desired attitude which is computed based on onboard measurements, models and predictions. The differences between the estimated and the desired attitude are analyzed and according to the attitude control algorithms, commands are sent to the actuators. The actuators apply the control torque in order to reach the desired attitude.

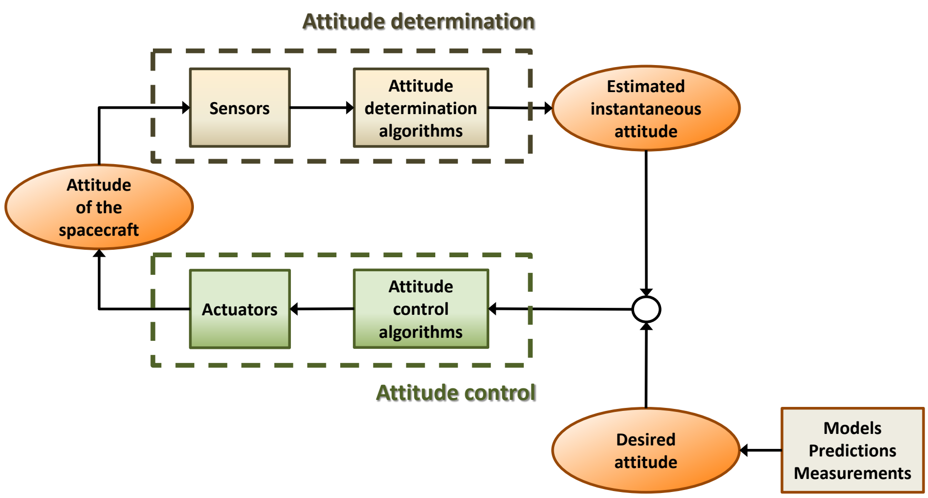

Figure 3.1: The attitude determination and control loop

GRACE operational modes

Onboard GRACE, both low accuracy sensors, i.e. Coarse Earth/Sun Sensor (CESS) and magnetometer, and high accuracy sensors, i.e. star cameras and Inertial Measurement Unit (IMU), are mounted. Each of them is used as the main sensor in different operational modes.

In the **coarse pointing mode** the main attitude sensors are CESS + IMU or CESS + magnetometer. This mode guarantees thermal and power survival of the spacecraft. The satellite is in this mode during rate damping, attitude acquisition, yaw steering maneuver or after onboard computer reboot. In contrast, in the **fine pointing** mode, i.e. **attitude hold mode** or **science mode**, the main attitude sensors are the star cameras. In the back-up attitude hold mode and back-up science mode the main sensors are star cameras together with the IMU. In the science mode and back-up science operational mode, all science instruments perform as required to meet the scientific objectives of the mission, i.e. the satellites collect all the high precise observation data which are necessary for the gravity field recovery. These modes require the precise inter-satellite pointing with a deadband of a few mrad with respect to the line-of-sight (for more details see Chapter 4). Up to now, both satellites were operating in the science mode or back-up science mode for almost 95% of the mission lifetime. In the attitude hold mode, the pointing deadbands are defined relative to orbit. The satellite is in attitude hold mode during e.g. orbit maintenance maneuvers, center of mass calibration or software upload. Science data is still collected but with lower accuracy. More information about the GRACE operational modes can be found in Herman *et al.* (2004).

As GRACE has high requirements on the satellite's orientation, the attitude control is performed by means of attitude actuators generating a control torque. The primary actuator are the magnetic torquers, which are supported by the cold gas thrusters if needed.

In the following, the characteristics of the GRACE attitude sensors and actuators are presented with the focus on the star cameras. The star cameras are the main attitude determination sensors in the science mode operation, hence their performance directly affects the satellite operation as well as the scientific data processing.

3.2 Attitude determination sensors

3.2.1 Coarse Earth/Sun sensor

The CESS provides a coarse state vector of the Sun and the Earth. CESS is excellent for initial acquisition and for recovering from the lost-in-space mode and hence it is set as the main attitude sensor in the coarse pointing mode. The Earth vector is estimated with an accuracy of $5° - 10°$ and the Sun vector with accuracy of $3° - 6°$ (Herman *et al.*, 2004). The CESS measurement data are provided with 0.1 Hz sampling frequency.

The CESS consists of 6 sensor heads which are orthogonally mounted at each of the six satellite panels (Figure 3.2). Each head carries 6 platinum thermistors, three of them are silvered, the other three are black coated, hence redundancy is ensured. Due to the different absorptance coefficient of these two types of thermistors, the measured temperature of the incident radiation (solar radiation and Earth albedo) is different.

The spacecraft orientation towards the Earth and the Sun is then estimated based on the temperature differences between the silvered and black coated thermistors as well as between the sensor heads from all six satellite panels (Doll and Wolters, 1999). The total measurement range of the CESS sensor is between $-273°\mathrm{C}$ and $+140°\mathrm{C}$ with a resolution below $0.2°\mathrm{C}$. The CESS temperature data can be used not only for attitude determination but also for further data analysis when correlations with the outside spacecraft temperature are searched.

The measured temperature reflects the amount and type of incident radiation and thus provides information about the orientation of the individual satellite's panels towards the Sun and the Earth, cf. Figure 3.3. In this figure, the dark red color characteristic for high temperatures indicates that the satellite's panel was directly illuminated by the sunshine. In contrast, the dark blue color typical for very low temperatures means that the satellite's panel was pointing to the outer space. Obviously, the port and the starboard panel were illuminated by the sunshine along the whole orbit for a certain periods of time (between Day Of the Year (DOY) 43-74 and 212-230), which means the satellite was operating in a full sun orbit. As the nadir panel is permanently oriented towards the Earth, the majority of the incident radiation comes from the Earth albedo. The intensity of the Earth albedo depends on illumination of the particular Earth's hemisphere by the Sun. This is very obvious in Figure 3.3(f), where the cyan color indicates that the satellite is flying in the Earth shadow, i.e. above the hemisphere which is currently not illuminated by the sunshine, compared to the orange color which is typical for the hemisphere which is currently illuminated. The red-color ring-shaped pattern where the sensed temperature increased just before entering the Earth shadow is caused by the very short direct illumination of the nadir panel by the sunshine.

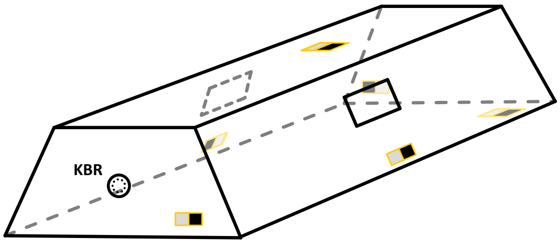

(a)

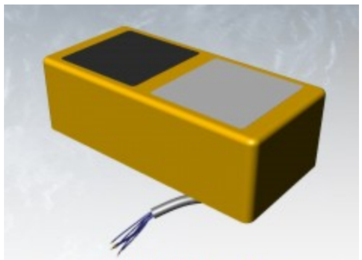

(b)

Figure 3.2: Coarse Earth/Sun sensor (CESS): mounting of the six sensor heads on GRACE satellite (a) and detail of the sensor head as pictured by SpaceTech GmbH Immenstaad (b)

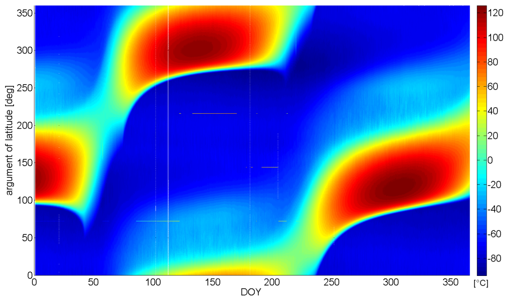

(a) front panel

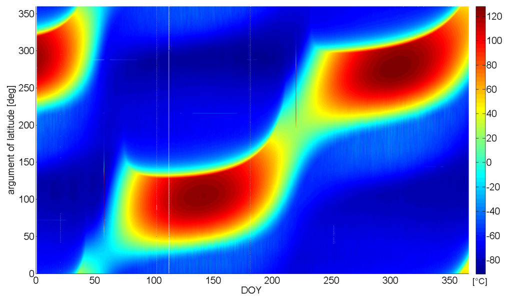

(b) rear panel

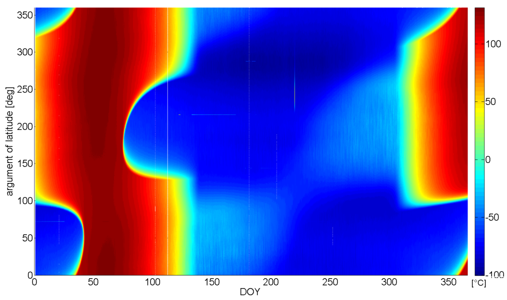

(c) port panel

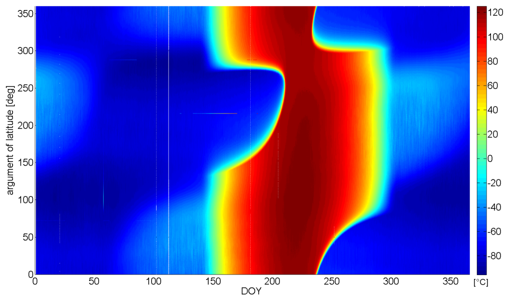

(d) starboard panel

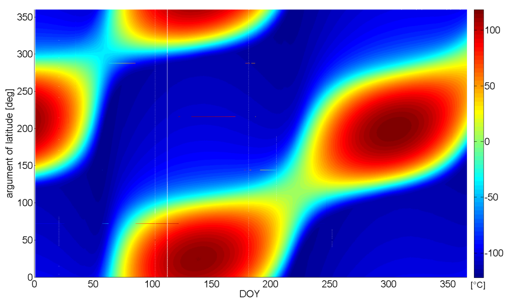

(e) zenith panel

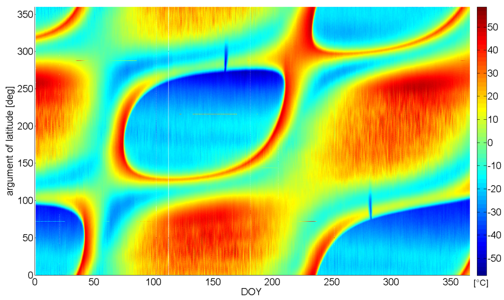

(f) nadir panel

Figure 3.3: Temperature due to the incident radiation measured by the CESS black coated thermistors in 2008, plotted along the orbit. Based on GRACE-A THCE data. The denomination of the satellite's panels can be found in Appendix A.1

3.2.2 Magnetometer

The very oldest sensor for attitude measurement based on the orientation with respect to the Earth's magnetic field is the compass. In space, the attitude determination can be done using a magnetometer. Onboard GRACE, a fluxgate magnetometer is mounted at the top of the boom at the nadir side of each satellite, which measures both the direction and the magnitude of the Earth's magnetic field. This 3-axes magnetometer is characterized by a measurement range of $\pm 50\,\mu$T and a resolution of 25 nT (Wang, 2003).

Figure 3.4 shows the individual components of the magnetic flux density vector, $\mathbf{B}$, along the ascending orbit. As the vector values are provided in a satellite body-fixed frame, the Satellite Frame (cf. Appendix A.2), their values differ along the ascending and descending orbit, hence $B_x^{desc} \approx -B_x^{asc}$, $B_y^{desc} \approx -B_y^{asc}$ and $B_z^{desc} \approx B_z^{asc}$. Along with the Earth's magnetic field, the magnetometer also senses artificial magnetic fields generated within the spacecraft. These artificial fields are especially due to magnetic torquer activity, cf. Section 3.4.1.

The main purpose of the magnetometer is for the attitude control. The control torque generated by the magnetic torquers depends on the instantaneous magnetic field vector and a dipole moment, which is a result of electric current flow through the torquer's coil (see also Section 3.4.1). Hence the magnetometer provides necessary input based on which the amount of electric current flow through the coil can be appropriately regulated.

Additionally, the magnetometer can be used as attitude determination sensor. While the information about the satellite's position is provided by the GPS, the measured magnetic flux density vector is compared with the onboard Earth's magnetic field model and the spacecraft's attitude is derived. The fundamental measurement principle can be expressed as

$$\mathbf{B} = \mathbf{A} \cdot \mathbf{B}_{model} \tag{3.1}$$

where $\mathbf{B} = [B_x, B_y, B_z]^T$ is the measured magnetic field vector by the magnetometer, $\mathbf{B}_{model} = [B_x^{model}, B_y^{model}, B_z^{model}]^T$ is the magnetic field model vector in Earth-fixed coordinates and $\mathbf{A}$ is the attitude matrix which represents the orientation of the satellite body-fixed frame with respect to the Earth-fixed frame. Equation 3.1 is solved using a Kalman filter (Psiaki *et al.*, 1990). In addition, the magnetometer attitude determination necessarily requires determination of the magnetometer bias and scaling factors (Crassidis *et al.*, 2005).

From the magnetometer measurement, both the attitude and attitude rate can be estimated with an accuracy of a few deg. The magnetometer-based attitude accuracy is limited by the artificial magnetic fields generated by the spacecraft itself and by the accuracy of the onboard Earth's magnetic field model and by the accuracy of the magnetometer bias and scaling factors. Therefore, the magnetometer attitude data are used only in combination with CESS in the coarse pointing mode in case the IMU cannot be used.

3.2.3 Inertial measurement unit

The IMU provides spacecraft's attitude rate about all three axes with high accuracy. It consists of three interferometric fiber optic gyroscopes which are mounted with their sensitive axes perpendicularly to each other. The IMU is pictured in Figure 3.5. The measurement principle is based on Sagnac effect, which occurs when a light beam propagates around a closed path in a frame that rotates with respect to the inertial frame (Jekeli, 2001). The fundamental equation for the phase shift due to the Sagnac effect is given by (Blockley and Shyy, 2010)

$$\phi = \frac{2\pi L D}{\lambda c}\omega \tag{3.2}$$

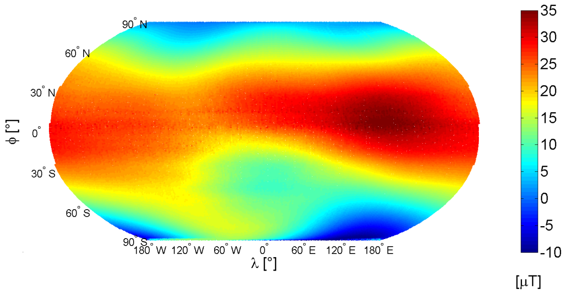

(a) B_x

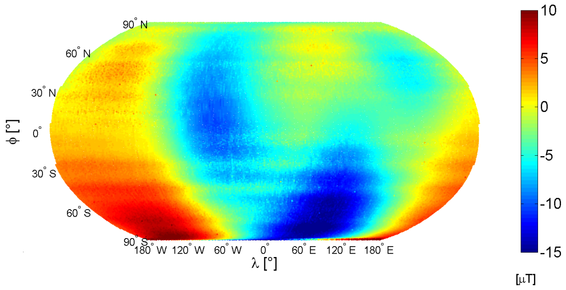

(b) B_y

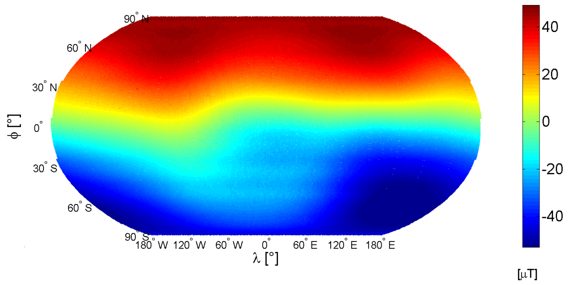

(c) B_z

Figure 3.4: The vector components of the the Earth's magnetic flux density **B** in SRF frame (cf. Appendix A.5) as sensed by the magnetometer onboard GRACE-A; shown for the ascending orbit only, Jan 1st-18th, 2008

where

L	...	length of the optical fiber
D	...	average diameter of the coil of optical fiber
c	...	speed of light
λ	...	wavelength of the laser light
ω	...	angular rate about the axis perpendicular to the coil

The angular rates determined by the IMU are characterized by their high accuracy in high frequency band. However, their accuracy in low frequency band is limited by the stability of bias and scaling factors. The measurement resolution is limited to $0.01\,\mathrm{mrad}\cdot\,\mathrm{s}^{-1}$, cf. Figure 3.6. As the IMU provides information about the relative spacecraft orientation, it is used in combination with sensors which provide the absolute inertial attitude of the spacecraft. It is used in the back-up operational modes for improvement the attitude information provided by CESS or the star cameras. Also, in case of short outages, the last measured valid attitude data are extrapolated using the IMU angular rates (Herman *et al.*, 2004). Unfortunately, the IMU onboard GRACE-A failed right after launch in 2002 and there is no redundant IMU available onboard. The IMU on GRACE-B is still functional, however, it is operating only when the satellite is switched to one of the back-up operational modes, which happens rather rarely compared to the operation in science mode.

Figure 3.5: Inertial measurement unit as pictured by Northrop Grumman (2013)

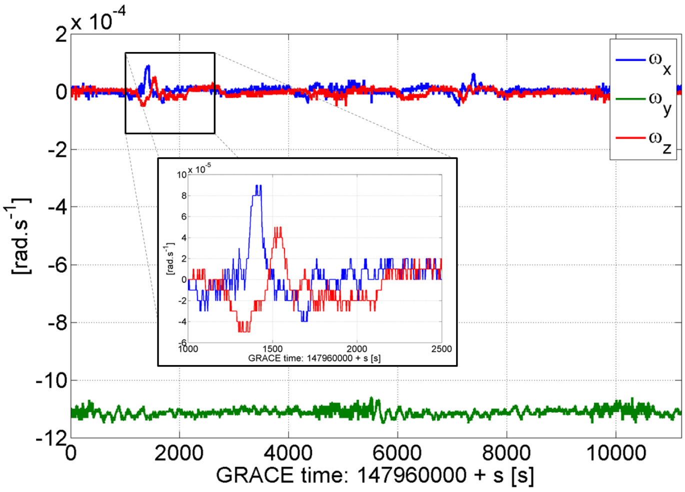

Figure 3.6: Time series of the angular rates measured by the IMU on GRACE-B on Sep 9th, 2004 and the demonstration of the measurement resolution which is 0.01 mrad·s^{-1}

3.2.4 Star camera

The key and most important attitude determination sensors onboard GRACE are the star cameras. Compared to all other available sensors, the star cameras provide the most accurate information about spacecraft's attitude. For that reason, the star cameras are set as the main sensor in the fine pointing mode in which the precise inter-satellite pointing is maintained and observations needed for the gravity field recovery are collected. In the scientific literature, several synonyms are used for the star camera such as star tracker or stellar compass, which are all equivalent.

Already the sensor name reveals that the reference objects for the attitude determination are the stars. The very basic concept of the star camera measurement is based on taking a picture of the stars in the field-of-view (FoV) on a charged coupled device (CCD) array, identifying these stars using an onboard star catalog and determining the attitude of the sensor frame with respect to the inertial frame. Onboard GRACE, two star camera heads are mounted pointing towards the port and the starboard panel.

Profound understanding of the star camera characteristics and performance is absolutely essential for the further analysis presented in this thesis. Therefore the following section is dedicated solely to the GRACE star cameras.

3.3 Characteristics of the GRACE star cameras

3.3.1 The star camera sensor

The star cameras (SCA) for GRACE were designed and built by the Technical University of Denmark (DTU) (Jørgensen and Pickles, 1998). The star camera assembly consists of two camera head units, which are rigidly mounted to the accelerometer CFRP (Carbon Fiber Reinforced Plastic) frame, two baffles and a data processing unit (Figure 3.7). The camera head unit #1 points with its boresight (i.e. optical axis) towards the starboard panel, whereas the camera head unit #2 points with its boresight towards the port panel. The boresight of both camera head units has a zenith offset of 45°, cf. Figure 3.8. Onboard GRACE, there is no separate star camera data processing unit. Instead, the associated software module, which was also developed by DTU, is executed at the Instrument Processing Unit (IPU), where also the K-band ranging data and GPS data are processed.

Figure 3.7: The star camera assembly consisting of the camera head units, baffles and the data processing unit as pictured by DTU. Note that onboard GRACE two (not three as shown here) star camera head units are mounted

A block diagram of the star tracker is sketched in Figure 3.9, which shows the main components of the camera head unit and the data processing unit (Jørgensen and Liebe, 1996). The camera head unit consists of optics and electronics necessary for generating highly accurate star images. This is done by integrating the light focused onto a photo-sensitive CCD array. After acquiring the image of stars within the FoV, the pattern on CCD is serially read out and fed into the data processing unit.

The task of the data processing unit (i.e. the IPU) is to compare all luminous objects on the digitalized image with a stored star pattern and to determine the inertial attitude. It consists of a powerful microprocessor, a power conditioning unit, a frame grabber and a communication interface. It also contains software, including the star catalog, advanced imaging functions and a search engine, which allow autonomous star pattern recognition and absolute attitude determination.

The baffle is mounted to the camera head unit in order to minimize the influence of the impacting light from other bright objects on the star camera performance. The baffle protects from the sunshine, the moonlight and also from the earthshine.

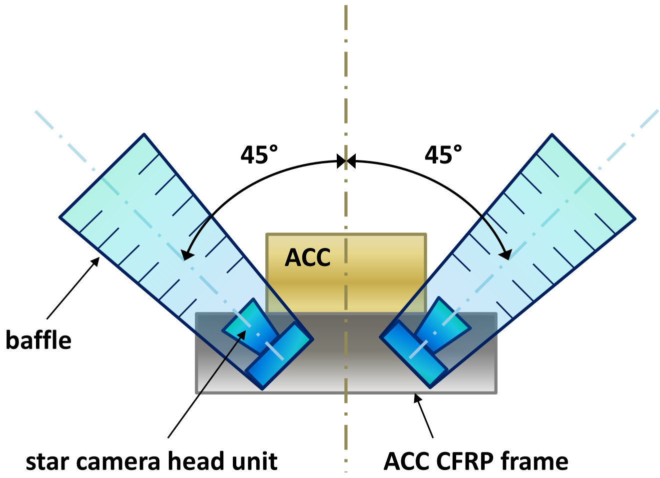

Figure 3.8: Mounting of the GRACE star cameras. The two camera head units are rigidly mounted to the accelerometer CFRP frame, their optical axes point towards the starboard and port panel with a zenith offset of 45°

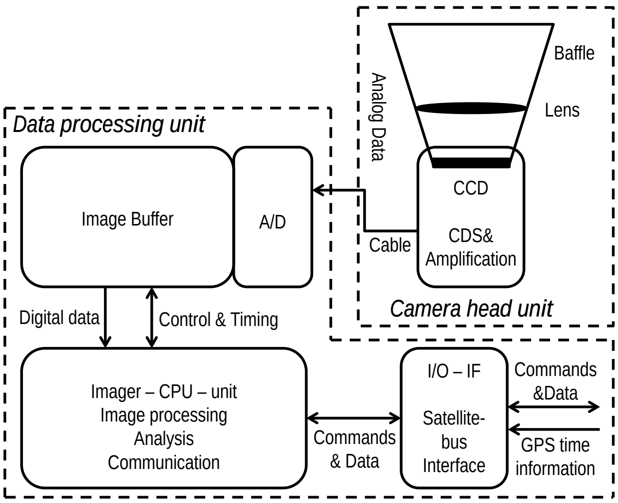

Figure 3.9: Block diagram of a star tracker (Jørgensen and Liebe, 1996)

3.3.2 The star camera measurement principle

The star camera measurement principle is sketched in Figure 3.10 and can be simplified as follows (Jørgensen and Pickles, 1998):

- The star picture is acquired by integrating the light of luminous objects within the FoV onto a CCD array.
- The pixel values are then digitized by the frame grabber, sifted for bright stars with apparent visual magnitude greater than a specified value, and corrected for lens distortion. Because the stars can be considered as point sources of light, the star images are defocused and spread over a number of pixels in order to increase the measurement accuracy which would be otherwise limited by the pixel size.
- For each star image, a centroid and its coordinates in the sensor frame with subpixel accuracy (approx. 1/10 of pixel size) is determined.

- Depending on the attitude determination mode, the stars are identified and the star pattern recognized using onboard database, which in case of GRACE is the Hipparcos star catalog. There are two attitude determination modes: the initial acquisition and the tracking mode.

- In the initial acquisition, the spacecraft's attitude is determined without any a priori attitude information. The computation algorithm is based on the computation of the so called triplets (a_{12}, a_{13}, u), i.e. angular distances between pairs of stars and plane angle between two arms connecting two pairs of stars. The star catalog contains not only the angular positions of the stars, but also multiple triples for possible three star combinations. For each star in the acquired picture, triplets are computed and matched with the database in order to identify the star. The database for the initial acquisition contains approx. 2000 brightest stars and in average 100 triplets for each star. If two or more stars are identified, attitude matrix can be determined. To get recovered from "lost in space" takes about less than 1 s.

- Once the inertial attitude is determined, the attitude determination is switched to the tracking mode. The gained attitude information is used together with the star catalog and an onboard orbital model to predict the star pattern in the FoV. The database for the tracking mode contains approx. 13000 stars. The measured star centroids are then matched with the predicted star positions in a least squares sense.

- Afterwards, the attitude is corrected for astronomical aberration and finally, the attitude transformation matrix describing the attitude of the SCA boresight and the rotation about this axis is determined.

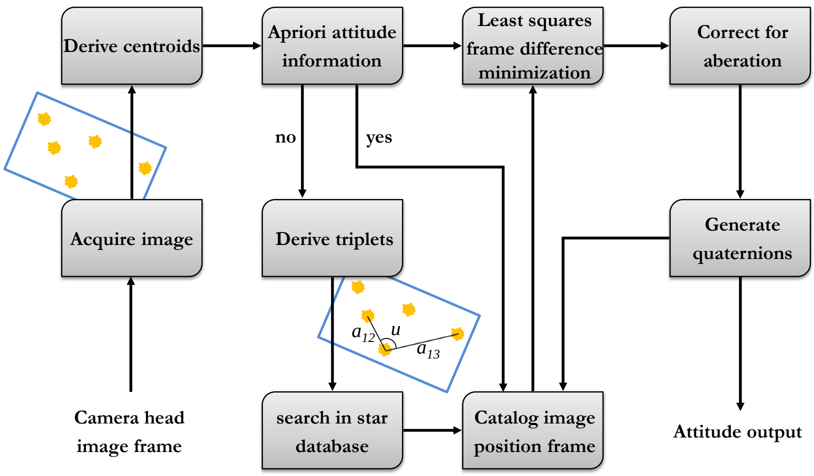

Figure 3.10: Block diagram of star camera attitude determination - from image acquisition to computation of attitude quaternions (source: DTU, 2010)

The star cameras provide information about the attitude of their own sensor frame, so called Star Camera Frame (SCF) (see Appendix A.3), with respect to the inertial frame, the International Celestial Reference Frame (ICRF) (see Appendix A.9) by comparing the measured star coordinates with known angular positions of these stars. The output is a transformation matrix rotating the star camera sensor reference frame into an inertial frame.

The attitude information is delivered in terms of quaternions. The quaternions are commonly used for spacecraft navigation because of their advantages: low requirement on memory capacity (1 quaternion consists of 4 elements, instead of 9 as it is in case of direction cosine matrix) and no ambiguity except for the sign. For the definition and operations with quaternions see Appendix C.

3.3.3 Star camera operation

One of the consequences of the GRACE orbital configuration with respect to the Earth and the Sun and the chosen mounting of the two GRACE star cameras is that one of the star cameras is continuously blinded by the sunshine or the moonlight along a part of the orbit. Consequently, no valid attitude data are provided during the blinding and data from only one star camera head is available. Figure 3.11 shows the availability of valid star camera data from GRACE-A and GRACE-B in 2008.

The partial blinding of the camera by the sunshine persists about 161 d. This is caused by the Earth's motion about the Sun and the very slow change of the ascending node of the GRACE orbit. When the angle between the orbital plane and the direction to the Sun, β' angle, passes through zero, the other side of the satellite becomes illuminated and the other camera is partially blinded for the next 161 d. More details on the β' angle can be found in Appendix D.2. The moonlight intrusions into the SCA FoV are short and last for 1.5 d. They occur regularly every 27 d.

The star camera data outages are not only related to the camera blinding. Certain outages occur systematically along a specific part of the orbit, which results in the striped pattern in Figure 3.11. The reason for these outages has not been found yet. One of the hypotheses is that some of these outages might be related to the sensitivity of the camera to the stray light which can be increased by the Earth albedo (Witkowski and Massmann, 2012).

One of the random phenomena resulting in star camera outages is the so called hole in the sky. This phenomenon is caused by low photometric gain of the star camera. This means that the number of bright stars identified in the image is lower than the threshold criterion, hence the attitude cannot be determined. This phenomenon was mitigated in 2011 by uploading new IPU SCA software in which the threshold criterion was reduced and new catalog, diagnostics and controls were incorporated (Witkowski and Massmann, 2011).

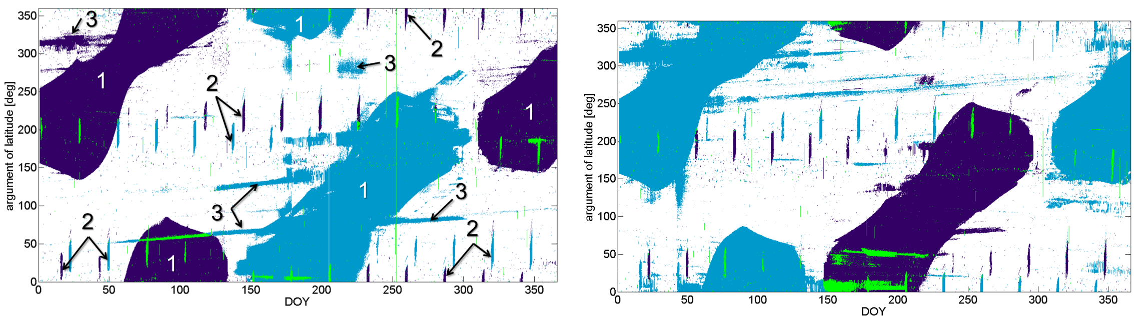

(a) (b)

Figure 3.11: Availability of valid star camera data in 2008 for GRACE A (a) and GRACE B (b). Legend: *white* - data available from both star camera heads, *dark blue* - data available solely from camera head #1, *light blue* - data available solely from camera head #2, *green* - no data available, *1* - Sun in FoV, *2* - Moon in FoV, *3* - outages not related to Sun or Moon blinding

Despite the fact that the two star cameras operate simultaneously, for the in-flight attitude determination, indeed, only one camera is necessary and the second camera is there for redundancy only. The GRACE AOCS uses the data from single camera only, so called primary camera. The notation of the primary and secondary camera was chosen according to the orientation towards the Sun. The primary camera is the one pointing away from the Sun which means it delivers valid information about the spacecraft's attitude along the whole orbit. The primary camera is regularly switched from SCA head #1 to head #2 and vice versa. The switches are routinely commanded by the German Space Operations Center in intervals of about 161 d when the β' angle passes through zero. Furthermore, temporary primary camera switches can occur when the moonlight intrudes into the primary camera FoV and when the other camera is not blinded by the Sun at the same time. In 2008, the primary camera on GRACE-A was head#1 between DOY 1-135 and DOY 305-366, and between DOY 135-305 it was head#2. On GRACE-B it was set vice versa. The primary camera operates on a sampling frequency of 1 Hz whereas the secondary camera operates partly on 1 Hz, 0.5 Hz or 0.2 Hz sampling frequency.

Using the data from only one star camera for the in-orbit operation has certainly some advantages but also several disadvantages. The advantage of the primary star camera data is their availability along the whole orbit except for the short outages caused by simultaneous blinding of both SCA heads. Also, the processing of single camera data is simpler than processing of data from both heads, which would include their combination and discarding of invalid data, and therefore it requires lower memory capacity of the onboard computer.

One of the disadvantages of using single camera data, however, is their anisotropic accuracy (see Section 3.3.4). This becomes critical when the data are rotated from one reference frame to another one. The rotated data are then less accurate because of the unfavorable error propagation. Additionally, the performance of the two star cameras is not the same as it is shown in the following section. Hence the accuracy of the estimated attitude is highly dependent on the selected primary camera. The consequences of using single camera data on mission operation are discussed in Chapter 6.

Of course, when valid data from both star camera heads are available, their combination is possible. Due to the mounting geometry, the data can be combined in such a way that the combined attitude solution carries full accuracy about all three axes. The data combination, however, is done only in the on-ground processing. The final attitude solution is then released as SCA Level-1B data product. The combination methods are presented in Chapter 5.

Note, there is a major difference between the SCA Level-1A (SCA1A) and Level-1B (SCA1B) data. The SCA1A data provide the original attitude quaternions which were obtained from the measurement of the two camera heads. The SCA1A quaternions rotate the inertial frame into the individual Star Camera Frame. The SCA1B data provide quaternions which were rotated from the individual SCF into a satellite body-fixed frame, the Science Reference Frame (SRF) (see Appendix A.5), and combined, if possible. The SCA1B quaternions rotate the inertial frame into SRF. The SCA1A to SCA1B data processing is described in detail in Sections 5.1 and 5.2.1.

3.3.4 Star camera measurement accuracy

The SCA measurement is characterized by its anisotropic accuracy, which is a consequence of the sensor construction geometry. The pointing of the boresight axis, i.e. the rotation about the $\mathbf{x}_{SCF}$ and $\mathbf{y}_{SCF}$ axes, is determined with a factor $\kappa = 8$ better than the rotation about the boresight ($\mathbf{z}_{SCF}$). The nominal measurement accuracy of the GRACE star cameras is assumed to be $\hat{\epsilon}_{\mathbf{x},\mathbf{y}} = 30\mu$rad for the rotation about the $\mathbf{x}_{SCF}$ and $\mathbf{y}_{SCF}$ and $\hat{\epsilon}_{\mathbf{z}} = 240\mu$rad for roll around the boresight axis (Stanton, 2000). The characteristic anisotropic noise distribution is obvious from Figure 3.12, where the attitude angles and angular rates about the SCF axes relative to the inertial frame are shown in both time and frequency domain. Between 0.01 Hz and 0.5 Hz the angular rates are dominated by noise which is characterized by f-behavior, i.e. in terms of attitude angles the PSD is flat.

For the GRACE star cameras, no error model is available which characterizes the sensor performance over the whole spectrum. The in-flight performance is not possible to be obtained precisely because of the lack of a reference and the many unpredictable factors influencing the performance (J.L.Jørgensen, DTU - private communication, March 2nd, 2015).

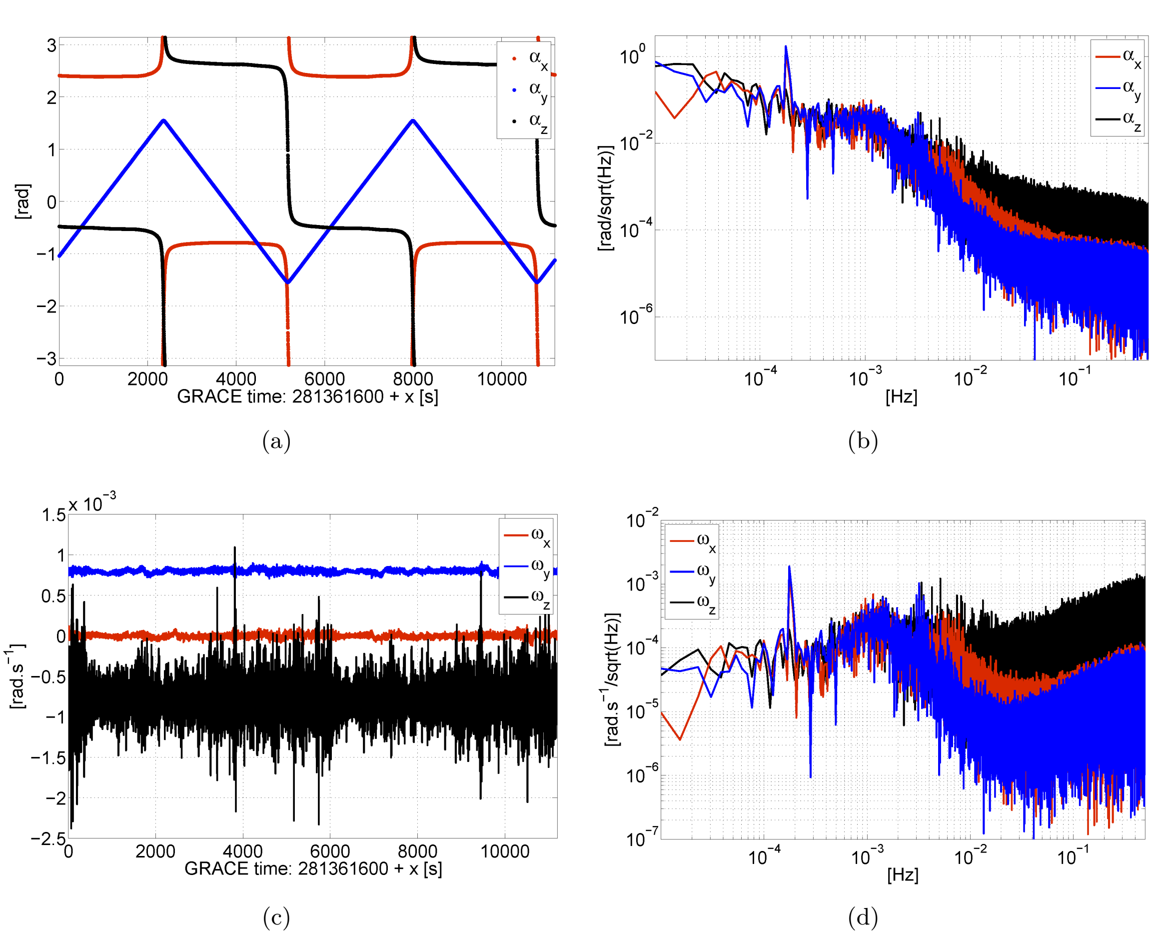

Figure 3.12: The attitude angles (a,b) and angular rates (c,d) about the star camera frame axes relative to the inertial frame demonstrating the anisotropic noise distribution of the SCA measurement in time (a,c) and frequency domain (b,d). Derived from the GRACE-A SCA Level-1A data of SCA head#1 on 2008-12-01 with 1 Hz sampling

The star camera measurement accuracy is limited by many different factors, which are discussed in detail e.g. by Eisenman and Liebe (1998); Jørgensen (2000); Liebe (2002). Absolute attitude error with respect to the mounting plane consists of:

- boresight error (*small mechanical excursions in the star tracker which cannot be calibrated out*)
  - thermal drift
  - ground calibration residuals
  - launch effects
  - gravity release effects
- Relative error (*the relative error is a measure of how accurately the star tracker can detect changes in attitude*)
  - optics error
    - ground calibration errors
    - thermal distortion
    - chromaticity

  - ▷ optical and point spread function distortion
- − centroiding error
  - ▷ pixel non-uniformity
  - ▷ quantization error
  - ▷ centroid algorithm uncertainty
  - ▷ CCD charge transfer efficiency effects
- − noise equivalent angle
  - ▷ readout noise
  - ▷ dark current noise
  - ▷ stray light noise
  - ▷ photon noise
- − algorithmic errors
  - ▷ time stamp uncertainty
  - ▷ erroneous star matches
  - ▷ algorithmic approximations
  - ▷ star catalog uncertainty

The in-flight performance of the four star cameras varies a lot despite of their nominally presumed identical performance. Although the star cameras on both spacecraft were calibrated in the early stage of the mission and parameters such as focal length, threshold for minimum number of stars in field-of-view and camera boresight were tuned in order to bring the performance of all 4 sensor heads to the level of the best one, there still remain certain differences (Herman *et al.*, 2004). On both satellites, the attitude data delivered by star camera head#2 are less noisy than the data from head#1. In other words, the good camera is head#2 and the bad camera is head#1 for both GRACE-A and GRACE-B according to Herman *et al.* (2004). However, the performance of the cameras changes with time and it depends on many factors which are listed above and which might also change with time. In 2014, the worst performing camera was head#1 on GRACE-B and the next worst performing camera was head#2 on GRACE-A (Witkowski and Massmann, 2014).

We have compared the measurement accuracy of the four star camera heads in 2008. The measurement accuracy was estimated as the mean noise level within 0.01 Hz and 0.5 Hz for the pointing of the boresight, $\epsilon_{\mathbf{x}_{SCF}}$ and $\epsilon_{\mathbf{y}_{SCF}}$, and for roll about the boresight, $\epsilon_{\mathbf{z}_{SCF}}$. Figure 3.13 shows the measurement accuracy for the primary camera of each satellite for the whole year 2008. The primary camera head switch was performed on DOY 135 and 305. The accuracy of the rotation about each SCF axis is quantified in Table 3.1.

Table 3.1: The measurement accuracy of the two star camera heads onboard GRACE-A and GRACE-B. The measurement accuracy is estimated as the mean noise level of the rotation about the SCF axes within the frequency band of 0.01-0.5 Hz. The results are based on the data from the whole year 2008, cf. Figure 3.13

	GRACE-A		GRACE-B	
	head#1	head#2	head#1	head#2
$\epsilon_{\mathbf{x}_{SCF}}$ [μrad]	25	25	32	20
$\epsilon_{\mathbf{y}_{SCF}}$ [μrad]	18	22	32	14
$\epsilon_{\mathbf{z}_{SCF}}$ [μrad]	235	170	240	140

For GRACE-A, the accuracy of the boresight pointing is practically the same and is slightly better than the estimated nominal measurement accuracy $\hat{\epsilon}_{\mathbf{x},\mathbf{y}} = 30\mu\text{rad}$. Moreover, the rotation about the $\mathbf{y}_{SCF}$ axis can be determined even slightly better than the rotation about $\mathbf{x}_{SCF}$, cf. Figure 3.13(a). Figure 3.13(b) reveals that the accuracy of roll about the boresight, $\epsilon_{\mathbf{z}_{SCF}}$, strongly differs for the two camera heads. Compared to the nominal accuracy of $\hat{\epsilon}_{\mathbf{z}} = 240\mu\text{rad}$, the SCA head#1 performs as expected, whereas head#2 performs much better than expected. Consequently, the factor κ, which represents the noise level ratio between boresight pointing and the roll about boresight, is then $\kappa = 11$ and $\kappa = 7$ for head#1 and head#2, respectively. The measurement accuracy of SCA head#1 on GRACE-B is exactly as expected and corresponds well with the nominally estimated values. From Figures 3.13(c) and 3.13(d) is obvious that the measurement accuracy of SCA head#2 is much better than of SCA head#1. The noise values are very close to those estimated during the on-ground tests. The corresponding noise level ratio factor is for both SCA heads $\kappa = 8$. Figure 3.13 also clearly shows the sensitivity of the SCA measurement accuracy to the moonlight intrusions which occur every 27 d.

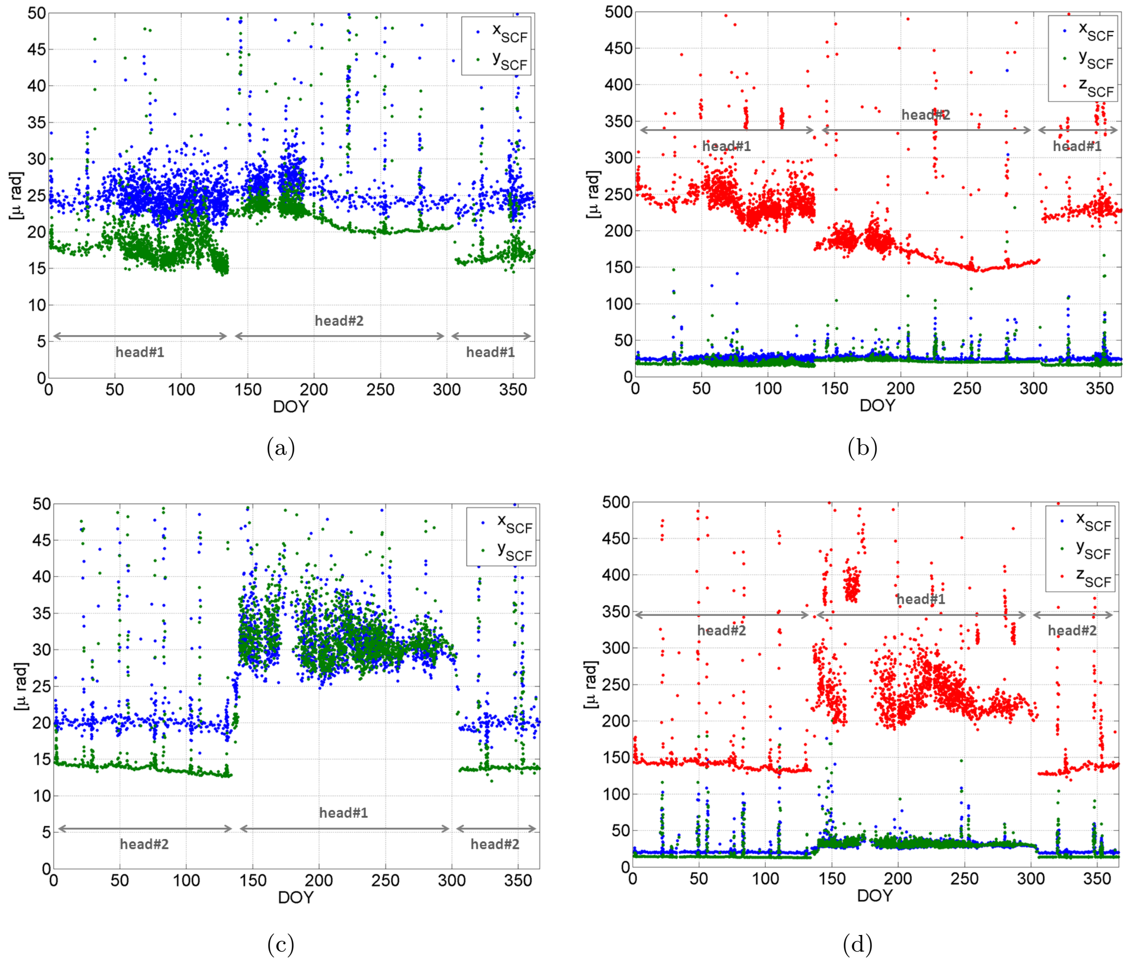

Figure 3.13: The measurement accuracy of the two star camera heads onboard GRACE-A (a,b) and GRACE-B (c,d). The measurement accuracy is estimated as the mean noise level of the rotation about the SCF axes within the frequency band of 0.01-0.5 Hz. Figures on the left represent the zoom in of the figures on the right, with focus on $\epsilon_{\mathbf{x}_{SCF}}$ and $\epsilon_{\mathbf{y}_{SCF}}$. The results are shown for the whole year 2008. The primary camera head switch was performed on DOY 135 and 305

As mentioned above, the measurement accuracy is influenced by many factors which might change over time. The most significant ones are the light intrusion into the FoV, number of stars in the FoV and thermo-elastic effects in the satellite. Some aspects of these factors are presented below.

The high sensitivity of the attitude measurement to the stray light was already discussed by Presti *et al.* (2004). Obviously, the cameras are not only sensitive to the light inside the FoV but also to the light outside the theoretical FoV which is limited by the baffles. As Presti *et al.* (2004) claim, it turned out that the effective FoV is larger than expected. The possible reason for the unexpected stray light are reflections.

The other factor affecting the measurement accuracy is the number of stars in the FoV. The more bright stars are identified in the digital star image, the better instantaneous attitude can be estimated. For precise attitude determination, a minimum number of stars in FoV is defined. The threshold for minimum number of stars can be adapted individually for each camera. The stars in the sky are not evenly distributed. There is a huge density of stars in the area of Milky Way compared to galactic poles where there are not so many stars. Therefore it does matter where the camera is pointing. Moreover, the ascending node of the GRACE orbit changes very slowly, it takes almost 8 years to finish the 360° circle. Hence the lack of stars in specific regions might influence the camera performance for long periods of time. As the two star cameras are pointing with their boresights to different parts of the sky, the number of stars in FoV is different for each camera, cf. Figure 3.14. This is one of the factors contributing to the different performance of the two cameras.

Interestingly, Figure 3.14 also shows the sensitivity of the number of stars in FoV to orbital configuration. Between DOY 43-74 and 212-233 the satellites were flying in the full sun orbit, which means the satellites did not pass through the Earth shadow. This means that the primary camera is less disturbed by the stray light as it is pointing more or less parallel to the Sun vector, but in the opposite direction. The white areas in Figure 3.14 are caused by the sunshine and moonlight intrusions into the FoV, cf. with Figure 3.11.

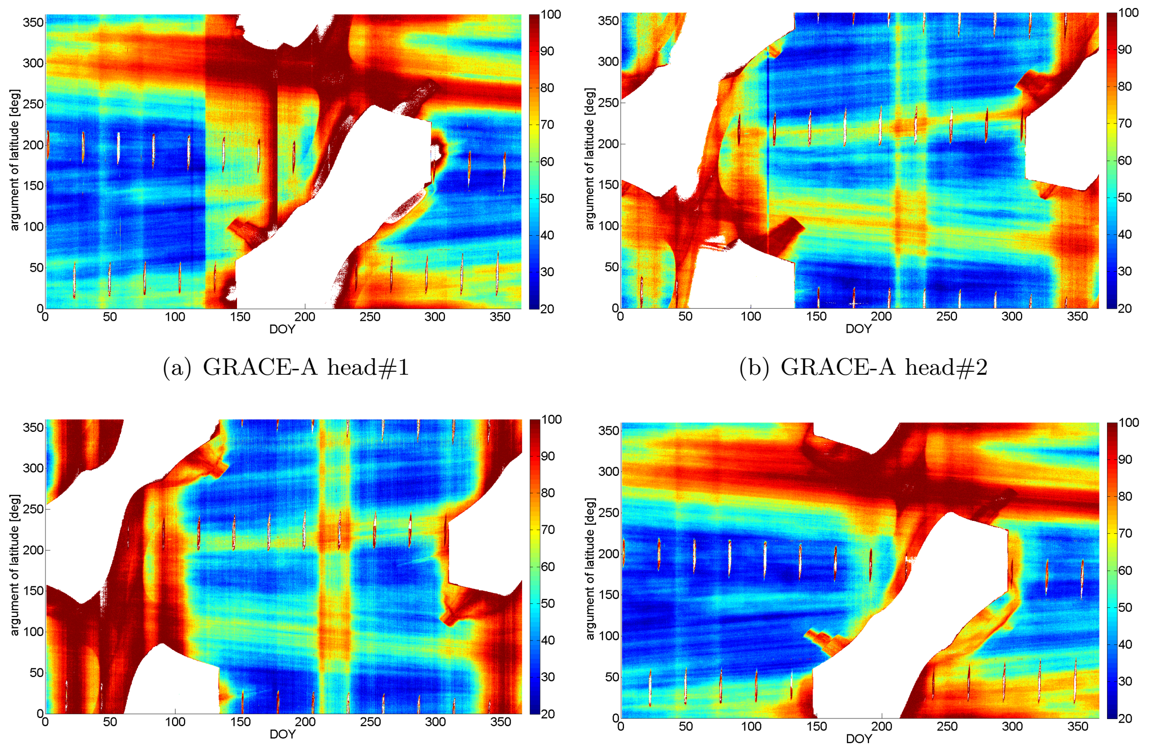

(a) GRACE-A head#1 (b) GRACE-A head#2

(c) GRACE-B head#1 (d) GRACE-B head#2

Figure 3.14: Number of stars in the star camera field-of-view for head#1 and head#2 on both satellites in 2008

The thermo-elastic effects of the star cameras and their neighborhood affect the star camera performance as well and cause possible biases and systematic effects. The satellite vehicle is exposed to extreme temperature differences which vary according to the satellite's position in orbit and its orientation towards the Sun. While one of the satellite panels is directly illuminated by the sunlight, the opposite panel is pointing into the outer space and hence is in shadow. The outside temperature difference reach up to 200 °C, cf. Figure 3.3. Inside the spacecraft, thermistors and heaters are mounted to sense and to change the inside temperature, in order to compensate the effect of the outside temperature differences and to ensure thermally homogeneous environment inside the vehicle. The effect of the temperature variations on the SCA measurement is shown in the following section.

The analysis of the impact of all these factors on the SCA measurement is beyond the scope of this thesis. The SCA performance analysis is a task for JPL, GSOC and DTU who have the required expertise and the access to the necessary housekeeping data, to the information about all satellites components and their properties and also to the onboard algorithms, which are confidential.

3.3.5 Inter-boresight angle variations

The mutual orientation of the star camera heads can be expressed in terms of the inter-boresight angle (IBA). IBA is the angle between the boresights of the star camera heads. It can be computed when valid data from both SCA heads are available. The computation details are given in Appendix D.1.

In case of GRACE, the IBA is nominally set to 90° and is supposed to be constant as the GRACE star camera heads are rigidly mounted on the accelerometer CFRP frame. However, temporal IBA variations of magnitude of 0.2 mrad (0.01 deg) exist. Daily variations of IBA are marked as well as systematic variations along the orbit which result in a striped pattern, cf. Figure 3.15. The IBA mean value is 89.26° and 89.21° for GRACE-A and GRACE-B, resp.

The magnitude of IBA variations is above the measurement accuracy level. The clear systematics in the IBA seem to be caused by continuous effect of one or more factors. Most likely the IBA varies due to the thermo-elastic effects within the satellite. However, the true reason remains unknown. Interestingly, similar inter-boresight variations have been found for CHAMP star cameras (Jørgensen *et al.*, 2004). The star cameras onboard CHAMP are similarly mounted as on GRACE, i.e. to the accelerometer frame. As for GRACE, systematic effects dominate the IBA variations which are of the same magnitude. For CHAMP it is believed that these variations are caused by thermal flexures of the optical bench. However, this phenomenon has not been further investigated. Recently, investigations of the IBA variations of the star cameras onboard the SWARM mission are ongoing (Michaelis, 2015). SWARM (Friis-Christensen *et al.*, 2008) is a low Earth orbiting satellite mission for the observation of the Earth's magnetic field, carrying 3 star cameras onboard manufactured by the DTU. The results from the calibration/validation phase, however, are expected to be released soon.

The sensitivity of the star cameras to temperature changes is obvious from Figure 3.16. Figure 3.16(a) shows the temperature drop sensed at the accelerometer frame after the so called DSHL (disabling of supplemental heater lines) event. In practice, the heaters onboard the satellite stopped working for a certain period of time which caused a temperature drop of 15 $°C$. Consequently, this caused a significant bias in the IBA (Figure 3.16(b)). The magnitude of this bias is 0.12 mrad which is above the measurement accuracy. The temperature is obviously not constant and variations with 1/revolution systematics exist which might be, indeed, the reason for the IBA variations shown in Figure 3.15.

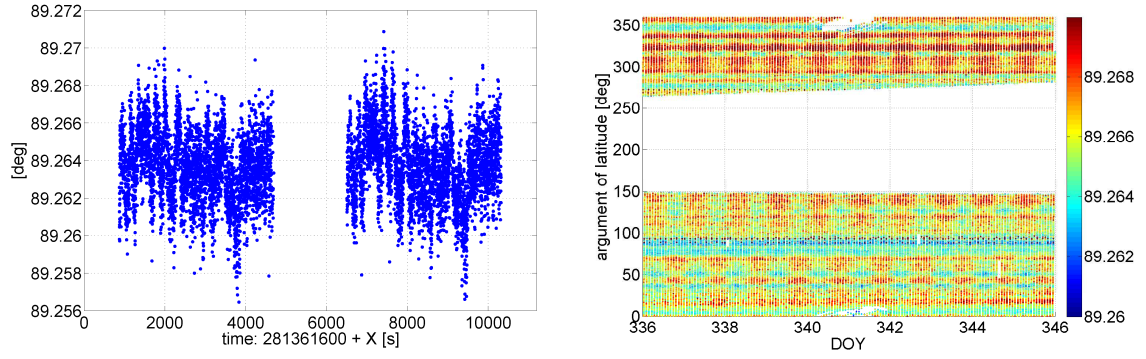

(a) (b)

Figure 3.15: The GRACE-A star camera inter-boresight angle shown in time domain for two orbital periods (a) and for 10 days in December 2008 along the orbit (b)

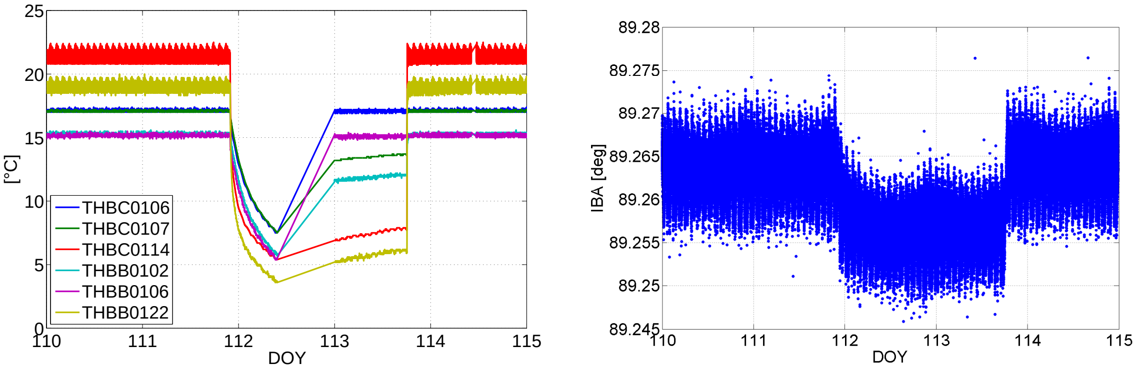

(a) (b)

Figure 3.16: Demonstration of sensitivity of the star cameras to temperature changes. The left figure shows the temperature of the acceleromter cage on which the star cameras are mounted. The temperature drop is caused by disabling of supplemental heater lines. The right figure shows the bias in the SCA inter-boresight angle which was caused by this temperature drop

3.4 Attitude actuators

The spacecraft's attitude is continuously perturbed by diverse torques due to the Earth's gravitational and magnetic field, residual Earth's atmosphere, solar radiation or due to motions inside the spacecraft like propellant motion inside the tanks or motion of the mass trim assembly. In order to keep the spacecraft in required attitude e.g. while maintaining the inter-satellite pointing or to intentionally change its actual attitude, as it is done e.g. during battery saving maneuvers, control torques generated by the attitude actuators are applied on the spacecraft. The attitude of the GRACE satellites is actively controlled by magnetic torquers and cold gas thrusters. Both actuators ensure 3-axis attitude control. The satellite is rotated about its roll (along-track), pitch (cross-track) and yaw (radial) axes (cf. Appendix B.3).

3.4.1 Magnetic torquers

The magnetic torquers are the primary attitude actuators for GRACE. Their advantage is that only power is needed for their operation. There is no need for any non-renewable consumable as it is in case of thrusters. The magnetic torquers (MTQ) generate a torque against the magnetic field of the Earth, which can be easily adjusted to the required value.

Onboard GRACE, three magnetic torquer rods of type MT30-2-GRC produced by ZARM/Microcosm (Figure 3.17(a)) are mounted (ZARM Technik, 2010). They are located off-center in the spacecraft parallel to the satellite body reference triad. Each rod consists of a cylindrical core and two coils. Direct electric current applied to the torquer creates a magnetic dipole $\mathbf{m}$ along the main axis of the torquer. The torque $\mathbf{T}$ applied to the spacecraft (Figure 3.17(b)) is then a reaction of the generated dipole moment to the Earth magnetic field flux density $\mathbf{B}$ (Blockley and Shyy, 2010):

$$\mathbf{T} = \mathbf{m} \times \mathbf{B} \tag{3.3}$$

or

$$\mathbf{T} = n \cdot I \cdot A \cdot \hat{\mathbf{n}} \times \mathbf{B} \tag{3.4}$$

with

n ... number of twists in the coil.
I ... applied electric current in [A]
A ... area in [m^2] that is encircled by the coil
$\hat{\mathbf{n}}$ ... unit vector along the coil axis

While the magnetic flux density is measured by the magnetometer and n and A are defined by the manufacturer, the magnitude and the direction of the torque depends on the applied electric current. The MTQ operate continuously, the magnitude and the sign of the current can be adjusted with a rate of 1 Hz. The maximum dipole moment of the GRACE MTQ is $30\,\mathrm{A} \cdot \mathrm{m}^2$.

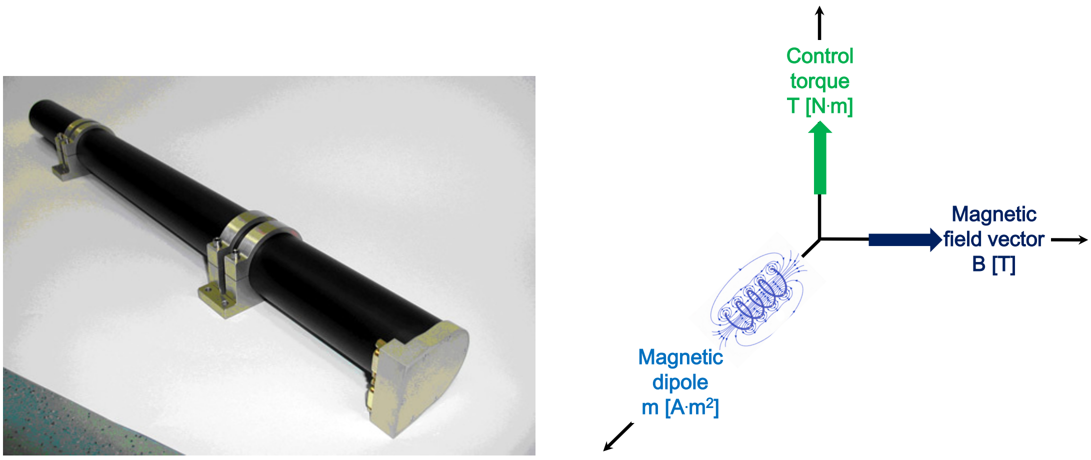

(a) (b)

Figure 3.17: Magnetic torquer rod as pictured by ZARM/Microcosm (a) and its principle of operation (b)

The efficiency of the attitude control using magnetic torquers depends on the mutual orientation of the torquer rods aboard the satellites and the Earth magnetic field lines. In case the main axis of the torquer rod becomes parallel to the geomagnetic field lines (Figure 3.18), i.e. $\mathbf{B} \parallel \mathbf{m}$, no torque can be generated about this axis. Due to the GRACE polar orbit, at particular locations over the globe torquer rods and the magnetic field lines become nearly parallel and so the generated control torque is not sufficient to adjust the attitude of the spacecraft as needed. Such constellation occurs along the geomagnetic equator and affect the rotation about the roll axis, and at high latitudes and over the geomagnetic poles where it affects the rotation about yaw axis. In these regions, the generated torque by magnetic torquers is not sufficient to fully control the spacecraft, which results in larger attitude variations, cf. Figure 4.5. Therefore, thrusters need to be activated to maintain the desired attitude. In contrast to roll and yaw, the satellite's attitude about the pitch axis can be controlled by MTQ very effectively. The pitch deviations are kept well below the deadband limits, pitch thrusters are needed to be activated very rarely.

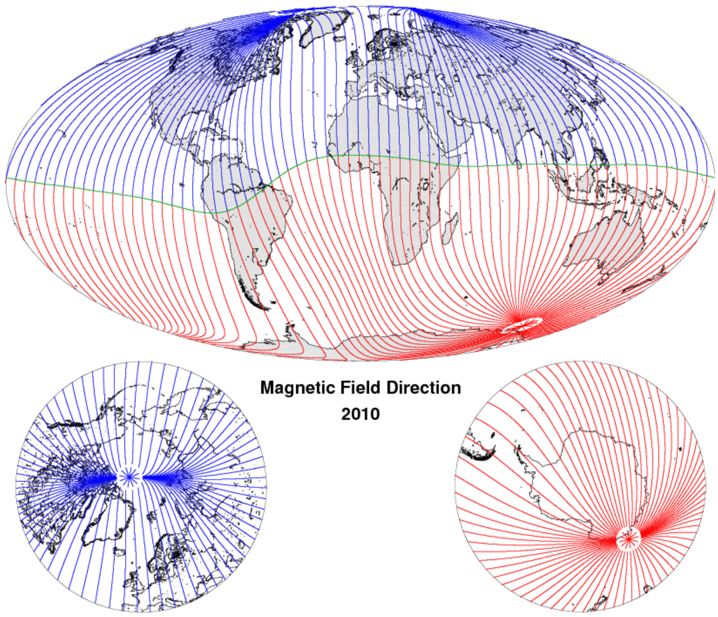

Figure 3.18: Earth's magnetic field direction in 2010, source: http://geomag.org

The attitude control using magnetic torquers has another prominent feature. That is the dominant frequency of the electric current flow through the torquer rods. Figure 3.19(d) shows the square root power spectral density of the electric current flow for all three torquer rods, from which the characteristic frequencies of the signal are obvious. Beside the characteristic frequency of 1/revolution (0.18 mHz) and 2/revolution (0.35 mHz), which are typical for practically all GRACE data because of the orbital configuration, the dominant frequency of the electric current is ∼3.3 mHz. This dominant frequency stays constant over long periods of time.

It is very unlikely that such periodicity would be caused by any natural or geophysical phenomena, or in other words that the external disturbing torques acting on the satellite would change its attitude with this frequency. Also, the construction and shape of the magnetic torquer rods do not cause such periodicity (D. Bindel, ZARM, personal communication, Sep 11th 2009). The analysis of the long time series of GRACE data revealed that in the early mission years this dominant frequency was ∼5 mHz. It suddenly changed to ∼3.3 mHz in February 2004 on GRACE-A and in January 2005 on GRACE-B (Figure 3.20). This sudden frequency switch was caused by changing the setting of one of the MTQ parameters in order to arrive at a quieter state of attitude motion (G. Kruizinga, S. Bettadpur, personal communication, Nov 15th 2010). As a result, the angular accelerations of the satellite were reduced and consequently the noise in acceleromter observations decreased (Flechtner, 2004). This means the MTQ dominant frequency is caused by the implemented onboard attitude control algorithms.

The consequence of the MTQ dominant frequency are systematic variations in the inter-satellite pointing. This feature is obvious especially in the pitch variations as the rotation about the pitch axis is controlled solely by the MTQ (cf. Figure 4.5(d)). Due to the magnetic torques operation, artificial magnetic fields are induced in the spacecraft. The magnitude of these artificial fields is not negligible and big enough to be sensed by the magnetometer located at the top of the boom. The perturbation is most obvious in the B_y component, resulting in apparent horizontal striping (cf. Figure 3.4(b) and 3.19).

As a consequence of this perturbation, the attitude control is negatively affected. This phenomenon was detected soon after launch and it is being solved in the onboard processing. Until 2007, a mixture of the measured magnetic field and an onboard model was used with a ratio of 0.7 to 0.3 in order to downweight disturbances in the magnetometer measurement.

Later, a magnetic compensation loop was implemented in the onboard processing to reduce the signal caused by magnetic torquer activity from the magnetometer measurements, (J. Herman, GSOC, C. Belle, Astrium, personal communication, Oct 21st 2009).

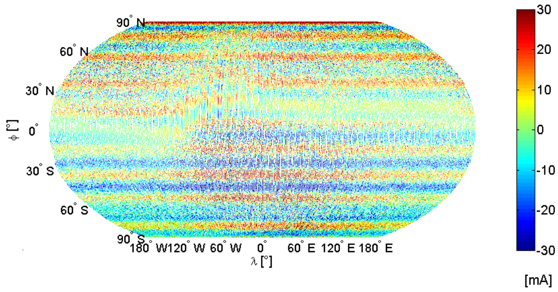

(a) MTQ rod1 (along track)

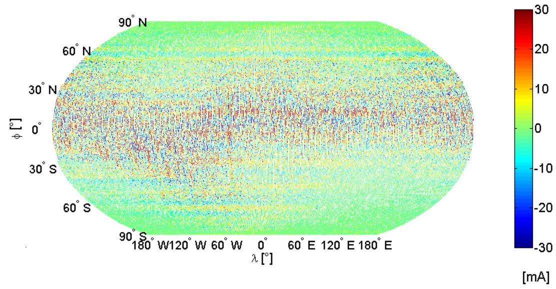

(b) MTQ rod2 (cross track)

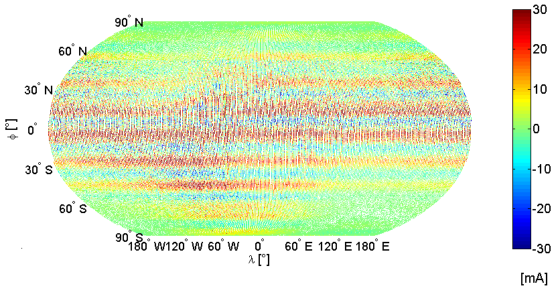

(c) MTQ rod3 (radial)

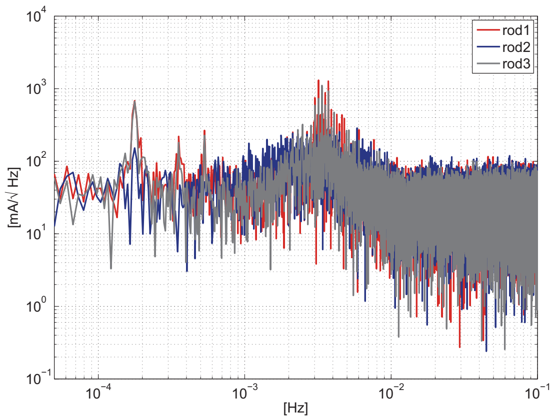

(d) PSD

Figure 3.19: Electric current flowing through the magnetic torquer rods along the ascending orbit from Jan 1st to Jan 18th, 2008, for GRACE-A (a-c) and their square root power spectral density (PSD) (d)

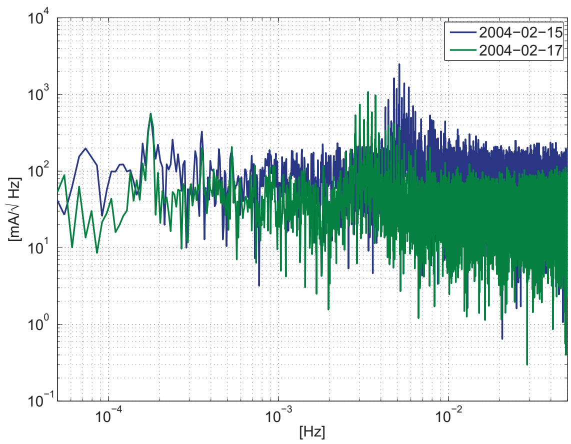

Figure 3.20: Change of the dominant frequency of the electric current flow through the magnetic torquers (here shown for rod1) from ∼5 mHz to ∼3.3 mHz occurred on GRACE-A in February 2004 due to updated setting of MTQ parameters for attitude control

3.4.2 Cold gas thrusters

Cold gas thrusters are implemented onboard GRACE for the purposes of attitude and also orbit control. Cold gas thrusters are highly reliable, flexible actuators at low cost and can be used in any environment. There are two 40 mN thrusters for orbit control mounted at the rear panel of each GRACE satellite. The orbit maneuvers are performed rarely, 2-3 times per year, to maintain the required orbit separation distance or to perform the satellite swap maneuver. The attitude is controlled by twelve 10 mN thrusters. In contrast to the orbital thrusters, the attitude control thrusters are activated very frequently, ~1000 times per day.

The mounting of the twelve 10 mN cold gas thrusters is pictured in Figure 3.21. They are characterized by low thrust level, hence allowing relatively smooth and accurate attitude control. The operation principle sketched in Figure 3.22. The executed thrust on the spacecraft, **F**, is equal to the amount of force applied to the satellite based on the expulsion of gases (Wertz and Larson, 1999), i.e.

$$\mathbf{F} = \dot{m}\mathbf{V}_e + A_e[P_e - P_\infty] \tag{3.5}$$

with

$\dot{m}$	...	propellant mass flow rate
$\mathbf{V}_e$	...	propellant exhaust velocity
A_e	...	nozzle exit area
P_e	...	gas pressure at the nozzle exit
P_∞	...	ambient pressure

The thrusters must be activated in pairs in order to execute the rotation of the spacecraft about its center of mass, cf. Figure 3.21(b). Detailed description and technical properties of the GRACE propulsion system can be found in Schelkle (2000).

Thrusters use up non-renewable propellant which for GRACE is gaseous nitrogen (GN_2) stored in two tanks disposed symmetrically about the center of mass of the spacecraft. Initially, there was ~16 kg of the propellant in each tank. While the thrusters are activated, the gas is used up simultaneously from both tanks in order to minimize the variations of the CoM. Over a long period of time, however, the CoM variations are inevitable due to the little fluctuations in the mass flow rate. As a result, the CoM has to be regularly calibrated using the mass trim system.

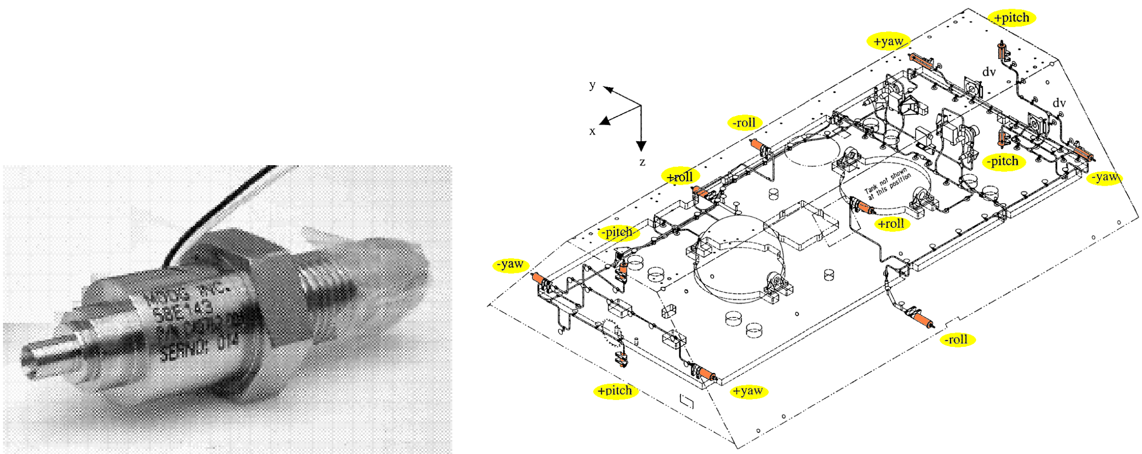

(a) (b)

Figure 3.21: Detail of a cold gas thruster (Usbeck *et al.*, 2004) (a) and the location of the attitude control thrusters onboard GRACE (Schelkle, 2000) (b)

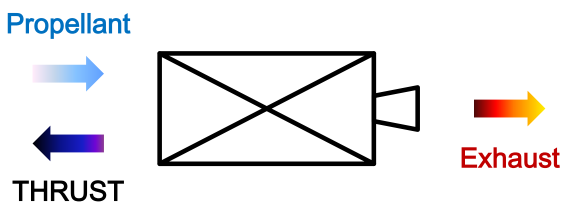

Figure 3.22: The principle of attitude control using cold gas thrusters

The thrusters are designed to be secondary attitude actuators for GRACE. They are activated only when the control torques generated by the magnetic torquers do not suffice to maintain the desired attitude. The thrusters operate based on adaptive strategy. This means the length of the pulse depends upon the strength and the results of the preceding ones. In other words, if the first correction was too small, the second will be slightly larger, the third even larger or smaller again etc. (Herman and Steinhoff, 2012).

The geographical location of the thruster activations is shown in Figure 3.23. The roll thrusters are activated mainly along the geomagnetic equator, because the efficiency of the attitude control about the roll axis using MTQ is very low in this region. In contrast, in this particular region, the attitude about the yaw axis can be controlled well using MTQ, but at high latitudes, thrusters need to be activated in order to generate the required control torque. The pitch thrusters are activated very rarely, because the magnetic torquers suffice to control well the rotation about the pitch axis at any position along the orbit. The statistics with the number of thruster activations per day and the propellant consumption can be found in Section 6.2.

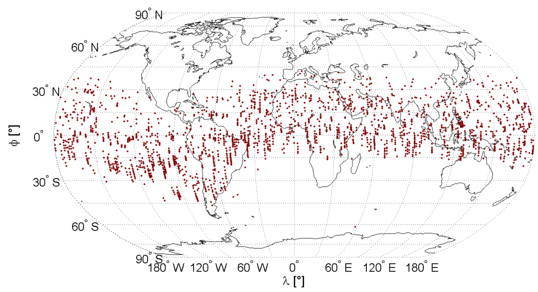

(a) roll

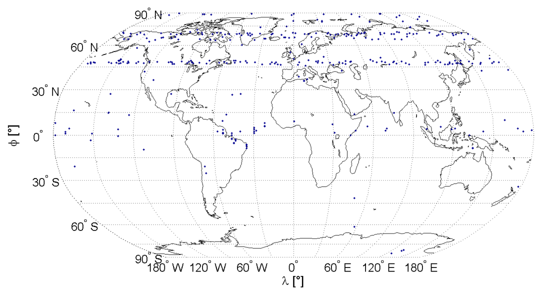

(b) pitch

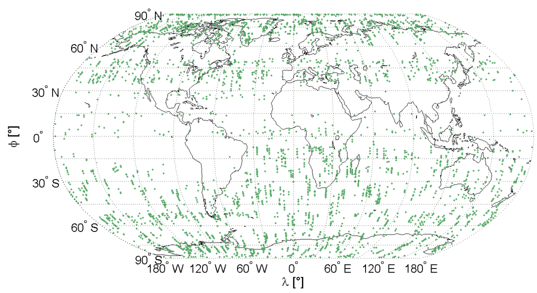

(c) yaw

Figure 3.23: Geographical location of thruster activations in roll, pitch and yaw for a time span of 18 days (Jan 1st-18th 2008) for GRACE-A ascending orbit

The attitude control using thrusters has two critical limitations for the mission operation. The first limitation arises from the fact that the propellant is non-renewable. The second

Table 3.2: Number of activation cycles of the roll, pitch and yaw thrusters during 2002-2007, i.e. at the planned mission lifetime, and during 2002-2014. The 10^6 cycles were exceeded already by the roll and yaw thrusters, pitch thrusters are well below this limit

	GRACE-A		GRACE-B	
	2007	2014	2007	2014
roll	$0.45\ 10^6$	$1.00\ 10^6$	$0.39\ 10^6$	$1.00\ 10^6$
pitch	$0.19\ 10^6$	$0.35\ 10^6$	$0.10\ 10^6$	$0.38\ 10^6$
yaw	$0.55\ 10^6$	$1.31\ 10^6$	$0.38\ 10^6$	$1.27\ 10^6$

limitation is thruster operation which is guaranteed only up to certain number of activation cycles.

Once GN_2 propellant is completely depleted, the attitude control using thrusters is no longer possible. Because the magnetic torquers alone do not suffice to control the satellite's attitude along the whole orbit, the thruster outage will be fatal for the maintenance inter-satellite pointing. Consequently, the inter-satellite ranging which is one of the primary observations needed for gravity field recovery, will not be performed anymore.

This fact was properly taken into account in the mission design. For the planned 5 years of GRACE operation, enough fuel was stored onboard for the mission operation. Figure 3.24 shows the amount of fuel onboard since the beginning of the mission until today. Clearly, in 2007, i.e. at the predicted mission end, only 10 kg onboard GRACE-A and 8 kg onboard GRACE-B out of 32 kg GN_2 was exhausted. Luckily, GRACE operated most of the time during the solar cycle minimum (Figure 3.25), hence the disturbing torques due to the atmosphere and the solar radiation were minimal. At the end of 2014, there was still ~9 kg and ~10 kg fuel left onboard GRACE-A and GRACE-B, respectively.

Today the mission keeps operating already 8 years after its planned termination. As the current goal is to operate the mission as long as possible, the fuel amount left onboard is one of the major concerns for the mission extension. The fuel consumption depends not only the efficiency of the attitude control strategy, on the magnitude of the disturbing torques acting upon the spacecraft and the efficiency of magnetic torquers, but also on the accuracy of the attitude data delivered by the primary star camera. The latter is further discussed in Chapter 6.

The functionality of the thrusters is guaranteed by the manufacturer up to 10^6 activation cycles. This apparent limitation became a concern first in the last years, when the nominal limit of 10^6 activation cycles was exceeded for the yaw and roll thrusters. Fortunately, all thrusters continue to operate well, hence this limitation seems to be not so critical so far.

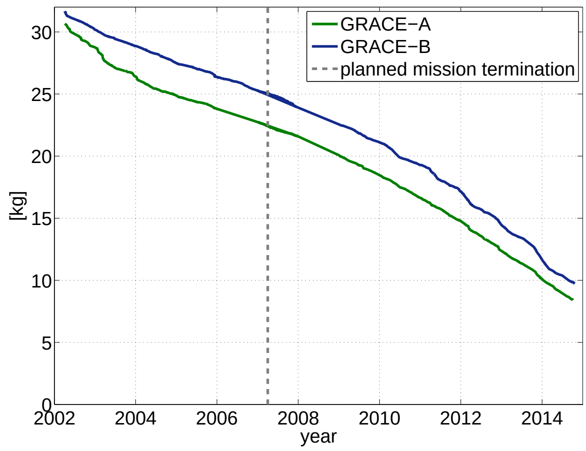

Figure 3.24: Propellant consumption onboard GRACE-A and GRACE-B during the whole mission operation

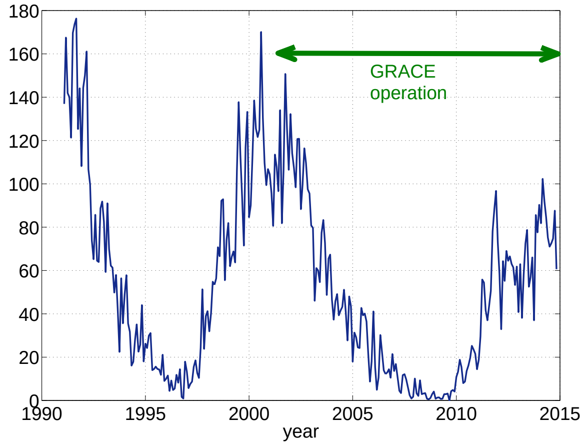

Figure 3.25: The solar activity (number of sunspots) during the GRACE mission operation period. Data source: http://solarscience.msfc.nasa.gov/SunspotCycle.shtml

For those determined to fly
having no wings
is just a little detail.

- Jane Lee Logan -

4 Inter-satellite pointing

The inter-satellite pointing is the very fundamental requirement for the inter-satellite ranging technique, which is one of the GRACE primary observation techniques (cf. Section 2.3.2). The measured range is related to the phase center (PhC) of each antenna horn and hence the goal is to keep the antenna phase centers aligned with the line-of-sight (LOS), which is the imaginary straight connection line between the satellites' center of mass.

One of the challenges related to the inter-satellite pointing is its maintenance in orbit. The precise pointing is maintained in the science mode and back-up science operational mode in which all scientific measurements needed for the gravity field recovery are collected. In the ideal case, the PhCs should be perfectly aligned with the LOS (Figure 4.1(a)). However, due to continuous attitude perturbations caused by both external and internal torques, such as the aerodynamic torque, magnetic torque, Earth's gravitational torque, solar radiation torque or due to propellant motion inside the tanks, the attitude variations are inevitable (Figure 4.1(b)). The characteristics of the inter-satellite pointing variations are discussed in Section 4.4.

The requirements on the inter-satellite pointing are defined by the so called deadband which is the maximum allowed angular deviation of the CoM-to-PhC vector relative to LOS. The deadband is set to 3 mrad for roll and 4 mrad for pitch. The value of the yaw deadband was changed several times during the mission operation, it was set to 4.0 mrad since 2002, 4.4 mrad since October 2007, 4.8 mrad since June 2008 and 5.2 mrad since January 2012 (Herman and Steinhoff, 2012).

There are two major reasons for keeping the inter-satellite pointing variations as small as possible. The first one is that the pointing jitter strongly affects the inter-satellite ranging observations. Consequently, the ranging observations need to be corrected for the imperfect pointing in the post-processing, cf. Section 4.5. The other reason is the multipath effect caused by the reflections of the microwave signal on the satellite's surface elements.

Another challenging aspect is the in-flight and on-ground determination of the inter-satellite pointing. This requires precise attitude information, precise orbit information, and various calibration parameters related to the star cameras and to the KBR horns. The in-flight and on-ground processing significantly differ (see Section 4.2 and 4.3), hence any inconsistency in these input data will affect the accuracy of the inter-satellite pointing and consequently also the ranging observations (see Section 4.6).

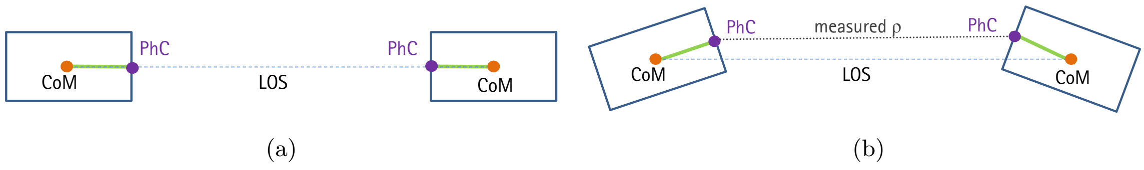

Figure 4.1: The ideal and the real inter-satellite pointing. In the ideal case, the PhC of the KBR antenna would be perfectly aligned with the LOS (a). In the real case, however, attitude variations due to continuous perturbations are inevitable (b)

4.1 Geometric interpretation of the inter-satellite pointing

Inter-satellite pointing can be geometrically interpreted as angular deviations of the CoM-to-PhC vector from the LOS, cf. Figure 4.1(b). In order to mathematically describe the inter-satellite pointing, two reference frames need to be defined: the K-Frame, of which the x-axis is identical with the CoM-to-PhC vector, and the LOS-Frame, of which the x-axis is aligned with the LOS. The full definition of these reference frames can be found in Appendix A, their mutual orientation is sketched in Figure 4.2.

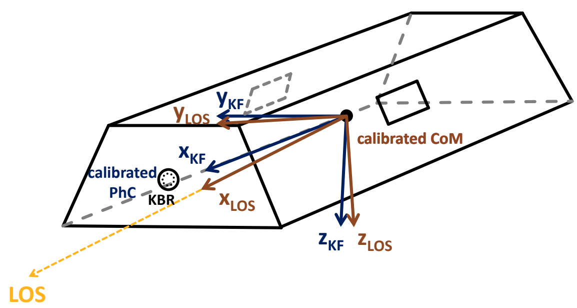

Figure 4.2: Mutual orientation of the K-Frame $\{\mathbf{x}_{KF}, \mathbf{y}_{KF}, \mathbf{z}_{KF}\}$ with respect to the LOS-Frame $\{\mathbf{x}_{LOS}, \mathbf{y}_{LOS}, \mathbf{z}_{LOS}\}$. The $\mathbf{x}_{KF}$ points from the satellite's center of mass (CoM) towards the calibrated KBR antenna phase center, the $\mathbf{x}_{LOS}$ is identical with the line of sight (LOS)

The mutual attitude of the K-Frame and the LOS-Frame can be expressed as sequence of rotations about the roll (x-), pitch (y-) and yaw (z-) axes about the respective roll ψ, pitch θ and yaw ϕ angles (Wertz, 1978). This rotation sequence is represented by the direction cosine matrix rotating the K-Frame into the LOS-Frame $\mathbf{R}_{KF\rightarrow LOS}$:

$$\mathbf{R}_{KF\rightarrow LOS} = \mathbf{R}_1(\psi)\mathbf{R}_2(\theta)\mathbf{R}_3(\phi) \tag{4.1}$$

where $\mathbf{R}_i$, i = 1,2,3, denote the elementary rotations about the x-, y- and z-axes (cf. Appendix B.3).

The elements of $\mathbf{R}_{KF\rightarrow LOS}$ matrix are

$$\mathbf{R}_{KF\rightarrow LOS} = \begin{pmatrix} R_{11} & R_{12} & R_{13} \\ R_{21} & R_{22} & R_{23} \\ R_{31} & R_{32} & R_{33} \end{pmatrix} = \begin{pmatrix} c\theta c\phi & c\theta s\phi & -s\theta \\ -c\psi s\phi + s\psi s\theta c\phi & c\psi c\phi + s\psi s\theta s\phi & s\psi c\theta \\ s\psi s\phi + c\psi s\theta c\phi & -s\psi c\phi + c\psi s\theta s\phi & c\psi c\theta \end{pmatrix} \tag{4.2}$$

with $c := \cos()$ and $s := \sin()$.

The roll ψ, pitch θ and yaw ϕ rotation angles (RPY) can be obtained from $\mathbf{R}_{KF\rightarrow LOS}$ as

$$\begin{aligned} \psi &= -\arctan\left(\frac{R_{23}}{R_{33}}\right) \\ \theta &= \arcsin(R_{13}) \\ \phi &= -\arctan\left(\frac{R_{12}}{R_{11}}\right) \end{aligned} \tag{4.3}$$

4.2 In-flight determination of the inter-satellite pointing

The in-flight maintenance of the inter-satellite pointing is the task of the AOCS (cf. Chapter 3). The attitude determination and control loop is sketched in Figure 3.1. From the comparison of the instantaneous orientation of the CoM-to-PhC vector with its desired orientation defined by the LOS direction, the inter-satellite pointing angles are computed. Subsequently, based on the attitude control algorithms, the satellite's attitude is adjusted using magnetic torquers and cold gas thrusters. The attitude determination and control is performed autonomously onboard the satellites. The values of the pointing angles computed onboard the satellites are stored in the Level-0 THAD data product.

Essentially, the following input data are needed to determine the direction cosine matrix rotating the K-Frame into LOS-Frame $\mathbf{R}_{KF\rightarrow LOS}$: the position of both satellites, the attitude of the local spacecraft and the location of the KBR antenna phase center within the local spacecraft. Note, as we do not have access to the onboard AOCS algorithms, in the following only the logic of the computation is shown. The scheme of the computation is sketched in Figure 4.3.

The position of both satellites in the inertial frame is needed for the computation of the instantaneous LOS vector. Although the position is measured by the GPS onboard each satellite, the data cannot be used directly as there is no link between the satellites for the data transmission. Instead, high-precision orbit predictions are computed on-ground and uploaded every day to the satellites in terms of two-line elements (TLE). The desired attitude is computed onboard each satellite by means of an orbit propagator based on GPS data and the TLEs. The relative position between the two satellites is obtained with accuracy below 50 m, resulting in pointing error smaller than 0.1 mrad (Arbinger *et al.*, 2003; Herman *et al.*, 2004). Based on this data, the direction cosine matrix $\mathbf{R}_{iner\rightarrow LOS}$ rotating the inertial frame into the LOS-Frame can be derived.

The information about the instantaneous attitude of the local spacecraft is delivered by the star cameras (cf. Section 3.3). The AOCS uses the attitude information delivered by the primary camera only (cf. Section 3.3.3). The star camera provides precise attitude of the respective Star Camera Frame with respect to the inertial frame in terms of quaternions from which the direction cosine matrix $\mathbf{R}_{iner\rightarrow SCF}$ can be derived.

The alignment of the KBR antenna phase center relative to the Star camera Frame is needed for the determination of the actual attitude of the CoM-to-PhC vector. The alignment of the PhC with respect to the SCF was estimated based on the KBR system calibration in 2003 (cf. Section 4.6.1) and uploaded to the satellites in terms of quaternions, denominated as QKS. The QKS quaternions provide the rotation of the respective Star Camera Frame into the K-Frame. The QKS are then transformed into direction cosine matrix $\mathbf{R}_{SCF\rightarrow KF}$.

Finally, the deviation of the CoM-to-PhC vector with respect to the LOS, i.e. the mutual orientation of the K-Frame with respect to the LOS-Frame ($\mathbf{R}_{KF\rightarrow LOS}$), can be obtained as

$$\mathbf{R}_{KF\rightarrow LOS} = \mathbf{R}_{iner\rightarrow LOS} \cdot (\mathbf{R}_{iner\rightarrow SCF})^T \cdot (\mathbf{R}_{SCF\rightarrow KF})^T \tag{4.4}$$

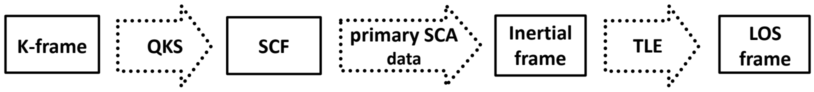

Figure 4.3: Flowchart of the in-flight determination of the inter-satellite pointing

4.3 On-ground determination of the inter-satellite pointing

In the data post-processing, the determination of the inter-satellite pointing is needed for the computation of the correction for the KBR observations. KBR observations are corrected for the imperfect pointing by applying so called antenna offset correction (see Section 4.5). In the on-ground processing, fully corrected satellite's attitude and position measurements are used as input for the pointing determination. This means, the predicted satellite orbits and attitude data from the primary star camera used in-flight processing are now replaced by the final orbit and attitude solutions, i.e. GNV1B and SCA1B data products. The KBR antenna phase center vector expressed in SRF coordinates is provided in the VKB1B data product. The scheme of the computation is sketched in Figure 4.4. The computation is done separately for GRACE-A and GRACE-B.

Based on the SCA1B and VKB1B data, direction cosine matrix rotating the inertial frame into K-Frame, $\mathbf{R}_{iner\rightarrow KF}$, can be obtained:

$$\mathbf{R}_{iner\rightarrow KF} = \begin{bmatrix} (\mathbf{x}_{KF})^T \\ (\mathbf{y}_{KF})^T \\ (\mathbf{z}_{KF})^T \end{bmatrix} \qquad \text{with} \qquad \begin{aligned} \mathbf{x}_{KF} &= (\mathbf{R}_{iner\rightarrow SRF})^T \frac{\mathbf{pc}}{|\mathbf{pc}|} \\ \mathbf{y}_{KF} &= \mathbf{z}_{KF} \times \mathbf{x}_{KF} \\ \mathbf{z}_{KF} &= \mathbf{x}_{KF} \times \mathbf{y}_{SRF} \end{aligned} \tag{4.5}$$

where

$\mathbf{R}_{iner\rightarrow SRF}$	is the matrix rotating the inertial frame into the Science Reference Frame derived from the SCA1B quaternions according to Equation C.21
$\mathbf{pc}$	is the CoM-to-PhC vector in SRF coordinates (as given in VKB1B)
$\mathbf{y}_{SRF}$, $\mathbf{x}_{KF}$, $\mathbf{z}_{KF}$	are the vectors representing the respective axes in inertial coordinates

The matrix rotating the inertial frame into the LOS-Frame $\mathbf{R}_{iner\rightarrow LOS}$ is derived from the final orbit solutions. As the GNV1B orbit data are given in the terrestrial frame, i.e. the International Terrestrial Reference Frame (ITRF), they need to be transformed into the inertial frame by applying the IERS conventions (cf. Appendix A.10). Then, the $\mathbf{R}_{iner\rightarrow LOS}$ can be computed as

$$\mathbf{R}_{iner\rightarrow LOS_j} = \begin{bmatrix} (\mathbf{x}_{LOS_j})^T \\ (\mathbf{y}_{LOS_j})^T \\ (\mathbf{z}_{LOS_j})^T \end{bmatrix} \qquad \text{with} \qquad \begin{aligned} \mathbf{x}_{LOS_j} &= \frac{\mathbf{r}_i - \mathbf{r}_j}{|\mathbf{r}_i - \mathbf{r}_j|} \\ \mathbf{y}_{LOS_j} &= \mathbf{x}_{LOS_j} \times \frac{\mathbf{r}_A}{|\mathbf{r}_A|} \\ \mathbf{z}_{LOS_j} &= \mathbf{x}_{LOS_j} \times \mathbf{y}_{LOS_j} \end{aligned} \tag{4.6}$$

where $i, j = A, B$, $i \neq j$ and $\mathbf{r}$ is the satellite's position vector in the inertial frame.

Finally, the direction cosine matrix rotating the K-Frame into LOS-Frame, $\mathbf{R}_{KF\rightarrow LOS}$, is obtained as

$$\mathbf{R}_{KF\rightarrow LOS} = \mathbf{R}_{iner\rightarrow LOS} \cdot (\mathbf{R}_{iner\rightarrow KF})^T \tag{4.7}$$

Obviously, the recovery of the pointing angles from the Level-1B data differs from the GRACE onboard processing carried out by the AOCS. Consequently, differences between the data computed onboard and in the post-processing exist. This phenomenon is further discussed in Section 4.6.

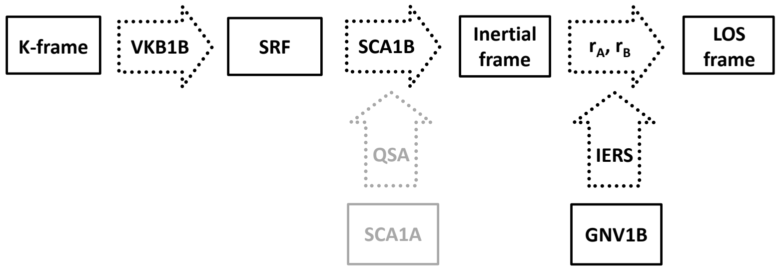

Figure 4.4: Flowchart of the on-ground determination of the inter-satellite pointing. Scheme of the derivation of the $\mathbf{R}_{KF\rightarrow LOS}$ matrix from the GRACE Level-1B data, from which the inter-satellite pointing angles are computed

4.4 Characteristics of the inter-satellite pointing variations

The inter-satellite pointing variations can be expressed in terms of roll, pitch and yaw rotation angles, derived from the $\mathbf{R}_{KF\rightarrow LOS}$ matrix. Figure 4.5 shows the RPY angles for 2 orbital periods as well as for a period of 18 d along the groundtrack. The RPY angles in Figure 4.5 were computed onboard the satellite and were recovered from the THAD data product. The characteristics of the pointing variations of GRACE-A and GRACE-B are the same, thus the following description is valid for both satellites.

It is very obvious that based on the available input data, the AOCS successfully keeps the pointing variations within the specified deadband which is different for roll, pitch and yaw. This means the requirements on the mission operation and the inter-satellite ranging are met successfully.

The pointing variations are dominated by several systematic effects which depend on the characteristics of the onboard attitude determination sensors and actuators rather then by satellite dynamics due to the disturbing environmental torques. Focusing on the pitch variations, the very prominent systematics is the oscillation at frequency about ~3.3 mHz which results in very regular horizontal stripes apparent in Figure 4.5(d). Clearly, such systematics cannot be related to any geophysical phenomena. It is the dominant frequency of the magnetic torquer operation (cf. Section 3.4.1) that causes this systematics. This is proved also by the fact that the frequency of pitch variations suddenly changed in February 2004 on GRACE-A and January 2005 on GRACE-B when the settings of magnetic torquers were changed. As pitch is almost entirely controlled by MTQs, this dominant frequency becomes particularly amplified.

Further, pitch variations reveal stronger and rather irregular variations at specific geographical regions. They are not random, but very steady in space and time. The regions are different for ascending and descending orbit. For GRACE-A ascending orbit and GRACE-B descending orbit this region is located at 75°W-100°E, 50°N-90°S and for GRACE-A descending orbit and GRACE-B ascending orbit at 160°E-50°W, 50°N-90°S. In these regions, the y-component of the Earth's magnetic flux density vector **B** has strongly negative values, compare Figure 3.4(b) and 4.5(d). The B_y values differ for ascending and descending orbit (cf. Section 3.2.2) and therefore the geographical regions of irregular pitch variations are orbit dependent as well. Obviously, the magnetic torquers do not manage to control the spacecraft in these regions as smoothly as in the other parts of the orbit. One possible explanation for that could be a particular constraint of the attitude control algorithms.

These two features are not so prominent in roll and yaw variations because the efficiency of MTQ attitude control is much lower due to the rather unfavorable orientation of the magnetic torquer rods with respect to the magnetic field lines. Hence the attitude deviations drift rapidly and attitude thrusters need to be activated to maintain the desired attitude. The attitude control with thrusters is not as smooth as with magnetic torquers. Moreover, the thrusters are activated when needed in contrast to torquers which operate continuously at 1 Hz sampling rate. As discussed in Section 3.4.1, the MTQs sufficiently control roll over the geomagnetic poles and yaw along the geomagnetic equator. In all other regions the thrusters need to support the MTQs and pointing variations become larger. This is very well reflected in the roll and yaw pointing variations (cf. Figure 4.5(b) and 4.5(f)).

The inter-satellite pointing variations are mainly influenced by the characteristics of the attitude determination sensors and actuators as just discussed. At the same time, however, pointing variations provide valuable information about the performance of the AOCS, and about some events carried out onboard when no other information is available. Especially the long time series reveal interesting phenomena. Figure 4.6 shows the pitch variations along the orbit for 2 years, 2007 and 2008. Along with the already discussed features, another eminent systematics was revealed and that is the one with characteristic duration of 161 days. Within one 161 d epoch the variations are stronger and within the next 161 d epoch the variations are milder. These epochs alternate regularly. This feature is the consequence of using attitude data from only one star camera for the in-flight maintenance of inter-satellite pointing. As the measurement accuracy of the two star cameras is not the same (see Section 3.3.4), such systematics is inevitable. This feature has crucial consequences on the attitude control and the gas consumption and it is further discussed in Chapter 6.

After zooming in, specific pitch variations are typical for different kind of events. Figure 4.7 shows the pitch variations along the orbit for approximately 4.5 months. Events such as CoM calibration maneuver, disabling of supplemental heater lines, Moon intrusion into SCA FoV, primary camera switches and switches to back-up science mode are obvious at first sight. This information is valuable to obtain indirect information about the satellite motion and to detect any irregular performance within the onboard laboratory in case of the absence of other data sources.

Although, the inter-satellite pointing variations are kept well within the deadband, the KBR inter-satellite ranging observations still need to be corrected for the imperfect pointing. This is done by applying so called antenna offset correction which is defined in the following section.

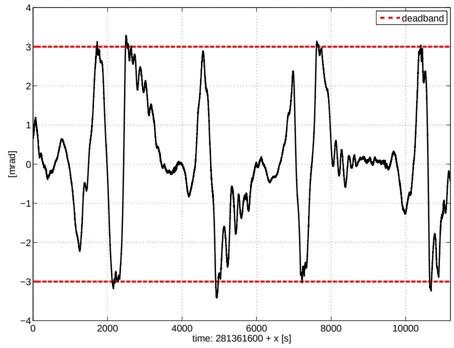

(a) roll

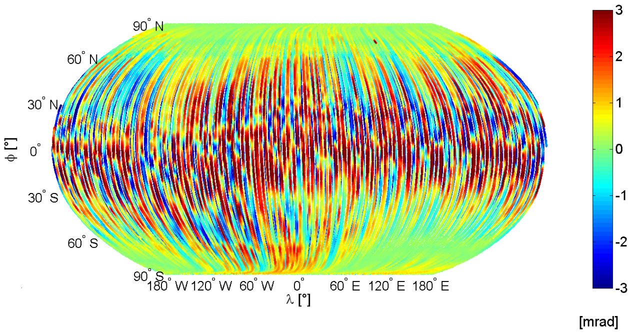

(b) roll

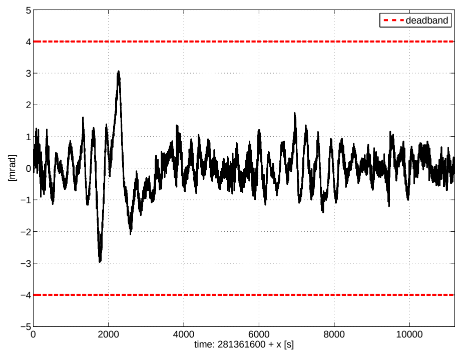

(c) pitch

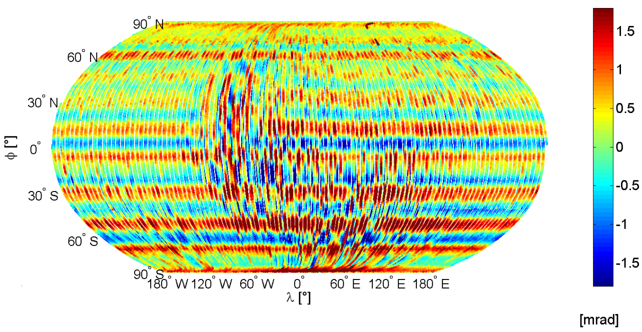

(d) pitch

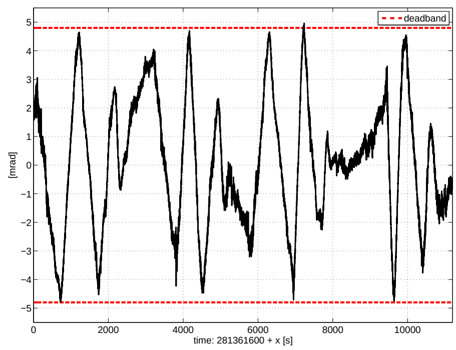

(e) yaw

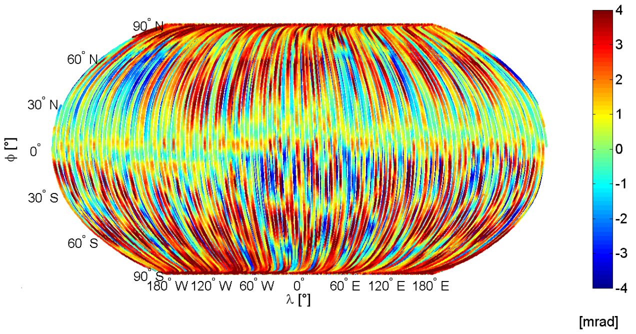

(f) yaw

Figure 4.5: The inter-satellite pointing variations expressed in terms of roll, pitch and yaw angles as time series plotted for two orbital periods together with the deadband (left column) and plotted with respect to the groundtrack for ascending orbit for a time span of 18 days (right column), recovered from the Level-0 data (THAD) for Dec 1st-18th,2008, GRACE-A

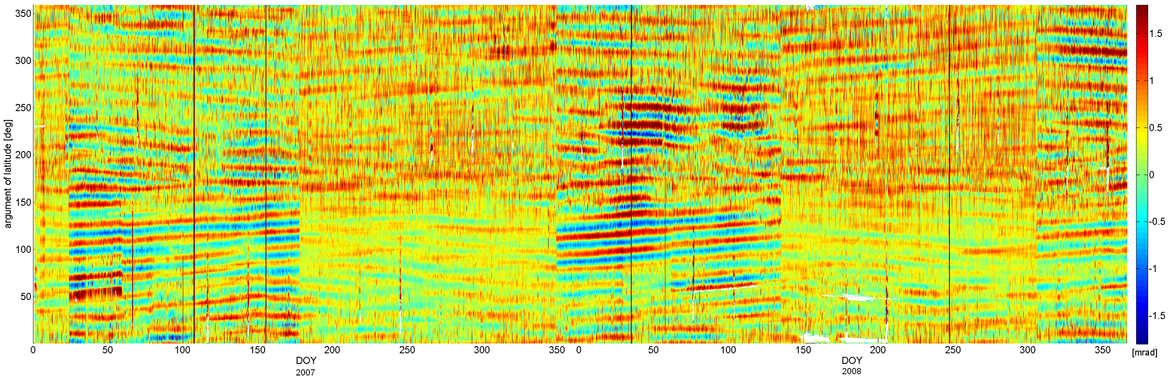

Figure 4.6: Variations of pitch inter-satellite pointing angle of GRACE-A in 2007 and 2008 plotted along the orbit, recovered from the THAD data

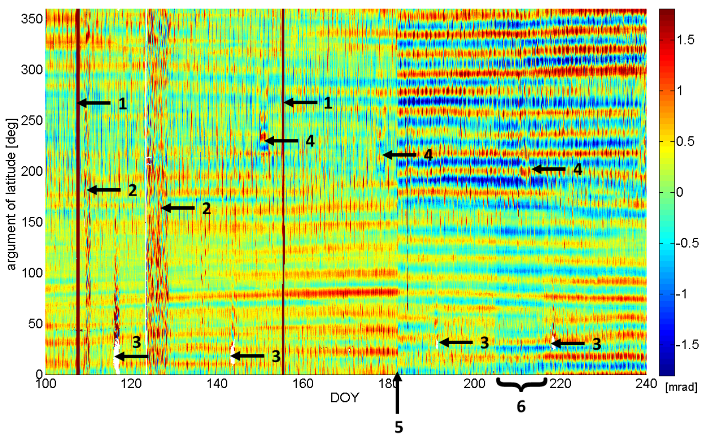

Figure 4.7: Long time series of pointing angles reflect well some events in the satellite operation. Here, the inter-satellite pointing pitch variations of GRACE-B in 2007 (April-August) are shown. Legend: 1 - Center of mass calibration maneuver, 2 - back-up science mode (the attitude was determined using SCA and IMU), 3 - simultaneous blinding of both SCA heads by the Sun and the Moon, followed by stronger attitude variations due to the residual stray light, 4 - short term primary camera switches due to blinding of the primary camera by the Moon, 5 - scheduled primary camera switch (β'=0), 6 - systematics due to the disabling of supplemental heater lines

4.5 Antenna offset correction

The KBR inter-satellite ranging observations are originally related to the KBR antenna phase center. However, for the purposes of the gravity field determination, the inter-satellite range, range rate and range acceleration have to be related to the center of mass of each satellite. This is done by applying so called antenna offset correction (AOC) which corrects for both the offset of the phase center from the center of mass and for the imperfect pointing, respectively.

The AOC for range (AOC_r) is the projection of the CoM-to-PhC vector of both satellites on the line-of-sight (Figure 4.8). The antenna offset correction for range rate ($AOC_{\dot{r}}$) and range acceleration ($AOC_{\ddot{r}}$) are then time derivatives of the AOC_r.

$$AOC_{\dot{r}} = \frac{d}{dt} AOC_r \tag{4.8}$$

$$AOC_{\ddot{r}} = \frac{d^2}{dt^2} AOC_r = \frac{d}{dt} AOC_{\dot{r}} \tag{4.9}$$

The antenna offset correction is determined based on the inter-satellite pointing pitch (θ) and yaw angles (ϕ) and their first ($\dot{\theta}$, $\dot{\phi}$) and second time derivatives ($\ddot{\theta}$, $\ddot{\phi}$) and on the length of the CoM-to-PhC vector ($|\mathbf{pc}|$) of both satellites GRACE-A and GRACE-B as follows

$$AOC_r = \sum_{i=A,B} |\mathbf{pc}_i| \cdot \cos\theta_i \cdot \cos\phi_i \tag{4.10}$$

$$AOC_{\dot{r}} = \sum_{i=A,B} -|\mathbf{pc}_i| \left(\dot{\theta}_i \sin\theta_i \cos\phi_i + \dot{\phi}_i \cos\theta_i \sin\phi_i\right) \tag{4.11}$$

$$\begin{aligned} AOC_{\ddot{r}} = \sum_{i=A,B} -|\mathbf{pc}_i|(\dot{\theta}_i^{\,2} \cos\theta_i \cos\phi_i + \ddot{\theta}_i \sin\theta_i \cos\phi_i - 2\dot{\theta}_i\dot{\phi}_i \sin\theta_i \sin\phi_i + \\ + \ddot{\phi}_i \cos\theta_i \sin\phi_i + \dot{\phi}_i^{\,2} \cos\phi_i \cos\theta_i) \end{aligned} \tag{4.12}$$

The antenna offset correction is computed and applied in the post-processing. The pitch and yaw pointing angles are computed from the GRACE Level-1B data as described in Section 4.3. The KBR phase center vector is obtained from the VKB1B data product. The AOC is also part of the official KBR1B data product. The order of magnitude of the AOC_r is about 2.9 m which is due to the PhC offset from the CoM. The order of magnitude of the $AOC_{\dot{r}}$ is about $\pm 0.5\,\mu\mathrm{m} \cdot \mathrm{s}^{-1}$ and of the $AOC_{\ddot{r}}$ about $\pm 0.2\,\mu\mathrm{m} \cdot \mathrm{s}^{-2}$.

Evidently, any systematic error in pointing angles and the PhC vector will directly affect the accuracy of the inter-satellite ranging observations and thus subsequently the accuracy of the gravity field model recovered from this data.

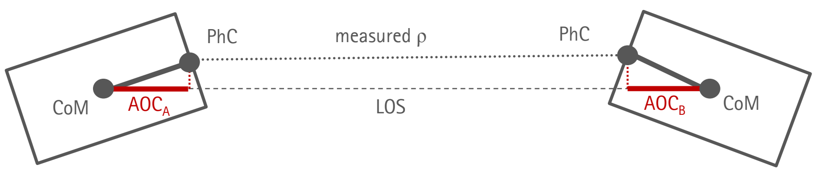

Figure 4.8: The antenna offset correction for range can be interpreted as projection of the CoM-to-PhC vector of each satellite on the line-of-sight. In this sketch, the $AOC_r = AOC_A + AOC_B$

4.6 Inconsistency of the QKS, QSA and VKB calibration parameters

The in-flight and on-ground determination of the inter-satellite pointing angles is different, not only in terms of the different input attitude and orbit solutions, but also in terms of the different calibration parameters needed in the data processing. Before presenting the comparison of the two sets of pointing angles, the relevant calibration parameters are introduced.

4.6.1 KBR calibration maneuver and the calibration parameters

For the determination of the inter-satellite pointing, three core calibration parameters, QKS, QSA and VKB, are required, which are related to the star cameras and to the KBR antenna phase center.

The QKS quaternions are needed in the in-flight data processing. They rotate the measured star camera data from the individual Star Camera Frame into K-Frame (Figure 4.9).

The QSA and the VKB calibration parameters are needed in the on-ground data processing. The QSA quaternions rotate the measured attitude data from the individual Star Camera Frame into the common Science Reference Frame (cf. Figure 4.9), where the attitude data are combined if possible. This star camera data processing is denoted as Level-1A to Level-1B data processing and is described in detail in Chapter 5. As the SRF axes are parallel to the accelerometer axes, the QSA quaternions actually represent the misalignment of the star cameras relative to the accelerometer. The VKB provides the coordinates of the CoM-to-PhC vector in the SRF coordinates. Based on this vector, the rotation from the SRF into K-Frame can be determined.

Obviously, QKS and QSA+VKB provide information about the same rotation, namely from the Star Camera Frame into K-Frame. Hence it is expected that the satellite's attitude obtained by the rotation of the measured quaternions from the SCF into the K-Frame according to these two approaches, will be the same. As we show in the following section, indeed, this is not the case.

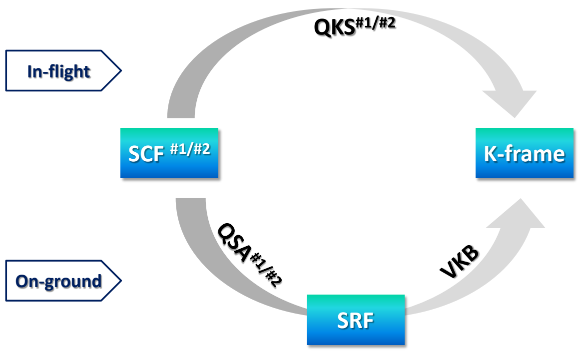

Figure 4.9: The rotation from the Star Camera Frame (SCF) into K-Frame is defined either by the QKS quaternions directly, or by the QSA quaternions and VKB coordinates of the KBR antenna phase center. The rotation using QKS is used in the in-flight data processing. In the on-ground processing, the rotation is performed via Science Reference Frame (SRF) using the QSA and VKB data

The values of these calibration parameters can be found in the corresponding data products: QKS1B, QSA1B or VKB1B (Case *et al.*, 2010). In the early phase of the mission, the values of these parameters differ slightly. The final values were estimated based on the measurements during the calibration maneuver of the KBR assembly (further noted as KBR calibration maneuver). The KBR calibration maneuver was performed in February 2003 for GRACE-B and in March 2003 for GRACE-A.

The KBR calibration maneuver was carried out as a periodic oscillation maneuver. While one satellite was oscillated by applying suitable torques about one selected axis, the other satellite was kept in its nominal attitude. Each satellite was oscillated first about yaw axis and subsequently about pitch axis within a certain attitude range while the variations about the other two axes were kept minimal. This means that four submaneuvers were performed: wiggling about yaw of GRACE-A, wiggling about pitch of GRACE-A and the same for GRACE-B. A detailed description of the calibration maneuver and the calibration estimation algorithms can be found in Wang (2003).

The main purpose of the calibration maneuver was to determine the location of the phase centers of the two KBR antennas. During the calibration maneuver the satellites were intentionally brought into relatively large angular motion (few degrees), which was detected by both the star cameras and the accelerometer. Therefore, along with the KBR antenna phase center, the misalignment of the star cameras with respect to the accelerometer could be determined as well.

The KBR calibration maneuver was performed only once during the mission operation. The values of the calibration parameters, however, were estimated twice. The first release of the calibration parameters was published in 2003 and was implemented in the standard processing routines for generating the Level-1B Release 01 data. In 2011, the data from the calibration maneuver were reprocessed while using improved GRACE orbits and GPS clock solutions (Kruizinga *et al.*, 2012). In the standard processing routines, the original QSA and VKB values were substituted by the new estimated values, which resulted in Level-1B Release 02 data. One of the major reasons for the re-processing was the large bias of the pointing angles, which is discussed thoroughly in the following section.

4.6.2 Pointing bias

The in-flight and the on-ground solution of the inter-satellite pointing angles differ significantly. The comparison of the in-flight and on-ground determined inter-satellite pointing roll, pitch and yaw angles is shown in Figure 4.10 in terms of time series for 2 orbital periods and in Figure 4.11 in terms of daily mean values of the RPY differences for a period of 2 years. The in-flight computed RPY angles were recovered from the Level - 0 THAD data. The on-ground solution was computed from both Level-1B Release 01 and Release 02 data.

At first sight, the major difference between these three solutions is their mutual bias. While the long-term mean value of the onboard computed pointing angles is below 0.03 mrad for all angles, the long-term mean value of the pointing angles based on the Level-1B data reach up to 2.8 mrad for Release 01 and 2.5 mrad for Release 02. The long-term mean values of the individual angles obtained from Level-1B Release 01 and Release 02 are given in Table 4.1. These values were computed based on RPY time series from two years, 2007 and 2008.

The pointing angles obtained from the Level-1B Release 02 data are characterized by significantly decreased bias compared to Release 01, especially in case of pitch and yaw angle. The differences between the Release 01 and Release 02 solutions are caused especially by the new estimated values of the QSA and VKB parameters, cf. Section 4.6.1. The pitch and yaw bias is of high interest, because the pitch and yaw angles are one of the core inputs for the computation of the antenna offset correction. Therefore any systematic error in these pointing angles will directly affect the inter-satellite ranging observations. The impact of the bias on the AOC is shown in the following section.

Considering the requirements on the inter-satellite pointing and the SCA and KBR measurement accuracy, the RPY bias is unexpectedly large and its source needs to be understood. The in-flight and on-ground solution differ in the input orbit and attitude data and also in the different calibration parameters needed in the data processing, i.e. QKS and QSA+VKB, respectively. The hypothesis is that the differences of the in-flight and on-ground orbit and attitude solutions would not cause such systematic bias. Instead, the bias is assumed to be caused by inconsistency of these three calibration parameters.

In order to prove that, two test solutions of RPY angles based on the same orbit and attitude data were generated and compared. The test solutions were obtained once for Release 01 data and once for Release 02 data. As input, the SCA1A quaternions from the primary camera and the GNV1B orbit data were used. The first test solution was obtained according to the approach presented in Section 4.2, in which the SCA1A data were rotated into K-Frame using the QKS. The second test solution was obtained according to the approach presented in Section 4.3, in which the SCA1A data were rotated using QSA and VKB into K-Frame via SRF (cf. also Figure 4.9). In both cases the LOS was obtained from the GNV1B orbit solution rotated into inertial frame. Hence, the only difference between the two generated sets of pointing angles were solely the calibration parameters used for the derivation of the $\mathbf{R}_{KF\rightarrow LOS}$ attitude matrix. The comparison of these two test data sets (not shown here) reveals the same RPY bias as given in Table 4.1. This means that the bias of the inter-satellite pointing angles, indeed, is caused by the inconsistency in the QKS and QSA + VKB parameters. As shown in Figure 4.9, theoretically they are expected to provide the same rotation, which in the reality is not the case.

As shown in Figure 4.11 the pointing RPY biases are relatively constant over long period of time. However, small temporal variations exist with a characteristic period of 322 d. Same temporal variations of the roll and yaw bias are present also in the THAD data. In case of pitch bias, distinct jumps up to 0.3 mrad occur at the time of primary camera switches. These jumps are present only in the on-ground solution derived from the Level-1B data. The reason for these jumps remains to be understood.

Table 4.1: Inter-satellite pointing bias of both GRACE-A and GRACE-B obtained as long-term mean value of the roll $\overline{\psi}$, pitch $\overline{\theta}$ and yaw $\overline{\phi}$ angles which were computed based on Level-1B Release 01 (RL01) and Release 02 (RL02) data from 2007 and 2008

	GRACE-A		GRACE-B	
	RL01	RL02	RL01	RL02
$\overline{\psi}$ [mrad]	2.82	2.45	-0.78	-0.44
$\overline{\theta}$ [mrad]	-0.11	0.63	1.58	-0.08
$\overline{\phi}$ [mrad]	2.59	-0.31	-1.70	0.29

4.6.3 Impact of the pointing bias on the antenna offset correction

The pointing bias crucially affects the antenna offset correction which is applied on the inter-satellite ranging observations. The impact of the bias on the AOC is demonstrated in Figure 4.12. Because the AOC for range, AOC_r, is obtained by the projection of the CoM-to-PhC vector on the LOS, its length strongly depends on the angle between CoM-to-PhC vector and the LOS, i.e. bigger angles result in shorter AOC_r. The bias represents the mean value of the pointing angle variations, hence when considering the full range of variations, the AOC_r related to the biased solution differs very significantly from that related to the solution with zero mean value. As the AOC for range rate, $AOC_{\dot{r}}$, and for range acceleration, $AOC_{\ddot{r}}$, are derived as the first and second time derivatives of the AOC_r, they are affected by the bias as well.

The effect of the pointing bias on the AOC is demonstrated in Figure 4.13. The first data set was derived from the in-flight computed pointing angles characterized with zero mean value (<0.03 mrad). The second data set was derived from the pointing angles computed from the Level-1B data, which are characterized by the non-zero mean value, cf. Table 4.1. The comparison is shown for both Level-1B Release 01 and Release 02. Especially in case of Level-1B Release 01, the differences relative to the in-flight solution are very large, reaching up to 40 μm for AOC_r, 0.7 $\mu\mathrm{m}\cdot\mathrm{s}^{-1}$ for $AOC_{\dot{r}}$ and 0.3 $\mu\mathrm{m}\cdot\mathrm{s}^{-2}$ for $AOC_{\ddot{r}}$, which is above the KBR

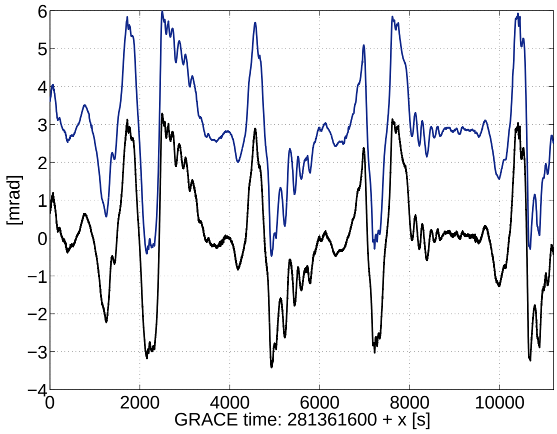

(a) roll

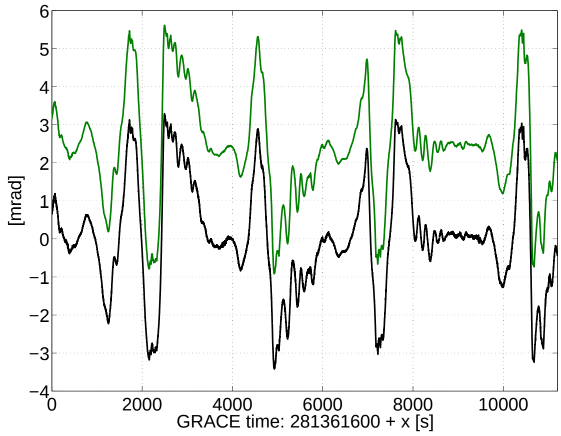

(b) roll

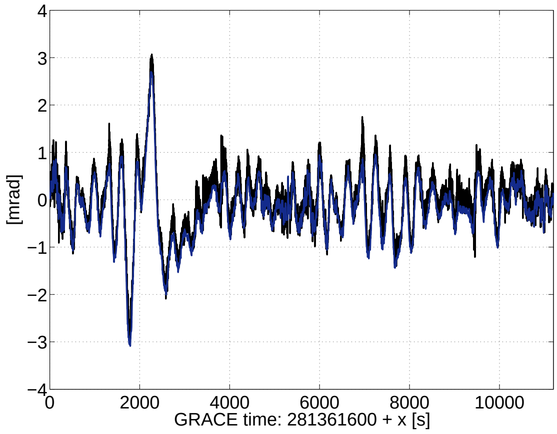

(c) pitch

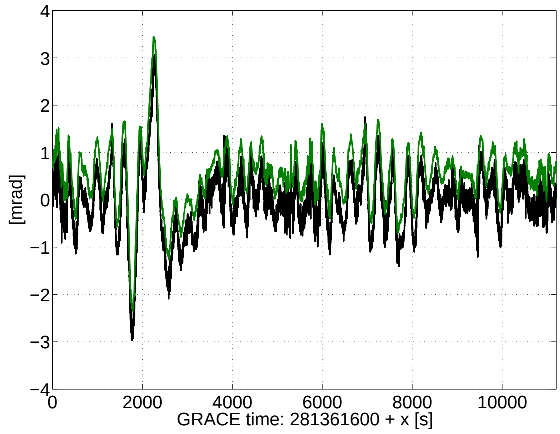

(d) pitch

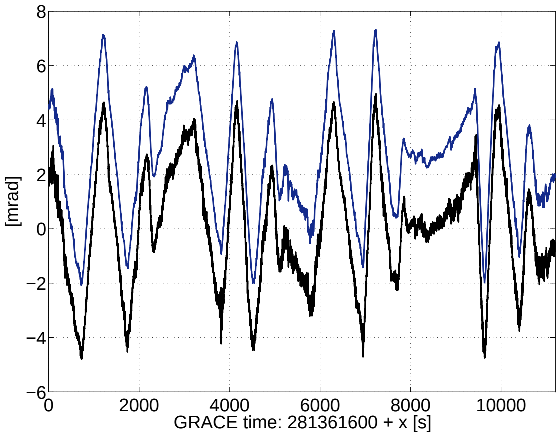

(e) yaw

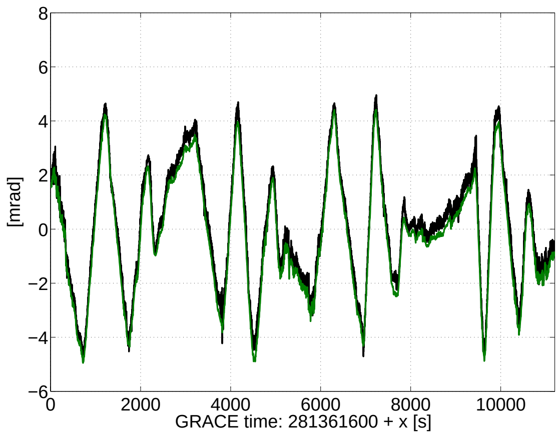

(f) yaw

Figure 4.10: Comparison of the in-flight and on-ground determined inter-satellite pointing angles. The black curves in all figures represent the pointing angles which were computed directly onboard the satellites. The blue and green curves represent the pointing angles recovered from the Level-1B Release 01 (left column) and Level-1B Release 02 (right column) data. Based on GRACE-A data from Dec 1st, 2008

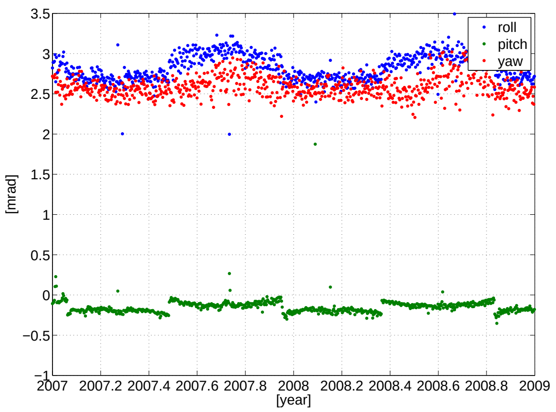

(a) GRACE-A RL01

(b) GRACE-A RL02

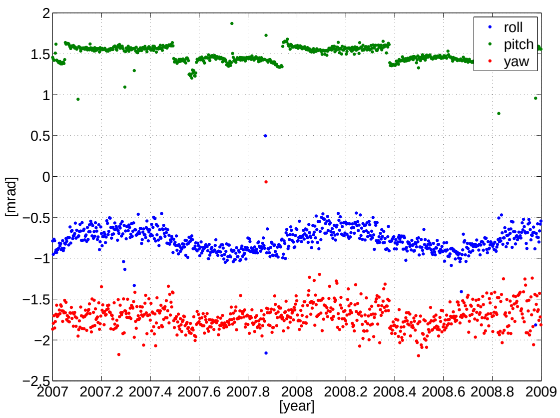

(c) GRACE-B RL01

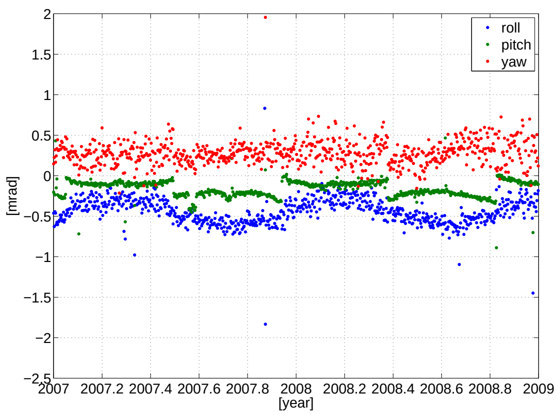

(d) GRACE-B RL02

Figure 4.11: Bias of the inter-satellite pointing roll, pitch and yaw angles computed based on Level-1B Release 01 (RL01) and Release 02 (RL02) data for both GRACE-A and GRACE-B in 2007 and 2008

ranging measurement accuracy. As the bias of the Release 02 pointing angles was reduced significantly, also the impact on the AOC decreased.

The impact of the biased AOC on the inter-satellite ranging observations turned out to be very crucial, especially in case of Level-1B Release 01 data. The problem of the pointing bias was pointed out by Horwath *et al.* (2010). The authors thoroughly investigated the effect of the pointing bias on the gravity field models. They showed that the effect on time-variable gravity field solutions generated at CNES/GRGS was in the order of 6-11 times the GRACE error baseline. The authors, however, did not discuss the possible source for this pointing bias. This was originally discussed by Bandikova *et al.* (2010). These studies became one of the key impulses for JPL to re-estimate the calibration parameters related to the star cameras and the KBR antenna phase centers in 2011, which resulted in Level-1B Release 02 data (cf. Section 4.6.1). Subsequently, major improvement of the gravity field models was achieved. The accuracy of the newly derived gravity field models based on Level1B Release 02 data, e.g. CSR RL05, significantly increased compared to the previous models, CSR RL04 (cf. Figure 2.9).

Although the in-flight pointing angles are characterized by the zero mean value, it does not necessarily mean that they are more accurate than the on-ground solution. Because of the lack of reference, it is not possible to state which of the two solutions is more accurate. The analysis of the in-flight data only proves that based on the input data the AOCS is capable to keep the satellites in the required orientation. Yet, the major challenge, i.e. the determination of the actual KBR antenna phase center, still remains.

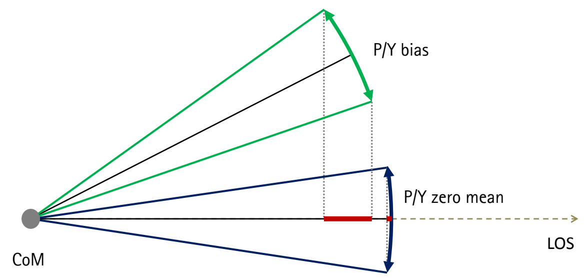

Figure 4.12: Demonstration of the effect of the pointing bias on antenna offset correction for range, while considering the pointing pitch (P) and yaw (Y) angles variations with zero mean value (blue) and with a bias (green)

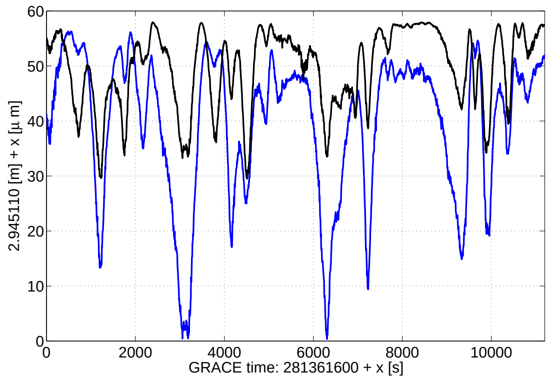

(a) AOC_r

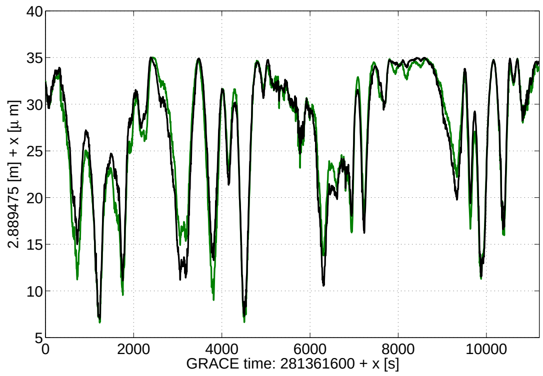

(b) AOC_r

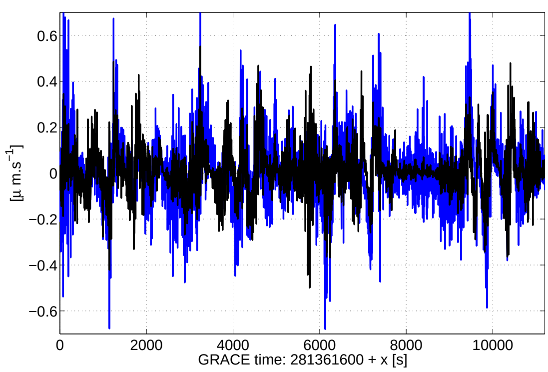

(c) $AOC_{\dot{r}}$

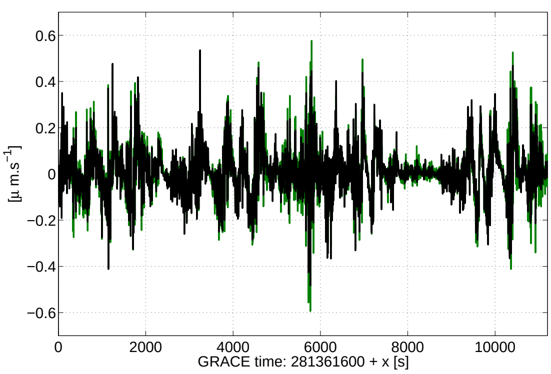

(d) $AOC_{\dot{r}}$

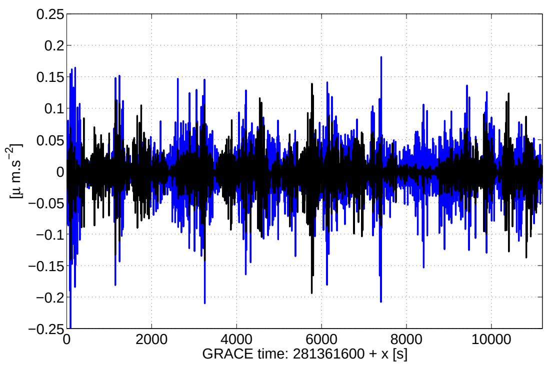

(e) $AOC_{\ddot{r}}$

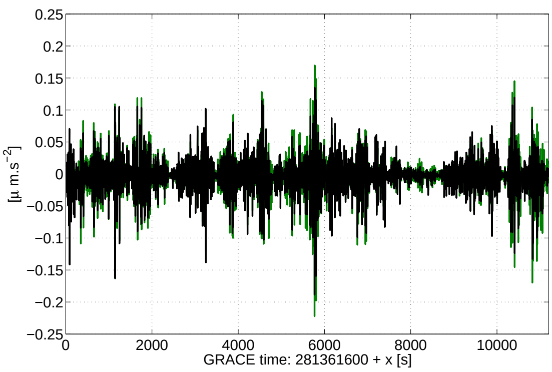

(f) $AOC_{\ddot{r}}$

Figure 4.13: Comparison of the antenna offset correction for range AOC_r, range rate $AOC_{\dot{r}}$ and range acceleration $AOC_{\ddot{r}}$ derived from the in-flight computed pointing angles characterized by zero mean value (black) with AOC derived from the Level-1B Release 01 (blue, left column) and Release 02 (green, right column) which are both characterized by non-zero mean value. Shown for GRACE-A 2 orbital periods on Dec 1st, 2008

If something is not impossible,
there must be a way of doing it.

- Sir Nicholas Winton -

5 Improved star camera attitude data

In this chapter we focus on the star camera Level-1A to Level-1B data processing, in which the final attitude solution (SCA1B) is obtained from the original observations (SCA1A) by their rotation into Science Reference Frame and their combination, if applicable. The final attitude solution is expected to be characterized by high accuracy about all three axes. However, the analysis of SCA1B Release 02 revealed their unexpectedly higher noise, cf. Section 5.1. As the star camera data are essential for the processing of the K-band ranging data, the accelerometer data and GPS data, their best possible accuracy is of high importance and priority. Therefore, in the following, we present a full reexamination of the SCA data processing from Level-1A to Level-1B with focus on the combination method of the attitude quaternions.

Two different combination methods are discussed in detail and applied on the GRACE attitude data. The first method introduces the information about the anisotropic accuracy of the star camera measurement in terms of a weight matrix (cf. Section 5.2.1). This method is also applied in the official processing, which is done by JPL. The alternative method merges only the well determined SCA boresight directions (cf. Section 5.2.2). This method is implemented on the GRACE SCA data for the first time. In the first step, these combination methods are compared (see Section 5.2.3). In the second step, the newly generated attitude solution is compared with the official SCA1B RL02 data in order to find the reason for its higher noise. The analysis of the differences of these two solutions is presented in Section 5.3. This analysis also proves that contrary to the SCA1B RL02, our generated attitude solution carries the full accuracy about all three axes. Subsequently, the effect of the improved SCA data on the fundamental scientific observations (Section 5.4) and on the GRACE monthly solutions (Section 5.5) is discussed. Note, part of the results presented in this chapter were already published by Bandikova and Flury (2014).

5.1 The GRACE SCA1B RL02 data

The GRACE SCA1B data provide information about the attitude of the spacecraft, represented by the Science Reference Frame, with respect to the inertial frame. The SCA1B data are derived from the SCA1A data, which are the measured attitude quaternions delivered by the SCA head#1 and head#2. The processing of the star camera data from Level-1A to Level-1B requires not only data combination and rotation from the individual Star Camera Frame into Science Reference Frame using the QSA quaternions, but also discarding of invalid data, sign flip, application of timetag correction, resampling and interpolation to integer 5 s (Wu *et al.*, 2006). The sign flip is needed because the quaternions are characterized by sign ambiguity as q and $-q$ represent the same rotation. The timetag correction is applied using the precise clock solution (CLK1B). The data combination is possible only for periods, when valid data from both SCA heads are available. The order of these processing steps is sketched in Figure 5.3.

Because of the characteristic anisotropic noise of the star camera measurement (see Section 3.3.4), the rotation from the SCF into SRF is affected by the unfavorable noise propagation, which is demonstrated in Figure 5.1. This figure shows the original attitude data in terms of angular rates[1] in the Star Camera Frame and in the Science Reference Frame, in both time and frequency domain. While in the SCF the rotation about $\mathbf{x}_{SCF}$ and $\mathbf{y}_{SCF}$ can be determined well and only the rotation about the $\mathbf{z}_{SCF}$ can be determined about a factor κ less accurately, in the SRF due to the noise propagation, only rotation about $\mathbf{x}_{SRF}$ axis can be determined with high accuracy contrary to the rotation about $\mathbf{y}_{SRF}$ and $\mathbf{z}_{SRF}$ axes.

The unfavorable noise propagation is the reason why the data from the two SCA heads are combined if possible. Thanks to the geometry of the SCA mounting, the noise of the rotated data can be efficiently reduced in such a way that the combined attitude solution is characterized by the full accuracy about all three axes. Obviously, the combination of the attitude quaternions is possible only when valid data from both SCA heads are available. This is not always the case because of the camera blinding by the sunshine or the moonlight. The availability of the SCA data is shown in Figure 3.11. In those periods, when the attitude data only from one star camera is available, the high noise of the SCA1B data is inevitable. For illustration see Figure 5.5.

Our analysis of the latest release of the star camera Level-1B data, the SCA1B Release 02 (RL02), focuses on those periods, when the attitude solution was obtained by the data combination. It is expected that the combined solution should be characterized by high accuracy about all three axes. However, the analysis of the combined data revealed their unexpectedly higher noise, cf. Figure 5.2. The noise level of the angular rates about the $\mathbf{y}_{SRF}$ and $\mathbf{z}_{SRF}$ is 4 times higher than the noise of the angular rates about the $\mathbf{x}_{SRF}$ axis. This means the noise due to the data rotation still partially propagates into the combined solution. This indicates that there might be some imperfections in the combination method applied in the official data processing. Therefore, in the following sections, a complete review of the star camera Level-1A to Level-1B data processing is presented with the main focus on the SCA data combination methods.

5.2 Star camera data combination methods

The combination of the attitude data delivered by multiple star camera heads is included in the data processing standards of all three gravity field missions, CHAMP, GRACE and GOCE. Two methods are commonly used for the star camera data combination. The first method introduces the anisotropic noise distribution as weighted information for the measurement. The other method merges only the well determined boresight directions. Both methods are expected to provide attitude information which carries the full accuracy about all three axes (Jørgensen *et al.*, 2008).

In the following, the mathematical background of these two combination methods and their implementation on the GRACE SCA1A data is presented. Based on these methods two star camera attitude solutions equivalent to the SCA1B solution were generated. All necessary processing steps, such as outlier discarding, sign flip, applying of timetag correction, downsampling and interpolation, were included, but are not further discussed here. The two generated attitude solutions allow mutual comparison of the combination methods and their efficiency of noise reduction. The combination of the SCA data is performed at the level of quaternions. The quaternion algebra is described in Appendix C.

[1] Note, the presentation of the attitude data and their noise level in terms of angular rates is more suitable than their presentation in terms of attitude angles. For angular rates, the characteristic noise level is obvious at first sight in both time and frequency domain, which is not the case for the attitude angles, cf. Figure 3.12. Therefore, in the following, we present the analysis results only in terms of angular rates.

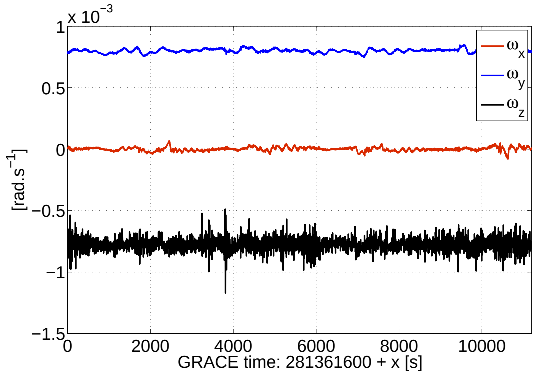

(a) SCF

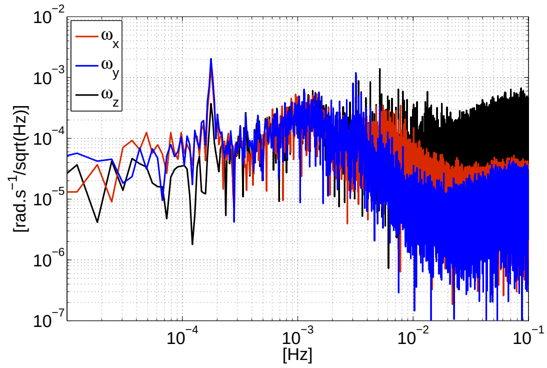

(b) SCF

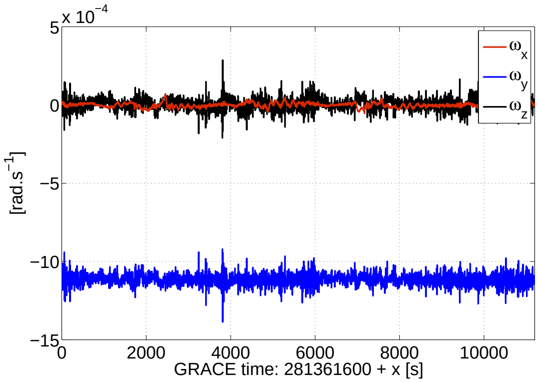

(c) SRF

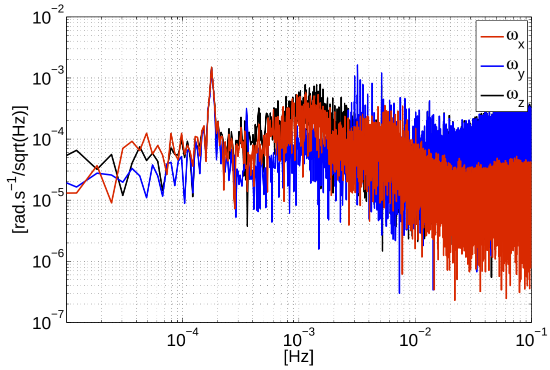

(d) SRF

Figure 5.1: Demonstration of noise propagation after SCA data rotation from SCF into SRF. The figures (a, b) show the measured attitude in terms angular rates about the Star Camera Frame axes in time (a) and frequency domain (b), and demonstrate the anisotropic accuracy of the SCA measurement. Figures (c, d) show the satellite's attitude in terms of angular rates about the Science Reference Frame and herewith demonstrate the unfavorable noise propagation after rotation of the single camera data from SCF into SRF. Based on GRACE-A SCA1A data from head#1 on Dec 1st, 2008, the data sample was downsampled to 0.2 Hz

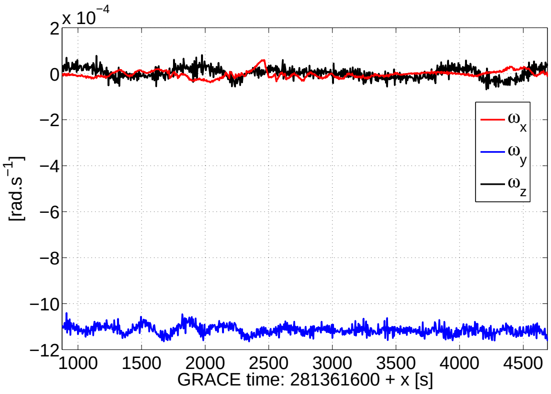

(a)

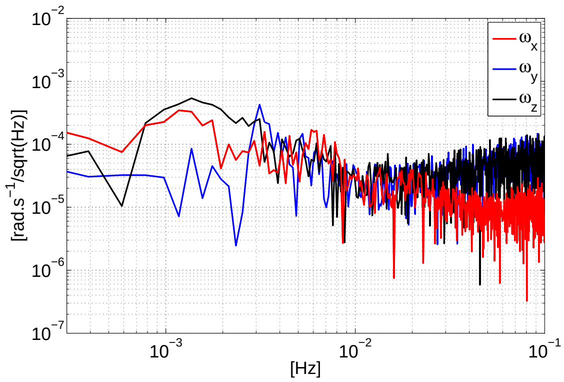

(b)

Figure 5.2: Demonstration of the unexpected higher noise of the SCA1B RL02 data. The figures show the spacecraft's attitude in terms of angular rates about SRF axes in time (a) and frequency domain (b). In the selected period the attitude data were obtained by combination of the data from both SCA heads. The noise level of the attitude about $\mathbf{y}_{SRF}$ and $\mathbf{z}_{SRF}$ is 4 times higher than the noise level of the attitude about the $\mathbf{x}_{SRF}$. Shown for GRACE-A SCA1B RL02 data from Dec 1st, 2008

5.2.1 Combination method based on a weight matrix

The first SCA data combination method was developed by L. Romans (Romans, 2003) and it integrates the information about the anisotropic noise of the SCA measurement in form of a weight matrix. This method is implemented in the GRACE and the GOCE official SCA data processing (Wu *et al.*, 2006; Siemes, 2011). The advantage of this combination method is that data from not only two SCA heads but also from three and more SCA heads can be combined simultaneously, which is not straightforward for the alternative combination method presented in the following section.

When implementing this combination method in the SCA Level-1A to Level-1B data processing, the quaternions delivered by the individual SCA heads are first rotated into the SRF and then these rotated quaternions are combined. Here we sum up general solution for the two GRACE star camera heads; the whole theory can be found in Romans (2003).

As first, the original attitude quaternions delivered by the SCA head #1 and #2, i.e. Q_1, Q_2, are rotated from the Star Camera Frame into Science Reference Frame by their multiplication with the QSA quaternions, denoted as Q_i^{QSA}:

$$\tilde{Q}_i = Q_i \cdot Q_i^{QSA} \qquad , \; i = 1, 2 \tag{5.1}$$

Theoretically, the two SCA heads should deliver the same attitude. However, small differences exist and are computed as follows

$$(1, \frac{1}{2}\Delta_{12}) = \tilde{Q}_1^{-1}\tilde{Q}_2 \tag{5.2}$$

where $\tilde{Q}_1, \tilde{Q}_2$ are the quaternions giving the attitude of the Science Reference Frame with respect to the inertial frame. $(1, \frac{1}{2}\Delta_{12})$ is again a 4-element quaternion, which is assumed to be close to unity.

The anisotropic measurement noise is expressed in terms of a weight matrix $\mathbf{P}_i$, which reflects the fact that the roll about the SCA boresight axis ($\mathbf{z}_{SCF}$) is κ times less accurate than pointing of the boresight, i.e. the attitude about the other two axes ($\mathbf{x}_{SCF}$ and $\mathbf{y}_{SCF}$). ϵ_i represents the sensor measurement noise about the high-sensitive axes, which is nominally assumed to be 30 μrad, cf. Section 3.3.4.

$$\mathbf{P}_i = \frac{1}{\epsilon_i^2} \begin{bmatrix} 1 & 0 & 0 \\ 0 & 1 & 0 \\ 0 & 0 & \frac{1}{\kappa^2} \end{bmatrix} \tag{5.3}$$

These weighted matrices are defined in the Star Camera Frame and hence need to be rotated into the Science Reference Frame as follows

$$\tilde{\mathbf{P}}_i = \mathbf{R}_{SCF_i \to SRF} \cdot \mathbf{P}_i \cdot (\mathbf{R}_{SCF_i \to SRF})^T \tag{5.4}$$

The rotation matrices $\mathbf{R}_{SCF_i \to SRF}$ are derived from the alignment parameters of the individual star camera heads with respect to the SRF, which are represented by the QSA quaternions.

Finally, the optimal quaternion $Q^\star$, i.e. combined and rotated into SRF, is obtained as

$$Q^\star = \tilde{Q}_1 \cdot (1, \frac{1}{2}(\tilde{\mathbf{P}}_1 + \tilde{\mathbf{P}}_2)^{-1}\tilde{\mathbf{P}}_2\Delta_{12}) \tag{5.5}$$

For the generation of our SCA data series, we set the variables as recommended in Wu *et al.* (2006), i.e.
$\kappa = 8$, $\epsilon_1 = \epsilon_2 = 30\,\mu$rad, $\mathbf{P}_1 = \mathbf{P}_2$ and

$$\mathbf{R}_{SCF_{1,2}\to SRF} = \begin{bmatrix} 1 & 0 & 0 \\ 0 & -\frac{1}{\sqrt{2}} & \pm\frac{1}{\sqrt{2}} \\ 0 & \mp\frac{1}{\sqrt{2}} & -\frac{1}{\sqrt{2}} \end{bmatrix} \tag{5.6}$$

hence arriving at (part of Equation 5.5):

$$(\tilde{\mathbf{P}}_1 + \tilde{\mathbf{P}}_2)^{-1}\tilde{\mathbf{P}}_2 = \frac{1}{2}\begin{bmatrix} 1 & 0 & 0 \\ 0 & 1 & -\frac{\kappa^2-1}{\kappa^2+1} \\ 0 & -\frac{\kappa^2-1}{\kappa^2+1} & 1 \end{bmatrix} \tag{5.7}$$

Note, $\mathbf{R}_{SCF_{1,2}\to SRF}$ matrix is needed solely for the rotation of the weight matrix into SRF, hence using an approximate SCA/ACC alignment, i.e. a nadir offset of $\pm 45°$, instead of the exact alignment given by QSA, is satisfactory.

Based on this combination method, the SCA1A data were processed to SCA1B data. The scheme of this SCA1A to SCA1B data processing is sketched in Figure 5.3. The timetag correction was derived from the satellite clock solutions stored in CLK1B data product. The newly generated attitude data are tagged as "SCA1B IfE"[2] and the quantities derived from this data are tagged as "IfE". Setting the κ, ϵ and $\mathbf{P}$ variables as recommended in Wu *et al.* (2006) allows for comparison of our solution to the official SCA1B RL02 generated by JPL, which is presented in Section 5.3.

5.2.2 SCA combination by merging exclusively the boresight axes

The alternative combination method is based on a different principle, namely on merging exclusively the boresight axes of the two star cameras into a so called Common Reference Frame (CR). This way, the uncertainty in the rotation about the SCA boresight axis is completely omitted. This combination method was developed by GFZ for the processing of the CHAMP SCA data (Mandea *et al.*, 2010). This method was also tested for GOCE star camera data (Stummer *et al.*, 2011). For GRACE SCA data, however, this method is implemented here for the first time. The details of the implementation are presented in the following.

The Common Reference Frame can be defined either as suggested by Mandea *et al.* (2010)

$$\begin{aligned} \mathbf{x}_{CR} &= -\frac{\mathbf{z}_1 \times \mathbf{z}_2}{|\mathbf{z}_1 \times \mathbf{z}_2|} \\ \mathbf{y}_{CR} &= \mathbf{z}_{CR} \times \mathbf{x}_{CR} \\ \mathbf{z}_{CR} &= -\frac{\mathbf{z}_1 + \mathbf{z}_2}{|\mathbf{z}_1 + \mathbf{z}_2|} \end{aligned} \tag{5.8}$$

or as suggested by Jørgensen *et al.* (2008)

$$\mathbf{x}_{CR} = \frac{\mathbf{z}_1 + \mathbf{z}_2}{|\mathbf{z}_1 + \mathbf{z}_2|}$$

[2] IfE stands for Institut für Erdmessung

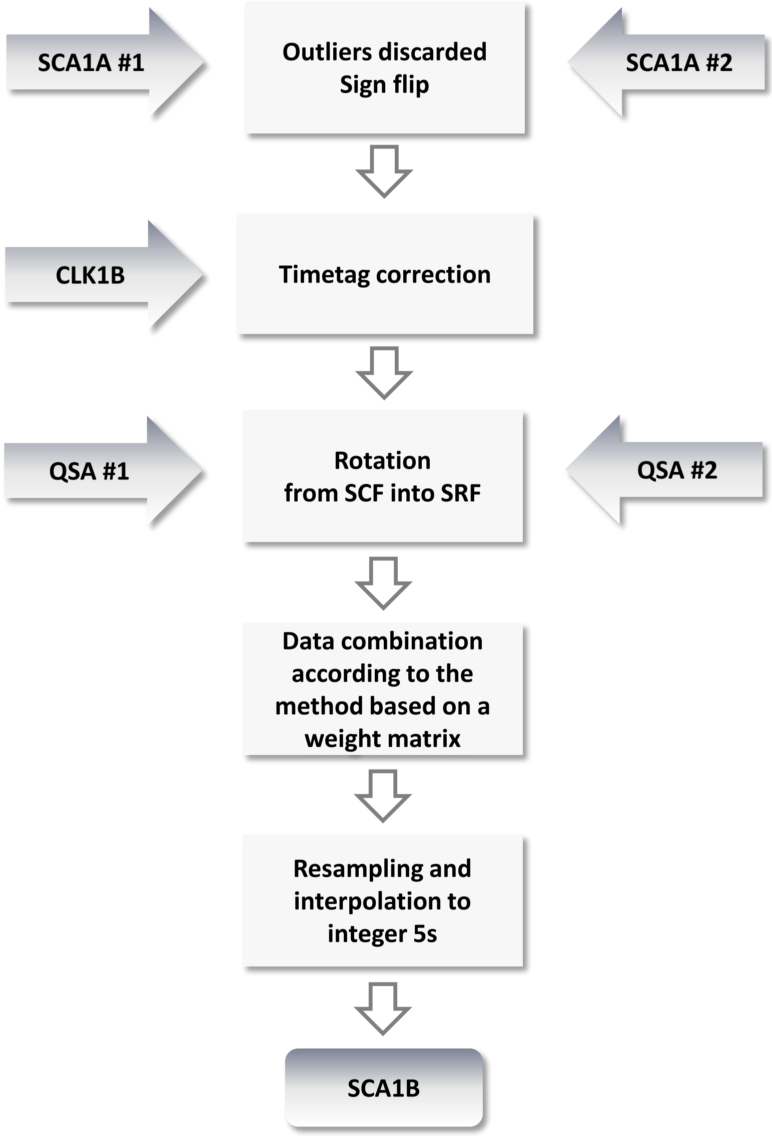

Figure 5.3: Scheme of the GRACE star camera Level-1A to Level-1B processing while implementing the method for SCA data combination based on a weight matrix

$$\begin{aligned} \mathbf{y}_{CR} &= \frac{\mathbf{z}_1 - \mathbf{z}_2}{|\mathbf{z}_1 - \mathbf{z}_2|} \\ \mathbf{z}_{CR} &= \mathbf{x}_{CR} \times \mathbf{y}_{CR} \end{aligned} \tag{5.9}$$

We tested both choices and both give an attitude solution with exactly the same accuracy. For this reason, from now on, we stick to Equation 5.8. Figure A.8 shows the accommodation of the CR obtained from Equation 5.8 in the satellite body.

When applying this method on the Level-1A quaternions, first the attitude data from the two star camera heads are simultaneously combined and rotated into the Common Reference Frame, followed by their rotation into the Science Reference Frame. This is done in three steps.

In the first step, the Common Reference Frame is formed by merging the two SCA boresight axes. The boresight axis $(\mathbf{z}_1, \mathbf{z}_2)$ can be extracted from the direction cosine matrix $\mathbf{R}_{iner \to SCF_i}$ derived from the original quaternions Q_1, Q_2 according to Equation B.7. This matrix describes the rotation from the inertial frame into the Star Camera Frame as it gives the SCF axis triad $\{\mathbf{x}_i, \mathbf{y}_i, \mathbf{z}_i\}$ in the inertial coordinates.

$$Q_i \to \mathbf{R}_{iner \to SCF_i} = \begin{bmatrix} x_{1,i} & x_{2,i} & x_{3,i} \\ y_{1,i} & y_{2,i} & y_{3,i} \\ z_{1,i} & z_{2,i} & z_{3,i} \end{bmatrix} = \begin{bmatrix} (\mathbf{x}_i)^T \\ (\mathbf{y}_i)^T \\ (\mathbf{z}_i)^T \end{bmatrix} \tag{5.10}$$

with $i = 1, 2$ for SCA head #1 and head #2

Using the boresight vectors $\mathbf{z}_1$, $\mathbf{z}_2$, the Common Reference Frame $\{\mathbf{x}_{CR}, \mathbf{y}_{CR}, \mathbf{z}_{CR}\}$ is obtained by applying Equation 5.8. From these vectors, a direction cosine matrix is derived which describes the rotation from the inertial frame into CR.

$$\begin{bmatrix} (\mathbf{x}_{CR})^T \\ (\mathbf{y}_{CR})^T \\ (\mathbf{z}_{CR})^T \end{bmatrix} = \mathbf{R}_{iner \to CR} \tag{5.11}$$

In the second step, direction cosine matrix giving the rotation from the Common Reference Frame into Science Reference Frame $(\mathbf{R}_{CR \to SRF})$ is derived from the QSA quaternions. At first, it is necessary to obtain the SCA boresight axes in SRF coordinates $(\hat{\mathbf{z}}_1, \hat{\mathbf{z}}_2)$. This can be done by the transformation of the QSA quaternions into a rotation matrix and its transposition, hence we get the $\mathbf{R}_{SRF \to SCF_i}$ describing SCF axis triad in SRF coordinates $\{\hat{\mathbf{x}}_i, \hat{\mathbf{y}}_i, \hat{\mathbf{z}}_i\}$

$$Q_i^{QSA} \to \mathbf{R}_{SCF_i \to SRF} \xrightarrow{T} \mathbf{R}_{SRF \to SCF_i} = \begin{bmatrix} (\hat{\mathbf{x}}_i)^T \\ (\hat{\mathbf{y}}_i)^T \\ (\hat{\mathbf{z}}_i)^T \end{bmatrix} \tag{5.12}$$

The boresight vectors $\hat{\mathbf{z}}_1, \hat{\mathbf{z}}_2$ can now be merged according to Equation 5.8, hence obtaining a new axis triad $\{\hat{\mathbf{x}}_{CR}, \hat{\mathbf{y}}_{CR}, \hat{\mathbf{z}}_{CR}\}$ from which the desired rotation matrix $\mathbf{R}_{CR \to SRF}$ can be obtained

$$\mathbf{R}_{CR \to SRF} = \mathbf{R}^T_{SRF \to CR} = \begin{bmatrix} (\hat{\mathbf{x}}_{CR})^T \\ (\hat{\mathbf{y}}_{CR})^T \\ (\hat{\mathbf{z}}_{CR})^T \end{bmatrix}^T \tag{5.13}$$

Finally in the third step, the optimal attitude quaternion describing the attitude of the Science Reference Frame with respect to the inertial frame is obtained by merging Eqs. 5.11 and 5.13

$$\mathbf{R}_{iner \rightarrow SRF} = \mathbf{R}_{CR \rightarrow SRF} \cdot \mathbf{R}_{iner \rightarrow CR} \tag{5.14}$$

$$\mathbf{R}_{iner \rightarrow SRF} \rightarrow Q^{\star} \tag{5.15}$$

Based on this combination method, a new set of SCA1B data was generated. The scheme of the SCA1A to SCA1B data processing when implementing this method is sketched in Figure 5.4. The newly generated data are tagged as "SCA1B IfE CR" and the quantities derived from this data are tagged as "IfE CR".

5.2.3 Mutual comparison of the combination methods

We compared the two newly generated star camera data sets, the "SCA1B IfE" and "SCA1B IfE CR", in terms of angular rates (ω) about the Science Reference Frame axes. Figure 5.5 shows the angular rates derived from "SCA1B IfE" data set in contrast to the angular rates obtained from the single camera head solution (identical to that shown in Figure 5.1(c)). In this figure, the combined solution exist for the following periods 875-4690 s and 6510-10320 s, the other epochs represent the single head solution, hence the higher noise. The rotation about the $\mathbf{x}_{SRF}$ axis can be determined well for both single head solution and the combined solution. This is because the $\mathbf{x}_{SRF}$ axis is perpendicular to the SCA boresight axes. But, in case of the angular rates about $\mathbf{y}_{SRF}$ and $\mathbf{z}_{SRF}$ axes, the noise has been effectively reduced in the combined solution. Figure 5.5(b) clearly shows, that the noise level of the angular rates about the $\mathbf{y}_{SRF}$ and $\mathbf{z}_{SRF}$ axes is the same as for the angular rate about the $\mathbf{x}_{SRF}$ axis and it is on the level of $\sigma_{\omega_{x,y,z}} \approx 17\,\mu\text{rad} \cdot s^{-1}$. The σ_{ω_i} represents the mean noise level of the angular rates within 0.01 Hz and 0.5 Hz.

Almost identical result was obtained from the angular rates derived from the "SCA1B IfE CR" attitude data. As obvious from Figure 5.6, the noise level is the same as for the "IfE" solution. The differences of these two solutions are 1.5 to 2 orders of magnitude below the actual signal. These small angular rate differences occur due to the different mathematical approaches applied on the quaternions. Considering the overall accuracy of the recent GRACE gravity field models, it can be stated that the two combination methods provide equivalent attitude solution.

We conclude that both combination methods provide an optimal star camera attitude solution, which confirms the hypothesis that both methods provide attitude information which carries the full accuracy about all three axes. This finding is very important for the validation of the results of the comparison of "SCA1B IFE" data set with the official SCA1B RL02 data in the following section.

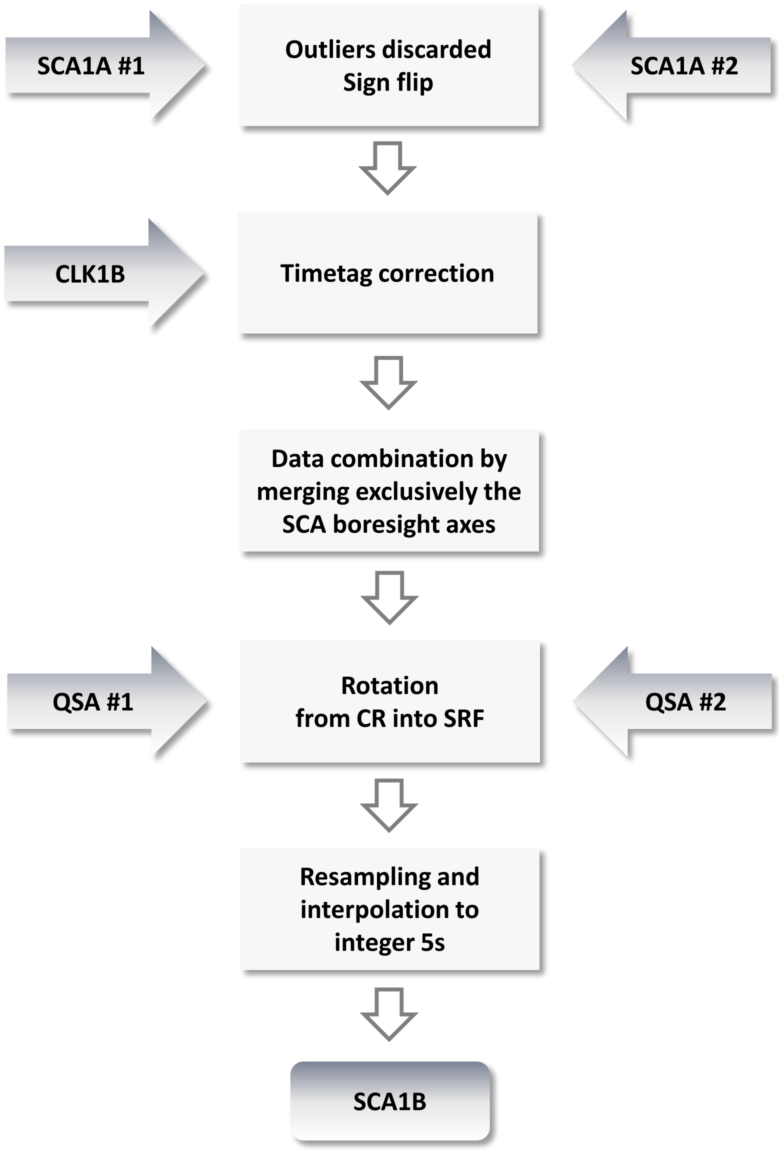

Figure 5.4: Scheme of the GRACE star camera Level-1A to Level-1B processing while implementing the combination method which is done by merging exclusively the boresight axes

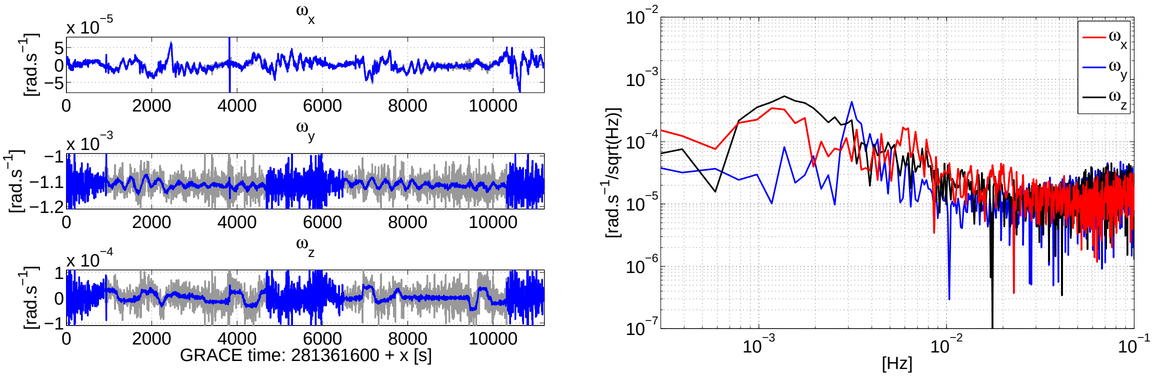

(a) (b)

Figure 5.5: a) The angular rates (ω) about the Science Reference Frame axes derived from the "SCA1B IfE" attitude data (blue), compared to the single head solution as presented in Figure 5.1(c) (grey). The GRACE-A angular rates are shown for two orbital periods on 2008-12-01. In the "SCA1B IfE" data set, the combined attitude solution exist in epochs 875-4690 s and 6510-10320 s. Figure b) shows the square root power spectral density of the "SCA1B IfE" angular rates, which proves that the attitude solution is characterized by full accuracy about all three axes

5.3 Improvement of the SCA1B RL02 attitude data

We compared the "SCA1B IfE" star camera data with the officially released data, the SCA1B RL02, generated by JPL. The combined attitude in both data sets was obtained by applying the same combination method, i.e. the method based on a weight matrix (Wu *et al.*, 2006), cf. Section 5.2.1. Based on the results presented in Section 5.2.3, it was proven that this combination method delivers attitude quaternions which do carry the full accuracy along all three axes. However, the SCA1B RL02 data clearly reveal significantly higher noise level, especially for the rotation about the $\mathbf{y}_{SRF}$ and $\mathbf{z}_{SRF}$ axes, cf. Figure 5.2. Figures 5.7 and 5.8 show then a mutual comparison of the two solutions, "SCA IfE" and SCA1B RL02, in terms of angular rates in both time and frequency domain.

Clearly, the "SCA1B IfE" solution is about a factor 3-4 better than the official SCA1B RL02 as the noise level has decreased from $\sigma_{\omega_{y,z}} \approx 47\,\mu\text{rad}\cdot s^{-1}$ (SCA1B RL02) to $\sigma_{\omega_{y,z}} \approx 17\,\mu\text{rad}\cdot s^{-1}$ ("SCA1B IFE"). Major improvement has been achieved especially within the frequency band above 5 mHz. Improvement in the frequency band below 5 mHz is expected as well. However, because the signal dominates the noise in this frequency band, the improvement might not be directly visible.

Evidently, the unfavorable noise propagation due to rotation from the Star Camera Frame into Science Reference Frame has not been compensated completely in the official SCA processing. In order to find the reason for such significant disagreements in these two star camera data sets, we revised the combination method thoroughly. We generated several SCA data sets with different settings of the variables introduced in Section 5.2.1 and compared these data sets to the official SCA1B RL02. We obtained the best fit when the variable κ was set to 1, cf. Figure 5.9 which shows comparison of the solutions in terms of the inter-satellite pointing angles. Setting $\kappa = 1$ practically means that the anisotropic noise distribution of the star camera measurement is not taken into account, in other words that the measurement accuracy about all axes is assumed to be the same, which is not correct. This explains the unexpectedly high noise level of the SCA1B RL02 quaternions. The software inspection done at JPL revealed that the combination method is correctly described in the GRACE official documents, but incorrectly implemented in the JPL processing routines (Kruizinga *et al.*, 2013).

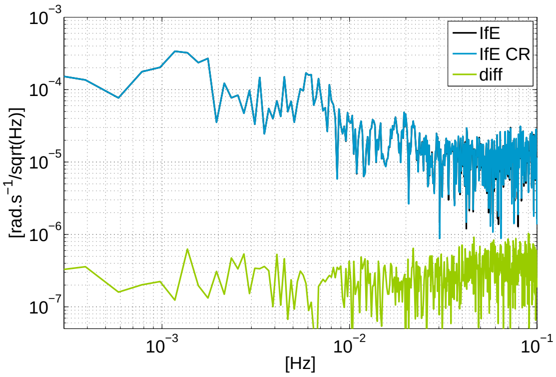

(a) ω_x

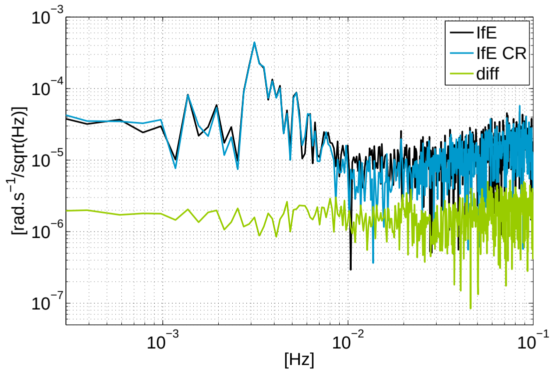

(b) ω_y

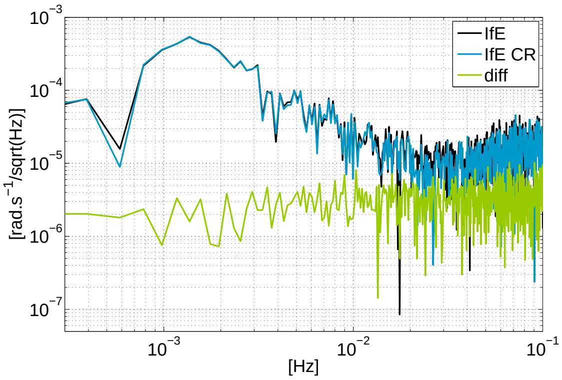

(c) ω_z

Figure 5.6: Mutual comparison of the angular rates derived from the "SCA1B IfE" (black) and "SCA1B IfE CR" (blue) GRACE A star camera data in terms of square root power spectral density. These two attitude data sets differs in the applied combination method. The green curve represents the differences of these angular rates. Derived from data from epoch 6510-10320 s - cf. Fig. 5.5)

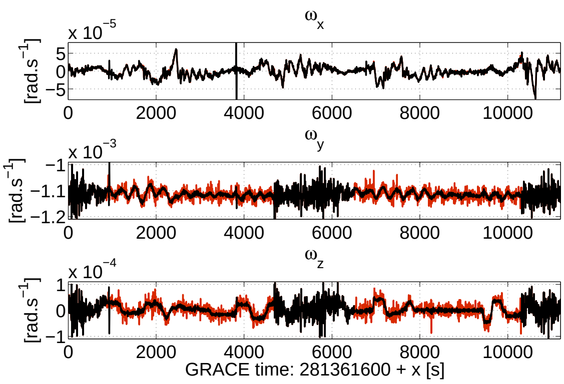

Figure 5.7: The angular rates about the Science Reference Frame axes derived from the "SCA IfE" solution (black) and from the official SCA Level-1B Release 02 (red). Shown for GRACE-A for 2 orbital periods on 2008-12-01

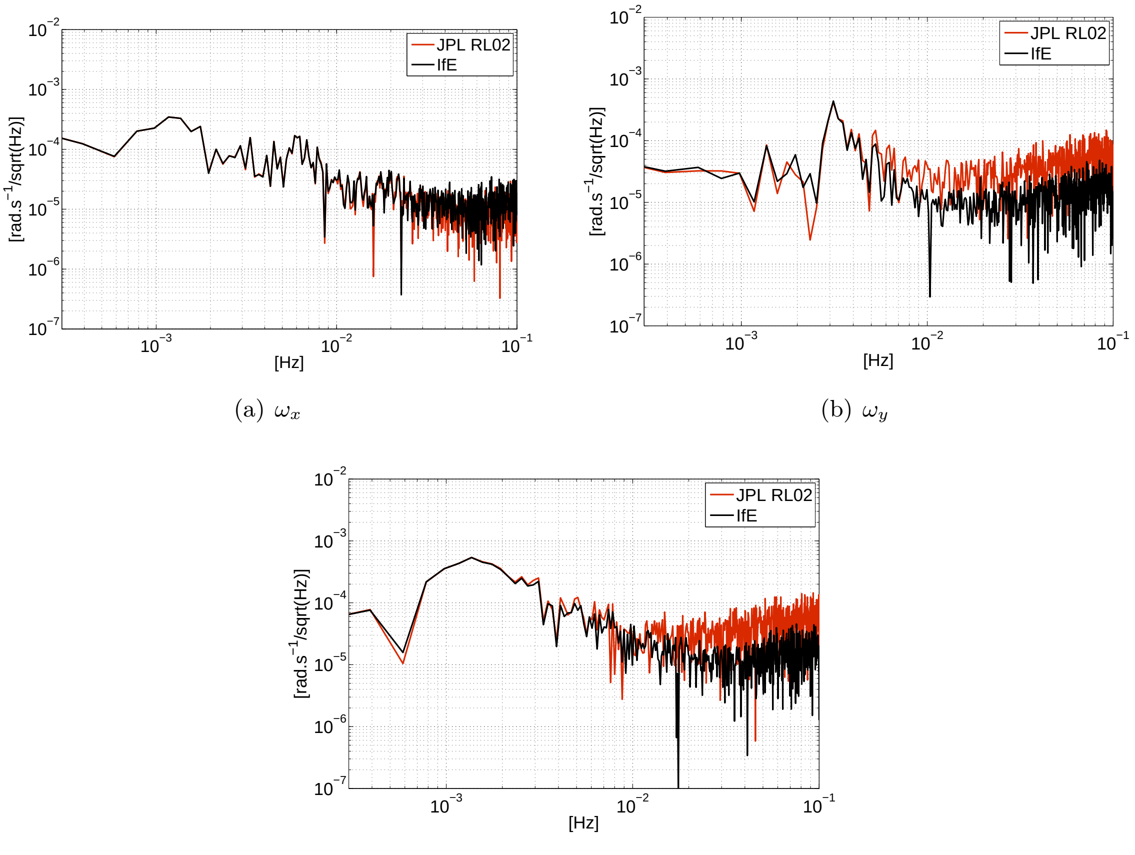

(a) ω_x (b) ω_y (c) ω_z

Figure 5.8: The angular rates about the Science Reference Frame axes derived from the "SCA IfE" solution and from the official SCA Level-1B Release 02 tagged as "JPL RL02" in terms of square root power spectral density. Derived from data from epoch 6510-10320 s - cf. Fig. 5.7). The noise level of these two solutions differs for ω_y and ω_z about a factor 3-4

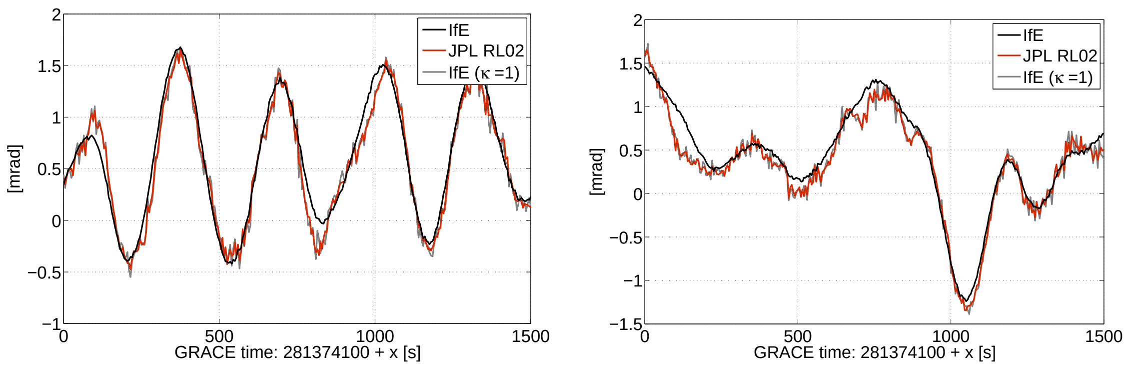

(a) pitch (b) yaw

Figure 5.9: Comparison of the "SCA IfE" attitude solution (black) with the official SCA Level-1B Release 02 solution tagged as "JPL RL02" (red) in terms of the inter-satellite pointing angles, shown for a part of a orbit of GRACE A on 2008-12-01. The grey curve represents a combined solution which was obtained by the same combination method but with the setting of $\kappa = 1$ instead of $\kappa = 8$

5.4 Effect of the improved SCA data on the GRACE fundamental observations

The analysis of the current SCA1B RL02 presented in the previous section, revealed their systematically higher noise than expected by about a factor 3-4 in periods, when the data were obtained by combination of the attitude data delivered by the two SCA heads. This inaccuracy is caused by the incorrect implementation of the combination method in the JPL processing routines. The improved "SCA IfE" attitude solution is now characterized by the full accuracy about all three axes. In the following, the effect of the improved solution on the fundamental GRACE observations needed for the gravity field recovery is presented.

5.4.1 Effect on the KBR observations

The inter-satellite K-band ranging observations (range r, range-rate $\dot{r}$, range-acceleration $\ddot{r}$) are corrected for the imperfect inter-satellite pointing and for the offset of the KBR antenna phase center from the CoM by applying the antenna offset correction (see Section 4.5). The KBR antenna offset corrections for range AOC_r, range-rate $AOC_{\dot{r}}$ and range-acceleration $AOC_{\ddot{r}}$ are derived from the inter-satellite pointing angles which are recovered from the SCA1B attitude data, cf. Section 4.3.

As first, the RPY pointing angles derived from "SCA1B RL02" and "SCA1B IfE" star camera data are compared. From Figure 5.9 showing the pitch and yaw angles is evident that the spacecraft's attitude recovered from the improved attitude data, i.e. "SCA1B IfE", is much smoother compared to the attitude derived from "SCA1B RL02" data. This meets well the assumption that the satellite attitude variations are expected to be rather smooth due to the spacecraft' mass and its moment of inertia. The differences of the pitch and yaw inter-satellite pointing angles reach up to 0.5 mrad, cf. Figure 5.10 which shows the RPY differences in both time and frequency domain. As expected, the roll angle reveals the smallest differences and they are well below 0.02 mrad. Concerning the SCA measurement accuracy and the requirements on the inter-satellite pointing, these differences are significant and cannot be neglected.

The effect on the KBR antenna offset correction for range rate is demonstrated in Figure 5.11. Additionally in Figure 5.11(b), the difference of the two solutions is compared to the KBR system error which is modeled as white noise of $1\,\mu\text{m}/\sqrt{\text{Hz}}$ at the range level (cf. Section 2.3.2). Clearly, at frequencies below $2 \cdot 10^{-2}$ Hz the differences are about a factor of 3-8 above the KBR error level. These results demonstrate that the error in the SCA1B RL02 due to the imperfect data combination has a significant effect on the AOC correction which should not be neglected as it directly affects the KBR ranging observations.

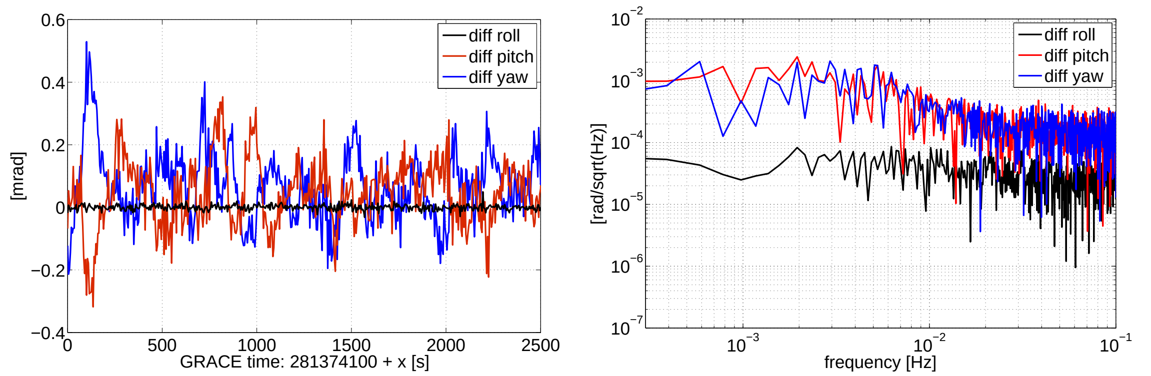

(a) (b)

Figure 5.10: Differences of the inter-satellite pointing angles derived from the "SCA1B IfE" and SCA1B RL02 star camera data in both time (a) and frequency domain (b). The differences of the roll, pitch and yaw angles are shown for a part of the orbit of GRACE-A on 2008-12-01

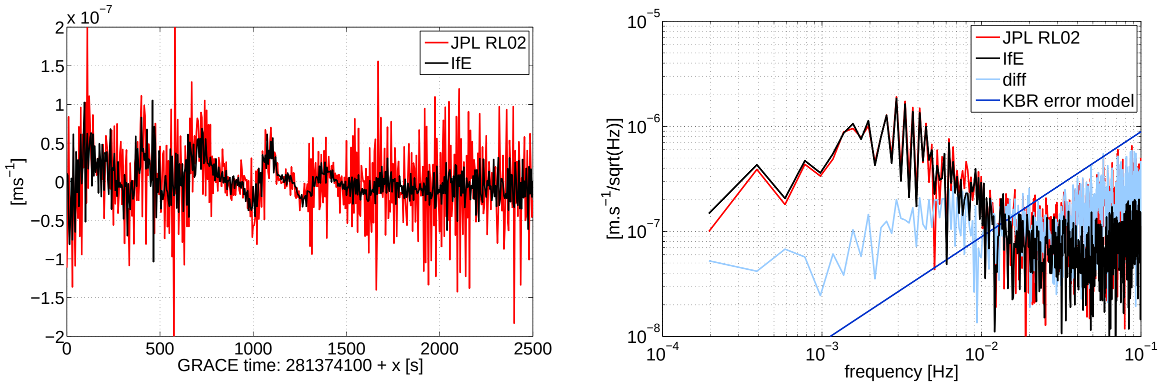

(a) (b)

Figure 5.11: The KBR antenna offset correction for range rate derived from the official SCA Level-1B Release 02 solution (red) and from the "SCA IfE" solution (black) in time domain (a) and in frequency domain (b). The differences of these two solutions (light blue) are compared to the KBR system error (blue), which is modeled as white noise of $1\,\mu\mathrm{m}/\sqrt{\mathrm{Hz}}$ at the range level

5.4.2 Effect on the ACC observations

The linear accelerations sensed by the accelerometer provide information about the non-gravitational forces acting on the satellite. Originally, they are provided in the Accelerometer Frame (see Appendix A.4), which is practically identical with the Science Reference Frame. For the gravity field recovery, these linear acceleration are required in the inertial frame or as in case of the Celestial mechanics approach (Beutler *et al.*, 2010) in the so called True Radial Reference Frame (TRRF).

The TRRF axes are defined as:

$$\begin{aligned} \mathbf{x}_{TRRF} &= \mathbf{y}_{TRRF} \times \mathbf{z}_{TRRF} \\ \mathbf{y}_{TRRF} &= \frac{\mathbf{r} \times \mathbf{v}}{|\mathbf{r} \times \mathbf{v}|} \\ \mathbf{z}_{TRRF} &= \frac{\mathbf{r}}{|\mathbf{r}|} \end{aligned} \tag{5.16}$$

where $\mathbf{r}$ and $\mathbf{v}$ are the satellite's position and velocity vectors in the inertial frame.

The rotation matrix rotating the inertial frame into TRRF ($\mathbf{R}_{iner \to TRRF}$) is then obtained as

$$\mathbf{R}_{iner \to TRRF} = \begin{bmatrix} (\mathbf{x}_{TRRF})^T \\ (\mathbf{y}_{TRRF})^T \\ (\mathbf{z}_{TRRF})^T \end{bmatrix} \tag{5.17}$$

The direction-cosine matrix rotating the Science Reference Frame into True Radial Reference Frame is obtained as

$$\mathbf{R}_{SRF \to TRRF} = \mathbf{R}_{iner \to TRRF} \cdot \mathbf{R}^T_{SRF \to iner} \tag{5.18}$$

where the latter rotation matrix, $\mathbf{R}_{SRF \to iner}$, is derived from the SCA1B quaternions according to Equation B.7.

The comparison of the linear accelerations rotated into TRRF using the $\mathbf{R}_{SRF \to TRRF}$ matrix derived from the "SCA1B RL02" and the "SCA1B IfE" is shown in Figure 5.12. The differences of the rotated ACC data reach up to $1.5 \cdot 10^{-8}\,\mathrm{ms}^{-2}$, cf. Figure 5.12(a). Figures 5.12(b)-5.12(d) show the comparison of the ACC differences with the expected error model of the ACC measurement. Although the ACC error models were originally defined for the Accelerometer Frame, they can be still considered as true in TRRF because of the very small differences in the mutual alignment of the Accelerometer Frame and TRRF along the orbit. In case of the high sensitive axes, i.e. radial and along-track axes, the differences reach up to two orders of magnitude above the expected error level. In case of the less accurate axis, i.e. the cross-track axis, the differences are smaller, but still above the expected error level.

These results show that the ACC sensor measurement accuracy cannot be fully exploited as the effects caused by the imperfect star camera data combination exceed the ACC measurement accuracy by up to two orders of magnitude. Moreover, this is even more critical for the periods when the attitude data are obtained from single camera solution, which for GRACE is inevitable due to SCA blinding by the Sun and the Moon, cf. Figure 5.7.

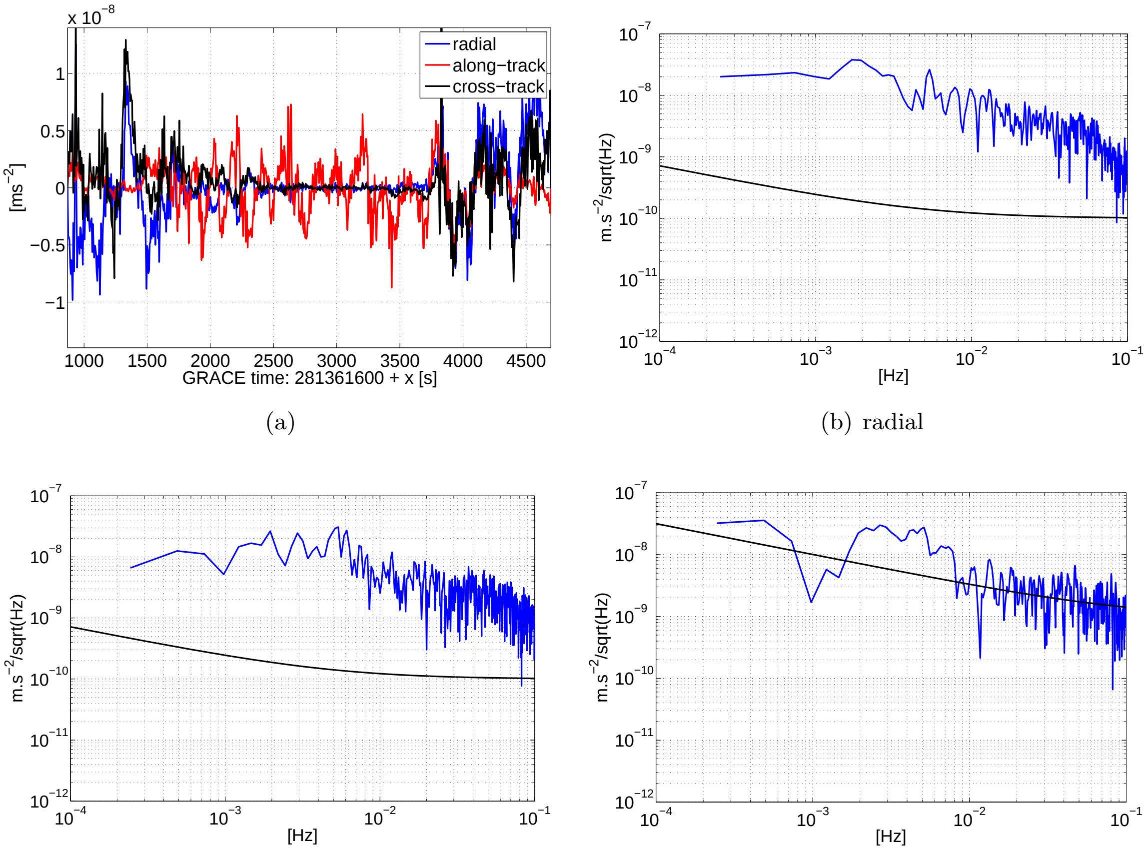

(a) (b) radial

(c) along-track (d) cross-track

Figure 5.12: Effect of the improved SCA data on ACC linear accelerations. Figure (a) shows the differences of the linear accelerations along the particular axes after their rotation into TRRF based on the SCA1B RL02 and "SCA1B IFE" data. In figures (b-d) these differences are shown in frequency domain (blue curves) and compared to the ACC error models (black curves). Based on GRACE-A data from Dec 1st, 2008

5.4.3 Effect on the GPS observations

Similarly to the KBR observations, which originally are related to the phase centers of the KBR antennas, also the original GPS observations are carried out between the phase center of the transmitter antenna onboard the GPS satellites and the phase center of the receiver antenna onboard GRACE. The main GPS navigation antenna is located on the zenith panel of each GRACE satellite, cf. Figure 2.8. As the final orbit solutions are required to be related to the satellite's center of mass, a geometric correction for the offset of the GPS antenna phase center from the CoM has to be applied during the GPS data processing. The location of GPS antenna phase center was determined from on-ground and in-flight calibration (Montenbruck *et al.*, 2008; Jäggi *et al.*, 2009). The PhC coordinates are then provided in SRF. The entire GPS processing is performed in ITRF, therefore the offset vector of the GPS antenna phase center ($\mathbf{pc}^{GPS}$) needs to be rotated first from the SRF into inertial frame using the SCA1B data, and from the inertial frame into the terrestrial frame using the IERS conventions:

$$\mathbf{pc}^{GPS}_{ITRF} = \mathbf{R}_{iner\rightarrow ITRF} \cdot \mathbf{R}_{SRF\rightarrow iner} \cdot \mathbf{pc}^{GPS}_{SRF} \tag{5.19}$$

The values for $\mathbf{pc}^{GPS}_{SRF}$ were obtained from the VGN1B data product, which represent the mean phase center location, i.e. phase center variation are not considered here. Figure 5.13 shows the differences of the $\mathbf{pc}^{GPS}_{ITRF}$ vector components for both L1 and L2 carrier frequencies, which was rotated using the SCA1B RL02 and "SCA1B IfE" attitude data. The differences reach up to 0.2 mm, while most of the values are well below 0.1 mm. According to Montenbruck *et al.* (2008), the phase center offset can be estimated with an accuracy between 0.1 mm and 0.5 mm. Because the magnitude of the $\mathbf{pc}_{ITRF}^{GPS}$ differences are very close to the currently achieved accuracy of the phase center location, they cannot be neglected.

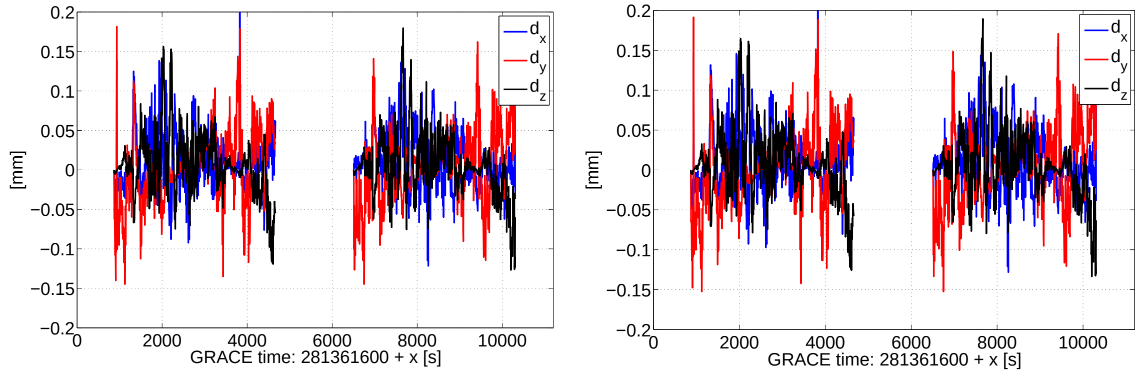

(a) L1

(b) L2

Figure 5.13: The effect of the improved SCA data on the GPS observations. The figures show the differences of the GPS antenna phase center offset vector $\mathbf{pc}_{ITRF}^{GPS}$ which was rotated using the SCA1B RL02 and "SCA1B IfE" attitude data. Shown for both L1 (a) and L2 (b) carrier frequencies. Based on GRACE-A data from Dec 1st, 2008

5.5 Effect of the improved SCA data on the monthly gravity field models

In the previous section, the effect of the improved star camera data on the fundamental observations needed for the gravity field recovery was demonstrated. Naturally, the next question to be answered is how big is the effect of the improved SCA data on the gravity field models, or in other words how much the attitude errors due to the imperfect star camera data combination propagate into the gravity field models.

For to answer this question, GRACE monthly field models were generated for December 2008 from the KBR, ACC and GPS observations which were processed using both SCA1B RL02 and "SCA1B IfE" data. The models were generated and analyzed in cooperation with the Astronomical Institute of the University of Bern (AIUB) and with the Institute of Theoretical Geodesy and Satellite Geodesy at the Graz University of Technology (ITSG). As the gravity field models can be determined based on different mathematical approaches, we have chosen two of them in order to compare and validate the results. Monthly gravity field models were generated up to spherical harmonic degree and order 90 using the AIUB Celestial mechanics approach (CMA) (Meyer *et al.*, 2012) and the ITSG Variational equations approach (VEA) (Mayer-Gürr, 2006).

In the first step, the generated gravity field models are compared in terms of difference degree amplitudes relative to the static field. The static field is different for the applied approaches, for CMA it is the AIUB-GRACE03s (Jäggi *et al.*, 2012) and for VEA it is GOCO03s (Mayer-Gürr *et al.*, 2012). In Figure 5.14(a) tiny differences between the CMA solutions are visible between degree 15 and degree 40. Above degree 30, the difference degree amplitudes are dominated by noise. In case of VEA (Figure 5.15(a)), the difference degree amplitudes relative to the static field for the two monthly solutions are almost identical as well. Tiny differences can be found between degrees 20-60.

In the second step, the global effect the attitude errors due to the SCA data combination on the geoid was analyzed. For this purpose, the differences between the two solutions were expressed in terms of geoid heights for each approach, cf. Figures 5.14(b) and 5.15(b). In case of both approaches, the geoid height changes are at mm-level. The global rms of these geiod height differences is 0.98 mm for AIUB and 1.4 mm for ITSG. The results of the AIUB and ITSG gravity field analysis match very well together. Both confirm that the effect of the improved star camera data on the monthly gravity field is at mm-level in terms of geoid heights.

This relatively small effect is caused also by the fact that the combined SCA attitude solution is available only for approx. 60% of the time. In the remaining time, only single camera solution is available due to the Sun and Moon blinding of the other camera. These results also indicate that the current gravity field models are dominated by errors coming from sources other than from the imperfect quaternion combination in the SCA1B RL02.

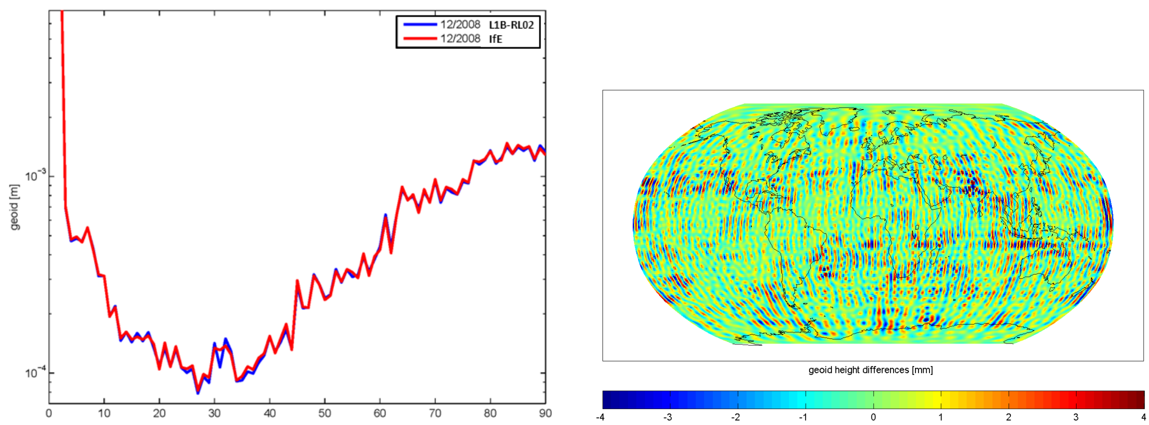

(a) (b)

Figure 5.14: Effect of the improved SCA data on monthly gravity field model obtained by Celestial mechanics approach. Figure (a) shows the difference degree amplitudes of the monthly model (December 2008) derived based on the SCA1B RL02 and "SCA1B IfE" data, relative to the AIUB-GRACE03s static field. Figure (b) shows then the difference between the two monthly solutions in terms of geoid heights

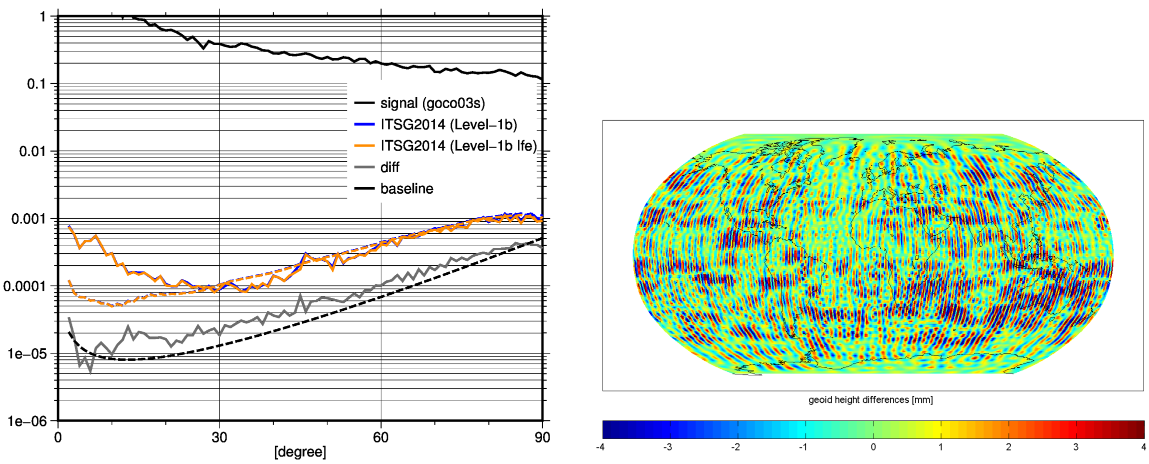

(a) (b)

Figure 5.15: Effect of the improved SCA data on monthly gravity field model obtained by Variational equation approach. Figure (a) shows the difference degree amplitudes of the monthly model (December 2008) derived based on the SCA1B RL02 and "SCA1B IfE" data, relative to the GOCO03s static field. Figure (b) shows then the difference between the two monthly solutions in terms of geoid heights

5.6 Further options for GRACE attitude data processing

The GRACE SCA1B RL02 data contain systematically higher noise than expected due to the imperfect implementation of the method for SCA data combination in the JPL processing routines, as we have proven in this chapter. As stated by Kruizinga *et al.* (2013), the correct implementation of the combination method will be a subject for the the next data reprocessing, if any. Further improvement of the GRACE attitude data, however, is still possible. It is based on further refinement of the star camera data processing and also on the attitude data fusion from multiple sensors. In the following, a brief discussion of the individual processing steps is presented. The implementation of these steps in the real data processing is, however, beyond the scope of this thesis.

In the currently implemented method for SCA data combination it is assumed that the measurement accuracy of the two star cameras is the same. But as we showed in Section 3.3.4, this is not the case. Therefore, by taking these performance differences into account, further improvement of the combined solution could be obtained. In the combination method based on the weight matrix (cf. Section 5.2.1) setting of the parameters ϵ, κ, $\mathbf{P}$ individually for each SCA head is possible. The weight matrix $\mathbf{P}$ given in Eqaution 5.3 will then be adjusted to:

$$\mathbf{P}_i = \begin{bmatrix} \frac{1}{\epsilon_x^2} & 0 & 0 \\ 0 & \frac{1}{\epsilon_y^2} & 0 \\ 0 & 0 & \frac{1}{\epsilon_z^2} \end{bmatrix} \tag{5.20}$$

Some of the key parameters for the attitude data processing and for the derivation of the inter-satellite pointing angles are the QSA, QKS and VKB calibration parameters. It is most likely, that these parameters were estimated based on the non-optimally combined attitude quaternions. Therefore, using the improved SCA attitude data, the reprocessing of the observations from the KBR calibration maneuver could lead to better results.

Another feature related to the star camera data are jumps in the SCA1B data at transitions from the combined SCA solution to single camera solution and vice versa, see Figure 5.16. This figure shows the inter-satellite pointing pitch angle, which was derived from both SCA head#1 and #2 data sets and from the combined SCA attitude solution. The jumps at transitions from single to dual camera data reach up to 0.3 mrad and are the consequence of the different performance of the two star camera heads. These jumps remain to be untreated in both SCA1B RL01 and RL02 data. They could be reduced by applying e.g. a smoothing filter.

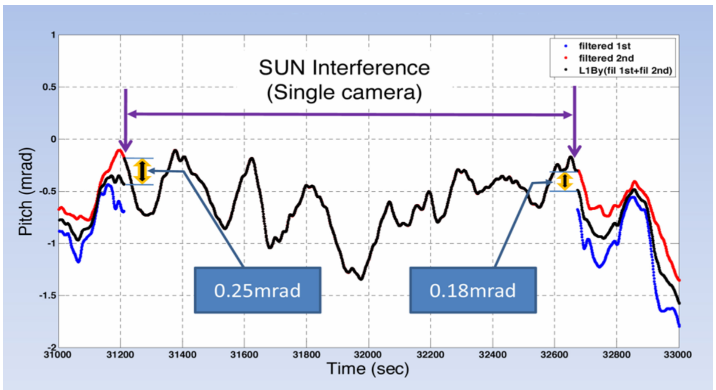

Figure 5.16: Jumps in SCA1B data at transitions from dual to single camera mode. The figure shows the pointing pitch angle computed based on SCA1A head#1 data (red), SCA1A head#2 data (blue) and SCA1B data (black). ©Ung-Dai Ko, CSR

The information about the spacecraft's attitude is provided not only by the star cameras, but also by the accelerometer and the IMU, which measure the satellite's angular accelerations and angular rates, respectively. Both of these sensors are characterized by lower measurement noise in the high-frequency band that the SCA, the long-term stability of the data is affected by drifts and biases, though. Therefore a frequency dependent attitude data fusion is possible and would further increase the attitude accuracy.

The combination of the star camera and accelerometer data was already tested by Frommknecht (2008). The data were combined on the level of angular rates by means of low-pass filter for the star camera data and high-pass filter for the accelerometer data with a cut-off frequency of $3 \cdot 10^{-2}$ Hz. Similar method, using Wiener filtering, was implemented for the combination of GOCE star camera and gradiometer data (Stummer *et al.*, 2011). Recently, the GRACE SCA/ACC data combination was implemented by Klinger and Mayer-Gürr (2014). The authors obtained the combined attitude solution not by data filtering but as a result of variance component estimation. Theoretically, the combination of the star camera data with the IMU data would be also possible. However, the IMU on GRACE-A failed right after launch and the IMU on GRACE-B is turned off most of the time. Therefore only the fusion of GRACE star camera and accelerometer data is practicable.

Attitude is a little thing
that makes a big difference.

- Sir Winston Churchill -

6 Attitude determination and mission lifetime

The GRACE mission lifetime is limited by several factors which are discussed in detail by Herman *et al.* (2012). One of the factors limiting the mission lifetime is the amount of propellant (gaseous nitrogen GN_2) onboard the satellites. In the absence of propellant, the inter-satellite pointing cannot be maintained and thus the inter-satellite ranging observations needed for the gravity field recovery cannot be collected. Also the communication with ground stations would be impossible if the RX/TX antennas would not be orientated towards the Earth as needed. The mission lifetime further depends on the energy which keeps the satellites' instruments, sensors and computers alive and which allows the performance of all measurements and communication with ground stations. The energy budget depends on the capacity of batteries and performance of solar cells. Another limiting factor is the thruster operation, which is guaranteed by the manufacturer up to 10^6 activations cycles. As the GRACE orbit is designed to be freely decaying, the satellites' altitude affects the mission lifetime as well. Lower orbit means higher air drag and disturbance torques due to the residual atmosphere, which would critically affect the mission performance. Also, the degradation of the KBR assembly due to front-end oxidation is another factor influencing the observation period. Generally, the mission operation depends on the health of the whole onboard laboratory.

It is a great accomplishment of the GRACE mission operations team to have kept the GRACE mission nominally operating despite several defunct components for more than 8 years after the planned mission termination. The very good performance of the twins is a result of continuous optimization, parameter adjustment, adaptations, software update, satellite maneuvers, etc. The current greatest challenges are to keep the energy budget stable and to optimize the propellant consumption. Demanding spacecraft maneuvers and handling are necessary to optimize the battery performance after 2 solar cells failed on each spacecraft and the battery capacity decreased from nominal 16 Ah to 3 Ah (Herman *et al.*, 2012). In order to minimize the propellant consumption, several approaches have been tested and implemented on GRACE, cf. Section 6.3. Also the health of the scientific instruments such as the K-band ranging assembly, accelerometer, GPS receiver and the star cameras is under critical observation. Although the nominal limit of 10^6 thruster activation cycles has been exceeded by some of the 12 attitude control thrusters (see Table 3.2), so far they continue to work nominally.

The relation between the mission lifetime and the attitude determination may not be very obvious at the first sight. However, the accuracy of the in-flight determined satellite's attitude critically affects the propellant consumption and the number of thruster activation cycles needed to keep the satellites in their required orientation. In this chapter, we present the impact of the different performance of the two star camera heads on both the propellant consumption and the number of thruster activation cycles, which are both considered as important factors limiting the mission lifetime. As first, we discuss the accuracy of the inter-satellite pointing angles, which were determined based on single star camera data (cf. Section 6.1). This is followed by demonstration of how the propellant consumption and thruster operation depends on the primary star camera (see Section 6.2). Finally, options for reduction of the propellant consumption are presented in Section 6.3.

6.1 Accuracy of inter-satellite pointing angles derived from single SCA data

In the in-flight spacecraft operation, the instantaneous attitude is obtained from the attitude data delivered solely by one star camera head which is set as the primary star camera. The data from the secondary camera are not used for the onboard computations at all. Using single camera data brings along two aspects which have to be considered. The first one is the different measurement accuracy of the two star camera heads. The second one is the anisotropic accuracy of the star camera measurement which is amplified when rotating the attitude data, cf. also Section 3.3.4. In the following, the effect of these two characteristics on the accuracy of the inter-satellite pointing angles is demonstrated.

The different measurement accuracy of the GRACE star cameras is very well reflected in the accuracy of the inter-satellite pointing angles. Figures 6.1(a) - 6.1(c) show the comparison of roll, pitch and yaw pointing angles determined based on the attitude data from SCA head#1 and head#2 of GRACE-A. We have computed these pointing angles based on the in-flight computational approach (see Section 4.2) using the GNV1B orbit solutions and the QKS quaterions for the SCA1A data rotation from SCF into K-frame. For better illustration, the RPY differences are shown separately in Figure 6.1(d) for two orbital periods. The differences can be computed only for the periods, when valid data from both SCA heads are available, hence the data gaps visible in Figure 6.1(d) are inevitable.

The roll angle differences are the smallest and reach up to 0.2 mrad. The roll axis is almost perpendicular to the SCA boresight axis whose pointing can be determined with high accuracy. For this reason the rotation about roll axis can be determined well, too. In contrast to roll, the differences of the pitch and yaw angles computed based on the attitude data from SCA head#1 and head#2 are much bigger. In case of pitch, the differences reach up to 1.3 mrad and in case of yaw up to 1 mrad.

The different accuracy of the RPY pointing angles is a result of the anisotropic SCA measurement accuracy. For the determination of the inter-satellite pointing, the measured attitude is needed to be rotated from the Star Camera Frame into K-Frame. Therefore the pitch and yaw angles become noisier than the roll angle. The unfavorable noise propagation is demonstrated in Figure 6.2, where the square root power spectral density of the angular rates about the SCF axes and K-frame axes are shown. While in the SCF the rotation about $\mathbf{x}_{SCF}$ and $\mathbf{y}_{SCF}$ can be determined well and only the rotation about the $\mathbf{z}_{SCF}$ can be determined about a factor κ less accurately, in the K-frame due to the noise propagation, only rotation about $\mathbf{x}_{KF}$ (roll) axis can be determined with high accuracy contrary to the rotation about $\mathbf{y}_{KF}$ (pitch) and $\mathbf{z}_{KF}$ (yaw) axes.

Considering the SCA measurement accuracy (nominally 30 μrad for SCA boresight pointing and 240 μrad for roll about the boresight) and the requirements on the inter-satellite pointing (deadband of 3-4.8 mrad), the RPY differences are very large and significantly affect the mission operation as we show in the following section.

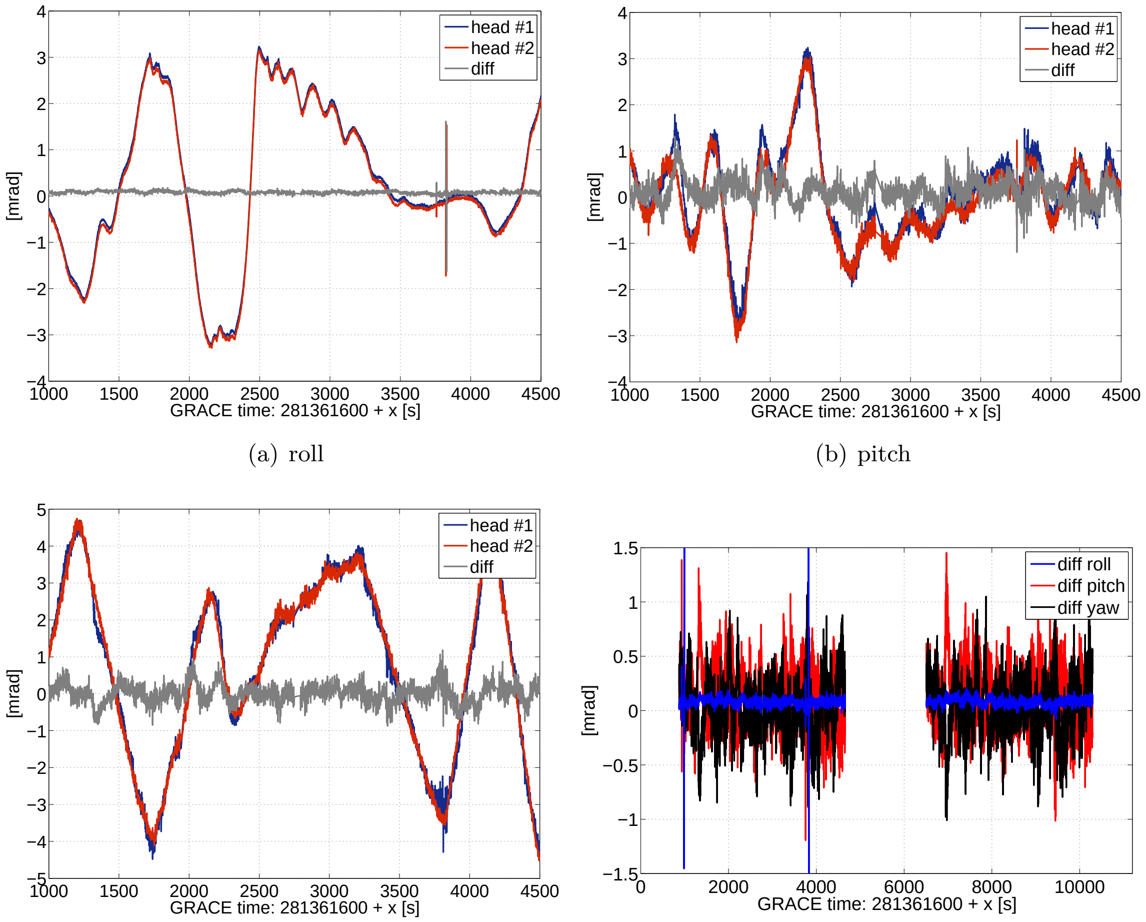

(a) roll (b) pitch

(c) yaw (d) RPY differences

Figure 6.1: Comparison of the inter-satellite pointing roll, pitch and yaw angles computed based on the attitude data from SCA head#1 and head#2 and their differences. GRACE-A, 2008-12-01

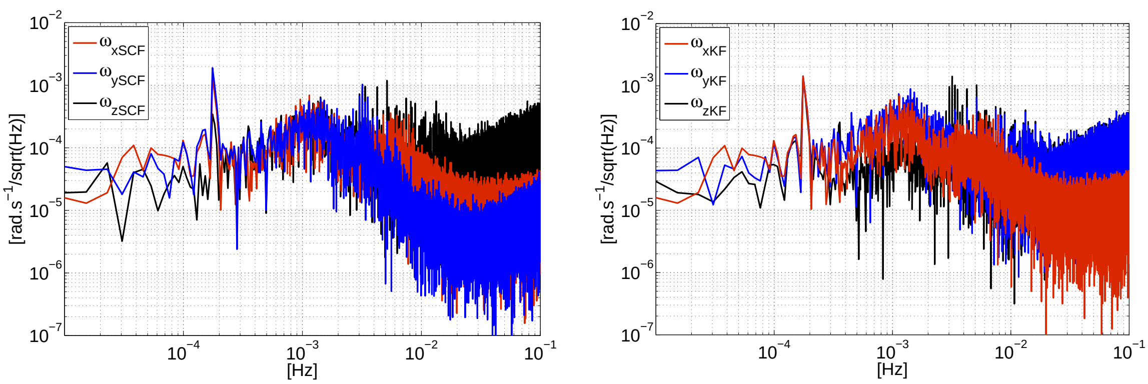

(a) (b)

Figure 6.2: Demonstration of the unfavorable noise propagation after single star camera data rotation from Star camera frame (SCF) into K-frame. The figure shows the angular rates about the SCF axes (a) and K-frame axes (b) in frequency domain, derived from the GRACE-A SCA Level-1A data on 2008-12-01

6.2 Propellant consumption dependence on the selected primary star camera

The gaseous nitrogen (GN_2) is consumed for thruster firings which are necessary to keep the satellites in the required formation and orientation. The twelve 10 mN attitude control thrusters are activated approximately 1000 times per day when control torques generated by the magnetic torquers do not suffice to maintain the desired attitude. More information about the GRACE attitude control can be found in Section 3.4. The torque needed to keep the satellite in the target attitude is computed based on the information about the instantaneous and the desired attitude. The instantaneous attitude is measured by the attitude determination sensors. In the science mode and back-up science mode, the attitude data are delivered to the AOCS by the primary star camera. Clearly, any inaccuracy in the measured attitude will directly propagate into the computed control torque which is subsequently generated by attitude actuators. When "the bad" star camera is set as the primary camera, the instantaneous attitude is determined less accurately. This results in larger differences between the instantaneous and the desired attitude and hence bigger control torque is needed to keep the satellite in the desired attitude. Consequently, the number of thruster activations as well as propellant consumption increase.

The dependence of the attitude control on the accuracy of the input attitude data is illustrated in Figure 6.3, where thruster events and their duration are shown for GRACE-A for the whole year 2008. The primary camera switches occurred on DOY 135 and 305. Between DOY 135 and 305, the primary camera was SCA head#2. In the other epoch, the primary camera was head#1. The dependence of the frequency of thruster firings and their duration on the selected primary camera is obvious at first sight, especially for pitch and yaw. The number of thruster firings per day increased more than 4 times for pitch and 2.3 times for yaw, when the SCA head#1 was set as the primary camera. The total duration of thruster firings per day increased 2 times for pitch and 2.8 times for yaw. As roll can be determined well by both star camera heads, the differences in number of thruster events and in the duration of thruster firings are much lower, characterized by a factor of 1.2.

In order to quantify the impact of the different performance of the two star cameras on the attitude control, the number of thruster activations, duration of thruster firings and propellant consumption, are shown for the period of 2006-2009 in Figure 6.4, according to the epochs defined by the selected primary camera.

As discussed above, the roll angle can be determined with high accuracy, hence the differences between the epochs are rather small. However, the number of thruster events is large, and more importantly, the duration of the firings is the biggest compared to pitch and yaw firings. This is because the efficiency of attitude control using magnetic torquers is extreme low along the geomagnetic equator. Although there are slightly more thruster activations in yaw compared to roll, their duration is significantly lower than for roll firings. The big differences between the epochs defined by the primary camera reflect well the different SCA measurement accuracy. The yaw thrusters are most frequent and the yaw thrusters have already exceeded the nominal limit of 10^6 activation cycles, cf. Table 3.2. Compared to roll and yaw, pitch thruster firings are rare (cf. also Figure 6.3) and hence they have the smallest effect on the propellant consumption.

The gas consumption depends on the absolute number of thruster firings in all directions as well as on their duration. In the epochs when the SCA head#1 was set as the primary camera, the gas consumption on GRACE-A is approximately 1.3 times bigger than when the SCA head#2 was the primary camera. Evidently, the impact on GRACE-B operation is even bigger than for GRACE-A. The propellant consumption in those periods, when SCA head#1 was the primary camera, is almost double. This is caused by the fact that the performance of GRACE-B SCA head#1 is the worst of all four GRACE star cameras (cf. Figure 3.13).

The selected period of 2006-2009 is special for two reasons. The first one is that the mission was operating during solar cycle minimum. The solar activity influence the overall satellite's performance. Among others, it affects the air drag and the disturbing atmospheric torques, which are low during the solar cycle minimum. The other reason is that the onboard laboratory was nominally operating. This is no more the case in the recent years when the SCA measurement accuracy of some SCA heads has substantially deteriorated. Also the satellite was more thermally stable than in the later years, because the thermal heating was switched off in 2011. Therefore the results obtained from the chosen sample period reflect well the impact of the SCA performance on the factors limiting the mission lifetime.

The differences in propellant consumption vary during the mission operation period, cf. Figure 6.5 which covers the epoch 2002-2014. For GRACE-A, the differences between the observed epochs decreased, but the overall GN_2 consumption became almost double compared to early years. Further, since 2012, "the bad" camera is no longer SCA head#1, but SCA head#2. On GRACE-B, the propellant consumption keep growing in the periods when the SCA head#1 is set as the primary camera. This is caused by the degradation of the SCA measurement accuracy. When SCA head#2 is the primary camera, the gas consumption is kept nominal, i.e. between 2-4 g/day. The overall increasing trend in the gas consumption depends on multiple factors. One of them is the decreasing SCA measurement accuracy. The other factors are increased frequency of special attitude maneuvers, i.e. yaw maneuver for battery discharge, and higher disturbance torques due to increased solar activity and lower satellite's orbit.

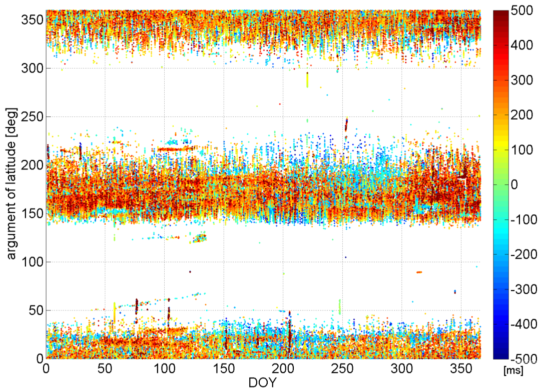

(a) roll

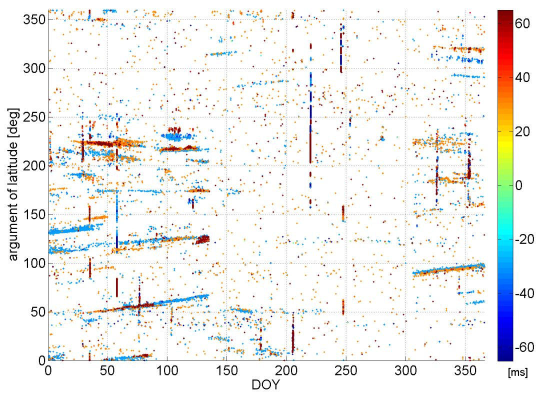

(b) pitch

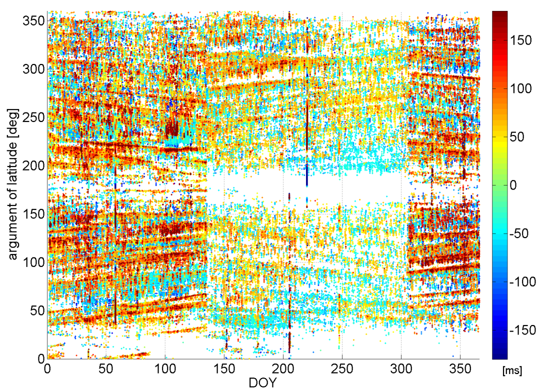

(c) yaw

Figure 6.3: Illustration of the dependence of the thruster activity on the selected primary star camera. Thruster firing events are plotted along the orbit for roll, pitch and yaw together their duration which is coded by color. The positive and negative values indicate the sense of rotation. Based on THR1B data from GRACE-A for the whole year 2008. The primary camera switches occured on DOY 135 and 305. Between DOY 135 and 305 the SCA head#2 was set as the primary camera

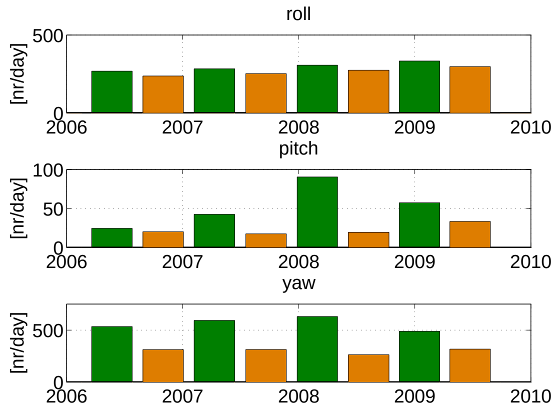

(a) number of thruster activations

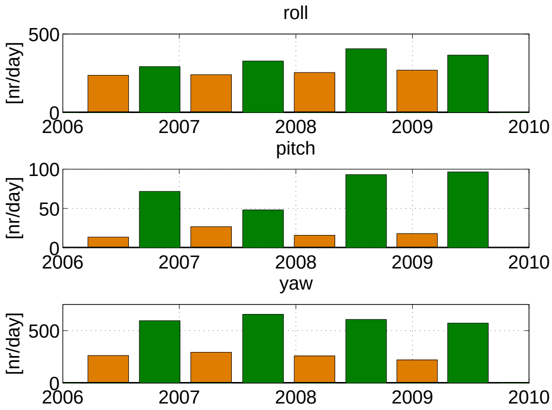

(b) number of thruster activations

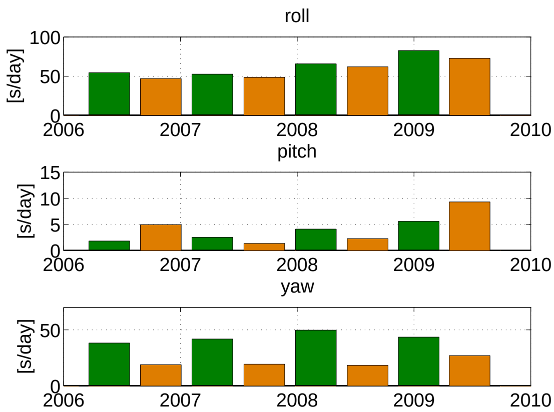

(c) duration of thruster firings

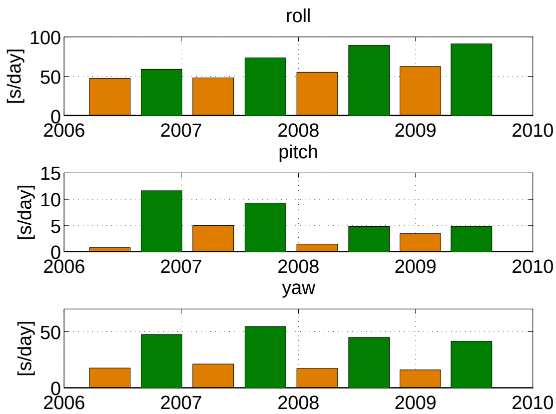

(d) duration of thruster firings

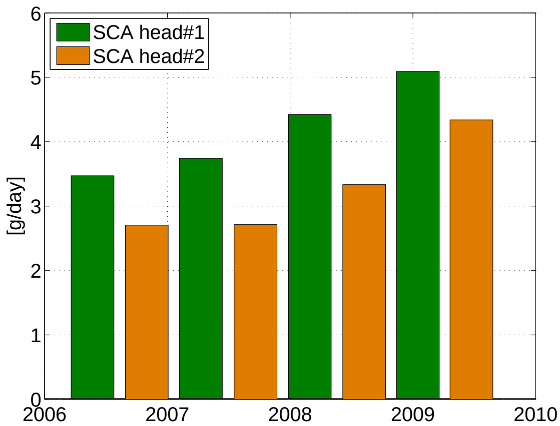

(e) propellant consumption

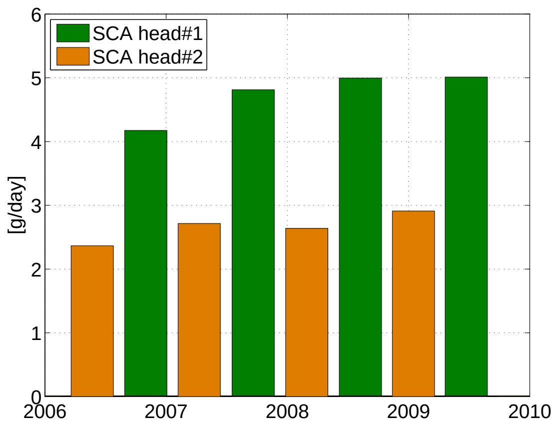

(f) propellant consumption

Figure 6.4: Dependence of thruster activity and propellant consumption on the primary star camera in 2006-2009 for GRACE-A (left column) and GRACE-B (right column). Based on THR1B and MAS1B data. All figures show the given parameter averaged per day

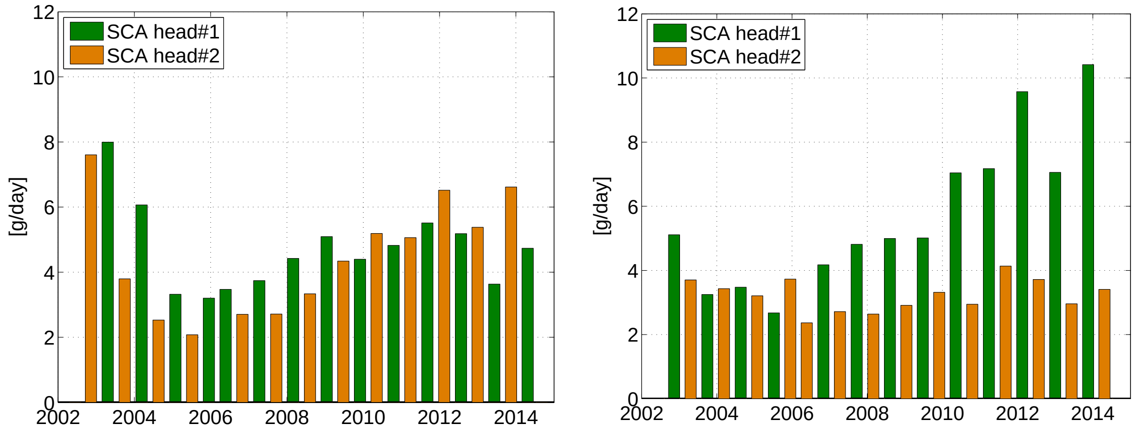

(a) (b)

Figure 6.5: Dependence of the propellant consumption on the selected primary camera in 2002-2014 for GRACE-A (a) and GRACE-B (b). The figures show the averaged GN_2 consumption per day. The satellite swap maneuver in December 2005 is taken into account

6.3 Options for propellant saving

The different performance of the two GRACE star cameras strongly affects the propellant consumption as demonstrated in the previous section. The GN_2 onboard the satellites is non-renewable, therefore the fuel management is a very important task not only during the mission operation, but also during the mission design and development phase. GRACE was originally planned to be operating for 5 years. Within 2002-2007, the fuel consumption was lower than expected because the mission was operating during a very low solar activity and the onboard laboratory was operating nominally. Until 2007, only about 25% of the total fuel amount was used up (cf. Figure 3.24). This was one of the key aspects which allowed the mission extension.

The current goal is to operate the mission as long as possible in order to provide continuous information about the Earth's gravity field and its time variations. The main goal is to minimize the gap between GRACE and GRACE Follow-On mission, which is planned to be launched in 2017. Keeping GRACE nominally operating requires big effort from the operations team, which includes GSOC and JPL, supported by CSR and GFZ. The team deals with many challenging issues, one of them is to keep the fuel consumption as low as possible. Approaches to minimize the propellant consumption and to lower the number of thruster activations, while considering the impact of the different SCA performance have been developed and implemented for GRACE. These approaches are very complex and are based on extended research studies and in-flight tests. In the following, the basic idea of these approaches is introduced.

The first approach is based on relaxation of the deadbands for inter-satellite pointing. While the deadband for roll and pitch remained constant over the years, the deadband for yaw was relaxed several times during the mission operation. In 2002, the deadband was set to 4.0 mrad, while in 2012 the deadband was already 5.4 mrad on GRACE-A and 5.2 mrad on GRACE-B. After relaxing the deadband, the number of yaw thruster activations was successfully reduced. For more information see Herman and Steinhoff (2012). This approach, however, does not deal with the dependence of the attitude control on the selected primary camera.

The second approach aims to keep the propellant consumption as low as possible while considering the impact of the primary camera on the attitude control. The impact of the primary camera on fuel consumption is critical especially for GRACE-B. In the recent years, when the SCA head#1 was set as the primary camera, the fuel consumption became 3 times higher than when SCA head#2 was the primary camera (cf. Figure 6.5). Further, since 2012 the "the bad" star camera on GRACE-A is no more SCA head#1, but SCA head#2. In other words, for both satellites the "the good" camera is now at the same side of the satellite relative to the flight direction. This constellation is ideal for the applied solution which requires that the satellites are kept operating only on "the good" star camera. In practice this means that the satellites need to be swapped every 161 d when $\beta' = 0$. The switch of the position of the leading and the trailing satellite was already performed in July 2014, December 2014 and June 2015. The next swap maneuver is planned for November 2015. Thanks to this maneuver, the fuel consumption is now kept between 3-4 g/day in comparison to the previous 10-12 g/day. More details can be found in Witkowski and Massmann (2014).

Both of these approaches have been already implemented on GRACE and they complement each other. Although they represent a good solution from the mission operation point of view, from the theoretical point of view they have one drawback. Both of them deal with the consequences of the problem, i.e. the different accuracy of the input attitude data, but they do not deal with the source of the problem itself.

The idea of our approach is to use combined star camera data as the input for the AOCS instead of the single camera data. The combined attitude solution is characterized by substantially improved accuracy. The combined solution solves both previously addressed issues related to usage of single camera data, i.e. the different SCA head performance and the anisotropic SCA measurement accuracy. The combined solution mitigates the impact of the different measurement accuracy of SCA head#1 and head#2, as it represents the optimal attitude. The SCA anisotropic measurement noise and its unfavorable propagation when rotating single camera data is no longer an issue, because the combined solution carries the full accuracy about all three axes and therefore the data quality is not affected by their rotation.

The comparison of the inter-satellite pointing angles computed based on the single camera data and the combined data is shown in Figure 6.6. Significant improvement is reached for both star camera heads. As expected due to the reasons discussed in Section 6.1, the roll differences are the smallest and reach up to 0.05 mrad. The pitch and yaw differences reach up to 0.8 mrad. The magnitude of the differences is slightly bigger for SCA head#1, which is caused by its lower measurement accuracy compared to SCA head#2 in the chosen epoch.

Comparison of Figures 6.6 and 6.1 reveals that the RPY differences are at the same order of magnitude. This means that using combined star camera data for the computation of the satellite's instantaneous attitude would significantly reduce the fuel consumption.

In order to quantify the effect of using combined data on the propellant consumption, extensive study is needed to be carried out. Such simulation study requires a profound knowledge of the attitude control laws and algorithms implemented onboard GRACE, as well as the simulation of all disturbing torques acting on the satellites. Such study, however, is beyond the scope of this thesis.

Although using combined star camera data as input for the AOCS would certainly significantly reduce the total propellant consumption, for GRACE the efficiency would be about 65%. This is because the combined solution can be obtained only when valid data from the two star camera heads are available. Due to the orbit constellation, one of the star cameras is continuously blinded by the sunshine or the moonlight along part of the orbit and thus in these periods no data combination is possible. The availability of the GRACE star camera data is shown in Figure 3.11. The combined solution is available in 65% of time (based on the data from 2008). The data combination onboard the satellites, however, might be very promising approach for GRACE Follow-On and for the future missions, which will carry 3 or more star camera heads onboard. The mutual geometry of the SCA mounting will allow the availability of the valid data from at least 2 star cameras at any time. Therefore the data combination will be possible at any time.

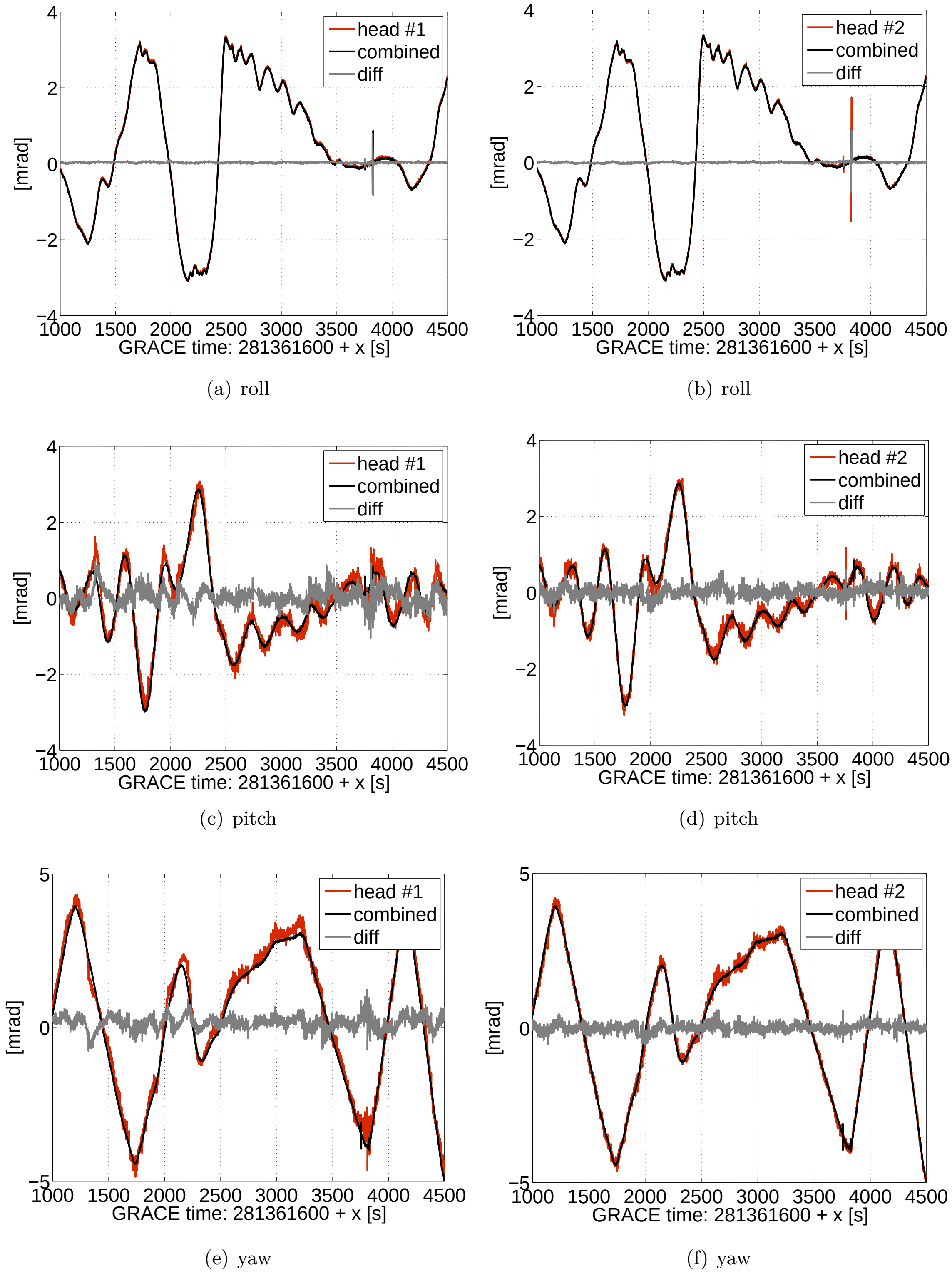

(a) roll (b) roll

(c) pitch (d) pitch

(e) yaw (f) yaw

Figure 6.6: Comparison of the inter-satellite pointing roll, pitch and yaw angles computed based on the attitude data from SCA head#1 (left column) and head#2 (right column) and on the combined solution from both SCA heads. The differences of the RPY pointing angles are shown also separately in Figure 6.7. Based on GRACE-A data from 2008-12-01

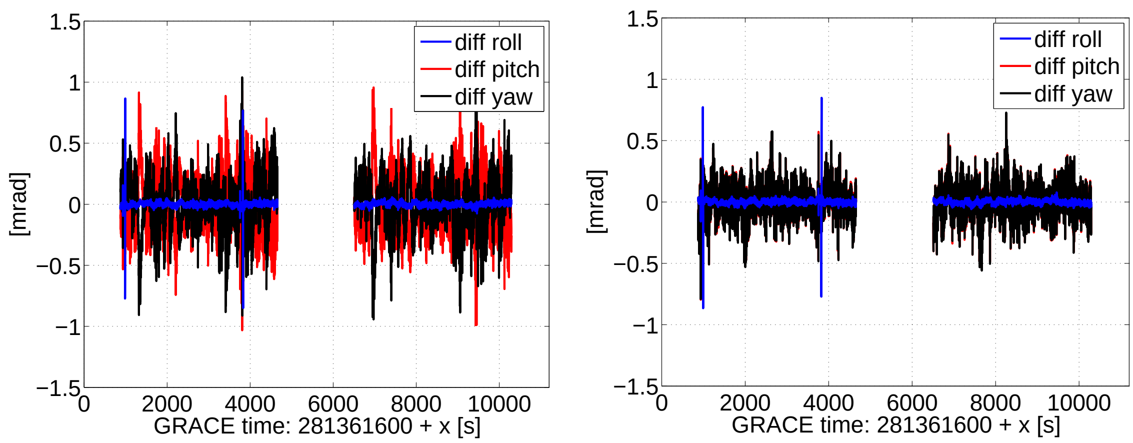

(a) differences

(b) differences

Figure 6.7: Differences of the inter-satellite pointing roll, pitch and yaw angles computed based on the attitude data from SCA head#1 (a) and head#2 (b) and the combined solution from both SCA heads. The RPY pointing angles are shown in Figure 6.6. Based on GRACE-A data from 2008-12-01

When you become comfortable with uncertainty,
infinite possibilities open up in your life.

- Eckhart Tolle -

7 Attitude determination and the future inter-satellite ranging missions

GRACE belongs to the first generation of the gravity field satellite missions (cf. Figure 7.1) and is the first mission based on the inter-satellite ranging technique for gravity field determination. Over the years, GRACE has proven its strengths in observing the Earth's gravity field and especially its temporal variations. The importance of the monitoring of the temporal gravity variations has substantially increased over the last two decades, because the gravity data contain valuable information about the Earth system which cannot be gained from any other observation data. For this reason, the continuation of monitoring the temporal variations of the Earth's gravity field is one of the current priorities of the geoscientific community.

Recently, several studies for the next generation of the gravity field satellite missions have been published, all considering one or multiple pairs of satellites performing the inter-satellite ranging, see e.g. Bender *et al.* (2008); Wiese *et al.* (2011); Elsaka (2012); Elsaka *et al.* (2013); Panet *et al.* (2013); NGGM-D Team *et al.* (2014). The future technique for inter-satellite ranging is considered to be the laser interferometry. The measurement accuracy of laser interferometry is expected to be more than one order of magnitude better than the measurement accuracy of the microwave interferometry. The combination of laser inter-satellite ranging with the constellation of multiple pairs of satellites placed in differently inclined orbits promise a significant improvement of the gravity field models.

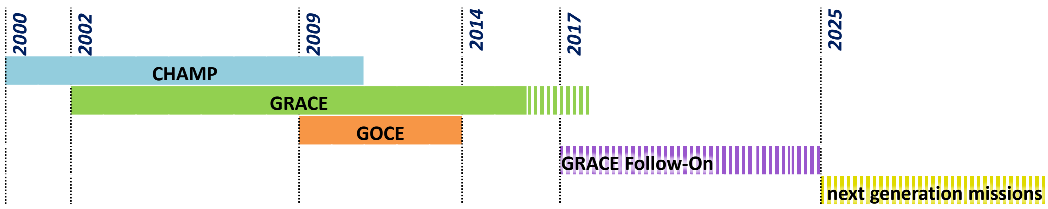

Figure 7.1: Timeline of the gravity field satellite missions

The very next mission, the GRACE Follow-On, is an interstage between the first and the next generation missions. The GRACE Follow-On will be a very close rebuild of the GRACE mission, but at the same time, it will be the first mission carrying a laser ranging interferometer (Watkins *et al.*, 2013; Flechtner *et al.*, 2014). The successful technology demonstration of space-based laser interferometry might then open the door for the next generation missions, which are designed to be based purely on inter-satellite laser ranging. The laser interferometry brings along several challenges related not only to spacecraft design and the development of the laser interferometer itself, but also related to attitude determination and control, for which original solutions are sought. For more details see Section 7.2.

Due to the unexpectedly long lifetime, GRACE offers highly valuable information about the performance of the satellite's subsystems as well as about the data processing algorithms applied onboard and on-ground. The experience from GRACE (cf. Section 7.1) is necessary to be taken into account when designing the future missions. While the technology of the measurement systems (inter-satellite ranging, orbit determination, accelerometry) is further improving, demands on the accuracy of attitude determination will increase. The total attitude accuracy depends not only on the sensor measurement accuracy itself, but also on the configuration of the attitude sensors within the spacecraft, accuracy of the related calibration parameters and data processing algorithms for possible attitude data fusion from multiple attitude determination sensors. As demonstrated in this thesis, highly accurate attitude information is not only critical for the mission operation itself, but also it is one of the key elements for the scientific data processing and the resulting gravity field recovery. Further, experience not only from GRACE, but also from the other missions for Earth observations can be taken into account, especially from GOCE and SWARM, both carrying three star cameras and ultra-sensitive accelerometers onboard.

The results presented in this thesis prove that the attitude determination has to be considered as the fourth fundamental observation technique along with the inter-satellite ranging technique, orbit determination and precise accelerometry. The so far available experience should be taken into account especially in the future missions' design phase, as discussed in Section 7.3.

7.1 The experience from GRACE

The results presented in the previous chapters demonstrated the impact of the inaccuracies in the attitude data on the mission operation as well as their impact on the scientific observations and gravity field models. Here, a natural question emerges: In retrospect, what could have been done differently for GRACE in order to gain more accurate attitude data? Or in other words, what should be done differently for the future missions than it was done for GRACE? Based on the findings presented in the previous chapters, the answer can be summarized in the following items:

i) three star camera heads onboard instead of two,

ii) SCA data combination onboard,

iii) fusion of attitude data in the on-ground processing,

iv) multiple calibration maneuvers for determination of the relevant calibration parameters,

v) independent analysis center for attitude determination,

vi) thorough understanding of the systematic effects in the measured attitude data.

ad i) In many aspects, the configuration of only two star cameras onboard is insufficient. Theoretically, for spacecraft attitude determination only one star camera is needed, hence the mounting of two SCAs onboard already means redundancy. However, when aiming for highly accurate attitude data, at least three star cameras need to be mounted onboard the spacecraft. The mutual geometry of the boresight axis of the three SCA heads need to be chosen appropriately to the satellite's orbital configuration and orientation towards the Sun and the Moon in such a way that valid data from at least two star camera heads are available at any time. This will allow to obtain a combined SCA attitude solution which carries the full accuracy about all three axes in contrast to the single head attitude solution which is characterized by its anisotropic accuracy. Also, in case of simultaneous blinding of two cameras by the sunshine and the moonlight, there will be valid data from the third camera, hence the periods when no valid data are available will be minimized. The combined solution also effectively mitigates the performance differences of the individual star cameras, which is important especially for the mission operation.

ad ii) It will be very beneficial for the mission operation to use the combined SCA attitude data directly for the in-flight maintenance of the inter-satellite pointing, because it will result in reduced propellant consumption. The combined attitude solution will allow to obtain more precise information about the instantaneous satellite's attitude. As it carries the full accuracy about all axes, it is independent of rotation, thus the roll, pitch and yaw pointing angles can be determined with the same level of accuracy. Consequently, the number of thruster firings in pitch and yaw will be effectively reduced. Moreover, as the combined solution mitigates the SCA performance differences, the overall propellant consumption will be significantly decreased because it will no longer depend on the measurement accuracy of the primary star camera. It is very likely that similarly to GRACE, the in-orbit operation of the future missions will be extended beyond the planned missions lifetime if possible. As the amount of cold-gas onboard the satellite is one of the elements limiting the mission lifetime, minimizing its consumption as much as possible is of high importance.

ad iii) Highly accurate attitude data are fundamental for the on-ground processing of the scientific observations. The final attitude solution can be obtained by combination of data from all star camera heads if possible, and further by fusion of the SCA data with data from other attitude determination sensors, such as accelerometer and IMU. The combination of attitude provided by an arbitrary number of SCA heads is straightforward when using the combination method based on a weight matrix (Romans, 2003), in which the setting of the parameter related to the measurement accuracy can be done individually for each SCA head. The data fusion of SCA data and data from the ultra-sensitive accelerometer will significantly improve the attitude solution especially in the high frequency band as shown by Stummer *et al.* (2011); Klinger and Mayer-Gürr (2014). Alternatively, the SCA data could also be combined with the IMU data, in case the sensors will be operating simultaneously with the star cameras.

ad iv) Another factor critically affecting the attitude accuracy is the accuracy of the calibration parameters related to the star cameras and to the ranging system. They are needed for the maintenance of the precise inter-satellite pointing, for reducing the pointing induced errors from the ranging observations in post-processing or for SCA Level-1A to Level-1B data processing. For attitude data fusion, the parameters of the mutual alignment of the SCAs, the accelerometer and IMU are further required. These calibration parameters are estimated based on calibration maneuvers, which are usually performed shortly after launch. However, as the SCA alignment with respect to the relevant sensors might change with time, multiple calibration maneuvers during the mission lifetime may possibly increase the accuracy of the estimates.

ad v) To assure the quality of the final attitude solution, the data processing should be performed independently by at least two analysis centers. The independent data processing is common for gravity field recovery or for orbit determination. However, as it turned out for GRACE, even after ten years of mission operation, fundamental errors in the official processing routines implemented at JPL were found, therefore the independent attitude data processing and mutual validation of the attitude solutions is of high importance.

ad vi) Thorough understanding of the systematic effects in the measured attitude data (e.g. related to SCA outages which are not caused by Sun or Moon blinding, related to IBA variations or to the different performance of the SCA heads, etc.) is fundamental for improving the attitude accuracy by proper correction of these systematics in the post-processing if possible. These systematics are mainly caused by the interaction of the spacecraft inner and outer environment (e.g. electrical fields, magnetic fields, charged particles, temperature variations, stray light, etc.) with the particular sensors. Many of these effects are predictable from on-ground tests, but many effect are discovered first during the mission operation. Better understanding of these interactions will further help to design a more stable inner environment of the spacecraft or more resistant sensor systems.

7.2 The challenge for GRACE Follow-On

GRACE Follow-On will be the second satellite mission using inter-satellite ranging observation technique for gravity field determination. It will carry two ranging systems onboard: the KBR microwave interferometer, which will serve as the primary system, and the laser ranging interferometer (LRI) (Heinzel *et al.*, 2012; Sheard *et al.*, 2012), which is mounted onboard for technology demonstration and therefore will be operating only in selected periods parallel to the KBR system. The LRI will measure the same variations of the inter-satellite range, but with more than one order of magnitude higher precision ($80\,\mathrm{nm}/\sqrt{\mathrm{Hz}}$ above 10^{-2}Hz) than the KBR interferometer. Additionally, it will provide accurate information about the relative pointing of the two satellites towards each other.

In the simplest case, the optical measurement axis of the LRI would coincide with the LOS connecting the accelerometer reference point of each satellite. The LOS, however, is occupied by the KBR interferometer and by fuel tanks. Therefore, a racetrack configuration was selected, in which the beam path is routed around the cold gas tank using a triple mirror assembly (TMA), cf. Figure 7.2. The TMA consists of three perpendicular mirror planes, just like a corner cube retroreflector. However, only those mirror sections are physically present, where the beam is incident. Therefore, the intersection point of the three mirror planes, the TMA vertex, lies outside the TMA structure and can be placed at the accelerometer reference point of each spacecraft. Because of the special properties of a corner cube retroreflector, this allows to measure distance changes between the reference points of both spacecraft and at the same time suppress spacecraft rotation-to-pathlength coupling (Schütze *et al.*, 2014b).

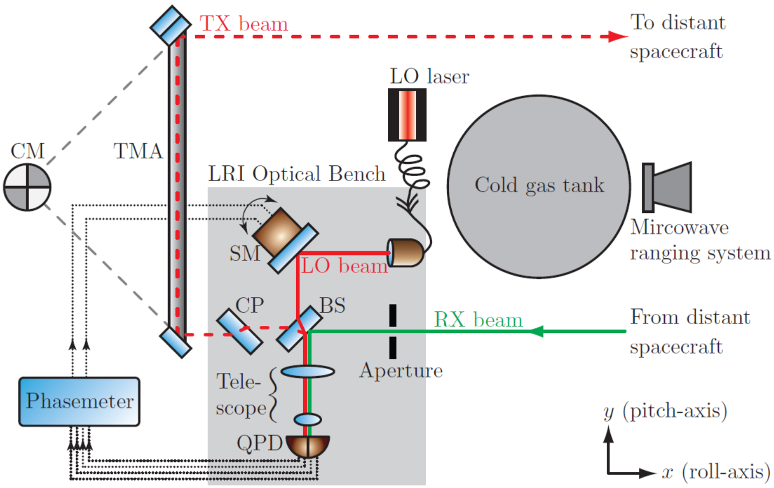

Figure 7.2: Laser ranging interferometer (LRI) of GRACE Follow-On as illustrated by Schütze (2015). Legend: RX beam - received laser beam, TX beam - transmitted laser beam, LO beam - local oscillator beam, BS - beam splitter, SM - steering mirror, QPD - quadrant photodetector, CP - compensation plate, TMA - triple mirror assembly, CM - spacecraft's center of mass

The precise inter-satellite pointing is one of the fundamental requirements for both microwave and laser inter-satellite ranging. While in case of the microwave ranging the deviation of the KBR antenna phase center from the LOS is sufficient to be maintained within a deadband of 3-5 mrad, in case of the laser ranging the transmitted and received laser beam need to be mutually aligned within less than 0.1 mrad (Heinzel *et al.*, 2012). This means, the inter-satellite pointing needs to be maintained about almost two orders of magnitude better than it was possible so far.

Since GRACE Follow-On is a very close rebuild of GRACE, the attitude determination and control system will be almost identical to GRACE, with only few upgrades. One of the upgrades will be mounting of three SCA heads onboard each spacecraft, which is very beneficial for reasons discussed in the previous section. At the moment, no further information about the sensor performance and mounting geometry has been published yet. Also, no information about the in-flight and on-ground SCA data processing have been provided yet. However, it is expected that the performance will be slightly better than the performance of the GRACE SCAs. Similarly to GRACE, using magnetic torquers and cold-gas thrusters for attitude control, the inter-satellite pointing will be maintained within a deadband of at most a few mrad. Such pointing precision will be sufficient for the microwave ranging, but surely the pointing requirements of the laser ranging interferometry will not be fulfilled. For this reason, the LRI features its own pointing control system. This is accomplished by using a quadrant photodetector, which allows for measuring tilt angles between the local oscillator wavefront and the received wavefront by using differential wavefront sensing (DWS) (Anderson, 1984). This tilt information is processed by a digital control loop and fed back to the steering mirror (SM) electronics (Schütze *et al.*, 2014a).

The principle of the beam steering control loop is sketched in Figure 7.3. Based on the DWS signal, the relative angle between the wavefronts of the local oscillator laser beam and the laser beam received from the other spacecraft can be determined in horizontal and vertical direction, i.e. yaw and pitch, respectively. Then, the local oscillator beam is aligned with the received beam by a corresponding tilt of the steering mirror. Consequently, the received beam points back to the other spacecraft independently of the local spacecraft orientation. For more details on the DWS measurement principle and the maintenance of the laser link see e.g. Sheard *et al.* (2012); Schütze (2015). The recent on-ground tests show that using the active beam steering method, the required laser beam pointing (<0.1 mrad) can be successfully achieved despite the relatively large spacecraft attitude variations (<5 mrad) (Schütze *et al.*, 2014a). The pointing pitch and yaw angles derived from the beam steering control loop may be further combined with the pointing angles derived from the SCA data which possibly will result in improved antenna offset correction for the microwave ranging observations.

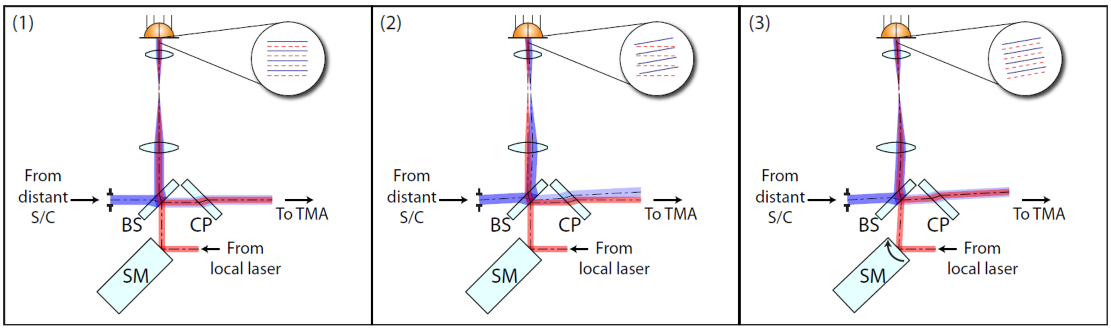

Figure 7.3: Laser beam steering control loop as illustrated by Sheard *et al.* (2012). (1) shows the ideal case of perfect alignment of the received and local beam, (2) shows the real case in which the received and local beam are tilted, (3) after rotating the steering mirror (SM) the two laser beam are now parallel

Another challenging task related to the attitude determination and control is the initial acquisition of the laser link. Prior the initial acquisition, the precise inter-satellite pointing of the two satellites needs to be already maintained by the AOCS, i.e. within a deadband of ±3 mrad. The acquisition process requires a search over five degrees of freedom, which are the ±3 mrad in pitch and yaw for each laser beam and ±1 GHz for the frequency difference between the two lasers (Wuchenich *et al.*, 2014). The GFO acquisition strategy combines spatial and frequency scanning run on each satellite. A detailed analysis of the laser link acquisition is presented by Mahrdt (2014).

7.3 The challenge for future missions

The concept of the next generation of the gravity field missions is already under development. One of the most recent studies presents a mission concept, the Earth System Mass Transport Mission (Square) (e^2.motion), which is based on two pairs of satellites orbiting the Earth in two different orbits with 90° and 70° inclination, using the laser interferometry as the primary technique for inter-satellite ranging (NGGM-D Team *et al.*, 2014).

A mission concept development is a very complex task which requires extensive expertise and cooperation of the scientific and industrial community and which needs to be solved iteratively. The approach for the e^2.motion concept development is shown in Figure 7.4. At first, based on the needs of the geoscientific community, the science requirements were defined in terms of temporal and spatial resolution of the gravity field models. Then a mission baseline scenario, i.e. the fundamental observation techniques and orbital configuration, were selected. To fulfill the science and mission goals, requirements on the AOCS were defined and a concept for AOCS designed and tested. At the same time, the instrument concept, i.e. design and performance requirements on the laser ranging interferometer and the ultra-sensitive accelerometer, were developed and tested. Finally, the satellite observations were simulated and verified in an end-to-end simulator.

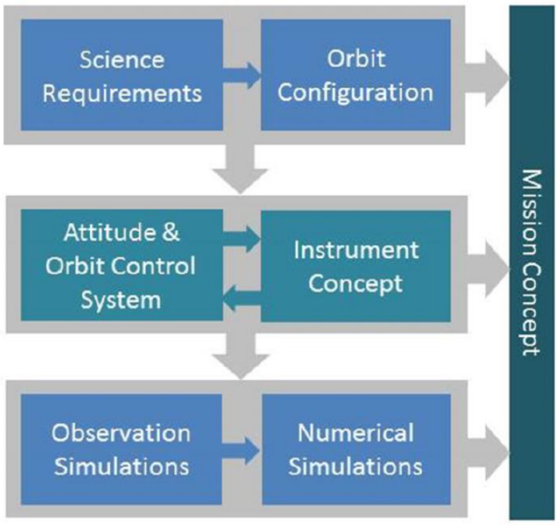

Figure 7.4: e^2.motion concept development approach (NGGM-D Team *et al.*, 2014)

The AOCS concept includes a design and performance study for attitude determination sensors and attitude actuators. The AOCS needs to fulfill science and mission requirements as well as requirements coming from the operation of the scientific instruments. In the e^2.motion study, the AOCS concept includes detailed design and testing only of a few selected components, namely of the thruster attitude control for drag compensation, laser beam steering control loop using DWS and SM, orbit and attitude control for initial acquisition of the laser inter-satellite ranging, and orbit control for maintenance of the satellite formation. For attitude determination, star cameras, IMU, CESS and magnetometer were considered (NGGM-D Team *et al.*, 2014). However, no further information and requirements on the design, measurement accuracy or data processing of these attitude determination sensors were provided.

The GRACE mission analysis results presented in the previous chapters indicate that the impact of the attitude determination on the satellite operation and on the scientific data processing must be taken into account already when developing a new satellite mission concept. An improved concept for attitude determination and upgraded satellite payload and data processing algorithms need to be designed and implemented in order to fully exploit the measurement accuracy of the scientific instruments and to optimally support the in-flight satellite operation. As the next generation of the gravity field missions is currently in the concept development phase, indeed, the experience from the previous satellite missions can and should be incorporated in the design study in order to find a best fitting concept for the attitude determination and control system. Possibly, this might also include further attitude sensor technology development.

For this purpose we have designed a basic approach for the determination of the requirements on the measurement accuracy of the attitude determination sensors, on the accuracy of the calibration parameters related to the attitude sensors and on the in-flight and on-ground data processing, see Figure 7.5. We focus here on the star cameras and on the fine pointing mode, in which the satellites are expected to operate most of the mission lifetime as in this mode all scientific observations needed for the gravity field recovery are collected. This approach, however, can be adjusted for any other operational mode and the relevant primary attitude determination sensor.

In the first step of the proposed approach, the role of the attitude determination for the mission operation and for the scientific data processing is identified based on the science and mission requirements, the instrument concept and the attitude control system. In case of the mission operation, the precise attitude determination is necessary for the maintenance of the inter-satellite pointing. The attitude data accuracy also influences the propellant consumption when using thrusters for attitude control. Also, for the GRACE Follow-On like missions, the data stream from the laser beam steering control loop will be used directly in the satellite's attitude determination and control loop. Based on the identified role, the requirements on the accuracy of the in-flight attitude solution, which is used as input for the attitude control loop, are defined.

Analogously, the role of attitude determination for the scientific data processing is identified. Here, the precise attitude data are required for the post-processing of the scientific observations, i.e. for correction of the pointing-induced errors from the ranging observations, for rotation of the accelerometer data into the inertial frame and for rotation of the GNSS phase center offset vector from the satellite-fixed reference frame into inertial frame. Considering the target accuracy of the scientific observations, the requirements on the accuracy of the final attitude solution, which is computed on-ground, are defined. Note that the listed role of the attitude determination for both the mission operation and the scientific data processing is only for illustration and might be slightly different for any particular future mission.

Based on the required accuracy of both the in-flight and the final attitude solution, the requirements not only on the sensor measurement accuracy itself, but also on the accuracy of the relevant calibration parameters and the data processing algorithms are defined. The data processing might be different for the in-flight and on-ground solution, it might also consider fusion of attitude data from multiple sensors such as SCA and ACC or IMU, or even the data from the steering mirror control loop. The optimal data processing strategy needs to be tested based on the measurement performance of all relevant attitude sensors. At the same time, the resulting optimal data processing strategy puts further requirements on the SCA measurement accuracy.

The required SCA measurement accuracy can be achieved by developing a proper sensor concept. On the one hand, such concept includes sensor design and performance, which is provided by the manufacturer. It is the task of the manufacturer to meet the requirements on the sensor measurement accuracy under consideration of the current available technology and the influence of satellite's inner and outer environment of the sensor performance. On the other hand, the sensor concept also includes the sensor constellation onboard the satellite, i.e. the number of SCA heads and their mounting geometry, and the algorithms for the raw data processing and for the possible combination of the attitude data from multiple SCA heads.

Furthermore, from the requirements on the in-flight and on-ground attitude accuracy, the needed accuracy of the calibration parameters related to the attitude determination sensors and their alignment (e.g. with respect to the ranging system, to the satellite body axes or to the other attitude sensors) is derived. Accordingly to these requirements, pre-flight and in-flight calibration maneuvers and data processing algorithms are designed.

In other words, based on this approach fundamental questions should be answered such as: what star camera measurement accuracy is needed; is such accuracy achievable with the current technology; what is the necessary mounting geometry of the star camera heads so that valid data from at least two cameras are available at any time; what is the necessary accuracy of the relevant calibration parameters, which calibration maneuvers are needed to be performed and how; is it necessary to combine the SCA data directly onboard the satellites and is any further fusion with attitude data from other sensors necessary for arriving at the required accuracy of the in-flight attitude solution; what is the required accuracy of the final attitude solution and does it allow the full exploitation of the measurement accuracy of the scientific observations; what are the limits of the designed attitude determination system; where are its weak points; what are the requirements on the satellite processing unit (hardware + software). These and other questions need to be answered already in the mission design phase.

The overall approach for the design of the attitude determination system requires an iterative solution based on simulated observations, numerical simulations and testing of various scenarios, while considering the performance of all other satellite systems such as attitude control system, scientific instruments systems. Also, the end-to-end simulations are a necessary part of this iterative solution. This is a very complex system which is unique for any particular mission. The numerical analysis is therefore beyond the scope is this thesis.

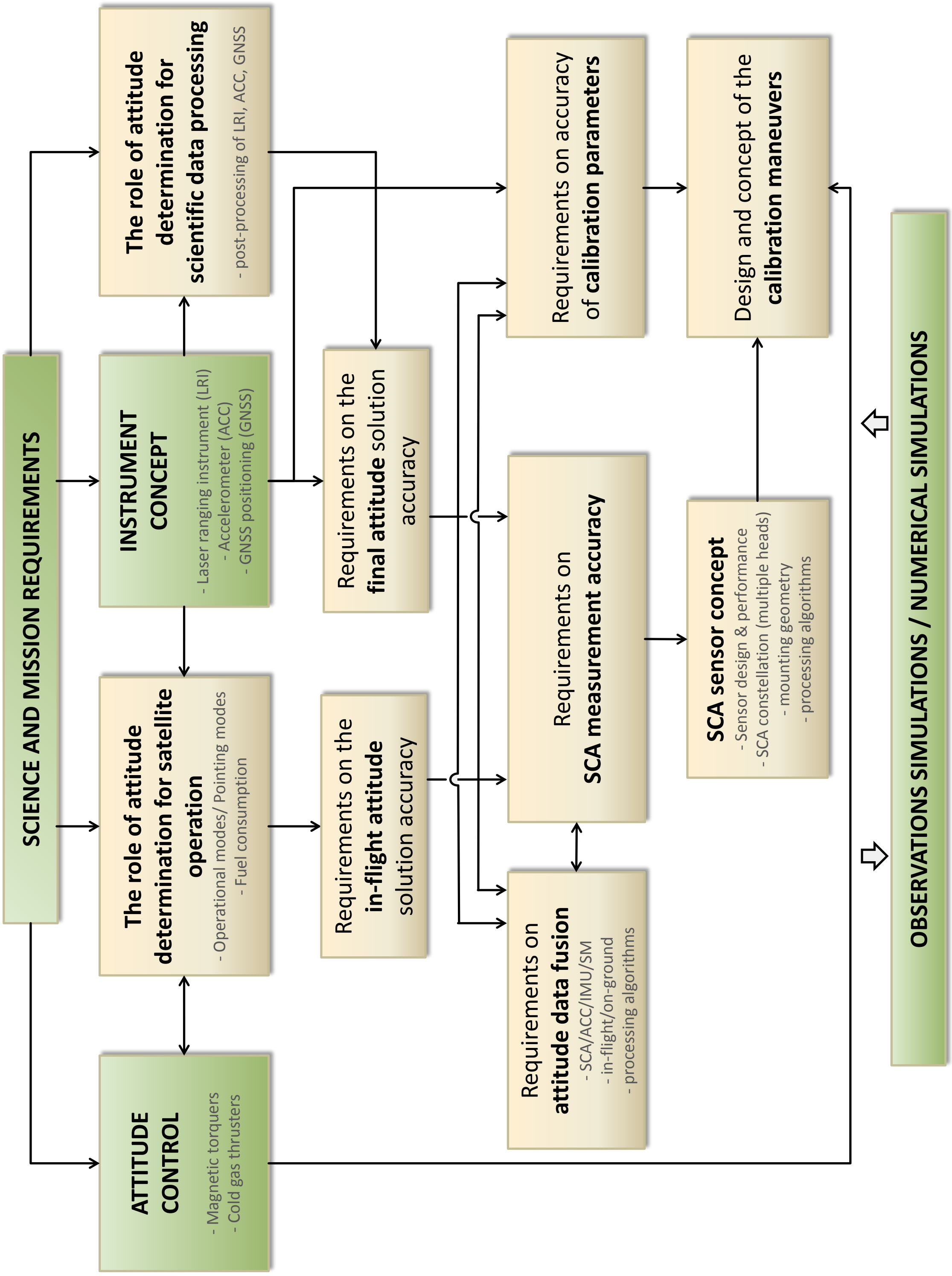

Figure 7.5: Proposed approach for defining the requirements on the attitude determination system for the future missions based on their science and mission requirements. The aim is the define the requirements on sensor measurement accuracy, on the accuracy of the relevant calibration parameters and on the attitude data processing

Just as every drop of the ocean carries the taste of the ocean,
so does every moment carry the taste of eternity.

- Sri Nisargadatta Maharaj -

8 Conclusions

We have presented the first comprehensive study on the role of attitude determination for inter-satellite ranging. This study is based on the data analysis from GRACE, which is the first and so far the only satellite mission using the inter-satellite ranging for the Earth's gravity field observation. The inter-satellite ranging is a very challenging measurement technique especially because of its requirements on the attitude determination and control. It requires the two satellites being precisely pointed with their ranging antennas towards each other while keeping the maximum deviation of the antenna phase center from the LOS below $\sim$5 mrad. The precise attitude determination is fundamental not only for the mission operation but also for the post-processing of the GRACE scientific observations needed for the gravity field recovery, i.e. of the inter-satellite ranging observations, GPS observations and linear accelerations sensed by the accelerometer.

Today efforts are still ongoing to improve the accuracy of the GRACE gravity field models as the predicted accuracy has not been reached yet. On the one hand, this requires an improvement of the background models for the atmosphere, ocean and tides in order to reduce the impact of the aliasing effects coming from the improper spatial and temporal sampling of the satellite observations. On the other hand and most importantly, an improvement of the satellite observations is needed, because any uncorrected error directly propagates into the gravity field models. As the attitude data are necessary for the post-processing of all primary scientific observations, the analysis of the performance of the star cameras, which are the primary attitude determination sensors, and of the star camera data processing was absolutely essential in order to ensure their highest possible accuracy of the attitude data.

One of the current highest priorities of the geoscientific community is the continuation of the Earth's gravity field observation from space. Therefore NASA and DLR decided to keep GRACE operating as long as possible and to launch a new satellite for the gravity field observation, the GRACE Follow-On, as soon as possible. Additionally, the next generation of the gravity field satellite missions is currently in the concept development phase. For both GRACE Follow-On and the future missions, the inter-satellite ranging was selected again to be the primary measurement technique. Profound understanding of the GRACE sensor characteristics and performance as well as the processing algorithms presented in this thesis is fundamental for the development of the future technology and for the optimal operation of the future missions. At the same time, it also allows for improvement of the current GRACE operation.

In the following, major findings of our data analysis are summarized and the implication of our research work is discussed. An outlook on further research work is provided as well.

Summary of major findings

We have provided a thorough analysis of the characteristics and accuracy of the GRACE star cameras, which deliver the attitude of their own sensor frame with respect to the inertial frame. The two star cameras onboard each satellite are operating simultaneously, however, due to the partial blinding of one of the cameras by the sunshine or the moonlight, valid data from both heads are available for about 60-70% of time. Due to the sensor construction geometry, the star camera measurement is characterized by its anisotropic accuracy. Moreover, the performance is significantly different for each star camera. So the pointing of the SCA boresight axis can be determined with an accuracy of 14-32 μrad and the rotation about the boresight with an accuracy of 140-240 μrad. Exactly these three characteristics, i.e. the limited availability of the dual camera data, the anisotropic measurement accuracy and the different performance of each star camera, are the most critical factors affecting the accuracy of the final attitude solution computed in-flight and on-ground, which consequently critically affect the mission operation and the accuracy of the scientific observations.

While maintaining the inter-satellite pointing, which is one of the fundamental requirements for the inter-satellite ranging, the star camera measurement accuracy directly affects propellant consumption and number of thruster activation cycles, which are both considered as factors limiting the mission lifetime. As we have shown here, the crucial aspect is that the in-flight determination of the instantaneous attitude is based on the data delivered by the primary star camera only. The primary star camera is routinely switched from the SCA head#1 to SCA head#2 or vice versa every ~161 d, except for the short term switches because of moonlight intrusions into primary camera FoV. When "the bad" star camera is set as the primary camera, the propellant consumption is about a factor 1.3 (for GRACE-A) and 1.8 (for GRACE-B) higher than when "the good" camera is set as the primary camera. In the recent years 2012-2014 for GRACE-B this factor has even increased to 2.5-3. Additionally, as the single camera attitude data are strongly affected by the anisotropic star camera measurement noise which unfavorably propagates into the rotated attitude data, the derived pointing pitch and yaw angles contain systematically higher noise than the roll angle. Consequently, the satellite's pitch and yaw attitude is over-controlled.

As we have discussed here, the number of thruster activation cycles and the propellant consumption could be efficiently reduced in case the satellite's instantaneous attitude would be computed based on the combined star camera attitude solution instead of on the single camera data only. Although it is possible the obtain the combined solution for 60-70% of the time, considering the current goal, i.e. to operate the mission as long as possible in order to minimize the gap between the GRACE and GRACE Follow-On, the data combination onboard would mean a significant reduction of both of these lifetime limiting factors.

The determination of the inter-satellite pointing remains to be very challenging not only because of the accuracy of the input attitude and orbit data, but also because of the accuracy of the needed calibration parameters related to the star cameras and the antenna phase center of the microwave interferometer. Our data analysis of the in-flight and on-ground determined inter-satellite pointing angles and the full review of the computation algorithms applied on-flight and on-ground, have revealed an unexpectedly large bias (up to 3 mrad) of the on-ground solution. As we have further shown, the reason for the pointing bias is the inconsistency between the calibration parameters used for the in-flight (QKS parameter) and on-ground (QSA and VKB parameters) computation, which in the theory should provide information about the same rotation, namely from the Star Camera Frame into K-Frame, but in the reality this is not the case. Consequently, the pointing bias critically affects the accuracy of the antenna offset correction which is needed for the correction of the inter-satellite ranging observations.

We have further shown that the official SCA1B RL02 attitude solution contains systematically higher noise about a factor 3-4 than it is expected for the periods when the combined solution exist. The SCA1B solution represents the final attitude solution obtained by the rotation and combination (if possible) of the originally measured attitude data, which is used for the post-processing of the inter-satellite ranging observations, GPS observations and the linear accelerations. By comparison of the combined SCA attitude solutions generated based on two different combination methods, we have proven that the combined solution carries the full accuracy about all three axes, which however is not the case for SCA1B RL02. Our results of the full reexamination of the GRACE SCA Level-1A to Level-1B processing have indicated that the reason for this unexpectedly higher noise is the incorrect implementation of the algorithms for the data combination in the JPL processing routines despite their correct description in the official GRACE documents. Based on the analysis of a monthly gravity field model, we have demonstrated that this systematically higher attitude noise has a global effect on the geoid at mm-level.

Moreover, we have discussed the need of precise attitude determination for the future missions which arises due to the fact that the measurement accuracy of the inter-satellite ranging and the ultra-sensitive accelerometry is assumed to be at least about one order of magnitude better than it is now for GRACE. Therefore, in order to fully exploit the accuracy of these measurements and to maximally support the mission operation, the experience from GRACE mission needs to be taken into account when designing an upgraded attitude determination and control system. In addition, simulation studies need to be carried out for to determine the requirements on the sensor measurement accuracy, on the accuracy of the relevant calibration parameters as well as on the data processing. Here we have presented a generic approach which can be used as a foundation for such simulation study.

Implication of this research work

This research study provides an insight not only into the role of attitude determination for inter-satellite ranging, but also into the in-flight and on-ground star camera data processing and into the in-flight and on-ground computation of the inter-satellite pointing angles. Especially it clearly demonstrates the importance of precise attitude determination for the gravity field recovery.

Because our results have been regularly presented at the GRACE Science Team Meetings and other international conferences, published as original articles in Advances in Space Research, and have been intensively discussed with CSR and JPL, they have already contributed to the improvement of the official products. This is especially the case of the report on large pointing bias caused by the inconsistency of the calibration parameters, which became one of the impulses for the reprocessing of the data from the KBR calibration maneuver and for the subsequent reprocessing of the Level-1B data, which resulted in Level-1B Release 02 data products.

Our research work emphasizes the need of an independent validation of the official data products. Even after more than 10 years of mission operation, we have discovered a fundamental software bug in the JPL processing routines, which probably would have been found much earlier if there would be an independent data analysis center. Such centers are common for orbit determination or for the gravity field modeling, but so far not common for the attitude determination. The SCA data reprocessing based on the correct implementing of the algorithms for the data combination is planned for the potential Level-1B Release 03.

Our work also proves that profound understanding of the characteristics and accuracy of the onboard sensors and the key satellite components as well as of the data processing algorithms is fundamental for the improvement of both the mission performance and of the data products, based on which the gravity field models are recovered. The full exploitation of the accuracy of the primary measurement techniques is not possible without highly precise attitude data.

Furthermore, this research work provides an information about the attitude determination, which is essential for the development of the future missions, and which might be already taken into account for the GRACE Follow-On operation. Our results emphasize the fact that the precise attitude determination must be considered as the fourth primary observation technique and as such being designed, developed and analyzed as extensively as the other primary measurement techniques.

Outlook on future research

The extension of this research work is further possible. Here we list some of the potential future research studies:

- *Further refinement of the SCA data combination and attitude data fusion for GRACE* - which includes e.g. taking the different performance of the two star cameras into account by more precise parameter setting in the combination method based on a weight matrix, smoothing of the jumps at the transitions from dual to single camera data, development of processing algorithms for the combination of the star camera data and the accelerometer data, testing of the effect of this combined attitude solution on the gravity field.
- *Attitude data analysis for GRACE Follow-On* - a pre-launch analysis may include development of algorithms for the combination of the attitude data from three star camera heads, as well as their fusion with acceleromter or IMU data, development of algorithms for fusion of the attitude data from the beam steering control loop with the pointing angles derived from the attitude data; an after-launch analysis may include the analysis of the performance of the star cameras, validation of the different attitude products and basically the same kind of study which has been presented here for GRACE.
- *Simulation study for the future missions* - a numerical simulation based on the approach presented in this thesis for the determination of the requirements on the sensor performance and accuracy, on the mounting geometry of SCA heads, on in-flight and on-ground data processing, on the accuracy of the relevant calibration parameters, etc. while aiming for the full exploitation of the measurement accuracy of the scientific instruments.

A

Reference frames

In the following, definitions of GRACE related reference frames are given, which are relevant for the data analysis presented in this thesis. The definitions of these frames were originally published by Bettadpur (2012).

A.1 Satellite panels

The regular shape of GRACE satellites allows clear nomenclature of their panels, which provide a helpful reference e.g. when speaking about the location of the payload within the satellites or about the mutual orientation of the twins. The nomenclature is for both satellites identical. Here, we distinguish between six satellite panels: front, rear, starboard, port, zenith and nadir, and the boom, see Figure A.1.

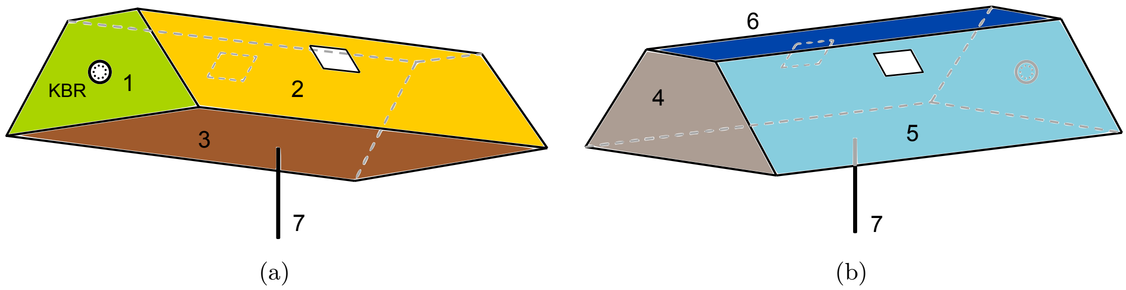

Figure A.1: Nomenclature of the satellite panels: 1-front, 2-port, 3-nadir, 4-rear, 5-starboard, 6-zenith; and 7-the boom

A.2 Satellite Frame

The Satellite Frame (SF) is necessary for the definition of the reference frames related to GRACE satellite body. In the pre-flight phase, the SF was used as the basis for satellite assembly and payload unit alignment orientation.

The Satellite Frame is defined as follows:

origin	target location of the center of mass of the proof mass of the accelerometer ([0, 0, 0])
$\mathbf{x}_{SF}$	points from the origin to a target location of the phase center on the boresight the K/Ka Band horn ([1.4 m, 0, 0])
$\mathbf{y}_{SF}$	forms a right-handed orthogonal triad with $\mathbf{x}_{SF}$ and $\mathbf{z}_{SF}$
$\mathbf{z}_{SF}$	is normal to $\mathbf{x}_{SF}$ and to the plane of the main equipment platform, and positive towards the nadir panel

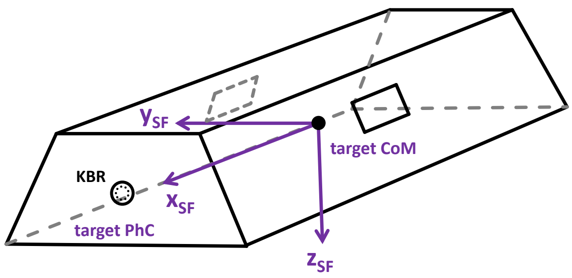

Figure A.2: Accommodation of the Satellite Frame in the GRACE satellite body

A.3 Star Camera Frame

On each GRACE spacecraft, two star camera heads are rigidly mounted to the accelerometer CFRP frame with their boresight, i.e. the optical axis, oriented towards the side panels with a zenith offset of ±45°. The star camera head #1 points with its boresight towards the starboard panel ($+\mathbf{y}_{SF}$), the star camera head #2 points with its boresight towards the port panel ($-\mathbf{y}_{SF}$).

The Star Camera Frame (SCF) is defined individually for each star camera head.

The Star Camera Frame is defined as follows:

origin	intersection of the boresight with the mounting plane for the star camera head
$\mathbf{x}_{SCF}$	parallel to $\mathbf{x}_{SF}$
$\mathbf{y}_{SCF}$	completes the right handed orthogonal triad
$\mathbf{z}_{SCF}$	identical with the SCA optical axis (boresight)

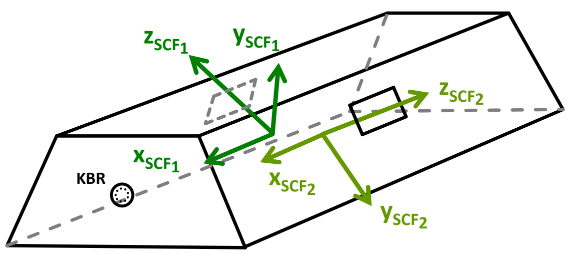

Figure A.3: Accommodation of the Star Camera Frame in the GRACE satellite body

The alignment of the Star Camera Frame with respect to the Science Reference Frame is represented by the QSA quaternions. The alignment of the Star Camera Frame with respect to the K-Frame is represented by the QKS quaternions.

A.4 Accelerometer Frame

The Accelerometer Frame (AF) is defined as:

origin	center of mass of the proof mass of the accelerometer
$\mathbf{x}_{AF}$	parallel to $\mathbf{y}_{SF}$
$\mathbf{y}_{AF}$	parallel to $\mathbf{z}_{SF}$
$\mathbf{z}_{AF}$	parallel to $\mathbf{x}_{SF}$

The accelerometer has two ultra-sensitive axes, the $\mathbf{y}_{AF}$ and $\mathbf{z}_{AF}$ and one less sensitive axis, the $\mathbf{x}_{AF}$.

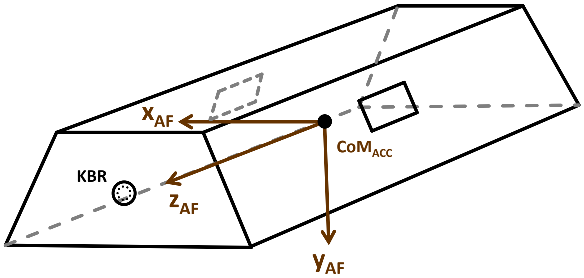

Figure A.4: Accommodation of the Accelerometer Frame within the GRACE satellite

A.5 Science Reference Frame

The Science Reference Frame (SRF) is the target reference frame for most of the GRACE Level-1B data. The SRF axes are parallel to the axes of the accelerometer.

The Science reference frame is defined as follows:

origin	center of mass of the satellite maintained by a Center of Mass Calibration & Trim maneuver
$\mathbf{x}_{SRF}$	parallel to $\mathbf{z}_{AF}$
$\mathbf{y}_{SRF}$	parallel to $\mathbf{x}_{AF}$
$\mathbf{z}_{SRF}$	parallel to $\mathbf{y}_{AF}$

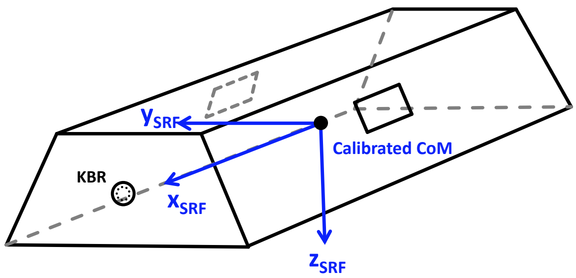

Figure A.5: Accommodation of the Science Reference Frame within the GRACE spacecraft

A.6 K-Frame

The K-Frame (KF) is related to the K-band ranging antenna horn. This reference frame is fundamental for the determination and maintenance of the inter-satellite pointing.

The K-Frame is defined as follows:

origin	center of mass of the satellite maintained by a Center of Mass Calibration & Trim maneuver
$\mathbf{x}_{KF}$	coincides with the CoM-to-PhC vector, i.e. the line joining the satellite's center of mass with the calibrated KBR antenna phase center
$\mathbf{y}_{KF}$	completes the right-handed orthogonal triad
$\mathbf{z}_{KF}$	cross product of $\mathbf{x}_{KF}$ and the y-axis of the Science Reference Frame $\mathbf{y}_{SRF}$

The vectors representing the K-Frame axes in inertial coordinates are realized as:

$$\begin{aligned} \mathbf{x}_{KF} &= (\mathbf{R}_{iner\to SRF})^T \frac{\mathbf{pc}}{|\mathbf{pc}|} \\ \mathbf{y}_{KF} &= \mathbf{z}_{KF} \times \mathbf{x}_{KF} \\ \mathbf{z}_{KF} &= \mathbf{x}_{KF} \times \mathbf{y}_{SRF} \end{aligned} \tag{A.1}$$

where

$\mathbf{R}_{iner\to SRF}$	is a direction cosine matrix rotating the inertial frame into the Science Reference Frame; it can be derived from the SCA1B quaternions
$\mathbf{pc}$ ...	is the CoM-to-PhC vector, i.e. KBR antenna phase center vector, given in SRF coordinates; its values are provided in the VKB1B data product

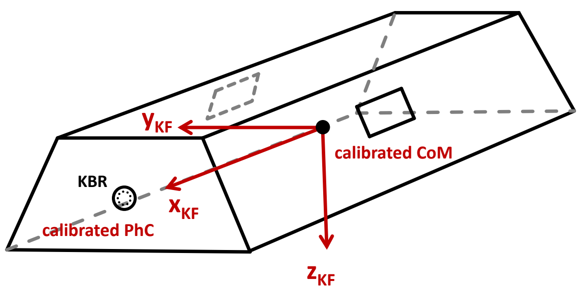

Figure A.6: Accommodation of the K-Frame within the GRACE spacecraft

A.7 Line-of-Sight Frame

Along with the K-Frame, the Line-of-Sight frame (LOS-frame) is fundamental for the determination and maintenance of the inter-satellite pointing.

The LOS-Frame is defined as follows:

origin	center of mass of the satellite maintained by a Center of Mass Calibration & Trim maneuver
$\mathbf{x}_{LOS}$	coincides with the LOS, i.e. the imaginary connection line between the center of mass of each satellite
$\mathbf{y}_{LOS}$	cross product of $\mathbf{x}_{LOS}$ and the geocentric position vector of GRACE-A
$\mathbf{z}_{LOS}$	completes the right-handed orthogonal triad

The axis triad of the LOS-frame is realized as:

$$
\begin{aligned}
\mathbf{x}_{LOS_j} &= \frac{\mathbf{r}_i - \mathbf{r}_j}{|\mathbf{r}_i - \mathbf{r}_j|} \\
\mathbf{y}_{LOS_j} &= \mathbf{x}_{LOS_j} \times \frac{\mathbf{r}_A}{|\mathbf{r}_A|} \\
\mathbf{z}_{LOS_j} &= \mathbf{x}_{LOS_j} \times \mathbf{y}_{LOS_j}
\end{aligned}
\tag{A.2}
$$

where $i, j = A, B$, $i \neq j$ and $\mathbf{r}$ is the satellite's position vector given in the inertial frame.

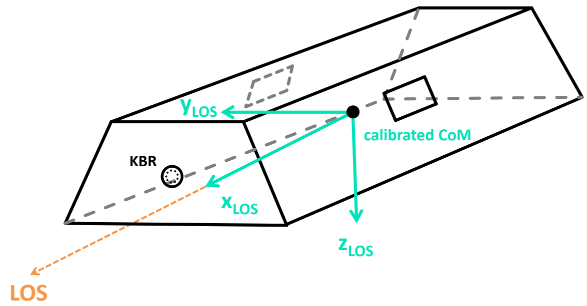

Figure A.7: accommodation of the LOS-frame within the GRACE spacecraft

A.8 Common Reference Frame

The Common Reference Frame (CR) is needed for the combination of the star camera attitude data when applying the method based on merging exclusively the boresight axes. There are at least two ways how to define this frame, cf. Mandea *et al.* (2010) and Jørgensen *et al.* (2008). These two definitions are discussed in Section 5.2.2. For the data analysis presented in this thesis we used the definition by Mandea *et al.* (2010).

The Common Reference Frame is defined as follows:

$$
\begin{aligned}
\mathbf{x}_{CR} &= -\frac{\mathbf{z}_1 \times \mathbf{z}_2}{|\mathbf{z}_1 \times \mathbf{z}_2|} \\
\mathbf{y}_{CR} &= \mathbf{z}_{CR} \times \mathbf{x}_{CR} \\
\mathbf{z}_{CR} &= -\frac{\mathbf{z}_1 + \mathbf{z}_2}{|\mathbf{z}_1 + \mathbf{z}_2|}
\end{aligned}
\tag{A.3}
$$

where $\mathbf{z}_1, \mathbf{z}_2$ are the star camera boresight vectors.

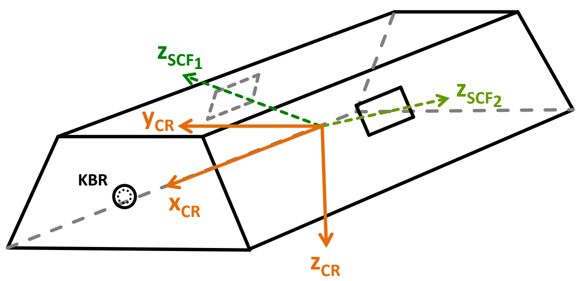

Figure A.8: Accommodation of the Common Reference Frame within the GRACE satellite

A.9 Inertial frame

The inertial frame refers to the International Celestial Reference Frame (ICRF), realized by the J2000.0 equatorial coordinates. The defintion can be found e.g. in McCarthy (1996).

A.10 Terrestrial frame

The terrestrial frame is represented by the International Terrestrial Reference Frame (ITRF). For the definition see e.g. McCarthy (1996).

The transformation between the ICRF and ITRF are performed based on the conventions published by the International Earth Rotation and Reference System Service (IERS) (McCarthy, 1996; Montenbruck and Gill, 2000).

A.11 GRACE time

The GRACE mission time is defined as the GPS atomic time expressed as seconds since January 1st, 2000, 12:00 h. The GRACE mission time is used for time-tagging of the Level-1A and Level-1B data.

B
Attitude representation

The spacecraft's attitude can be expressed as coordinate transformation, which transforms a particular reference frame into a target reference frame. The representations of the spacecraft's attitude used in this thesis are based on the direction cosine matrix, quaternions and roll, pitch and yaw angles. There is no single best approach for the attitude representation as every approach has its specific advantages and disadvantages related to physical interpretation, processing time, ambiguities, etc., which determine the choice for any particular representation. A comprehensive theory about the attitude representation is provided e.g. by Wertz (1978).

B.1 Direction cosine matrix

The direction cosine matrix $\mathbf{R}_{A\to B}$, sometimes called as attitude matrix, transforms a vector $\mathbf{v}$ from an original reference frame A into a target reference frame B:

$$\mathbf{v}_B = \mathbf{R}_{A\to B} \cdot \mathbf{v}_A \tag{B.1}$$

The direction cosine matrix is a real orthogonal 3×3 matrix with $det(\mathbf{R}_{A\to B}) = 1$:

$$\mathbf{R}_{A\to B} = \begin{bmatrix} a_{11} & a_{12} & a_{13} \\ a_{21} & a_{22} & a_{23} \\ a_{31} & a_{32} & a_{33} \end{bmatrix} \tag{B.2}$$

The inverse transformation is defined as

$$\mathbf{v}_A = (\mathbf{R}_{A\to B})^{-1} \cdot \mathbf{v}_B = (\mathbf{R}_{A\to B})^T \cdot \mathbf{v}_B \tag{B.3}$$

A sequence of rotations is defined as

$$\mathbf{R}_{A\to C} = \mathbf{R}_{B\to C} \cdot \mathbf{R}_{A\to B} \tag{B.4}$$

Considering the original frame being defined by a right-handed orthogonal triad $\{u, v, w\}$ and analogically the target frame by $\{x, y, z\}$, then the matrix elements are the components of the original frame unit vectors in target frame coordinates, i.e.

$$\mathbf{R}_{uvw\to xyz} = \begin{bmatrix} x_u & x_v & x_w \\ y_u & y_v & y_w \\ z_u & z_v & z_w \end{bmatrix} \tag{B.5}$$

B.2 Quaternions

The spacecraft's attitude can be further expressed in terms of a quaternion q. The quaternion is represented by a 4-tuple of real numbers

$$q = (q_0, q_1, q_2, q_3) \tag{B.6}$$

The definition and the operations with quaternions are provided separately in Appendix C.

The quaternion can be converted into a direction cosine matrix by

$$\mathbf{R}_{A\to B} = \begin{bmatrix} 2q_0^2 - 1 + 2q_1^2 & 2q_1q_2 + 2q_0q_3 & 2q_1q_3 - 2q_0q_2 \\ 2q_1q_2 - 2q_0q_3 & 2q_0^2 - 1 + 2q_2^2 & 2q_2q_3 + 2q_0q_1 \\ 2q_1q_3 + 2q_0q_2 & 2q_2q_3 - 2q_0q_1 & 2q_0^2 - 1 + 2q_3^2 \end{bmatrix} \tag{B.7}$$

and vice versa, cf. Equation C.23.

B.3 Roll, pitch, yaw

The orientation of rigid body to a desired attitude can be performed by three successive rotations about the body frame axes. The first rotation is about any arbitrary axis, the second rotation is about one of the two axes not used for the first rotation, and the third rotation is about one of the two axes not used for the second rotation. There are 12 sets of possible successive rotations about body-fixed axes. In the literature, these rotations are commonly called as Euler angle rotations.

For satellite control, the 3-2-1 rotation is commonly used, which means rotation of the satellite first about its z- (yaw-) , then about its y- (pitch-) and then about its x- (roll-) axis about the respective yaw (ϕ), pitch (θ) and roll (ψ) angles:

$$\mathbf{R}_{A\to B} = \mathbf{R_1}(\psi) \cdot \mathbf{R_2}(\theta) \cdot \mathbf{R_3}(\phi) \tag{B.8}$$

where $\mathbf{R_{1-3}}$ are the elementary rotation about the x-, y- and z-axes:

$$\mathbf{R_1} = \begin{bmatrix} 1 & 0 & 0 \\ 0 & \cos\alpha & \sin\alpha \\ 0 & -\sin\alpha & \cos\alpha \end{bmatrix} \tag{B.9}$$

$$\mathbf{R_2} = \begin{bmatrix} \cos\alpha & 0 & -\sin\alpha \\ 0 & 1 & 0 \\ \sin\alpha & 0 & \cos\alpha \end{bmatrix} \tag{B.10}$$

$$\mathbf{R_3} = \begin{bmatrix} \cos\alpha & \sin\alpha & 0 \\ -\sin\alpha & \cos\alpha & 0 \\ 0 & 0 & 1 \end{bmatrix} \tag{B.11}$$

Consequently, the resulting direction cosine matrix of the 3-2-1 rotation is

$$\mathbf{R}_{A\to B} = \begin{pmatrix} c\theta c\phi & c\theta s\phi & -s\theta \\ -c\psi s\phi + s\psi s\theta c\phi & c\psi c\phi + s\psi s\theta s\phi & s\psi c\theta \\ s\psi s\phi + c\psi s\theta c\phi & -s\psi c\phi + c\psi s\theta s\phi & c\psi c\theta \end{pmatrix} \tag{B.12}$$

with $c := \cos()$ and $s := \sin()$.

In the inverse process, from a known direction cosine matrix $\mathbf{R}_{A \to B}$, the roll, pitch and yaw angles can be obtained as:

$$\begin{aligned} \psi &= -\arctan\left(\frac{a_{23}}{a_{33}}\right) \\ \theta &= \arcsin(a_{13}) \\ \phi &= -\arctan\left(\frac{a_{12}}{a_{11}}\right) \end{aligned} \tag{B.13}$$

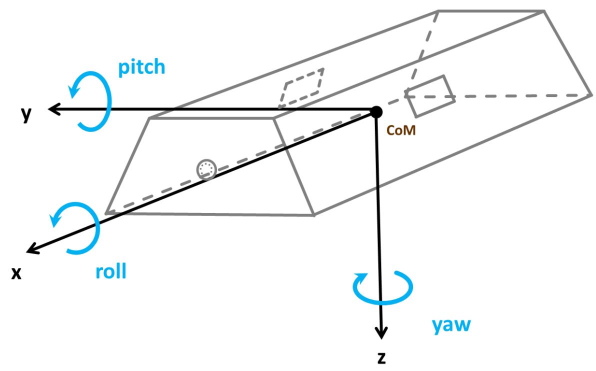

Figure B.1: Roll, pitch and yaw rotation about satellite's body-fixed frame axes

C
Quaternions

The GRACE Level-1A and Level-1B star camera data are provided in terms of quaternions. For the SCA data processing and analysis, the operations with quaternions are inevitable. In the following, the fundamentals of the quaternion algebra are introduced, which are based on the theory presented by Kuipers (1999).

C.1 Defintion

The quaternions were introduced in 1843 by William Rowan Hamilton and can be seen as hyper-complex numbers of rank 4.

A quaternion is denoted by a some lower case letter p, q or r. The quaternion can either be represented as a 4-tuple of real numbers, i.e. as an element of R^4

$$q = (q_0, q_1, q_2, q_3) \tag{C.1}$$

where q_0, q_1, q_2, q_3 are real numbers or scalars;

or be represented by its scalar part q_0 and vector part $\mathbf{q}$

$$q = q_0 + \mathbf{q} = q_0 + \mathbf{i}q_1 + \mathbf{j}q_2 + \mathbf{k}q_3 \tag{C.2}$$

where $\mathbf{i}$, $\mathbf{j}$, $\mathbf{k}$ denote the standard orthonormal basis for R^3

$$\begin{aligned} \mathbf{i} &= (1,0,0) \\ \mathbf{j} &= (0,1,0) \\ \mathbf{k} &= (0,0,1) \end{aligned} \tag{C.3}$$

Products of these basis vectors are needed e.g. for the definition of multiplication of two quaternions. They are defined as

$$\begin{aligned} \mathbf{i}^2 = \mathbf{j}^2 = \mathbf{k}^2 = \mathbf{ijk} &= -1 \\ \mathbf{ij} = \mathbf{k} &= -\mathbf{ij} \\ \mathbf{jk} = \mathbf{i} &= -\mathbf{kj} \\ \mathbf{ki} = \mathbf{j} &= -\mathbf{ik} \end{aligned} \tag{C.4}$$

Further, a complex conjugate of a quaternion can be defined. The complex conjugate of a quaternion q defined in Eq. C.2, is denoted as q^* and is given by

$$q^* = q_0 - \mathbf{q} = q_0 - \mathbf{i}q_1 - \mathbf{j}q_2 - \mathbf{k}q_3 \tag{C.5}$$

The complex conjugate of two quaternions is defined as

$$(pq)^* = q^*p^* \tag{C.6}$$

C.2 Operations with quaternions

Equality

Two quaternions p and q are equal if and only if they have exactly the same components. If

$$p = p_0 + \mathbf{i}p_1 + \mathbf{j}p_2 + \mathbf{k}p_3$$

and

$$q = q_0 + \mathbf{i}q_1 + \mathbf{j}q_2 + \mathbf{k}q_3$$

then $p = q$ if and only if

$$\begin{aligned} p_0 &= q_0 \\ p_1 &= q_1 \\ p_2 &= q_2 \\ p_3 &= q_3 \end{aligned} \tag{C.7}$$

Addition

The sum of two quaternions p and q is defined by adding the correspondent components. The sum of two quaternions is again a quaternion.

$$p + q = (p_0 + q_0) + \mathbf{i}(p_1 + q_1) + \mathbf{j}(p_2 + q_2) + \mathbf{k}(p_3 + q_3) \tag{C.8}$$

The addition of quaternions is both assosiative and commutative.

Multiplication

Product of a quaternion and a scalar

A product of a scalar c and a quaternion q is defined by multiplication of each quaternion component by the scalar. The product is again a quaternion.

$$c \cdot q = cq_0 + \mathbf{i}cq_1 + \mathbf{j}cq_2 + \mathbf{k}cq_3 \tag{C.9}$$

Product of two quaternions

The multiplication of two quaternions can be defined as

$$pq = (p_0 + \mathbf{p})(q_0 + \mathbf{q}) = p_0q_0 - \mathbf{p} \cdot \mathbf{q} + p_0\mathbf{q} + q_0\mathbf{p} + \mathbf{p} \times \mathbf{q} \tag{C.10}$$

The product of two quaternions is again a quaternion, its components can be computed as

$$pq = r = r_0 + \mathbf{i}r_1 + \mathbf{j}r_2 + \mathbf{k}r_3 \tag{C.11}$$

$$\begin{aligned} r_0 &= p_0q_0 - p_1q_1 - p_2q_2 - p_3q_3 \\ r_1 &= p_0q_1 + p_1q_0 + p_2q_3 - p_3q_2 \\ r_2 &= p_0q_2 - p_1q_3 + p_2q_0 + p_3q_1 \\ r_3 &= p_0q_3 + p_1q_2 - p_2q_1 + p_3q_0 \end{aligned} \tag{C.12}$$

The product of two quaternions is not commutative, hence

$$pq \neq qp \tag{C.13}$$

Inverse

The inverse of a quaternion fulfills the following condition

$$q^{-1}q = qq^{-1} = 1 \tag{C.14}$$

The inverse of a non-zero quaternion is defined as

$$q^{-1} = \frac{q^*}{|q|^2} \tag{C.15}$$

with q^* being complex conjugate of the quaternion (Eq. C.5)
$|q|$ being the norm of the quaternion
$|q| = \sqrt{q^*q}$

The inverse of a unit quaternion, i.e. $|q| = 1$, is equal to its complex conjugate

$$q^{-1} = q^* \tag{C.16}$$

C.3 Quaternion as rotation operator

The quaternions are particularly well suited for use as rotation operators. The relation between the rotation through an angle ψ about an axis $\mathbf{u}$ and a normalized or unit quaternion q is following (cf. Fig. C.1(a)):

$$\begin{aligned} q = q_0 + \mathbf{q} &= \cos\frac{\psi}{2} + \mathbf{u}\sin\frac{\psi}{2} \\ &= \begin{pmatrix} \cos\frac{\psi}{2} \\ \sin\frac{\psi}{2}\cos\alpha \\ \sin\frac{\psi}{2}\cos\beta \\ \sin\frac{\psi}{2}\cos\gamma \end{pmatrix} \end{aligned} \tag{C.17}$$

where $\cos\alpha, \cos\beta, \cos\gamma$ are the direction cosines for the rotation axis u.

The angle related to the quaternion is only half the angle of the desired rotation. This is because the rotation operator based on a quaternion is defined as a product of two quaternions (Eq. C.19).

In linear algebra, one of the classic rotation operators is the direction cosine matrix $\mathbf{R}$. The rotation of vector $\mathbf{v}$ is then given as

$$\mathbf{w} = \mathbf{R}\mathbf{v} \tag{C.18}$$

Analogically, the rotation of a vector $\mathbf{v}$ when using quaternions as the rotation operator (Fig. C.1(b)) is defined as

$$\mathbf{w} = q^*\mathbf{v}q \qquad \textit{or} \qquad \mathbf{w} = q\mathbf{v}q^* \tag{C.19}$$

Here, the vector $\mathbf{v}$ can be considered as pure quaternion, i.e. a quaternion with a zero scalar part: $v = 0 + \mathbf{v}$. From the geometrical point of view, the operator $q^*\mathbf{v}q$ can be considered as a *frame* rotation (i.e. the vector $\mathbf{v}$ is considered as fixed, while the reference frame is rotated) and the operator $q\mathbf{v}q^*$ as a *point* rotation (i.e. the reference frame is considered to be fixed, while the vector is rotated).

The Eq. C.19 can be further expanded so that the rotation operator can be expressed in terms of a direction cosine matrix rotating a reference frame $\mathbf{a}$ into reference frame $\mathbf{b}$:

$$\begin{aligned} \mathbf{w} = q^*\mathbf{v}q &= (q_0 - \mathbf{q})(0 + \mathbf{v})(q_0 + \mathbf{q}) \\ &= (2q_0^2 - 1)\mathbf{v} + 2(\mathbf{v}\cdot\mathbf{q})\mathbf{q} + 2q_0(\mathbf{v}\times\mathbf{q}) \end{aligned} \tag{C.20}$$

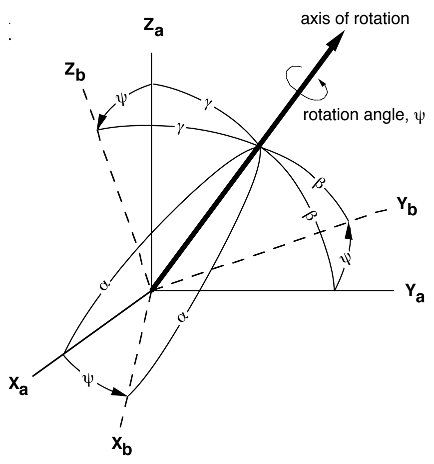

(a) A sketch of a frame rotation. The rotation of a frame **a** through an angle ψ about the axis of rotation **u** into a frame **b** (Wu *et al.*, 2006)

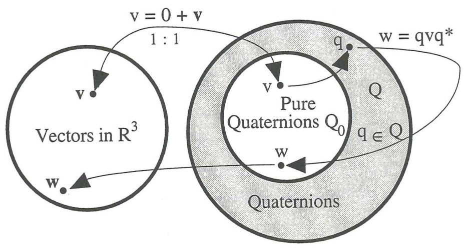

(b) Quaternion operation on vectors (Kuipers, 1999)

Figure C.1: Quaternion as rotation operator

$$
\begin{aligned}
\mathbf{w} = q^* \mathbf{v} q \quad &= \mathbf{R}_{\mathbf{a}\to\mathbf{b}} \cdot \mathbf{v} \\
&= \begin{bmatrix} 2q_0^2 - 1 + 2q_1^2 & 2q_1q_2 + 2q_0q_3 & 2q_1q_3 - 2q_0q_2 \\ 2q_1q_2 - 2q_0q_3 & 2q_0^2 - 1 + 2q_2^2 & 2q_2q_3 + 2q_0q_1 \\ 2q_1q_3 + 2q_0q_2 & 2q_2q_3 - 2q_0q_1 & 2q_0^2 - 1 + 2q_3^2 \end{bmatrix} \begin{bmatrix} v_1 \\ v_2 \\ v_3 \end{bmatrix}
\end{aligned} \tag{C.21}
$$

The relation between the quaternion and the direction cosine matrix (Eq. C.21) clearly suggest the derivation of the quaternion from any given rotation matrix **R** with r_{ij} elements: If

$$
\mathbf{R} = \begin{bmatrix} r_{11} & r_{12} & r_{13} \\ r_{21} & r_{22} & r_{23} \\ r_{31} & r_{32} & r_{33} \end{bmatrix} \tag{C.22}
$$

then

$$
\begin{aligned}
q_0 &= \tfrac{1}{2}\sqrt{r_{11} + r_{22} + r_{33} + 1} \\
q_1 &= \frac{(r_{23} - r_{32})}{4q_0} \\
q_2 &= \frac{(r_{31} - r_{13})}{4q_0} \\
q_3 &= \frac{(r_{12} - r_{21})}{4q_0}
\end{aligned} \tag{C.23}
$$

Quaternion to angular rate

When time series of quaternions rotating a reference frame **a** into a reference frame **b** are available, angular rates about the axes of frame **b** can be computed.

First, the difference of the two quaternions given to epoch t and $t + \Delta t$ is determined:

$$
q(t)^{-1} q(t + \Delta t) = \begin{pmatrix} v_0 \\ v_1 \\ v_2 \\ v_3 \end{pmatrix} \tag{C.24}
$$

Then, the angle of rotation which occurred within Δt epoch is computed:

$$\Delta\Phi = 2 \cdot \arccos(v_0) \tag{C.25}$$

And as next, the angular rate and its components can be determined:

$$\omega = \frac{\Delta\Phi}{\Delta t} \tag{C.26}$$

$$\begin{aligned} \omega_x &= v_1 \frac{\omega}{\sin(\frac{\Delta\Phi}{2})} \\ \omega_y &= v_2 \frac{\omega}{\sin(\frac{\Delta\Phi}{2})} \\ \omega_z &= v_3 \frac{\omega}{\sin(\frac{\Delta\Phi}{2})} \end{aligned} \tag{C.27}$$

D
Auxiliary computations

D.1 Inter-boresight angle

The inter-boresight angle θ is the angle between the unit vectors $\mathbf{z}_{SCF_1}$ and $\mathbf{z}_{SCF_2}$ which represent the boresights of the two star camera heads (Fig. D.1).

The inter-boresight angle can be computed as

$$\theta = \arccos \frac{\mathbf{z}_{SCF_1} \cdot \mathbf{z}_{SCF_2}}{\mid \mathbf{z}_{SCF_1} \mid \cdot \mid \mathbf{z}_{SCF_2} \mid} \tag{D.1}$$

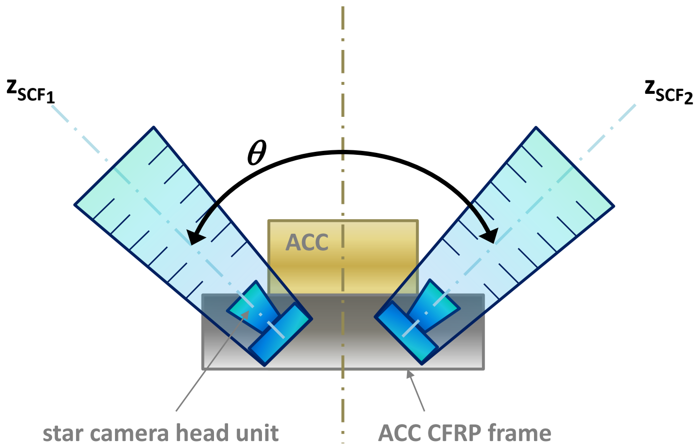

Figure D.1: The star camera inter-boresight angle θ is the angle between the optical axes of the two star camera heads

There are two ways how to obtain the unit vectors of the star camera boresight. The first alternative is (Bock and Lühr, 2001):

$$\mathbf{z}_{SCF_i} = \begin{pmatrix} \cos\delta \cdot \cos\alpha \\ \cos\delta \cdot \sin\alpha \\ \sin\delta \end{pmatrix} \tag{D.2}$$

with

$$\alpha = \arctan \frac{q_2 q_3 - q_1 q_4}{q_1 q_3 + q_2 q_4} \tag{D.3}$$

$$\sin\delta = -q_1^2 - q_2^2 + q_3^2 + q_4^2 \tag{D.4}$$

$$\cos\delta = \sqrt{1-\sin^2\delta} \tag{D.5}$$

where α, δ ... right ascension and declination of the star camera boresight in the inertial frame

q_1, q_2, q_3, q_4 ... quaternion elements giving the rotation from the inertial frame into the star camera frame, i.e. the GRACE Level-1A SCA quaternions

i ... star camera head identifier, i = 1,2

The second alternative suggests obtaining the $\mathbf{z}_{SCF_i}$ from the direction-cosine matrix derived from the attitude quaternions:

$$SCA1A\ [q_0, q_1, q_2, q_3] \rightarrow \mathbf{R}_{iner\rightarrow SCF_i} = \begin{bmatrix} x_1 & x_2 & x_3 \\ y_1 & y_2 & y_3 \\ z_1 & z_2 & z_3 \end{bmatrix}_i = \begin{bmatrix} (\mathbf{x}_{SCF_i})^T \\ (\mathbf{y}_{SCF_i})^T \\ (\mathbf{z}_{SCF_i})^T \end{bmatrix} \tag{D.6}$$

D.2 β' angle

The β' is the angle between the direction to the Sun and the orbital plane of the satellite. When the Sun is in the orbital plane, $\beta' = 0$.

The β' angle can be computed as

$$\beta' = \arccos \frac{\mathbf{n} \cdot \mathbf{r}_{Sun}}{|\mathbf{n}| \cdot |\mathbf{r}_{Sun}|} - 90° \tag{D.7}$$

with $\mathbf{r}_{Sun}$ ... position vector of the Sun in the inertial frame (ICRF/J2000.0), which can be obtained from e.g. the JPL HORIZONS SYSTEM
$\mathbf{n}$ ... normal vector of the satellite's orbit $\mathbf{n} = -(\mathbf{r}_{sat} \times \mathbf{v}_{sat})$
$\mathbf{r}_{sat}, \mathbf{v}_{sat}$ ... satellite's position and velocity in the inertial frame

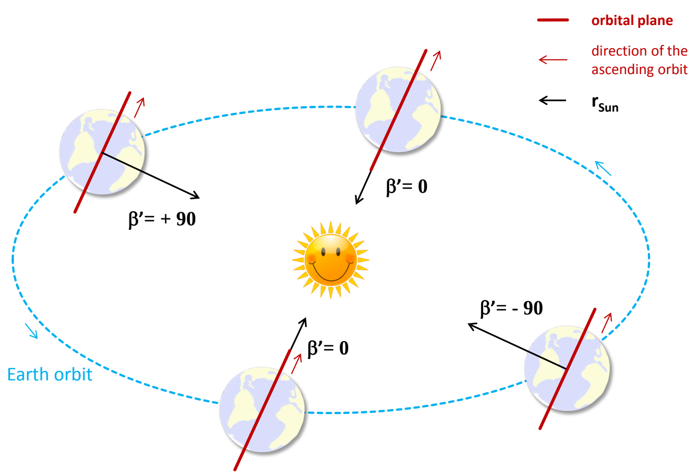

Figure D.2: β' angle is the angle between the direction to the Sun and the satellite's orbital plane

Figure D.3 shows the β' angle of the GRACE satellites for the period 2002 - 2009. The β' angle does not reach exactly $\pm 90°$ because of the drift of the ascending node of the satellite orbit. The β' angle passes through zero every 161 ± 3 d.

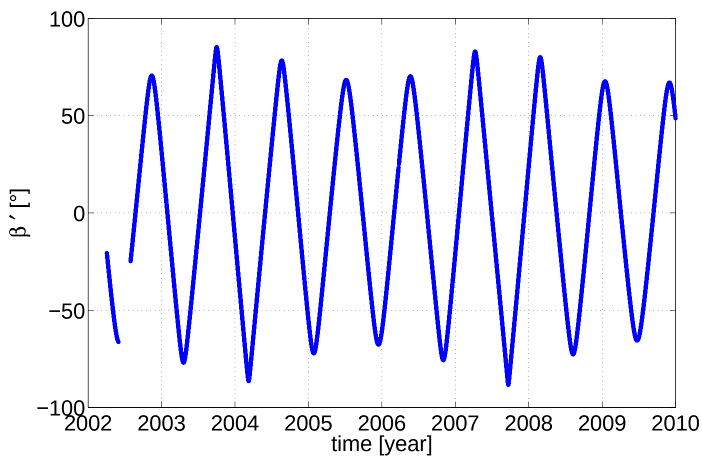

Figure D.3: β' angle of the GRACE satellites in 2002-2009

D.3 Argument of latitude

The argument of latitude u describes the position of the satellite along its orbit. u is the angle between the ascending node and the satellite, measured in the satellite's orbital plane, cf. Figure D.4.

The argument of latitude is defined as

$$u = \omega + v \tag{D.8}$$

where ω and v are the Keplerian orbital elements: ω-argument of perigee, v-true anomaly. The values of the argument of latitude are within $u = \langle 0; 360°\rangle$. The argument of latitude can be derived from the satellite's position $\mathbf{r}_{sat} = (x, y, z)^T$ and velocity $\mathbf{v}_{sat} = (v_x, v_y, v_z)^T$ vectors in inertial coordinates as

$$\mathbf{h} = \frac{\mathbf{r}_{sat} \times \mathbf{v}_{sat}}{|\mathbf{r}_{sat} \times \mathbf{v}_{sat}|} = \begin{pmatrix} h_x \\ h_y \\ h_z \end{pmatrix} \tag{D.9}$$

$$u = \arctan\left(\frac{z}{-x \cdot h_y + y \cdot h_x}\right) \tag{D.10}$$

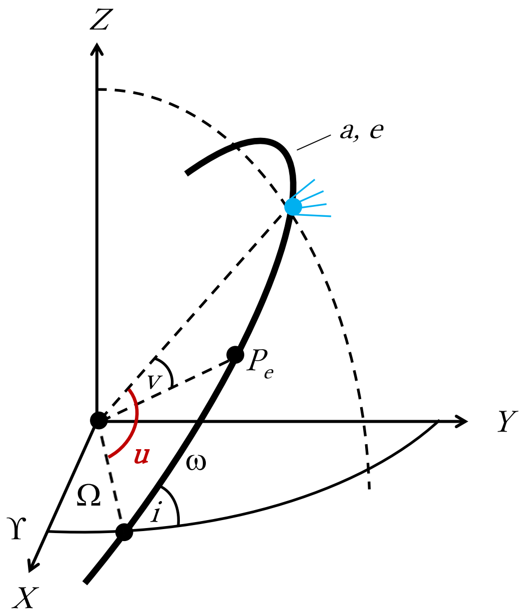

Figure D.4: Keplerian orbital elements: a - semi-major axis, e - numerical eccentricity, i - orbit inclination, Ω - right ascension of ascending node, ω - argument of perigee, v - true anomaly, u - argument of latitude

In this thesis, some of the parameters of interest are plotted as a function of time and argument of latitude. This allows to plot the values along the whole orbit for unlimited period of time, which is advantageous especially for observing the long-term systematic effects. Figure D.5 shows the argument of latitude as a funtion of time for 1 day. The values of the parameter of interest are then expressed by color, cf. e.g. Figure 3.3.

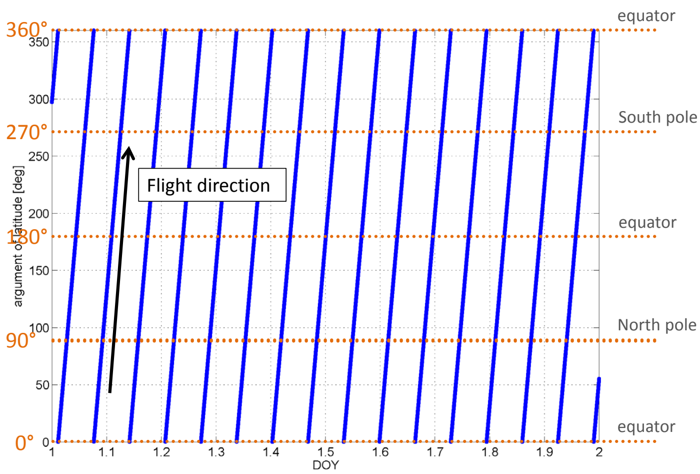

Figure D.5: Argument of latitude

Bibliography

A, G., Wahr, J., and Zhong, S. (2013). Computations of the viscoelastic response of a 3-D compressible Earth to surface loading: an application to Glacial Isostatic Adjustment in Antarctica and Canada. *Geophysical Journal International*, 192, Pages 557–572, doi: 10.1093/gji/ggs030.

Anderson, D. (1984). Alignment of resonant optical cavities. *Applied Optics*, 23, Pages 2944–2949, doi: 10.1364/AO.23.002944.

Arbinger, C., D'Amico, S., Feucht, U., and Finzi, A. (2003). The GRACE formation: science mode pointing performance. *3rd International Workshop on Satellite Constellations and Formations Flying, Pisa, Italy, Feb 24-26, 2003.*

Bandikova, T. and Flury, J. (2014). Improvement of the GRACE star camera data based on the revision of the combination method. *Advances in Space Research*, 54, Pages 1818–1827, doi: 10.1016/j.asr.2014.07.004.

Bandikova, T., Flury, J., and Ko, U.-D. (2010). Analysis of systematic effects in GRACE inter-satellite pointing. *GRACE Science Team Meeting, Nov 11-12, 2010, Potsdam.* GSTM proceedings 2010.

Bandikova, T., Flury, J., and Ko, U.-D. (2012). Characteristics and accuracies of the GRACE inter-satellite pointing. *Advances in Space Research*, 50, Pages 123–135, doi: 10.1016/j.asr.2012.03.011.

Baur, O., Kuhn, M., and Featherstone, W. (2013). Continental mass change from GRACE over 2002–2011 and its impact on sea level. *Journal of Geodesy*, 87, Pages 117–125, doi: 10.1007/s00190-012-0583-2.

Bender, P., Wiese, D., and Nerem, R. (2008). A possible dual-GRACE mission with 90 degree and 63 degree inclination orbits. In *Proc. 3rd Int. Symp. on Formation Flying, Missions and Technologies, Noordwijk ,The Netherlands.*

Bettadpur, S. (2012). Gravity Recovery and Climate Experiment: Product specification document. Technical Report GRACE 327-720, Center for Space Research, The University of Texas at Austin.

Bettadpur, S. and the CSR Level-2 Team (2012). Insights into the Earth System mass variability from CSR-RL05 GRACE gravity fields. *EGU General Assembly, 2012.*

Beutler, G., Jäggi, A., Mervart, L., and Meyer, U. (2010). The celestial mechanics approach: theoretical foundations. *Journal of Geodesy*, 84, Pages 605–624, doi: 10.1007/s00190-010-0401-7.

Blockley, R. and Shyy, W. (2010). *Encyclopedia of Aerospace Engineering. Volume 5 Dynamics and Control.* Wiley, ISBN: 978-0-470-75440-5.

Bock, R. and Lühr, H. (2001). CHAMP attitude aberration correction. Technical Report CH-GFZ-TN-2702, GFZ Potsdam.

Bruinsma, S., Lemoine, J.-M., Biancale, R., and Vales, N. (2010). CNES/GRGS 10-day gravity field models (release 2) and their evaluation. *Advances in Space Research*, 45, Page 587–601, doi: 10.1016/j.asr.2009.10.012.

Case, K., Kruizinga, G., and Wu, S.-C. (2010). GRACE level-1B data product user handbook. Technical Report JPL D-22027, Jet Propulsion Laboratory.

Cazenave, A. and Llovel, W. (2010). Contemporary sea level rise. *Annual Review of Marine Science*, 2, Pages 145–173, doi: 10.1146/annurev-marine-120308-081105.

Crassidis, J., Lai, K.-L., and Harman, R. (2005). Real-time attitude-independent three-axis magnetometer calibration. *Journal of Guidance, Control and Dynamics*, 28, Pages 115–120, doi: 10.2514/1.6278.

Dahle, C., Flechtner, F., Gruber, C., König, D., König, R., Michalak, G., and Neumayer, K.-H. (2014). *Observation of the System Earth from Space - CHAMP, GRACE, GOCE and future missions*, Chapter GFZ RL05: An Improved Time-Series of Monthly GRACE Gravity Field Solutions, Pages 29–39. Springer, doi: 10.1007/978-3-642-32135-1_4.

de Angelis, M., Bertoldi, A., Cacciapuoti, L., Giorgini, A., Lamporesi, G., Prevedelli, M., Saccorotti, G., Sorrentino, F., and Tino, G. (2009). Precision gravimetry with atomic sensors. *Measurement Science and Technology*, 20, Page 022001, doi: 10.1088/0957-0233/20/2/022001.

Doll, B. and Wolters, R. (1999). GRACE Coarse Earth- & Sun Sensor Specification 327-40230. Technical Report GR-DSS-SP-2230, DaimlerChrysler Aerospace.

Doornbos, E., Förster, M., Fritsche, B., van Helleputte, T., van den Ijssel, J., and et al. (2009). Air density models derived from multi-satellite drag observations. Technical Report ESTEC contract 210022/07/NL/HE, TU Delft.

Eisenman, A. R. and Liebe, C. C. (1998). The advancing state-of-the-art in second generation star trackers. In *Aerospace Conference, 1998 IEEE*, Volume 1, Pages 111–118. doi: 10.1109/AERO.1998.686810.

Elsaka, B. (2012). *Simulated satellite formation flight for detecting the temporal variations of the Earth's gravity field*. PhD thesis, University of Bonn.

Elsaka, B., Raimondo, J.-C., Brieden, P., Reubelt, T., Kusche, J., Flechtner, F., Iran Pour, S., Sneeuw, N., and Müller, J. (2013). Comparing seven candidate mission configurations for temporal gravity field retrieval through full-scale numerical simulation. *Journal of Geodesy*, 88, Pages 31–43, doi: 10.1007/s00190-013-0665-9.

ESA (1999). Gravity Field and Steady-State Ocean Circulation Mission. Report for mission selection of the four candidate Earth Explorer missions ESA SP-1233(1), European Space Agency.

Famiglietti, J. S. and Rodell, M. (2013). Water in the balance. *Science*, 340, Pages 1300–1301, doi: 10.1126/science.1236460 .

Flechtner, F. (2004). GRACE Science Data System Monthly Report February 2004. Technical Report, JPL/GFZ.

Flechtner, F., Morton, P., Watkins, M., and Webb, F. (2014). Status of the GRACE Follow-On mission. In *Gravity, Geoid and Height Systems*. Springer, doi: 10.1007/978-3-319-10837-7_15.

Flury, J., Bettadpur, S., and Tapley, B. (2008). Precise accelerometry onboard the GRACE gravity field satellite mission. *Advances in Space Research*, 42, Pages 1414–1423, doi: 10.1016/j.asr.2008.05.004.

Förste, C., Bruinsma, S., Abrikosov, O., Lemoine, J.-M., Schaller, T., Götze, H.-J., and et al. (2014). The latest combined global gravity field model including GOCE data up to degree and order 2190 of GFZ Potsdam and GRGS Toulouse. *5th GOCE User Workshop, Paris*. http://icgem.gfz-potsdam.de/ICGEM/documents/Foerste-et-al-EIGEN-6C4.pdf.

Frappart, F., Papa, F., Santos da Silva, J., Ramillien, G., Prigent, C., Seyler, F., and Calmant, S. (2012). Surface freshwater storage and dynamics in the Amazon basin during the 2005 exceptional drought. *Environmental Research Letters*, 4, Page 044010, doi: 10.1088/1748-9326/7/4/044010.

Friis-Christensen, E., Lühr, H., Knudsen, D., and Haagmans, R. (2008). Swarm – an Earth observation mission investigating geospace. *Advances in Space Research*, 41, Pages 210–2016, doi: 10.1016/j.asr.2006.10.008.

Frommknecht, B. (2008). *Integrated Sensor Analysis of the GRACE Mission*. PhD thesis, Technische Universität München.

Goodkind, J. (1999). The superconductiong gravimeter. *Review of Scientific Instruments*, 70, Pages 4131–4152, doi: 10.1063/1.1150092.

Han, S.-C., Jekeli, C., and Shum, C. (2004). Time-variable aliasing effects of ocean tides, atmosphere, and continental water mass on monthly mean GRACE gravity field. *Journal of Geophysical Research*, 109, Page B04403, doi: 10.1029/2003JB002501.

Han, S.-C., Shum, C. K., Bevis, M., Ji, C., and Kuo, C.-Y. (2006). Crustal Dilatation Observed by GRACE After the 2004 Sumatra-Andaman Earthquake. *Science*, 313, Pages 658–662, doi: 10.1126/science.1128661.

Heinzel, G., Sheard, B., Brause, N., Danzmann, K., Dehne, M., Gerberding, O., Mahrdt, C., and et al. (2012). Laser Ranging Interferometer for GRACE Follow-On. In *Proceedings of the International Conference on Space Optics (ICSO2012)*. ISCO proceedings.

Herman, J. and Steinhoff, M. (2012). Balancing, turning, Saving: Special AOCS operations to extend the GRACE mission. *SpaceOps 2012, Stockholm, Sweden, June 11-15*. doi: 10.2514/6.2012-1275114.

Herman, J., Presti, D., Codazzi, A., and Belle, C. (2004). Attitude control for GRACE: the first low-flying satellite formation. In *ESA SP-548: 18th International Symposium on Space Flight Dynamics*.

Herman, J., Davis, A., Chin, K., Kinzler, M., Scholz, S., and Steinhoff, M. (2012). Life with a weak heart - prolonging the GRACE mission despite degraded batteries. In *SpaceOps 2012, Stockholm, Sweden, June 11-15*.

Hofmann-Wellenhof, B. and Moritz, H. (2005). *Physical geodesy*. SpringerWienNewYork, ISBN: 3-211-23584-1.

Hofmann-Wellenhof, B., Lichtenegger, H., and Wasle, E. (2008). *GNSS - Global navigation satellite system. GPS, GLONASS, Galileo & more.* SpringerWienNewYork, ISBN: 978-3-211-73012-6.

Horwath, M., Lemoine, J.-M., Biancale, R., and Bourgogne, S. (2010). Improved GRACE science results after adjustment of geometric biases in the Level-1B K-band ranging data. *Journal of Geodesy*, 85, Pages 23–38, doi: 10.1007/s00190-010-0414-2.

Hudson, D. (2003). *In-flight characterisation and calibration of the SuperSTAR accelerometer.* Master thesis, CSR, The University of Texas at Austin.

Inacio, P., Ditmar, P., Klees, R., and Hashemi Farahani, H. (2015). Analysis of star camera errors in GRACE data and their impact on monthly gravity field models. *Journal of Geodesy*, 89, Pages 551–571, doi: 10.1007/s00190-015-0797-1.

Jäggi, A., Hugentobler, U., Bock, H., and Beutler, G. (2007). Precise orbit determination for GRACE using undifferenced or doubly differenced GPS data. *Advances in Space Research*, 39, Pages 1612–1619, doi: 10.1016/j.asr.2007.03.012.

Jäggi, A., Dach, R., Montenbruck, O., Hugentobler, U., Bock, H., and Beutler, G. (2009). Phase center modeling for LEO GPS receiver antennas and its impact on precise orbit determination. *Journal of Geodesy*, 83, Pages 1145–1162, doi: 10.1007/s00190-009-0333-2.

Jäggi, A., Beutler, G., Meyer, U., Prange, L., Dach, R., and Mervart, L. (2012). AIUB-GRACE02S: Status of GRACE Gravity Field Recovery Using the Celestial Mechanics Approach. In S. Kenyon, M. C. Pacino, and U. Marti (Ed.), *Geodesy for Planet Earth*, Volume 136, *International Association of Geodesy Symposia*, Pages 161–169. Springer Berlin Heidelberg, doi: 10.1007/978-3-642-20338-1_20.

Jekeli, C. (2001). *Inertial navigation systems with geodetic applications.* de Gruyter, ISBN: 3-11-015903-1.

Jørgensen, J. L. (2000). In-orbit performance of a fully autonomous star tracker. In *Spacecraft Guidance, Navigation and Control Systems.* 4th ESA International Conference, Oct 18-21, 199, ESTEC, Noordwijk.

Jørgensen, J. L. and Liebe, C. C. (1996). The advanced stellar compass, development and operations. *Acta Astronautica*, 39, Pages 775–783.

Jørgensen, J. L. and Pickles, A. (1998). Fast and robust pointing and tracking using a second generation star tracker. *Proceedings of the International Society for Optical Engineering*, 3351, Pages 51–61.

Jørgensen, P., Jørgensen, J., Denver, T., and Betto, M. (2004). In-flight quality and accuracy of attitude measurements from the CHAMP advanced stellar compass. *Acta Astronautica*, 56, Pages 181–186, doi: 10.1016/j.actaastro.2004.09.012.

Jørgensen, P. S., Jørgensen, J. L., and Denver, T. (2008). On-the-fly merging of attitude solutions. In Sandau et al. (Ed.), *Small satellites for Earth observation.* Springer, ISBN: 978-1-4020-6942-0.

Kang, Z., Tapley, B., Bettadpur, S., Ries, J., and Nagel, P. (2006). Precise orbit determination for GRACE using accelerometer data. *Advances in Space Research*, 38, Pages 2131–2136, doi: 10.1016/j.asr.2006.02.021.

Kim, J. (2000). *Simulation study of a low-low satellite-to-Satellite tracking mission.* PhD thesis, University of Texas at Austin.

Kim, J. and Tapley, B. (2002). Error Analysis of a Low–Low Satellite-to-Satellite Tracking Mission. *Journal of Guidance, Control and Dynamics*, 25, Page 6.

Klinger, B. and Mayer-Gürr, T. (2014). Combination of GRACE star camera and angular acceleration data. *Geophysical Research Abstracts*, 16, Pages EGU2014–5340.

Ko, U.-D. (2008). *Analysis of the characteristics of the GRACE dual one-way ranging system.* PhD thesis, University of Texas at Austin.

Kruizinga, G., Bertiger, W., Byun, S., Finch, C., and et al. (2012). GRACE Level-1 processing status. *GRACE Science Team Meeting, Potsdam, Sep 17-19, 2012.* GSTM 2012 proceedings.

Kruizinga, G., Bertiger, W., Byun, S., Finch, C., and et al. (2013). GRACE Level-1 processing status. *GRACE Science Team Meeting, Austin, TX, Oct 23-25, 2013.* GSTM 2013 proceedings.

Kuipers, J. B. (1999). *Quaternions and ratation sequences. A primer with applications to orbits, aerospace, and virtual reality.* Princeton University Press, Princeton, New Jersey, ISBN: 0-691-05872-5.

Liebe, C. C. (2002). Accuracy performance of star trackers - a tutorial. *IEEE Transactions on Aerospace Electronic Systems*, 38, Pages 587–599, doi: 10.1109/TAES.2002.1008988.

Liu, X. (2008). *Global gravity field recovery from satellite-to-satellite tracking data with acceleration approach.* PhD thesis, Technical University of Delft.

Lundquist, C. A. and Veis, G. (1966). Geodetic Parameters for a 1966 Smithsonian Institution Standard Earth. Sao special report #200, Smithsonian Astrophysical Observatory.

Luthcke, S. B., Zwally, H., Abdalati, W., Rowlands, D. D., Ray, R. D., Nerem, R., Lemoine, F., McCarthy, J. J., and Chinn, D. (2006). Recent Greenland ice mass loss by drainage system from satellite gravity observations. *Science*, 314, Pages 1286–1289, doi: 10.1126/science.1130776.

Luthcke, S. B., Arendt, A. A., Rowlands, D. D., McCarthy, J. J., and Larsen, C. F. (2008). Recent glacier mass changes in the Gulf of Alaska region from GRACE mascon solutions. *Journal of Glaciology*, 54, Pages 767–777, doi: 10.3189/002214308787779933.

Mahrdt, C.rdt, C. (2014). *Laser link acquisition for the GRACE Follow-On laser ranging Interferometry.* PhD thesis, Gottfried Wilhelm Leibniz Universität Hannover.

Mandea, M., Holschneider, M., Lesur, V., and Lühr, H. (2010). *System Earth via geodetic-geophysical space techniques*, Chapter The Earth's magnetic field at the CHAMP satellite epoch. Springer, doi: 10.1007/978-3-642-10228-8_42.

Mayer-Gürr, T. (2006). *Gravitationsfeldbestimmung aus der Analyse Kurzer Bahnbögen am Beispiel der Satellitenmissionen CHAMP und GRACE.* PhD thesis, University of Bonn.

Mayer-Gürr, T., Rieser, D., Höck, E., Brockmann, J.-M., Schuh, W.-D., Krasbutter, I., and at al. (2012). The new combined satellite only model GOCO03s. *International Symposium on Gravity, Geoid and Height Systems GGHS 2012.*

McCarthy, D. (1996). IERS Conventions (1996). Technical Report IERS Technical Note 21, U.S. Naval Observatory.

Meyer, U., Jäggi, A., and Beutler, G. (2012). Monthly gravity field solutions based on GRACE observations generated with the Celestial Mechanics Approach. *Earth and Planetary Science Letters*, 345–348, Pages 72 – 80, doi: 10.1016/j.epsl.2012.06.026.

Michaelis, I. (2015). Star tracker / VFM activities. *Swarm - National CalVal-Meeting, 12.-13.5.2015, GFZ Potsdam.*

Montenbruck, O. and Gill, E. (2000). *Satellite orbits: models, mmethod, applications.* Springer, ISBN: 3-540-67280-X.

Montenbruck, O., van Helleputte, T., Kroes, R., and Gill, E. (2005). Reduced dynamic orbit determination using GPS code and carrier measurements. *Aerospace Science and Technology*, 9, Pages 261–271, doi: 10.1016/j.ast.2005.01.003.

Montenbruck, O., Garcia-Fernandez, M., Yoon, Y., Schön, S., and Jäggi, A. (2008). Antenna phase center calibration for precise positioning of LEO satellites. *GPS Solutions*, 13, Pages 23–34, doi: 10.1007/s10291-008-0094-z.

Müller, J., Naeimi, M., Gitlein, O., Timmen, L., and Denker, H. (2012). A land uplift model in Fennoscandia combining GRACE and absolute gravimetry data. *Physics and Chemistry of the Earth*, 53-54, Pages 54–60, doi: 10.1016/j.pce.2010.12.006.

NGGM-D Team, with contributions by Baldesarra, M., Brieden, P., Danzmann, K., Daras, I., Doll, B., Feili, D., Flechtner, F., Flury, J., Gruber, T., Heinzel, G., Iran Pour, S., Kusche, J., Langemenn, M., Löcher, A., Müller, J., Müller, V., Murböck, M., Naeimi, M., Pail, R., Raimondo, J., Reiche, J., Reubelt, T., Sheard, B., Sneeuw, N., and Wang, X. (2014). *e^2.motion - Earth System Mass Transport Mission (Square) - Concept for a Next Generation Gravity Field Mission - Final Report of Project "Satellite Gravimetry of the Next Generation (NGGM-D)".* Deutsche Geodätische Kommission, ISBN: 978-3-7696-8596-1.

Northrop Grumman (2013). LN-200s Inertial measurement unit. http://www.northropgrumman.com/Capabilities/LN200FOG/Documents/ln200s.pdf.

Panet, I., Flury, J., Biancale, R., Gruber, T., Johannessen, J., van den Broeke, M., and van Dam, T. (2013). Earth System Mass Transport Mission (e.motion): A Concept for Future Earth Gravity Field Measurements from Space. *Surveys in Geophysics*, 34, Pages 141–163, doi: 10.1007/s10712-012-9209-8.

Peterseim, N. (2014). *Twangs - high-frequency disturbing signals in 10 Hz accelerometer data of the GRACE satellites.* PhD thesis, Technische Universität München.

Presti, D., Herman, J., and Codazzi, A. (2004). Mission operations system design and adaptations for the twin-satellite mission GRACE. *Space OPS 2004 Conference.* doi: 10.2514/6.2004-382-219.

Psiaki, M., Martel, F., and Pal, P. (1990). Three-axis attitude determination via Kalman filtering of magnetometer data. *Journal of Guidance, Control and Dynamics*, 13, Pages 506–514, doi: 10.2514/3.25364.

Ray, R. D. and Luthcke, S. B. (2006). Tide model errors and GRACE gravimetry: towards a more realistic assessment. *Geophysical Journal International*, 167, Pages pp. 1055–1059, doi: 10.1111/j.1365-246X.2006.03229.x.

Reigber, C., Schwintzer, P., and Lühr, H. (1999). The CHAMP geopotential mission. *Bollettino di Geofisica Teorica ed Applicata*, 40, Pages 285–289.

Rodell, M., Famiglietti, J. S., Chen, J., Seneviratne, S. I., Viterbo, P., Holl, S., and Wilson, C. R. (2004). Basin scale estimates of evapotranspiration using GRACE and other observations. *Geophysical Research Letters*, 31, Page 20504, doi: 10.1029/2004GL020873.

Rodell, M., Velicogna, I., and Famiglietti, J. S. (2009). Satellite-based estimates of groundwater depletion in India. *Nature*, 460, Pages 999–1003, doi: 10.1038/nature08238.

Romans, L. (2003). Optimal combination of quaternions from multiple star cameras. Technical Report, JPL Internal Memorandum.

Sasgen, I., Konrad, H., Ivins, E., Van den Broeke, M., Bamber, J., Martinec, Z., and Kleemann, V. (2013). Antarctic ice-mass balance 2003 to 2012: regional reanalysis of GRACE satellite gravimetry measurements with improved estimate of glacial-isostatic adjustment based on GPS uplift rates. *The Cryosphere*, 7, Pages 1499–1512, doi: 10.5194/tc-7-1499-2013.

Schelkle, M. (2000). The GRACE cold gas attitude and orbit control system. In *3rd International conference on spacecraft propulsion, ESA SP-465*.

Schütze, D. (2015). *Intersatellite laser interferometry. Test environments for GRACE Follow-On*. PhD thesis, Gottfried Wilhelm Leibniz Universität Hannover.

Schütze, D., Stede, G., Müller, V., Gerberding, O., Bandikova, T., Sheard, B., Heinzel, G., and Danzmann, K. (2014a). Laser beam steering for GRACE Follow-On intersatellite Interferometry. *Optics Express*, 22, Pages 24117–24132, doi: 10.1364/OE.22.024117.

Schütze, D., Müller, V., Stede, G., Sheard, B., Heinzel, G., Danzmann, K., Sutton, A., and Shaddock, D. (2014b). Retroreflector for GRACE Follow-On: Vertex vs. point of minimal coupling. *Optics Express*, 22, Pages 9324–9333, doi: 10.1364/OE.22.009324.

Sheard, B. S., Heinzel, G., Danzmann, K., Shaddock, D. A., and et al. (2012). Intersatellite laser ranging instrument for the GRACE Follow-On mission. *Journal of Geodesy*, 86, Pages 1083–1095, doi: 10.1007/s00190-012-0566-3.

Siemes, C. (2011). GOCE gradiometer calibration and Level 1b data processing. Technical Report EWP-2384, European Space Agency.

Stanton, R. (2000). Science & Mission requirements document. Technical Report JPL D-15928, Jet Propulsion Laboratory, University of Texas Center for Space Research, GeoForschungszentrum Potsdam.

Steffen, H., Denker, H., and Müller, J. (2008). Glacial isostatic adjustment in Fennoscandia from GRACE data and comparison with geodynamical models. *Journal of Geodynamics*, 46, Pages 155–164, doi: 10.1016/j.jog.2008.03.002.

Stummer, C., Fecher, T., and Pail, R. (2011). Alternative method for angular rate determination within the GOCE gradiometer processing. *Journal of Geodesy*, 85, Pages 585–596, doi: 10.1007/s00190-011-0461-3.

Svendsen, P., Andersen, O., and Nielsen, A. (2013). Acceleration of the Greenland ice sheet mass loss as observed by GRACE: Confidence and sensitivity. *Earth and Planetary Science Letters*, 364, Pages 24–29, doi: 10.1016/j.epsl.2012.12.010.

Tapley, B., Bettadpur, S., Watkins, M., and Reigber, C. (2004). The Gravity Recovery and Climate Experiment: Mission overview and early results. *Geophysical Research Letters*, 31, doi: 10.1029/2004GL019920.

Tapley, B., Flechtner, F., Bettadpur, S., and Watkins, M. (2013). The status and future prospect for GRACE after the first decade. *AGU, Fall Meeting 2013, abstract G32A-01*.

Thomas, J. (1999). An analysis of gravity-field estimation based on intersatellite dual 1-way biased ranging. Technical Report JPL 98-15, Jet Propulsion Laboratory.

Torge, W. (1989). *Gravimetry*. Walter de Gruyter, Berlin, New York, ISBN: 3-11-010702-3.

Torge, W. and Müller, J. (2012). *Geodesy*. De Gruyter, ISBN: 978-3-11-020718-7.

Touboul, P., Foulon, B., and Willemenot, E. (1999). Electrostatic space accelerometers for present and future missions. *Acta Astronautica*, 45, Pages 605–617, doi: 10.1016/S0094-5765(99)00132-0.

Usbeck, T., Wohlfart, J., and Schelkle, M. (2004). A flexible cold gas propulsion system concept for different space applications. In *4th Int. Spacecraft Propulsion Conference, June 2-4, 2004*.

van Helleputte, T. and Visser, P. (2008). GPS based orbit determination using accelerometer data. *Aerospace Science and Technology*, 12, Pages 478–484, doi: 10.1016/j.ast.2007.11.002.

Velicogna, I. and Wahr, J. (2006). Measurements of time-variable gravity show mass loss in Antarctica. *Science*, 311, Pages 1754–1756, doi: 10.1126/science.1123785.

Vey, S., Steffen, H., Müller, J., and Boike, J. (2013). Inter-annual water mass variations from GRACE in central Siberia. *Journal of Geodesy*, 87, Pages 287–299, doi: 10.1007/s00190-012-0597-9.

Wang, F. (2003). *Study on Center of Mass Calibration and K-band Ranging System Calibration of the GRACE Mission*. PhD thesis, The University of Texas at Austin.

Wang, L., Shum, C. K., Simons, F., Tassara, A., Erkan, K., Jekeli, C., and et al. (2012). Coseismic slip of the 2010 Mw 8.8 Great Maule, Chile, earthquake quantified by the inversion of GRACE observations. *Earth and Planetary Science Letters*, 335–336, Pages 167–179, doi: 10.1016/j.epsl.2012.04.044.

Wang, W., Shi, Y., Sun, W., and Zhang, J. (2011). Viscous lithospheric structure beneath Sumatra inferred from post-seismic gravity changes detected by GRACE. *Science China Earth Sciences*, 54, Pages 1257–1267, doi: 10.1007/s11430-011-4217-y.

Watkins, M., Gruber, T., and Bettadpur, S. (2000). Science data system development plan. Technical Report 327-710, JPL, GFZ, CSR.

Watkins, M., Flechtner, F., and Morton, P. (2013). Status of the GRACE Follow-on mission. *GRACE Science Team Meeting*. GSTM proceedings.

Wertz, J. R. (1978). *Spacecraft Attitude Determination and Control*. D. Reidel Publishing company, Dordrecht, Holland, ISBN: 90-277-0959-9.

Wertz, J. R. (2001). *Orbit and Constellation Design and Management*. Microcosm Press, Springer, ISBN: 1881883078.

Wertz, J. R. and Larson, W. (1999). *Space mission analysis and design*. Microcosm Press, Springer, ISBN: 978-1881883-10-4.

Wickert, J., Beyerle, G., Koenig, R., Heise, S., Grunwaldt, L., Michalak, G., Reigber, C., and Schmidt, T. (2005). GPS radio occultation with CHAMP and GRACE: A first look at a new and promising satellite configuration for global atmospheric sounding. *Annales Geophysicae*, 23, Pages 653–658.

Wickert, J., Michalak, G., Schmidt, T., Beyerle, G., CChen, C.-Z., Healy, S., Heise, S., and et al. (2009). GPS Radio Occultation: Results from CHAMP, GRACE and FORMOSAT-3/COSMIC. *Terrestrial Atmospheric And Oceanic Sciences*, 20, Pages 35–50, doi: 10.3319/TAO.2007.12.26.01(F3C).

Wiese, D., Nerem, R., and Lemoine, F. (2011). Design considerations for a dedicated gravity recovery satellite mission consisting of two pairs of satellites. *Journal of Geodesy*, 86, Pages 81–98, doi: 10.1007/s00190-011-0493-8.

Witkowski, M. and Massmann, F.-H. (2011). Status GRACE mission operations. *GRACE Science Team Meeting*. GSTM proceedings 2011.

Witkowski, M. and Massmann, F.-H. (2012). Status GRACE mission operations. *GRACE Science Team Meeting*. GSTM proceedings 2012.

Witkowski, M. and Massmann, F.-H. (2014). Status GRACE mission operations. *GRACE Science Team Meeting*. GSTM proceedings 2014.

Wolff, M. (1969). Direct measurements of the Earth's gravitational potential using a satellite pair. *Journal of Geophysical Research*, 74, Pages 5295–5300.

Wu, S.-C., Kruizinga, G., and Bertiger, W. (2006). Algorithm theoretical basis document for GRACE Level-1B data processing v1.2. Technical Report GRACE 327-741, Jet Propulsion Laboratory.

Wuchenich, D., Mahrdt, C., Sheard, B., Francis, S., Spero, R., Miller, J., Mow-Lowry, C., Ward, R., Klipstein, W., Heinzel, G., Danzmann, K., McClelland, D., and Shaddock, D. (2014). Laser link acquisition demonstration for the GRACE Follow-On mission. *Optics Express*, 22, Pages 11351–11366, doi: 10.1364/OE.22.011351.

Yuan, D.-N., Byun, S., and Kuang, D., e. a. (2012). GRACE JPL L2 RL05 status. *GRACE Science Team Meeting, Potsdam, Sep 17-19, 2012*. GSTM 2012 proceedings.

ZARM Technik (2010). Magnetic torquers for spacecraft attitude control. http://www.zarm-technik.de/downloadfiles/ZARMTechnikAG_MagneticTorquers_web2010.pdf.

Zenner, L. (2013). *Atmospheric and oceanic mass variations and their role for gravity field determination*. PhD thesis, Technische Universität München.

Zuber, M., Smith, D., Watkins, M., Asmar, S., Konopliv, A., Lemoine, F., and et al. (2013). Gravity field of the Moon from the Gravity Recovery and Interior Laboratory (GRAIL) mission. *Science*, 339 (6120), Pages 668–671, doi: 10.1126/science.1231507.

List of Figures

List of Tables

List of acronyms

ACC	Accelerometer
ACC SU	Accelerometer Sensor Unit
ACC ICU	Accelerometer Interface Control Unit
AIUB	Astronomical Institute of the University of Bern
AOC	Antenna Offset Correction
AOCS	Attitude and Orbit Control System
ATH	Attitude Control Thrusters
CCD	Charged Coupled Device
CESS	Coarse Earth/Sun Sensor
CFRP	Carbon Fiber Reinforced Plastic
CHAMP	Challenging Minisatellite Payload
CMA	Celestial Mechanics Approach
CNES	Centre National d'Études Spatiales
CoM	Center of Mass
COSPAR	Committee on Space Research
CR	Common Reference Frame
CSR	University of Texas at Austin, Center for Space Research
DLR	Deutsches Zentrum für Luft-und Raumfahrt (German Aerospace Center)
DOY	Day Of the Year
DSHL	Disabling Supplemental Heater Lines
DTU	Technical University of Denmark
DWS	Differential Wavefront Sensing
e^2.motion	Earth System Mass Transport Mission (Square)
FoV	Field-of-View
GFZ	GeoForschungszentrum (German Research Centre for Geosciences) Potsdam
GN_2	Gaseous Nitrogen
GOCE	Gravity Field and Steady State Ocean Circulation Explorer
GPS	Global Positioning System
GRACE	Gravity Recovery and Climate Experiment
GRAIL	Gravity Recovery and Interior Laboratory
GRGS	Le Groupe de Recherche de Géodésie Spatiale
GSOC	German Space Operations Center
IBA	Inter-Boresight Angle
ICRF	International Celestial Reference Frame
IERS	International Earth Rotation and Reference System Service
IfE	Institut für Erdmessung at the Leibniz Universität Hannover
IMU	Inertial Measurement Unit
IPU	Instrument Processing Unit
ISDC	Integrated System and Data Center
ITRF	International Terrestrial Reference Frame
ITSG	Institute of Theoretical Geodesy and Satellite Geodesy
JPL	Jet Propulsion Laboratory
KBR	K-Band Ranging
KF	K-Frame
LOS	Line-of-Sight
LRI	Laser Ranging Instrument
LRR	Laser Retro-Reflector
MTM	Mass Trim Mechanism
MTE	Mass Trim Electronics
MTQ	Magnetic Torquer
NASA	National Aeronautics and Space Administration
OBDH	On-Board Data Handler
OTH	Orbit Control Thrusters
ONERA	Office National d'Études et de Recherches Aérospatiales
PCDU	Power Conditioning and Distribution Unit
PhC	Phase Center
PSD	Power Spectral Density
RFEA	Radio-Frequency Electronics Assembly

RL	Release
RPY	Roll, Pitch, Yaw
SCA	Star Camera
SCF	Star Camera Frame
SF	Satellite Frame
SH	Spherical Harmonic functions
SLR	Satellite Laser Ranging
SM	Steering Mirror
SRF	Science Reference Frame
SST	Satellite to Satellite Tracking
SZA TX/RX	S-band Zenith Transmitter and Receiver Antenna
TLE	Two-Line Elements
TMA	Triple Mirror Assembly
TN SOE	Technical Note Sequence-of-Events
TRRF	True Radial Reference Frame
TX/RX Antenna	Transmitter/Receiver antenna
USO	Ultra-Stable Oscillator
VEA	Variational Equation Approach
ZARM	Center of Applied Space Technology and Microgravity

List of GRACE data products used for the analysis presented in this thesis

data level	product	description
Level-0	THAD	AOCS data
	THBB	Pt1000 thermistor data
	THBC	YSI thermistor data
	THCE	CESS temperature data
Level-1A	SCA1A	star camera data
Level-1B	ACC1B	accelerometer science data
	CLK1B	satellite clock solution
	GNV1B	GPS orbit solution
	KBR1B	KBR ranging data
	MAG1B	magnetometer data and magnettorquer activation data
	MAS1B	spacecraft mass data
	QSA1B	SCA/ACC calibration parameters
	QKS1B	SCA/KBR calibration parameters
	SCA1B	star camera data
	THR1B	thruster activation data
	TNK1B	gas tank sensor data
	VGN1B	vector offset for the GPS main navigation antenna
	VKB1B	KBR antenna phase center offset
Level-2	GSM-2	geopotential SH coefficients

Acknowledgements

First of all, I would like to thank my parents from the bottom of my heart for giving me both roots and wings. Thank you for all your support throughout the past years. Thank you for believing in me and for encouraging me to live my dreams. I am deeply grateful for everything and am proud of both of you.

Mami, tati, děkuju!

I deeply appreciate the cooperation with my supervisor Prof. Dr.-Ing. Jakob Flury. Thank you, Jakob, for your guidance, for believing in me, and for widening my horizons. Thank you for supporting me in all the different projects I was involved in. Especially thank you for giving me the freedom to choose my own way and to do what I feel most enthusiastic about.

I also want to thank Prof. Dr.-Ing. habil. Jürgen Müller who introduced me to space geodesy during the time I spent in Hannover as a bachelor student. Thanks to your enthusiasm and expertise I became passionate about this exciting field of study. I particularly want to thank you for making it possible for me to come back to Hannover for my PhD studies.

Further, I would like to thank Prof. Dr.-Ing. Martin Horwath and apl. Prof. Dr. Gerhard Heinzel for their review of my thesis, constructive feedback and interesting discussions.

I am very thankful for the wonderful cooperation with my colleagues which resulted in joint projects and publications. Special thanks goes to (in alphabetical order): Beate Klinger (TU Graz), Ung-Dai Ko (UT CSR), Torsten Mayer-Gürr (TU Graz), Ulrich Meyer (AIUB), Majid Naeimi (LUH), Robbie Robertson (VirginiaTech), Daniel Schütze (AEI/MPG), Paul Tregoning (ANU), and Matthias Weigelt (UL).

My research would not have been possible without the numerous discussions with the members of the GRACE science team. Thank you Christian Belle (Astrium), Srinivas Bettadpur (UT CSR), Jaap Herman (GSOC), Gerhard L. Kruizinga (JPL), and Furun Wang (UT CSR) for sharing your valuable insights.

Furthermore, I would like to thank the University of Texas Center for Space Research for providing us with the GRACE Level-1A star camera data, and the German Space Operations Center for providing us with the GRACE telemetry (Level-0) data. I would also like to thank the German Space Operations Center (GSOC) of the German Aerospace Center (DLR) for providing continuously and nearly 100% of the raw telemetry data of the twin GRACE satellites.

I gratefully acknowledge the following institutions that provided funding for my research:

- Centre for Quantum Engineering and Space-Time Research (QUEST) at Leibniz University of Hannover
- Leibniz University of Hannover, funding program: "Förderung des weiblichen Nachwuchses auf dem Weg zur Professur"
- Collaborative Research Center SFB 1128 "Relativistic Geodesy and Gravimetry with Quantum Sensors"

Last but not least, I truly thank you, my soul-mates, my friends, my teachers and my mentors for accompanying me on my life journey. Thank you for your love and support, thank you for believing in me, and for sharing your knowledge and wisdom. Thank you for inspiring me and for giving me the courage to follow my dreams.